frontiers | Research Topics

Recent advances in biotechnological applications of microbial secondary metabolites

Edited by
Paola Angelini, Ajay Kumar, Vijay K. Sharma and Ragini Bodade

Published in
Frontiers in Microbiology

ISSN 1664-8714
ISBN 978-2-8325-5577-4
DOI 10.3389/978-2-8325-5577-4

About Frontiers

Frontiers is more than just an open access publisher of scholarly articles: it is a pioneering approach to the world of academia, radically improving the way scholarly research is managed. The grand vision of Frontiers is a world where all people have an equal opportunity to seek, share and generate knowledge. Frontiers provides immediate and permanent online open access to all its publications, but this alone is not enough to realize our grand goals.

Frontiers journal series

The Frontiers journal series is a multi-tier and interdisciplinary set of open-access, online journals, promising a paradigm shift from the current review, selection and dissemination processes in academic publishing. All Frontiers journals are driven by researchers for researchers; therefore, they constitute a service to the scholarly community. At the same time, the *Frontiers journal series* operates on a revolutionary invention, the tiered publishing system, initially addressing specific communities of scholars, and gradually climbing up to broader public understanding, thus serving the interests of the lay society, too.

Dedication to quality

Each Frontiers article is a landmark of the highest quality, thanks to genuinely collaborative interactions between authors and review editors, who include some of the world's best academicians. Research must be certified by peers before entering a stream of knowledge that may eventually reach the public - and shape society; therefore, Frontiers only applies the most rigorous and unbiased reviews. Frontiers revolutionizes research publishing by freely delivering the most outstanding research, evaluated with no bias from both the academic and social point of view. By applying the most advanced information technologies, Frontiers is catapulting scholarly publishing into a new generation.

What are Frontiers Research Topics?

Frontiers Research Topics are very popular trademarks of the *Frontiers journals series*: they are collections of at least ten articles, all centered on a particular subject. With their unique mix of varied contributions from Original Research to Review Articles, Frontiers Research Topics unify the most influential researchers, the latest key findings and historical advances in a hot research area.

Find out more on how to host your own Frontiers Research Topic or contribute to one as an author by contacting the Frontiers editorial office: frontiersin.org/about/contact

Recent advances in biotechnological applications of microbial secondary metabolites

Topic editors

Paola Angelini — University of Perugia, Italy

Ajay Kumar — Amity University, India

Vijay K. Sharma — Agricultural Research Organization (ARO), Israel

Ragini Bodade — Savitribai Phule Pune University, India

Citation

Angelini, P., Kumar, A., Sharma, V. K., Bodade, R., eds. (2024). *Recent advances in biotechnological applications of microbial secondary metabolites*. Lausanne: Frontiers Media SA. doi: 10.3389/978-2-8325-5577-4

Table of contents

frontiers | Frontiers in Microbiology

TYPE Editorial
PUBLISHED 09 December 2024
DOI 10.3389/fmicb.2024.1525146

OPEN ACCESS

EDITED AND REVIEWED BY
Sabine Kleinsteuber,
Helmholtz Association of German Research Centres (HZ), Germany

*CORRESPONDENCE
Ragini Bodade
ragini.bodade@iasst.gov.in
Ajay Kumar
ajaykumar_bhu@yahoo.com

RECEIVED 08 November 2024
ACCEPTED 26 November 2024
PUBLISHED 09 December 2024

CITATION
Bodade R, Kumar A, Sharma VK and Angelini P (2024) Editorial: Recent advances in biotechnological applications of microbial secondary metabolites.
Front. Microbiol. 15:1525146.
doi: 10.3389/fmicb.2024.1525146

Editorial: Recent advances in biotechnological applications of microbial secondary metabolites

Ragini Bodade[1]*, Ajay Kumar[2]*, Vijay K. Sharma[3] and Paola Angelini[4]

[1]Life Science Division, Institute of Advanced Study in Science and Technology, Vigyan Path, Guwahati, Assam, India, [2]Amity Institute of Biotechnology, Amity University, Noida, India, [3]Agricultural Research Organization, The Volcani Center, Rishon LeZion, Israel, [4]Department of Chemistry, Biology and Biotechnology, University of Perugia, Perugia, Italy

KEYWORDS

secondary metabolites, microbial strains, fermentation, human health, microbial metabolites

Editorial on the Research Topic
Recent advances in biotechnological applications of microbial secondary metabolites

Secondary metabolites are low molecular weight organic compounds synthesized by microbes during the late growth stage. Although secondary metabolites do not play a direct role in growth, but they have important ecological functions for microbes. The synthesis and production of microbial secondary metabolites are influenced by various factors such as growth conditions, media composition, feedback regulation and enzyme activation/inductions. Moreover, secondary metabolites are derived from primary metabolites, produced under the control of biosynthetic gene clusters that are regulated by tRNA, low molecular weight metabolites and gene products formed during post-exponential development. Recent advancements in biotechnological applications of microbial secondary metabolites have highlighted their potential uses in various sectors including sustainable agriculture, environment contamination and human health management.

The Research Topic "*Recent advances in biotechnological applications of microbial secondary metabolites*" has compiled 10 intriguing papers on production, characterization, regulation, and diverse applications of microbial secondary metabolites.

For example Narsing Rao et al. reported about exopolysaccharides secreted by the thermophilic strain *Bacillus paralicheniformis* CamBx3, which exhibit strong antioxidant and β-glucosidase inhibitory activities and form viscoelastic gels at acidic pH levels. The genome analysis of the strain provided information about EPS gene clusters.

Li et al. characterized four new polyketides and seven known compounds from fermented extracts of *Paecilomyces gunnii* YMF1.00003. Among different compounds 3β-hydroxy-7α-methoxy-5α,6α-epoxy-8(14),22*E*-dien-ergosta showed potent cytotoxic activity against five tumor cell lines, while the compounds gunniiol A, 7*R*-[[4*R*,5*S*-dihydroxy-1-oxo-2*E*-hexen-1-yl]oxy]-4*S*-hydroxy-2*E*-octenoicacid and (3*R*,5*R*)-3-hydroxy-5-decanolide exhibited protein kinase Cα inhibitory activity. The potential of extracted secondary metabolites can be significantly enhanced by manipulating specific transcription factors.

Kaliaperumal et al. discovered seven compounds from fermentation extracts of *Penicillium verruculosum* (XWSO1F60), endophytes of *Spongia officinalis*. These compounds were averufin, aspergilol-A, sulochrin, monomethyl sulochrin, methyl emodin, citreorosein, and diorcinol. Notably, averufin showed anticancer activity against myeloid leukemia HL60 cell lines at IC_{50} concentration of 1.00 μM compared to the standard taxol (0.002 μM) by *in vitro* assay. Moreover, virtual computational molecular docking studies confirmed the considerable binding between averufin and HL60 antigens.

Wang et al. investigated the cyclosporin A (CsA) production from *Tolypocladium inflatum* and the effect of varying concentrations of fructose and sucrose on its mycelium growth. They observed that high levels of fructose in the medium resulted in enhanced CsA production. This study provides valuable information about potential candidate genes that could be modified through metabolic engineering to create strains for higher CsA yield.

Shahbaz et al. reported the capabilities of probiotics in improving meat quality. This study reported the isolation of four lactobacilli strains from chicken gut. All strains showed strong resistance to salt and bile salts, as well as good viability and adherence ability to chicken ileum epithelial cells. *Lactobacillus delbrueckii* PUPro2 displayed a faster growth rate compared to the other strains. Furthermore, all the strains exhibited antagonistic behavior against the tested pathogens, cholesterol assimilation capabilities, and γ-hemolysis. The study revealed that these bacteria have the potential to enhance chicken growth and improve meat quality.

Lu et al. isolated a salt-tolerant rhizobacteria, *Micromonospora profundi* TRM 95458, from the rhizosphere of chickpea plant (*Cicer arietinum* L.) and extracted a novel osmotic compound named 2-(2-(2,3-dihydroxypropoxy)-2-oxoethyl) amino) benzoic acid (ABAGG) from its fermentation broth. The strain *M. profundi* TRM 95458 showed the capability to convert glycerol into ABAGG. Additionally, accumulation of ABAGG was found to depend on the concentration of glycerol and glycine in the medium. The study suggests the accumulation of ABAGG in the *M. profundi* TRM 95458 enables the strain to thrive in saline-alkaline environments.

Shi et al. investigated the antagonistic activity of *Bacillus velezensis* BHZ-29, which has shown the ability to combat *Verticillium dahliae*, a plant pathogen responsible for *Verticillium* wilt in cotton. This strain exhibited a high potential for inhibition, achieving a disease control ability of 93.8% in treated cotton. The strain increases the activities of peroxidase and superoxide dismutase, indicating that it employs antibiosis while also inducing resistance, thereby showcasing its promising role in agricultural applications.

Kim et al. conducted a comparative genomics study to analyze secondary metabolite gene clusters in 366 different *Burkholderia* species. Their research revealed distinct patterns of these gene clusters within different groups of *Burkholderia* species and examined the relationships between species and metabolite synthesis (polyketide synthase, terpene, and siderophore) through network analysis. The study highlighted similar patterns of siderophore gene clusters among various species, providing insights into their species-specific mechanisms of environmental adaptation.

Yuan et al. reported that microalgae accumulate fatty acids and astaxanthin in response to abiotic stress. Their research emphasized the significant role of NADPH oxidase-derived reactive oxygen species in accumulation of fatty acids and astaxanthin in *Chromochloris zofingiensis* under high-salinity, nitrogen and phosphorus stress. They identified 1,445 shared differentially expressed genes through transcriptome analysis. Additionally, enrichment analysis suggested the importance of biotin, betalain, thiamine, and glucosinolate in stress responses. The heat map illustrated that diphenyleneiodonium notably suppressed gene expression in the fatty acid and carotenoid biosynthesis pathways.

Xu et al. examined the dynamics of microbial flora associated with musk during its secretion period using a metagenomics approach. Male musk deer secrete a malodorous liquid from their musk glands, which, upon fermentation, turns into a blackish-brown solid in the musk pod, resulting in the distinct musk scent. The serum testosterone level, chemical composition, and microbiota of musk exhibit dynamic changes during its secretion. GC-MS analysis of natural musk revealed maximum production of 3-methyl cyclopentadecanone followed by 3a-hydroxy-5b-androstan-17-one and cholesterol. Studies of mascon using 16S rRNA sequencing from different stages of animals showed *Actinobacteria, Firmicutes,* and *Proteobacteria* were the dominant bacterial phyla throughout the musk secretion cycle. Moreover, *Pseudomonas* and *Corynebacterium* were identified as the biomarkers during the vigorous musk secretion period, while *Clostridium* appeared in the late period. *Actinobacteria* and *Corynebacterium* were predicted to be involved in the synthesis of muscone and etiocholanone during musk secretion.

The studies presented in this Research Topic highlight the synthesis, structural characterization and diverse potential applications of secondary metabolites across various fields. They emphasize the relevance of these compounds in environmental sustainability, human health, and animal welfare. It is our hope that this Research Topic offers valuable scientific insight into microbial secondary metabolites while addressing critical knowledge gaps in the field.

Author contributions

RB: Conceptualization, Investigation, Writing – original draft, Writing – review & editing. AK: Writing – review & editing. VS: Writing – review & editing. PA: Writing – review & editing.

Conflict of interest

The authors declare that the research was conducted in the absence of any commercial or financial relationships that could be construed as a potential conflict of interest.

Publisher's note

frontiers | Frontiers in Microbiology

TYPE Original Research
PUBLISHED 07 September 2023
DOI 10.3389/fmicb.2023.1236906

OPEN ACCESS

EDITED BY
Ajay Kumar,
Agricultural Research Organization (ARO), Israel

REVIEWED BY
Parul Chaudhary,
Graphic Era Hill University, India
Rubee Devi,
Eternal University, India

*CORRESPONDENCE
Chuan-xing Wan
✉ wanchuanxing@163.com

RECEIVED 08 June 2023
ACCEPTED 11 August 2023
PUBLISHED 07 September 2023

CITATION
Lu D, Shen H-l, Wang L and Wan C-x (2023) *Micromonospora profundi* TRM 95458 converts glycerol to a new osmotic compound. *Front. Microbiol.* 14:1236906. doi: 10.3389/fmicb.2023.1236906

Micromonospora profundi TRM 95458 converts glycerol to a new osmotic compound

Di Lu[1,2], Hong-ling Shen[1,2], Lei Wang[1,2] and Chuan-xing Wan[1,2]*

[1]Key Laboratory of Protection and Utilization of Biological Resources in Tarim Basin Co-funded by Xinjiang Production & Construction Corps and The Ministry of Science & Technology, Tarim University, Alar, China, [2]College of Life Sciences and Technology, Tarim University, Alar, China

Plant growth and agricultural productivity was greatly limited by soil salinity and alkalization. The application of salt-tolerant rhizobacteria could effectively improve plant tolerance to saline-alkali stress. *Micromonospora profundi* TRM 95458 was obtained from the rhizosphere of chickpea (*Cicer arietinum* L.) as a moderate salt-tolerant rhizobacteria. A new osmotic compound (ABAGG) was isolated from the fermentation broth of *M. profundi* TRM 95458. The chemical structure of the new compound was elucidated by analyzing nuclear magnetic resonance (NMR) and high-resolution mass (HRMS) data. *M. profundi* TRM 95458 could convert glycerol into ABAGG. The accumulation of ABAGG varied depending on the amount of glycerol and glycine added to the fermentation medium. In addition, the concentration of NaCl affected the ABAGG content obviously. The highest yield of ABAGG was observed when the salt content of the fermentation medium was 10g/L. The study indicated that salt stress led to the accumulation of ABAGG using glycerol and glycine as substrates, suggesting ABAGG might aid in the survival and adaptation of the strain in saline-alkaline environments as a new osmotic compound.

KEYWORDS

ABAGG, compatible solutes, conversion of glycerol, *Micromonospora profundi* TRM 95458, salt-tolerant rhizobacteria

Introduction

Salinity is one of the major abiotic stress factors that threaten plant growth and agricultural productivity (Wang et al., 2022). This phenomenon is attributed to osmotic stress, which leads to water loss and impedes the absorption of water by plant roots. Additionally, ionic stress caused by high levels of Na^+ and Cl^- ions can result in toxicity and hinder the uptake of other essential ions (Robles et al., 2018). Due to the widespread drought conditions in recent years and the lack of confident water resources, there has been an increase in saline soil levels, particularly in arid regions. Soil microbes such as plant growth-promoting rhizobacteria (PGPR) play a vital role in improving plant growth, soil health, abiotic stress and enhance crop productivity (Kong et al., 2018; Kumar Arora et al., 2020; Kumawat et al., 2020). The rhizosphere refers to the soil zone surrounding plant roots, which has a significant impact on the biological and chemical properties of the soil. In the rhizosphere, bacterial concentrations are approximately 10–1,000 times higher compared to the bulk soil (Gouda et al., 2018; Liu et al., 2020). The microorganisms present in their rhizosphere play a crucial role in enhancing the plants' stress tolerance (Ferreira et al., 2019; Liu et al., 2022). The application of PGPR has effectively improved plant tolerance to saline-alkali stress (Nordstedt and Jones, 2020). Actinomycetes have been reported to alleviate salt stress. For instance, *Streptomyces* sp. strain PGPA39 isolated from agricultural soil has been stated to alleviate

salt stress in tomato plants (Rani et al., 2020). Actinomycetes produce many compatible solutes such as ectoine, trehalose, glycine betaine, and glucosylglycerol, and thus have a great capacity to increase salt-tolerance (Wang et al., 2021; Xu et al., 2021; Narsing Rao et al., 2022). *Micromonospora* is a highly productive genus within the rare actinomycetes group, with over 740 bioactive microbial metabolites discovered up to date (Mercedes et al., 2018). Most of the *Micromonospora* species contain salt-tolerant gene clusters such as NAGGN gene cluster, which may be a resource for discovering new osmotic compound. In light of the tremendous potential of actinomycetes in mitigating salt stress conditions, this study focused on isolating and identifying the salt stress tolerance of actinomycetes in the rhizosphere soil of Chickpea (*Cicer arietinum* L.). Chickpea is a crucial pulse crop that is widely cultivated and consumed globally, with a particular emphasis on Afro-Asian countries (Varshney et al., 2021; Grasso et al., 2022). Chickpea is a popular food crop in China, particularly in the northern and southern Tianshan Mountains of Xinjiang. Mulei County in Xinjiang is known as the hometown of chickpeas and is the largest chickpea planting base of China. This crop is well-suited for the region due to its ability to withstand salt stress conditions. Soil salinisation is a global and dynamic problem which is predicted to intensify in the future under the changing realms of climate (Amro et al., 2022). Rhizobacteria including *Rhizobium* and *Micromonospora* are abundantly existed in the rhizosphere of chickpea. Previous studies have shown that plant growth-promoting rhizobacteria (PGPR), which are beneficial soil microorganisms, can enhance plant growth and yield even under stress conditions. The salt-tolerant antagonistic bacteria CZ-6 has the potential to act as a biological control agent in saline soil. It is expected that the addition of salt-tolerant antagonistic bacteria will help alleviate plant damage and economic losses caused by pathogenic fungi and salt stress (Zhou et al., 2021). Halophytes, which exhibit extreme salt tolerance, are cultivated in saline-alkaline environments. The microorganisms present in their rhizosphere play a crucial role in enhancing the plants' stress tolerance (Ferreira et al., 2019). However, there are few studies on the salt-tolerant active monomer components of chickpea soil microorganisms. In order to find out the beneficial actinomyces and active ingredient with salt tolerance, *M. profundi* TRM 95458 was isolated and screened from the rhizosphere soil of chickpea in Mulei County, Xinjiang. The investigation of compatible solutes in *M. profundi* TRM 95458 resulted in findinig a new osmotic pressure regulator ABAGG.

Materials and methods

General experimental procedures

The high-performance liquid chromatography (LC-20AT, Shimadzu) with an Agilent ODS column (4.6 × 250 mm) was used for HPLC analysis. Preparative HPLC (pHPLC) was carried out using Waters 2,767 coupled with a Shim-park RP-C18 column (250 × 20 mm i.d., Shimadzu). NMR spectra were measured in MeOD at 298 K on a Bruker Ascend™ 500 M NMR (^{1}H NMR, 500 MHz; ^{13}C NMR, 125 MHz) spectrometer with TMS as internal standard. HRMS (ESI) m/z measurements were obtained on a Thermo Scientific Q Exactive mass spectrometer. SEM photos were taken by an S3400n scanning electron microscopy (Hitachi). Software MEGA 5.05 was used to establish phylogenetic tree.

Isolation of *M. profundi* TRM 95458

The strain was isolated from soil samples taken from the chickpea rhizosphere in Mulei County, Xinjiang (90.14° East longitude, 43.56°North and 1,562 m altitude) in July, 2021. This was achieved using the dilution coating plate method with 1/10 ISP2 medium (0.4% yeast extract, 1% wort, 0.4% glucose, 0.1% NaCI, and 1.6% agar, which was made up to 1 L with water, pH 7.0) in a 28°C constant temperature culture. The strain TRM 95458 was further cultured by a glycerol-amino acid medium.

Taxonomic identification of *M. profundi* TRM 95458

Morphological observation

Scanning electron microscopy required a solid plate culture, using a blade to cut off a block (size of about 0.5 cm × 0.5 cm). The excess medium was cut off, with the mycelium medium of thin and uniform thickness. The morphology of mycelium, the growth of aerial mycelium and basal mycelium, whether the mycelium produces spore filaments, and the arrangement and shape of spore filaments were observed and recorded.

Molecular biological identification of strain TRM 95458

Extraction of genomic DNA from strain TRM 95458

The TRM 95458 cells on the culture plate were collected and placed in a sterile 1.5-mL centrifuge tube, and 480 μL 1 × TE buffer was added. Then, 20 μL of lysozyme (50 mg·mL^{-1}) were added, and it was put in a 37°C water bath overnight. Each tube had 50 μL 20% SDS, 5 μL 20 mg·mL^{-1} protease K and was placed in a 60°C water bath for 2 h. Then, 55 μL of phenol: chloroform: isoamyl alcohol (25:24:1) were added, the tubes were centrifuged at 12,000 rpm for 5 min. The supernatant was moved into another centrifuge tube, which was repeated twice. The supernatant was mixed with 300 μL of 95% isopropanol and 70 μL of sodium acetate (3 mol·L^{-1}), centrifuged at 12,000 rpm for 10 min, and the supernatant was discarded. The centrifuged product was washed with 500 μL of 70% ethanol once, centrifuged at 12000 rpm for 5 min, and the supernatant was discarded to volatilise the ethanol completely. The DNA at the bottom was fully dissolved with 30 μL of sterile ultra-pure water, and the quality of DNA extraction was detected by 1% agarose gel electrophoresis. The extracted DNA was stored in a refrigerator at −20°C.

Amplification of 16S rRNA gene of strain TRM 95458

The 16S rRNA gene fragment in the genomic DNA of actinomycetes was amplified by using the universal primers 27F (5'-AGAGTTTGATCCTGGCTC-3′) and 1492R (5'-CGGCTACCT TGTTACGACTT-3′). The 50 μL PCR reaction system was as follows: 34 μL dd H_2O, 5 μL 10× buffer, 2.5 μL dNTPs, 2 μL primer 27F (10 μmol·L^{-1}), 2 μL primer 1492R (10 μmol·L^{-1}), 2 μL 50% DMSO, 0.5 μL Taq DNA polymerase and 2 μL template DNA.

The PCR reaction conditions were pre-denaturation at 94°C for 4 min. Denaturation was done at 94°C for 1 min, annealing at 56°C for 1 min, extension at 72°C for 2 min for 30 cycles and then total extension at 72°C for 8 min. The reaction was detected by 1% agarose gel electrophoresis. The sequencing results were spliced by DNAMAN5.2, and the sequences were compared with the published strains in the GenBank database by BLAST. The 16S rRNA gene sequences of the published strains with high similarity were downloaded. The phylogenetic tree was constructed by MEGA5.05 software to determine the taxonomic status of strain TRM 95458.

Genome sequencing of strain TRM 95458

Strain TRM 95458 was cultured in a liquid medium. When the strain grew to the logarithmic phase, the bacteria were collected and sent to the Xi'an Branch of Beijing Qingke Biotechnology Co., Ltd. for equencing by Nanopore PromehION.

Fermentation, isolation, and purification of compounds

A single colony in the solid medium was selected to seed the liquid medium (0.4% yeast extract, 1% wort, 0.4% glucose, and 0.1% NaCI, which was made up to 1 L with water, pH 7.0), and incubated at 30°C on a rotary shaker (150 rpm) to produce fermentation for five days. Then, 4% of the seed liquid medium was inoculated into the fermentation medium (glycerol 2%, peptone 1%, glycine 1% and yeast extract 1%, which was made up to 1 L with water, pH 7.0) and cultured at 30°C for 7 days. The bacterial solution was centrifuged, and the fermentation products were separated into fermentation broth and mycelia. The fermentation broth was adsorbed with D101 macroporous resin and washed with distilled water to remove sugars, salts, and extracellular proteins. Then, it was eluted with 30% methanol. Finally, 95% methanol was used to elute into colourlessness, and the eluent was concentrated under reduced pressure by a rotary evaporator to obtain the crude extract of secondary metabolites. The crude extract products were packed into an ODS column (50 cm × 6.0 cm) and eluted with MeOH-H_2O (30%, 50%, 80%, and 100% MeOH) to give four fractions. The 80% methanol eluent was further purified by preparative HPLC. The solvent systems for pHPLC were A: 30% MeOH-H_2O (0.075% HCOOH), B: 100% MeOH and a flow rate of 10 mL/min. The gradient elution conditions were 0–40 min, 0–65% B; 40–45 min, 65–100% B; and 45–50 min, 100% B. The DAD detector wavelength was 350 nm. Compounds 1, 2, 3, and 4 were harvested from the peaks at 21.85 min, 19.38 min, 28.28 min, and 33.13 min, respectively.

Functional determination of converting from glycerol to ABAGG by TRM 95458

The purified ABAGG was prepared in a 1.0 mg/mL mother liquor. It was then diluted to concentrations of 1.0, 0.5, 0.25, 0.125, 0.0625, 0.03125, and 0.0156 mg/mL to create a standard curve using the area normalisation method with HPLC. Varying amounts of glycerol and glycine were added to the fermentation media, the fermentation broth was subjected to detect the production amount of ABAGG.

The relationship between salt stress and ABAGG accumulation in TRM 95458

The effect of different concentrations of NaCl (2.5, 5, 10, 15, and 20 g/L) was investigated on the production of ABAGG in TRM 95458 fermentation broth.

Results

Taxonomy of the isolated organism

The strain TRM95458 isolated from chickpea rhizosphere soil was an actinomycetes judging by the single warty-globular spore of colony (Figure 1A) and the toruliform spores observed in the scanning electron microscopy (SEM) photo (Figure 1B). Based on 16S rRNA phylogenetic analysis, the strain was further classified as *M. profundi*, with 100% similarity to *M. profundi* DS3010 (Figure 1C).

Structure elucidation of the new compound

The organic extract of TRM 95458 cultured in a 20 L fermentation media was separated and purified to obtain compounds 1, 2, 3, and 4 (Figures 2, 3), among which compound 1 was a new compound. Compound 1 was obtained as a brown solid. Its HRESIMS (high-resolution electrospray ionization mass) data showed an $(M+Na)^+$ ion peak at m/z 292.0793, indicating a molecular formula of $C_{12}H_{15}NO_6$ (Figure 4). The ^1H and ^{13}C NMR spectra showed typical signals for the derivative of anthranilic acid (Figures 5, 6; Table 1). The high field area shows 7 proton signals according to the typical H signal. The peak at δ_H 4.11 (2H, s) is the methylene peak of C-8. The peak at δ_H 4.34 (2H, m) was the methylene peak of C-10. The peak at δ_H 4.23 (^1H, m) was the peak of C-11. The peak at δ_H 4.16 (2H, m) was the methylene peak of C-12. The four H signals at 6 ~ 8 ppm were signals on the benzene ring. The ^{13}C NMR spectrum as well as HSQC spectrum showed 12 carbon atoms, consisting of 3 secondary carbons, 5 tertiary carbons and 4 quaternary carbons with two carbonyl signals at δ_C 170 ~ 173 (Supplementary Figure S1). According to the HMBC spectrum, H-8 (δ_H 4.11) was associated with two quaternary carbon atoms (C-2, δ_C 151.70; C-9, δ_C 172.34), indicating glycine group connected with anthranilic acid. H-10 (δ_H 4.34) showed HMBC relationship to C-9 and C-12 (C-9, δ_C 172.34; C-12, δ_C 71.94), indicating glycerol group connected with glycine (Figure 7 and Supplementary Figure S2). Based on the 1D & 2D NMR (Supplementary Figure S3) spectroscopic analyses the new compound was ABAGG (compound **1**, 2-((2-(2,3-dihydroxypropoxy)-2-oxoethyl) amino) benzoic acid), together with three known compounds including 2-aminobenzoic acid (compound **2**), 2-((carboxymethyl) amino) benzoic acid (compound **3**), and 2-((2-methoxy-2-oxoethyl) amino) benzoic acid (compound **4**).

Conversion from glycerol to ABAGG by TRM 95458

The standard curve was determined by HPLC through the area normalisation method (Figure 8). The standard curve equation of

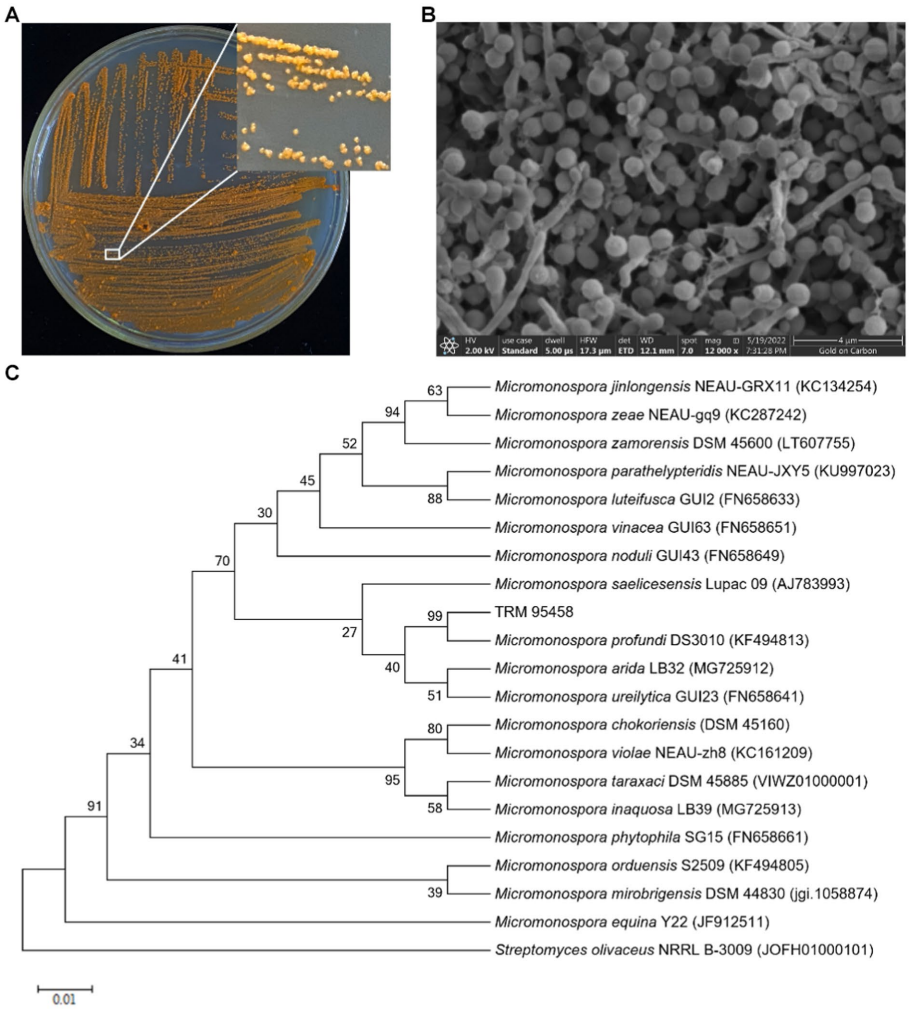

FIGURE 1
Colony characteristics and scanning electron micrograph of TRM95458 grown on ISP2 agar at 28°C for 7 days. **(A)** Colony characteristics of TRM95458. **(B)** The spores of TRM95458. **(C)** Neighbour-joining phylogenetic tree from the 16S rRNA sequences of TRM95458 and related species constructed by MEGA 5.05. Numbers at nodes indicate levels of bootstrap support (%) based on a neighbour-joining analysis of 1,000 resampled datasets; only values >50% are given. NCBI accession numbers are given. Bar, 0.01 nucleotide substitutions per site. *Streptomyces olivaceous* NRRL B-3009 was selected as the outgroup.

ABAGG is $y = 4.2905x + 0.3875$, where x was the relative peak area, and y was the content of ABAGG. According to $R^2 = 0.9929$, the linear relationship was good and was used to determine the content of ABAGG. Different contents of glycerol and glycine were added to the fermentation media resulted in accumulation of different amounts of ABAGG. The highest yield of ABAGG was obtained when 0.1 mL glycerol and 1 g glycine were added. Figure 9 showed the yield of ABAGG produced by *M. profundi* TRM 95458 with different glycerol additions. Figure 10 showed the yield of ABAGG produced by *M. profundi* TRM 95458 with different glycine addition.

Salt stress regulation of the accumulation of ABAGG

Changing NaCl concentration in the fermentation media varying from 2.5, 5, 10, 15 to 20 g/L, the yield of ABAGG in fermentation broth increased at first and then decreased with the increasing of NaCl concentration. When the NaCl content was 10 g/L, the yield of ABAGG was the highest (Figure 11). The results indicated that the salt tolerance of *M. profundi* TRM 95458 was improved by transforming glycerol and glycine and accumulating ABAGG in the cells under high salt concentration, indicating ABAGG as a new structure of an osmoregulatory-compatible substance.

Screening of genes related to the conversion of glycerol and glycine

The genome size of strain TRM 95458 was 6.90 Mb, and the G + C content was 70%. Through the whole genome analysis of strain TRM 95458, the gene cluster contained salt tolerance-related genes, and the genes related to glutamine-related hydrolase, synthetase and aspartic acid synthase were screened (Table 2).

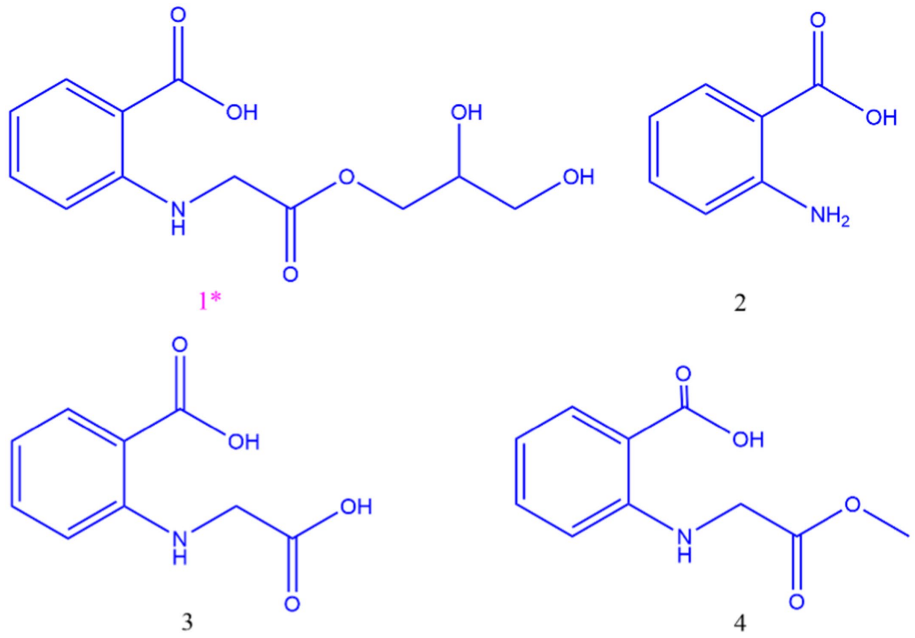

FIGURE 2
Structure of compounds 1, 2, 3,4.

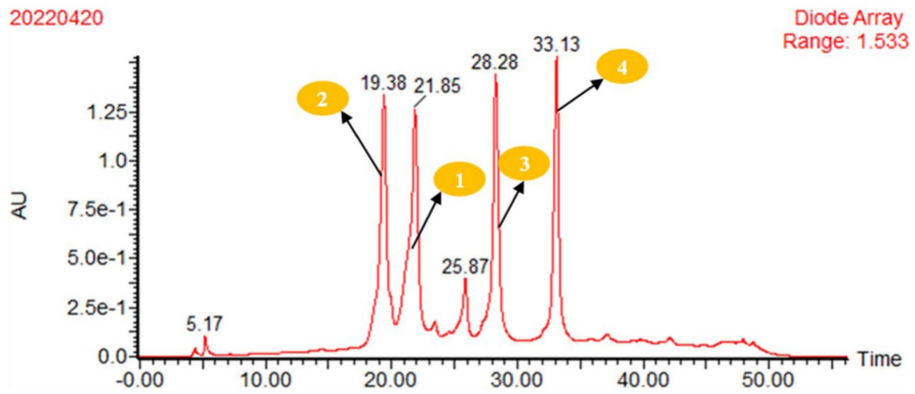

FIGURE 3
pHPLC analysis of the crude extract of strain TRM95458 fermented in liquid fermentation medium (Glycerol 2%, peptone 1%, glycine 1%, yeast extract 1%), 80% methanol eluent was purified by preparative HPLC, Conditions: A: 30% MeOH-H2O (0.075% HCOOH); B: 100% MeOH; flow rate:10mL/min; gradient elution conditions: 0–40 min 0–65% B; 40–45 min 65–100%B; 45–50 min 100%B; DAD detector wavelength: 350 nm. 2, tR = 19.38 min; 1, tR = 21.85 min; 3, tR = 28.28 min; and 4, tR = 33.13 min. The crude extract was isolated by pHPLC equipped.

Discussion

The increasing global population and decreasing availability of cultivated land pose threats to sustainability due to the loss of irrigation water resources, soil salinization, and water and environmental pollution. Among these challenges, soil salinity is particularly devastating. Soil microbes play a crucial role in mitigating salt stress (Wang et al., 2020; Yukun et al., 2021). A significant number of published studies have focused on the isolation of salt-tolerant bacteria from soil rhizosphere microorganisms. Many actinomyces were isolated from the plant rhizosphere and were known to enhance plant growth and protect plant health (Liu et al., 2019). *Streptomyces* strain D2-8 was isolated from the rhizosphere of Phragmites, a plant that thrives in saline and alkaline environments. Strain D2-8 exhibited moderate tolerance to saline and alkaline stress, as it was able to grow in solutions containing 10% NaCl and 120 mM soda saline (Gao et al., 2022). The CZ-6 strain of antagonistic bacteria was isolated from the rhizosphere of wheat in saline soil. This strain has the ability to survive in a medium with a NaCl concentration of 10% and produces indole acetic acid (IAA) and 1-aminocyclopropane-1-carboxylic acid (ACC) deaminase. Due to these characteristics, CZ-6 shows potential as a biological control agent in saline soil (Zhou et al., 2021). In light of the significant potential of actinomycetes in mitigating salt stress conditions, this study focused on isolating and identifying *M. profundi* TRM 95458 from the chickpea rhizosphere soil in saline-alkali land in Xinjiang. The strain was found to possess the ability to convert glycerol

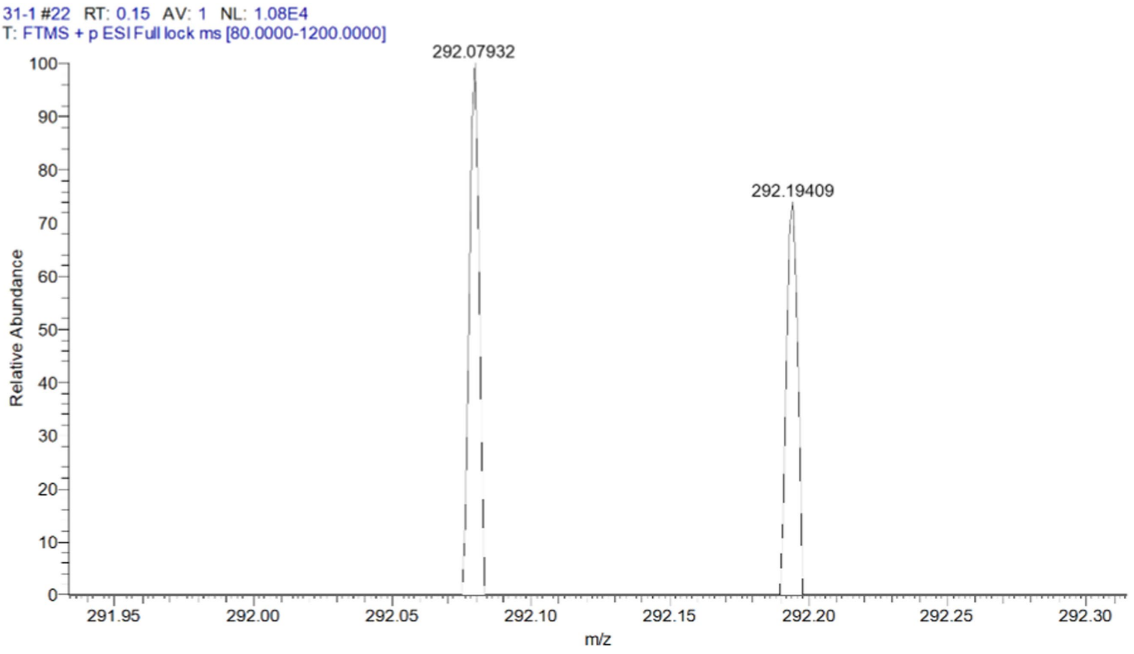

FIGURE 4
HRMS spectrum of compound 1 C12H15NaNO6+ (M+Na)+ 292.0791584.

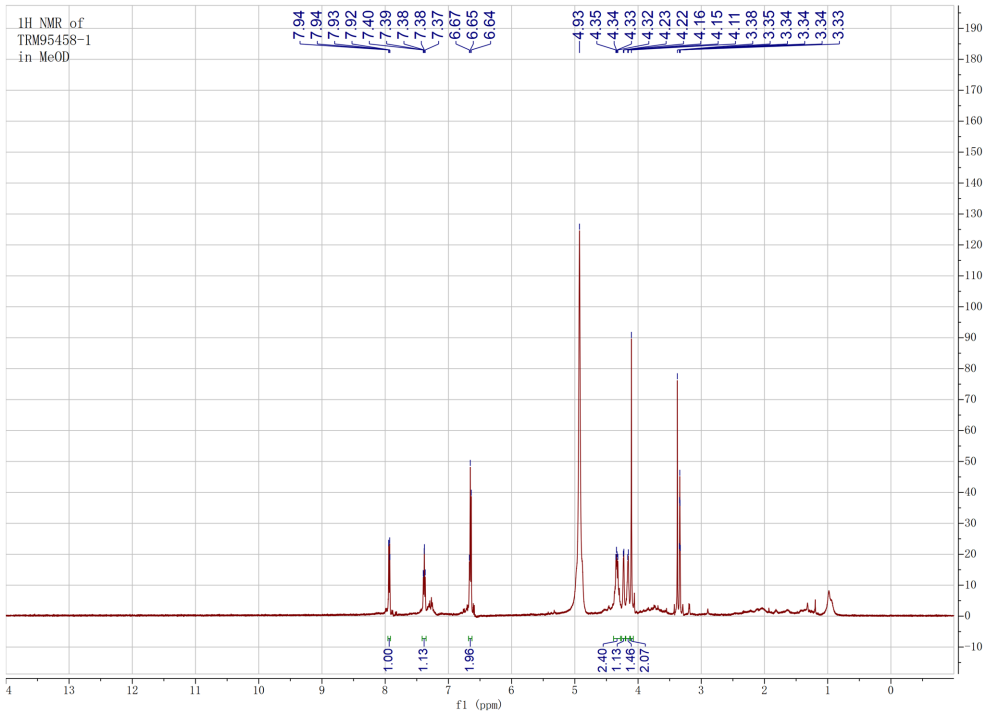

FIGURE 5
^{1}H NMR of compound 1 in MeOD.

and glycine into a novel osmotic compound called ABAGG. Under salt-stressed conditions, the majority of rhizospheric bacteria secrete osmo-protectants such as glutamate, trehalose, proline, proline betaine, and ectoine to maintain their cytoplasmic osmolarity (Kumar and Verma, 2018). These solutes, with their small molecular weight, are highly soluble. They play a crucial role in increasing intracellular water activity without disrupting normal cell metabolism (Kloska et al., 2022). The accumulation of these compatible solutes helps to balance the osmotic pressures inside and outside the cells, thereby alleviating the stress caused by high-salt environments. Additionally,

10.3389/fmicb.2023.1236906

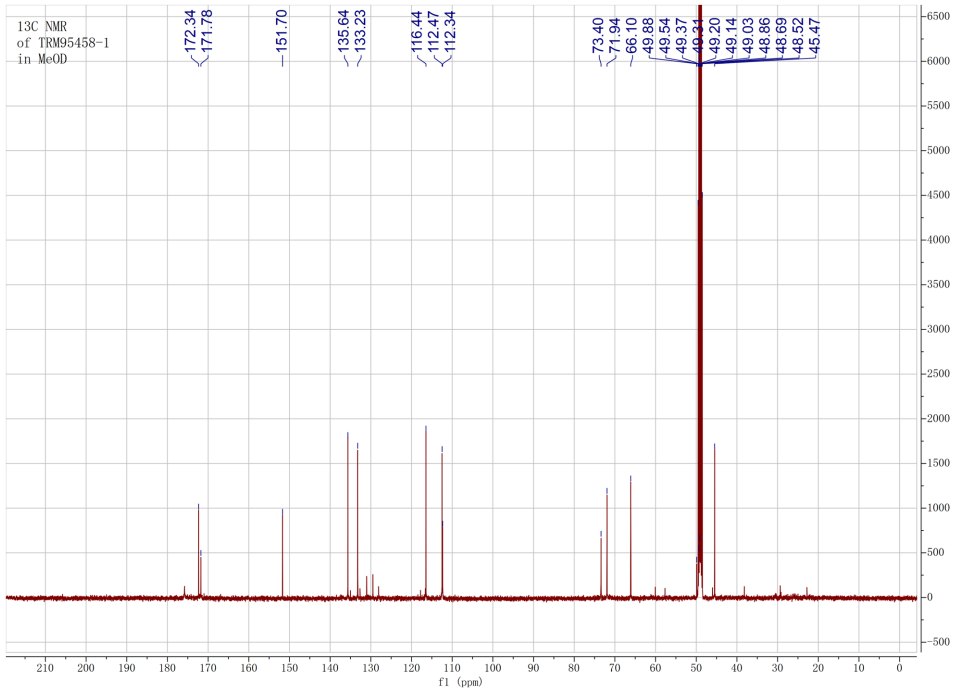

FIGURE 6
^{13}C NMR of compound 1 in MeOD.

TABLE 1 ^{1}H NMR and ^{13}C NMR data (125 MHz, MeOD) of 1.

Position	δ_C	δ_H (J in Hz)
1	112.47	
2	151.70	
3	112.34	6.64 d (7.5)
4	135.64	7.38 t (7.5)
5	151.70	6.65 t (7.5)
6	133.23	7.94 d (7.5)
7	171.78	
8	45.47	4.11 2H, s
9	172.34	
10	66.10	4.23 2H, m
11	73.40	4.23 m
12	71.94	4.16 2H, m

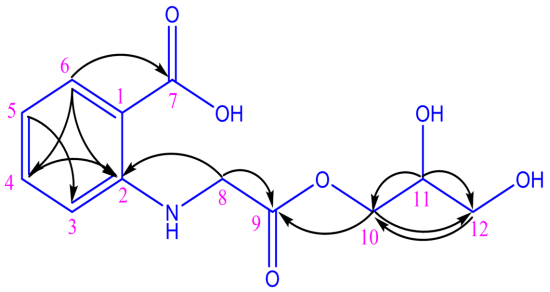

FIGURE 7
HMBC correlations of compound 1.

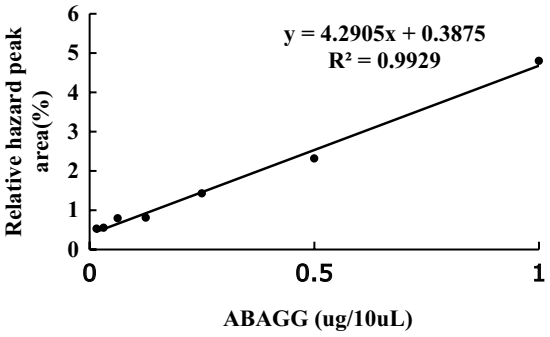

FIGURE 8
The standard curve of ABAGG by HPLC.

the rapid synthesis and degradation of these solutes are advantageous for halophilic microorganisms in adapting to high osmotic pressures. Halophilic microorganisms can synthesize different compatible solutes according to the external conditions, such as duration of the osmotic stress, level of salinity, availability of substrates, and osmolytes in the surroundings. Beneficial microorganisms, such as *Azospirillum, Burkholderia, Arthrobacter, Bacillus, Pseudomonas,* and *Rhizobium*, have been found to contribute to the development of osmo-protectants. These osmo-protectants include proline, betaine, trehalose, glycine, phenols, and flavonoids (Hashem et al., 2019). *Streptomyces albidoflavus* OsiLf-2 is an endophytic actinomycete that

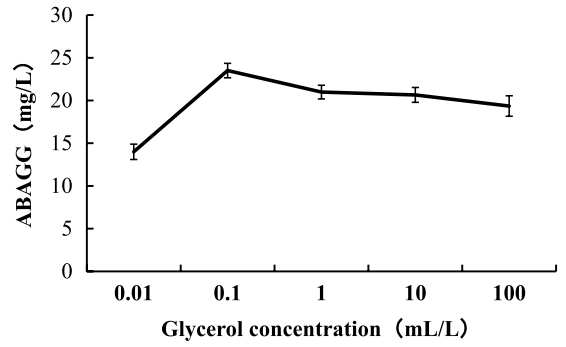

FIGURE 9
Production of ABAGG by TRM 95458 with different glycerol addition.

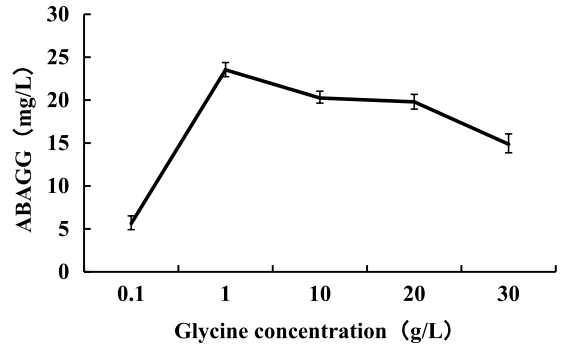

FIGURE 10
Production of ABAGG by TRM 95458 with different glycine addition.

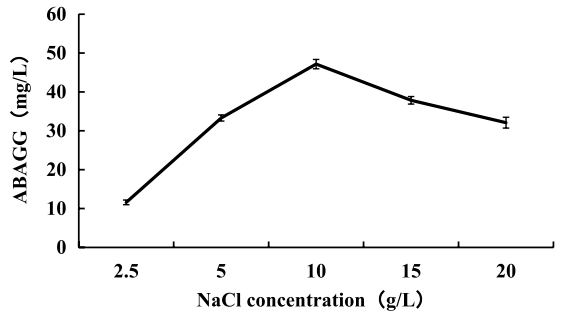

FIGURE 11
Relationship between salt stress and ABAGG accumulation in TRM 95458.

TABLE 2 Genes related to salt tolerance of strain TEM95458.

Seq ID	Function	Gene-name	Total
ctg_02190	Glutamine-hydrolyzing GMP synthase	guaA	1
ctg_03194	Glutamine amidotransferase	gatD	1
ctg_03398	Asparagine synthase (glutamine-hydrolyzing)	asnB	4
ctg_04519			
ctg_04667			
ctg_04771			
ctg_06205	Glutamine synthetase	glnA	3
ctg_03015			
ctg_02988			

exhibits moderate salt tolerance, with a tolerance of approximately 6% NaCl. This strain is capable of synthesizing important osmolytes such as proline, polysaccharides, and ectoine. Upon inoculation, the proline content in rice increased by 250.3% and 49.4%, respectively, under higher salinity. Similarly, the soluble sugar content in rice also showed an increase of 20.9% and 49.4%, respectively, under higher salinity (Niu et al., 2022). The three seaweeds used as soil amendments effectively mitigated the detrimental impact of salinity on canola plants. The seaweeds increased the levels of antioxidative compounds like phenols, flavonoids, anthocyanin, and osmo-protectants, including total carbohydrates and proline (Hashem et al., 2019). *Nocardiopsis* is an intriguing halophilic microorganism known for its ability to synthesize a diverse range of compatible solutes. These include ectoine, hydroxyectoine, trehalose, glutamate, and β-glutamate, among others. Halotolerant The ectABC from *Nocardiopsis gilva* YIM 90087T was activated under the salt stress (Han et al., 2018). The production of hydroxyectoine was observed in six bacterial isolates, namely *Nesterenkonia xinjiangensis, Halobacillus* sp., *Halomonas neptunia, Thalassobacillus devorans, Nesterenkonia sp.*, and *Bacillus agaradhaerens*. The production was found to be dependent on NaCl concentration and temperature. Additionally, the study identified these bacterial isolates as novel producers of ectoine or hydroxyectoine (Orhan and Ceyran, 2023). All osmolytes share the common characteristic of reducing the osmotic potential in the cytosolic compartment at higher concentrations, without impeding metabolic reactions (Lou et al., 2018). Certain stress conditions are employed during the production of specific metabolites. *Cyanobacteria* have been observed to adapt to changing environmental conditions by adjusting the concentration of metabolites (Yadav et al., 2022). It is important to note that micro-based products have the potential to be more effective than microbial strains for different crop varieties and under various environmental conditions (Kumawat et al., 2020). The concentration of NaCl in the fermentation media had a clear impact on the production of ABAGG, indicating that salt stress resulted in the accumulation of ABAGG. Together, these results suggest that ABAGG and *M. profundi* TRM 95458 could potentially play a role in enhancing the survival and adaptation of plants in saline environments.

Conclusion

In summary, *M. profundi* TRM 95458, a strain capable of converting glycerol and glycine, was isolated and identified from rhizosphere of chickpea. A new osmotic compound (ABAGG) was identified from the fermentation broth of *M. profundi* TRM 95458 by 1D & 2D NMR and HRMS data. The accumulation of ABAGG varied depending on the amount of glycerol and glycine added to the fermentation media. The concentration of NaCl in the fermentation media obviously affected the production of ABAGG,

suggesting that salt stress led to the accumulation of ABAGG. ABAGG and *M. profundi* TRM 95458 might be implicated for improving the survival and adaptation of plants in saline environments.

Data availability statement

The datasets presented in this study can be found in online repositories. The names of the repository/repositories and accession number(s) can be found at: NCBI – PRJNA994917, SAMN36452542, OR269619.

Author contributions

C-xW: generated ideas, obtained funding, directed the work, chemical investigation, and reviewed the manuscript. DL: performed the experiments, collected, analyzed, and interpreted the data, prepared, and edited the manuscript. H-lS: isolated and identificated the strain of TRM 95458. LW: performed part of the experiments, analyzed, and interpreted the data. All authors contributed to the article and approved the submitted version.

Funding

This study was supported by Bingtuan Science and Technology Program (2021BB007) and Tarim University Principal's Fund Project (TDZKKY202201).

Acknowledgments

The authors would like to thank the Key Laboratory of Protection and Utilization of Biological Resources in Tarim Basin Co-funded by Xinjiang Production & Construction Corps and The Ministry of Science & Technology / College of Life Science and Technology, Tarim University.

Conflict of interest

The authors declare that the research was conducted in the absence of any commercial or financial relationships that could be construed as a potential conflict of interest.

Publisher's note

All claims expressed in this article are solely those of the authors and do not necessarily represent those of their affiliated organizations, or those of the publisher, the editors and the reviewers. Any product that may be evaluated in this article, or claim that may be made by its manufacturer, is not guaranteed or endorsed by the publisher.

Supplementary material

The Supplementary material for this article can be found online at: https://www.frontiersin.org/articles/10.3389/fmicb.2023.1236906/full#supplementary-material.

References

Amro, A., Harb, S., Farghaly, K. A., Ali, M. M. F., Mohammed, A. G., Mourad, A. M. I., et al. (2022). Growth responses and genetic variation among highly ecologically diverse spring wheat genotypes grown under seawater stress. *Front. Plant Sci.* 13:996538. doi: 10.3389/fpls.2022.996538

Ferreira, C. M. H., Soares, H. M. V. M., and Soares, E. V. (2019). Promising bacterial genera for agricultural practices: an insight on plant growth-promoting properties and microbial safety aspects. *Sci. Total Environ.* 682, 779–799. doi: 10.1016/j.scitotenv.2019.04.225

Gao, Y., Han, Y., Li, X., Li, M., Wang, C., Li, Z., et al. (2022). A salt-tolerant *Streptomyces paradoxus* D2-8 from rhizosphere soil of *Phragmites communis* augments soybean tolerance to soda saline-alkali stress. *Pol. J. Microbiol.* 71, 43–53. doi: 10.33073/pjm-2022-006

Gouda, K., Kerry, R. G., das, G., Paramithiotis, S., Shin, H.-S., and Patra, J. K. (2018). Revitalization of plant growth promoting rhizobacteria for sustainable development in agriculture. *Microbiol. Res.* 206, 131–140. doi: 10.1016/j.micres.2017.08.016

Grasso, N., Lynch, N. L., Arendt, E. K., and O'Mahony, J. A. (2022). Chickpea protein ingredients: a review of composition, functionality, and applications. *Compr. Rev. Food Sci. Food Saf.* 21, 435–452. doi: 10.1111/1541-4337.12878

Han, J., Gao, Q. X., Zhang, Y. G., Gao, Q. X., Zhang, Y. G., Li, L., et al. (2018). Transcriptomic and Ectoine analysis of halotolerant *Nocardiopsis gilva* YIM 90087 T under salt stress. *Front. Microbiol.* 9:618. doi: 10.3389/fmicb.2018.00618

Hashem, H. A., Mansour, H. A., El-Khawas, S. A., and Hassanein, R. A. (2019). The potentiality of marine macro-algae as bio-fertilizers to improve the productivity and salt stress tolerance of canola (*Brassica napus* l.) plants. *Agronomy* 9:146. doi: 10.3390/agronomy9030146

Kloska, A., Cech, G. M., Nowicki, D., Maciąg-Dorszyńska, M., Bogucka, A. E., Markert, S., et al. (2022). Three microbial musketeers of the seas: *Shewanella baltica*, *Aliivibrio fischeri* and *Vibrio harveyi*, and their adaptation to different salinity probed by a proteomic approach. *Int. J. Mol. Sci.* 23:619. doi: 10.3390/ijms23020619

Kong, Z., Hart, M., and Liu, H. (2018). Paving the way from the lab to the field: using synthetic microbial consortia to produce high-quality crops. *Front. Plant Sci.* 9:1467. doi: 10.3389/fpls.2018.01467

Kumar Arora, N., Fatima, T., Mishra, J., Mishra, I., Verma, S., Verma, R., et al. (2020). Halo-tolerant plant growth promoting rhizobacteria for improving productivity and remediation of saline soils. *J. Adv. Res.* 26, 69–82. doi: 10.1016/j.jare.2020.07.003

Kumar, A., and Verma, J. P. (2018). Does plant-microbe interaction confer stress tolerance in plants: a review? *Microbiol. Res.* 207, 41–52. doi: 10.1016/j.micres.2017.11.004

Kumawat, K. C., Sharma, P., Nagpal, S., Gupta, R. K., Sirari, A., Nair, R. M., et al. (2020). Dual microbial inoculation, a game changer? – bacterial biostimulants with multifunctional growth promoting traits to mitigate salinity stress in spring Mungbean. *Front. Microbiol.* 11:600576. doi: 10.3389/fmicb.2020.600576

Liu, B., Hu, Y., Wang, Y., Xue, H., Li, Z., and Li, M. (2022). Effects of saline-alkali stress on bacterial and fungal community diversity in Leymus chinensis rhizosphere soil. *Environ. Sci. Pollut. Res. Int.* 29, 70000–70013. doi: 10.1007/s11356-022-20270-6

Liu, F., Mo, X., Kong, W., and Song, Y. (2020). Soil bacterial diversity, structure, and function of Suaeda salsa in rhizosphere and non-rhizosphere soils in various habitats in the Yellow River Delta, China. *Sci. Total Environ.* 740:140144. doi: 10.1016/j.scitotenv.2020.140144

Liu, D., Yan, R., Fu, Y., Wang, X., and Xiang, W. (2019). Antifungal, plant growth-promoting, and genomic properties of an endophytic actinobacterium *streptomyces sp*. neau-s7gs2. *Front. Microbiol.* 10:2077. doi: 10.3389/fmicb.2019.02077

Lou, D., Wang, H., and Yu, D. (2018). The sucrose non-fermenting-1-related protein kinases SAPK1 and SAPK2 function collaboratively as positive regulators of salt stress tolerance in rice. *BMC Plant Biol.* 18:203. doi: 10.1186/s12870-018-1408-0

Mercedes, P.-B., Daniel, O.-C., Cruz, D. L., Maria, K., Martín, J., Vicente, F., et al. (2018). Phocoenamicins b and c, new antibacterial spirotetronates isolated from a marine *micromonospora sp*. *Mar. Drugs* 16:95. doi: 10.3390/md16030095

Narsing Rao, M. P., Lohmaneeratana, K., Bunyoo, C., and Thamchaipenet, A. (2022). Actinobacteria-plant interactions in alleviating abiotic stress. *Plants (Basel)* 11:2976. doi: 10.3390/plants11212976

Niu, S., Gao, Y., Zi, H., Liu, Y., Liu, X., Xiong, X., et al. (2022). The osmolyte producing endophyte *Streptomyces albidoflavus* OsiLf-2 induces drought and salt tolerance in rice via a multi-level mechanism. *Crop. J.* 10, 375–386. doi: 10.1016/j.cj.2021.06.008

Nordstedt, N. P., and Jones, M. L. (2020). Isolation of rhizosphere bacteria that improve quality and water stress tolerance in greenhouse ornamentals. *Front. Plant Sci.* 11:826. doi: 10.3389/fpls.2020.00826

Orhan, F., and Ceyran, E. (2023). Identification of novel halophilic/halotolerant bacterial species producing compatible solutes. *Int. Microbiol.* 26, 219–229. doi: 10.1007/s10123-022-00289-y

Rani, K., Yadav, D., Parashar, A., and Wati, L. (2020). Assessment of stress tolerance properties of chickpea actinomycetes. *Ind. J. Pure Appl. Biosci* 8, 639–646. doi: 10.18782/2582-2845.7954

Robles, P., Navarro-Cartagena, S., Ferrández-Ayela, A., Núñez-Delegido, E., and Quesada, V. (2018). The characterization of Arabidopsis *mterf6* mutants reveals a new role for mTERF6 in tolerance to abiotic stress. *Int. J. Mol. Sci.* 19:2388. doi: 10.3390/ijms19082388

Varshney, R. K., Roorkiwal, M., and Sun, S. (2021). A chickpea genetic variation map based on the sequencing of 3,366 genomes. *Nature* 599, 622–627. doi: 10.1038/s41586-021-04066-1

Wang, J., Liu, Y., Hu, S., Xu, J., Nian, J., Cao, X., et al. (2022). *LEAF TIP RUMPLED 1* regulates Leaf morphology and salt tolerance in Rice. *Int. J. Mol. Sci.* 23:8818. doi: 10.3390/ijms23158818

Wang, X., Sun, R., Tian, Y., Guo, K., and Liu, B. (2020). Long-term phytoremediation of coastal saline soil reveals plant species-specific patterns of microbial community recruitment. *mSystems* 5:e00741-19. doi: 10.1128/mSystems.00741-19

Wang, P., Yang, L., Sun, J., Yang, Y., Qu, Y., Wang, C., et al. (2021). Structure and function of rhizosphere soil and root endophytic microbial communities associated with root rot of. *Front. Plant Sci.* 12:752683. doi: 10.3389/fpls.2021.752683

Xu, T., Cui, K., Chen, J., Wang, R., Wang, X., Chen, L., et al. (2021). Biodiversity of culturable endophytic actinobacteria isolated from high yield camellia oleifera and their plant growth promotion potential. *Agriculture* 11:1150. doi: 10.3390/agriculture11111150

Yadav, P., Singh, R. P., Rana, S., Joshi, D., Kumar, D., Bhardwaj, N., et al. (2022). Mechanisms of stress tolerance in *cyanobacteria* under extreme conditions. *Stresses* 2, 531–549. doi: 10.3390/stresses2040036

Yukun, G., Jianghui, C., Genzeng, R., Shilin, W., Puyuan, Y., Congpei, Y., et al. (2021). Changes in the root-associated bacteria of sorghum are driven by the combined effects of salt and sorghum development. *Environ. Microbiome* 16:14. doi: 10.1186/s40793-021-00383-0

Zhou, Y., Hao, L., Ji, C., Zhou, Q., Song, X., Liu, Y., et al. (2021). The effect of salt-tolerant antagonistic bacteria CZ-6 on the rhizosphere microbial Community of Winter Jujube (*Ziziphus jujuba* mill. "Dongzao") in saline-alkali land. *Biomed. Res. Int.* 2021:5171086. doi: 10.1155/2021/5171086

frontiers | Frontiers in Microbiology

TYPE Original Research
PUBLISHED 02 October 2023
DOI 10.3389/fmicb.2023.1216928

OPEN ACCESS

EDITED BY
Vijay K. Sharma,
Agricultural Research Organization (ARO), Israel

REVIEWED BY
Kin Israel Notarte,
Johns Hopkins University, United States
Afzal Basha Shaik,
Jawaharlal Nehru Technological University, Kakinada, India

*CORRESPONDENCE
Rohini Karunakaran
✉ rohini@aimst.edu.my

†These authors share first authorship

RECEIVED 04 May 2023
ACCEPTED 31 May 2023
PUBLISHED 02 October 2023

CITATION
Kaliaperumal K, Salendra L, Liu Y, Ju Z, Sahu SK, Elumalai S, Subramanian K, M. Alotaibi N, Alshammari N, Saeed M and Karunakaran R (2023) Isolation of anticancer bioactive secondary metabolites from the sponge-derived endophytic fungi *Penicillium sp.* and *in-silico* computational docking approach. *Front. Microbiol.* 14:1216928. doi: 10.3389/fmicb.2023.1216928

Isolation of anticancer bioactive secondary metabolites from the sponge-derived endophytic fungi *Penicillium sp.* and *in-silico* computational docking approach

Kumaravel Kaliaperumal[1†], Limbadri Salendra[2†], Yonghong Liu[3], Zhiran Ju[4], Sunil Kumar Sahu[5], Sanniyasi Elumalai[6], Kumaran Subramanian[7], Nahaa M. Alotaibi[8], Nawaf Alshammari[9], Mohd Saeed[9] and Rohini Karunakaran[10,11,12]*

[1]Unit of Biomaterials Division, Department of Orthodontics, Saveetha Dental College and Hospitals, SIMATS, Saveetha University, Chennai, India, [2]New Use Agriculture and Natural Plant Products Program, Department of Plant Biology, Rutgers University, New Brunswick, NJ, United States, [3]Key Laboratory of Tropical Marine Bio-Resources and Ecology, Center for Marine Microbes, South China Sea Institute of Oceanology, Chinese Academy of Sciences, Guangzhou, China, [4]Institute of Pharmaceutical Science and Technology, Zhejiang University of Technology, Hangzhou, China, [5]State Key Laboratory of Biocontrol, Guangdong Provincial Key Laboratory of Plant Resources, Sun Yat-sen University, Guangzhou, China, [6]Department of Biotechnology, University of Madras, Guindy Campus, Chennai, Tamil Nadu, India, [7]Research Department of Microbiology, Sri Sankara Arts and Science College (Autonomous), Kanchipuram, Tamil Nadu, India, [8]Department of Biology, College of Science, Princess Nourah bint Abdulrahman University, Riyadh, Saudi Arabia, [9]Department of Biology, College of Science, University of Hail, Hail, Saudi Arabia, [10]Unit of Biochemistry, Faculty of Medicine, AIMST University, Semeling, Bedong, Malaysia, [11]Centre for Excellence for Biomaterials Science AIMST University, Semeling, Bedong, Malaysia, [12]Department of Bioinformatics, Saveetha School of Engineering, Saveetha University, Chennai, India

Introduction: Fungus-derived secondary metabolites are fascinating with biomedical potential and chemical diversity. Mining endophytic fungi for drug candidates is an ongoing process in the field of drug discovery and medicinal chemistry. Endophytic fungal symbionts from terrestrial plants, marine flora, and fauna tend to produce interesting types of secondary metabolites with biomedical importance of anticancer, antiviral, and anti-tuberculosis properties.

Methods: An organic ethyl acetate extract of *Penicillium verruculosum* sponge-derived endophytic fungi from *Spongia officinalis* yielded seven different secondary metabolites which are purified through HPLC. The isolated compounds are of averufin (1), aspergilol-A (2), sulochrin (3), monomethyl sulochrin (4), methyl emodin (5), citreorosein (6), and diorcinol (7). All the seven isolated compounds were characterized by high-resolution NMR spectral studies. All isolated compounds', such as anticancer, antimicrobial, anti-tuberculosis, and antiviral, were subjected to bioactivity screening.

Results: Out of seven tested compounds, compound (1) exhibits strong anticancer activity toward myeloid leukemia. HL60 cell lines have an IC_{50} concentration of 1.00μm, which is nearly significant to that of the standard anticancer drug taxol. A virtual computational molecular docking approach of averufin with HL60 antigens revealed that averufin binds strongly with the protein target alpha, beta-tubulin (1JFF), with a −10.98 binding score. Consecutive OSIRIS and Lipinski ADME pharmacokinetic validation of averufin with HL60 antigens revealed that averufin has good pharmacokinetic properties such as drug score, solubility, and mutagenic nature. Furthermore, aspergilol-A (2) is the first report on the *Penicillium verruculosum* fungal strain.

Discussion: We concluded that averufin (1) isolated from *Penicillium verruculosum* can be taken for further preliminary clinical trials like animal model *in-vivo* studies and pharmacodynamic studies. A future prospect

of *in-vivo* anticancer screening of averufin can be validated through the present experimental findings.

KEYWORDS

anticancer, averufin, fungi, HL60, molecular docking, sponges, cytotoxicity, environment

1. Introduction

Marine natural products are of great interest in the field of the pharmaceutical industry, where diverse classes of bioactive substances are derived from marine organisms. Marine sponges are sessile invertebrates that contribute the majority of natural products that possess antiviral, anticancer, antiprotozoal, antifungal, and anti-inflammatory properties (Mehbub et al., 2014). Sponges produce these bioactives as a chemical defense to protect them from predators (Pawlik et al., 2002). Marine sponges are a rich source of natural products that exhibit a wide range of chemical diversity, including xanthones, alkaloids, steroids, cyclic peptides, isoprenoids, quinones, and terpenes. Whether these natural products are secreted independently or by their endophytic symbionts has long been a contentious topic. Endophytic fungi derived from marine and terrestrial fauna and flora possess immense biomedical values in terms of therapeutic targets. Endophytic fungi, *Pullularia* sp., isolated from a terrestrial plant *Culophyllum* sp., produces cytotoxic hexadepsipeptides named pullulans A-D, which exhibited cytotoxicity against human epidermoid cancer cells and human breast cancer cells. (Thomas Edison et al., 2020). Species richness in fungal endophytic diversity was quantified from a Chinese medicinal plant (Cycdales) *Cycas debaoensis* and *Cycas fairylakea*, revealing that these plants possess 33 known genera and 62 different species of fungal endophytes, which include *Taloromyces*, *Penicillium*, and *Fusarium* spp. (Pecundo et al., 2021). Marine-derived endophytic fungi yielded many bioactive compounds. One such type is Malformin A1, an anti-trypanosomal cyclic peptide that was isolated from a marine seaweed-derived fungi *Aspergillus tubingensis*, followed by isolation of 5-hydroxy-2-pyrone derivatives isolated from green algae *Enteromorpha tubulosa* to produce cAMP on GPR12 cells (Notarte et al., 2017, 2018). Mangroves, a marine plant, harbor enormous endosymbiotic fungi, and various reports share that mangrove-derived endophytic fungi possess antimicrobial properties (Ramirez and Notarte, 2020).

Marine-derived fungi tend to be a potential candidate for bioactive compounds. Fungi associated with those marine organisms, majorly as invertebrates such as sponges, mangroves, and marine algae, were found to represent a vast untapped reservoir of metabolic diversity with growing attention during recent years (Suay et al., 2000; Bugni and Ireland, 2004; Paz et al., 2010; Rateb and Ebel, 2011). These secondary metabolites are products synthesized by the symbiotic-associated microbes within the sponges, such as cyanobacteria, microalgae, fungi, archaea, and bacteria (Unson et al., 1994; Koopmans et al., 2009). Therefore, much attention has been paid to these endophytic microbes and their cultural condition. Since harvesting sponges for their immense pharmacological importance may endanger their community, an effective and alternate method of trapping such endophytes and culturing them in laboratory conditions may yield the targeted secondary metabolites on a pilot scale.

Spongia officinalis is a marine sponge that has been used for bioprospecting for many years. An interesting class of chemical moieties like furanosesterpenes and scalarene sesquiterpenes with antibacterial and anticancer properties were isolated from *Spongia officinalis* (Manzo et al., 2011). Whether these bioactive compounds are produced by host organisms or from their endophytic symbionts is a topic of debate. As an ongoing attempt of our continuous exploration for bioactive compounds from the sponge-derived endophytes (Yang et al., 2009; Sun et al., 2015; Wang et al., 2015a), we isolated a fungal strain *Penicillium verruculosum* (XWSO1F60) derived from a marine sponge *Spongia officinalis*. The fungus was fermented on a large scale and extracted, and its bioactive compound isolation was conducted through chromatographic purification, like HPLC. Structural elucidation of isolated compounds was carried out through NMR spectroscopic studies. Herein, we have reported on the fermentation, extraction, and isolation strategies of those bioactive metabolites.

2. Materials and methods

2.1. General experimental procedures

NMR studies were recorded on a Bruker AC 500MHz NMR (Bruker, Fällanden, Switzerland) spectrometer using TMS as an internal standard. Chemical shifts were expressed in "d" (ppm) and coupling constant 'J' in Hz. HR-ESI-MS were measured using a Bruker micro TOF-QII mass spectrometer (Bruker, Fällanden, Switzerland). Size exclusion chromatography was conducted using Sephadex LH-20 gel (GE Healthcare, Uppsala, Sweden). Column chromatography was performed using a silica gel (200–300) at Qingdao Marine Chemical Factory (Qingdao, China). TLC spots were detected under UV light and by heating after spraying with 12% H_2SO4 in H_2O. Semi-preparative HPLC (RP-HPLC) was conducted on Agilent HPLC (Agilent 1260 infinity series with DAD detector, Santa Clara, CA, USA). All the positive control standard drugs used in the bioassay were procured from Sigma Aldrich (USA).

2.2. Sponge material collection

Fresh sponges of *S. officinalis* were collected from the Xidao Island (18°23.18'N and 109°36.71'E), Hainan province of the

South China Sea coast, in July 2014, during a marine cruise collection. Sponges were transported to the laboratory in ice-freeze conditions and stored at−20°C until further use. Sponges were identified based on morphological and spicule identification by the Department of Marine Bioresources and Ecological Sciences, SCISO, China. A voucher specimen (Voucher Number: SCISO 45874/2018) was deposited at SCSIO marine biological collections.

2.3. DNA extraction and phylogenetic sequence analysis

The endophytic fungus XWSO1F60 was isolated from the sponge *S. officinalis*. The strain was grown on a MactoBalt (MB) agar slant at 25°C. Two-week-old fungal hyphae were scraped for genomic DNA isolation using the Ultraclean Microbial DNA Kit (MoBio Laboratories). The internal transcribed spacer of ribosomal nucleotide sequence (ITS rDNA) primers ITS1 (5′-GCACAGGCAGCAGGAGCTG CCCCTCAGCTGTCTCCTCGTGCTCAAC-3′) and ITS (5′-AGAGCAAGCCGAGCAGGTCTATCGCCAAGTATCCTCAG AAGCTGTGCT-3′) were used (Volkov et al., 2014). The PCR reaction was conducted using Eppendorf equipment (Eppendorf, NY, USA). The reaction mixture of 50 μL consisted of polymerase chain reaction (PCR) buffer, 2.5 mM Mg^{2+}, 100 μM dNTPs, 0.5 μM each primer, 10 ng extracted DNA, and 2 U Taq polymerase. The thermocycling steps involved an initial denaturation at 95°C for 5 min, followed by 20 cycles consisting of 1.5 min at 95°C, 2 min at 50°C, and 2 min at 68°C. This was followed by another set of 20 cycles with 10 min at 68 C and a final extension step of 10 min at 4°C. The resulting PCR product was processed from agarose gel using QIA quick Gel Extraction Kit (QIAGEN, Valencia, CA, USA) and sequenced using an ABI 3730 sequencer (Applied Bio-systems, USA). Sequences were analyzed using the BLAST program (Basic Local Alignment Search Tool). The phylogenetic tree was constructed based on the neighbor-joining (NJ) method using MEGA-5.0 by using 1,000 bootstrap replicates. The sequence was deposited in GenBank and assigned an accession number (Genbank: KU891245).

2.4. Fermentation, extraction, and isolation of compounds

A stock culture of the strain XWSO1F60 was grown on MB agar solid medium at 25°C for a week. The stock culture was inoculated in an optimized seed medium (malt extract 15 g, sea salt 2.5 g, NaCl 2.5 g, distilled water 1000 mL, pH 7.4 −7.8) and incubated at 25°C for 72 h on a rotating shaker (180 rpm). The optimization of the growth medium was selected based on previous experimental validation with maximum fungal growth and UV-HPLC metabolite fingerprinting. The mass quantity of fermentation of fungal isolates XWSO1F60 was carried out using a solid rice medium in 1000 mL flasks (rice 200 g, sea salt 2.5 g, distilled water 200 mL), which were inoculated with 10 mL of seed solution. Flasks were incubated at 25°C under a day-night cycle. 60 days old of fungal cultures from 40 flasks were subjected to organic extraction using Acetone /Ethyl acetate (EtOAc). The combined acetone/EtOAc fungal culture extracts were partitioned between 90% aqueous MeOH and petroleum ether. The resultant MeOH yield was fractionated using a silica column, Sephadex LH-20, and finally, semi-preparative reversed-phase HPLC to yield compounds (1–7).

The EtOAc crude extracts were then purified by silica gel column chromatography eluted with $CHCL_3$-MeOH in a gradient eluent (v/v, 75:1, 50:1, 30:1, 20:1, 5:1, 1:1, 0:1) to obtain fractions 1–8 based on the TLC spots. Fr. 4 (950 mg) was purified by Sephadex LH-20 ($CHCl_3$/MeOH, 1:1) to obtain three subfractions (fr. 4.1–4.3). Fr.4.1 (226 mg) was further purified by SP-RP HPLC eluting with CH_3CN/H_2O (55:45) to afford compound diorcinol (7) (16.7 mg) and compound methyl emodin (5) (9.6 mg). Fraction 3 (1.9 g) was purified using Sephadex LH-20 ($CHCl_3$/MeOH, 1:1) and SP-RP HPLC using a C-18 column (Agilent 1260 infinity, YMC-Pack, ODS-A S-5 μm× 12 nm 250 × 20mm i.d., 3 mL per minute) eluting with MeOH/H_2O (10:90) to afford compound citreoresin (6) (13.2 mg). Fr. 7 (1.8 g) was subjected to Silica gel chromatography eluted with Acetone/MeOH in a step-wise eluent (1:8, 3:5, 3:3, 5;1, 8:1) to give three subfractions (fr. 7.1–7.3). Fr. 7.2 (159 mg) was purified using SP-RP HPLC eluting with CH_3CN / H_2O (79:21) to afford compound averufin (1) (5.6 mg) and compound apergilol-A (2) (12.2 mg). Fr. 8 (3.9 g) was subjected to silica gel column chromatography eluted with a $CHCL_3$/MeOH in a gradient elution of (50:1, 35:1, 15:1, 10:1 and 0:100) (v/v), which yielded six fractions (fr 8.1 – 8.3). Fr. 8.3 (700 mg) was subjected to ODS chromatography eluted with MeOH/H_2O (linear gradient, 50–100% MeOH) to obtain five subfractions (fr. 8.3.1–8.3.3). Fr. 8.3.1 (96.1mg) was further purified using SP-RP HPLC eluting with CH_3CN- H_2O (50:50) to afford the compound monomethyl sulochrin (4) (14.9mg). Fr. 8.2.4 (23 mg) was purified using (SP-RP) HPLC eluting with CH_3CN-H_2O (67:33) to afford the compound sulochrin (3) (11.6mg).

2.5. NMR spectroscopy characterization

All the isolated compounds were checked for purity using Thin-layer Chromatography (TLC). After ensuring the purity, the compounds were subjected to ^1H and ^{13}C-Nuclear Magnetic Resonance (NMR) spectroscopy (500 MHz, Bruker). Trimethylsilane (TMS) was used as an internal standard. The NMR spectrum was analyzed using MestreNova spectral processing (Version. 14.2.0).

2.6. Anticancer screening

Cytotoxicity was assessed using the Cell Counting Kit (CCK-8) (Dojindo, Japan) method adopted by Wang et al. (2015a). Cancer cell lines used in this study included K562, MCF-7, A549, HuH-7, H1975, HeLa, HL7702, DU145, HL60, MOLT-4. Additionally, a normal cell line, MCF10A, was included. All cell lines were procured from Shanghai Cell Bank, Chinese Academy of Sciences. Cells were routinely grown and maintained in RPMI or DMEM media with 10% Fetal Bovine Serum and 1%

penicillin/streptomycin. Various concentrations of seven isolated compounds from *Penicillium* sp. were dissolved in 100% DMSO with a maximum concentration of 200 μg/mL and serially diluted to a final 0.1% DMSO concentration to treat cells for 2 h. Taxol was used as a positive control, and DMSO was used as a negative control. Cytotoxicity screening assay experiments were conducted in triplicate to obtain the standard error ± mean value. The percentage of cytotoxicity (IC_{50}) alongside the selectivity index was then calculated using the formula:

$$IC_{50} = (\text{absorbance of the cell without treatment} - \text{absorbance of cells with treatment}/\text{absorbance of the cell without treatment}) \times 100$$

$$\text{Selective index (SI)} = CC_{50}\text{value for normal cells}/IC_{50}\text{for cancer cells}$$

2.7. Anti-tuberculosis assay

The H37Ra strain of *Mycobacterium tuberculosis* (ATCC 25177) purchased from the American Type Culture Collection (ATCC) was used in the anti-TB bioassay. The anti-tuberculosis assay was based on the one used by Wang et al. (2015b). INH (Isoniazid) was used as the positive control, and DMSO was used as a negative control. For the minimum inhibitory concentration (MIC) analysis, 100 μl of *Mycobacterium* suspension was prepared in a 96-well microtiter plate. A total of 10 mL of double serial dilution of various concentrations of 7 isolated compounds (from 0.08 to 20 μg/mL) alongside the positive control isoniazid (1 to 417 μg/mL) was added to the well. The anti-tubercular assay was done in triplicate to obtain the SD± mean value.

2.8. Antiviral activity

Influenza A virus strains H1N1 (ATCC, VR-1520) and H3N2 (ATCC, VR-1679) were used in the present study. The antiviral activities against H1N1 and H3N2 were evaluated by the CPE inhibition assay based on the methodology (Fang et al., 2014). The IC_{50} was determined by the concentration required to inhibit the influenza virus yield at 48 h post-infection by 50%. The antiviral assay was conducted in triplicate to obtain the SD± mean value.

2.9. Antimicrobial assay

The antimicrobial activities against *Staphylococcus aureus* (CGMCC 1.230) and *Escherichia coli* (CGMCC 1.2385) were evaluated by an agar dilution method based on the study by Wang et al. (2014). Microbial strains used in the present study were procured from the China General Microbiological Culture Collection Center (CGMCC). The isolated compounds were dissolved in dimethyl sulfoxide (DMSO) and added to a 96-well plate in a concentration ranging from 0.3 to 50 μg/mL. Then, malto broth liquid medium with grown bacterial suspension was added to each well, and the cell density was adjusted to ~106 cfu/mL. The plates were kept in the incubator at 37°C for 24 h. The minimum inhibitory concentrations (MIC) were denoted at least at a concentration where no microbial growth could be observed. Ciprofloxacin was used as a positive control, and DMSO was used as a negative control. The antimicrobial assay was done in triplicate to obtain the SD± mean value.

2.10. Data analysis

Each experimental data obtained after triplicate assays were computed as a standard error deviation. A p-value of ≤ 0.05 was calculated as statistically significant using a one-way ANOVA. The analysis was performed using SPSS statistical package version 19.0.

2.11. Molecular docking

Computational docking studies based on the structure-activity relationship obtain a better understanding of drug-target interactions. Based on the biological screening test compound (1), averufin was docked with four major cancer antigens of HL60 cell lines, namely, human serum transferrin, CD-5 antigen, CD-20, and alpha-beta tubulin from zinc-induced sheet based upon the methodology derived by Notarte et al. (2023). The antigenic drug targets were selected based on the previous literature survey and prominent antigens that are over-expressed on myeloid leukemia cancer cells (Taetle et al., 1985; Launder et al., 1996; Shariftabrizi et al., 2012; Lagorce et al., 2015). Taxol was used as a standard reference drug. Three dimensional (3D) structures of those target proteins human serum transferrin (1A8E), CD-5 antigen (2JOP), CD-20 (3BKY) antigen, and the refined structure of alpha-beta tubulin from zinc-induced sheets (1JFF), stabilized with taxol (PDB ID: 1A8E, 2JOP, 3BKY, and 1JFF, respectively) were retrieved from the protein data bank (PDB). The chemical structures of the natural inhibitors (taxol), as well as the averufin (1), were generated from SMILES notation (Simplified Molecular Input Line Entry Specification) using the Chemsketch Software.

2.12. Protein-ligand docking

For docking analysis, Argus Lab 4.0.1 software was used, followed in accordance to the methodology described by Duverna et al. (2010). The active sites on the target proteins were obtained from RCSB ligand explorer software. The proteins and ligands were geometrically optimized, and hydrogen bonds were added. The genetic algorithm (GA) was used as the docking engine, and the grid resolution was set to 0.40 A^o. The calculation type was set to "Dock" mode, whereas "flexible mode" was selected for the ligand. The lowest energy represented the easy binding character of ligands and receptors. Molecular interactions between ligands and target proteins were visualized using Discovery Studio (Ver 3.1) software.

2.13. *In-silico* pharmacokinetic ADME predictions

The pharmacokinetic properties of compound (1) averufin were predicted by using the Swiss ADME software (Swiss Institute of Bioinformatics, 2019) based on the methodology derived by

Quimque et al. (2021a). Pharmacokinetic ADME predictions were evaluated as Lipinski's "rule of five," which includes the basic molecular weight, hydrogen bond acceptors and donors, and lipophilicity properties of the drug. The boiled egg prediction for compound (1) averufin was also assessed to check the water solubility. Apart from that, the OSIRIS property explorer program (Thomas Sander, Idorsia Pharmaceuticals Ltd., 2017) was employed for assessing the *in-silico* toxicity prediction to evaluate the mutagenicity, tumorigenicity, irritant effects, and reproductive toxicity efficacy of compound (1), i.e., averufin (de Leon et al., 2021; Quimque et al., 2021b; Brogi et al., 2022).

2.14. Molecular dynamic study

A molecular dynamic (MD) analysis was performed using Schrödinger maestro based on the methodology of Wu et al. (2018). Targets and ligands with maximum binding energy and clinical relevance based on docking results were selected and subjected to molecular dynamic drug target binding efficacy. Here, the target human serum transferrin (1A8E) protein was selected to dock with compound (1) averufin based on the good docking score. As a prerequisite for the dynamic studies, the parameters were fixed as the tetrahedron water box with water molecules were used to soak, and the edge of the box was 1 nm. Then, the surface charges of complexes were neutralized by adding 30 Na^+ and 10 Cl^-. The energy minimization was conducted and equilibrated by NVT at 300 K and 1 bar for 100 ns and then subjected to a molecular dynamics study using an NPT ensemble. A molecular dynamic (MD) prediction of drug and target was performed at 100 nanoseconds (ns) to assess the bonding stability and displacement of ligand with that of the target.

3. Results

3.1. Identification of fungi

Two-week-old fungal colonies reached a diameter of 2–3 cm wide. The colonies appeared pale green by visual observations. Under confocal microscopy (Leica Microsystems, Mannheim, Germany), the fungal hyphae stained with lactophenol blue appears to be slender with dispersed conidiophores (Figure 1). The fungal strain XWSO1F60 was identified as *P. verruculosum* based upon the sequence obtained from the internal transcribed spacer (ITS) regions (Genbank accession number: KU891245), and it has 99% similarity with that of *P.verruculosum* strain C2-8 (JQ717338) (Figure 2).

3.2. Metabolite isolation

The organic extract of *P.verruculosum* strain XWSO1F60 yielded seven different metabolites, which comprise polyketides, xanthones, and alkaloid derivatives. Structural determinations were carried out manually and referred to previously published NMR spectral data for their consistency (Figure 3).

3.2.1. Averufin (1)

Amorphous powder with orange-red color: ^{1}H-NMR (500MHz, DMSO): δH: 1.52(3H, s, H-6′), 1.62(2H, m, H-4′), 1.72 - 2.01(2H, m, H-3′), 1.82 - 1.99 (2H, m, H-2′), 5.28(1H, d, J = 2 0.5 Hz, H-1′), 6.58(1H, d, J= 2.6 Hz, H-7),7.03(1H, s, H-4), 7.11 (1H, d, J= 2.6 Hz, H-5), 12.109(1H, s, OH-8), 12.54(1H, br s, OH-1); ^{13}C-NMR (125 MHz, DMSO): δC: 15.2 (C-4′), 26.8 (C-3′), 27.3 (C-6′), 35.1 (C-2′), 66.1(C-1′), 101.1 (C-5′), 107.1 (C-4), 108.0 (C-7), 108.4 (C-9a), 108.6 (C-8a), 108.9 (C-5), 115.9 (C-2), 133.1 (C-10a), 134.9 (C-4a), 158.1 (C-3), 159.8 (C-8), 164.2 (C-1),165.2 (C-6), 180.9 (C- 10), and 188.8 (C-9) (Hong et al., 2007).

3.2.2. Aspergilol – A (2)

Amorphous Red powder: ^{1}H-NMR (500MHz, DMSO): δH: 0.83 (3H, t, J = 6.0Hz, H3-16), 1.22 (1H, m, H-13), 1.26 (2H, m, H-15), 1.26 (2H, m, H-14), 1.40 (1H, m, H-13), 1.75 (1H, m, H-12), 1.87 (3H, s, H-7″), 2.39 (3H, s, H-7′), 2.56 (1H, m, H-12), 4.40 (1H, t, J = 8.0Hz, H-11), 5.66 (1H, br s, H-4″), 5.68 (1H, br s, H-2″), 5.85 (1H, br s, H-6″), 5.96 (1H, d, J = 1.5Hz, H-4′), 6.37 (1H, d, J =2.2 Hz, H-2′), 6.54 (1H, d, J = 2.2 Hz, H-2), 6.98 (1H, s, H-5), 7.03 (1H, d, J = 2.3 Hz, H-4), 8.98 (s,-OH-5″), 9.14 (br s, - OH-5′), 10.87 (s, OH-3), 11.20 (br s, OH-6), 12.20 (s, OH-1),12.87 (s, OH-8); ^{13}C-NMR (125 MHz, DMSO): δC: 14.4 (C-16), 20.7 (C-7′), 21.2 (C-7″), 22.6 (C-15), 28.8 (C-13), 32.1 (C-14), 33.1 (C-12), 37.3 (C-11), 101.5 (C-4″), 105.8 (C-4′), 108.3 (C-2), 108.5 (C-5), 108.5 (C-8a), 108.7 (C-4), 108.8 (C-2″), 109.2 (C-1a), 109.6 (C-6″), 113.7 (C-2′), 122.9 (C-7), 126.4 (C-6′), 131.8 (C-5a), 135.2 (C-4a), 139.1 (C-1″), 139.7 (C-1′), 155.1 (C-5′), 155.9 (C-3′), 158.2 (C-3″), 158.8 (C- 5″), 164.1 (C-3), 164.2 (C-6), 164.4 (C-8), 165.1 (C-1), 181.6 (C-9), and 189.2 (C-10) (Wu et al., 2016).

3.2.3. Sulochrin (3)

Yellow color: ^{1}H NMR (500MHz, DMSO): δH: 2.31 (3H, s, CH_3-7′), 3.64 (3H, s, OCH_3-3), 3.65 (3H, s, $COOCH_3$), 6.09 (1H, s, H-5′ and 3′), 6.68 (1H, d, J = 2.5, H-4), 6.91 (1H, d, J = 2.5, H-6), 10.02 (1H, s, OH-5), 12.48 (1H, s, OH-2′); ^{13}C NMR (125 MHz, DMSO): δC: 21.5 (C-7′), 52.1 (C-9′), 55.9 (OCH_3, C-7), 103.3 (C-4), 107.1(C-6), 107.5 (C-5′ and3′), 109.1 (C-1′), 126.1 (C-2), 127.8 (C-1), 143.3 (C-4′), 156.7 (C-3), 158.1 (C-5), 161.6 (C-6′ and 2′), 165.6 (C-7), and 199.6 (C-8′) (Huang et al., 1996).

3.2.4. Monomethyl sulochrin (4)

Colorless powder: ^{1}H NMR (500MHz, DMSO): δH: 2.25 (3H, s, CH_3-7′), 3.33 (3H, s, OCH_3-9′), 3.62 (3H, s, OCH_3-7), 3.63 (3H, s, OCH3-8), 6.26 (1H, s, H-5′), 6.38 (1H, s, H-3′), 6.69 (1H, d, J = 1.5, H-4),6.90 (1H, d, J = 1.5, H-6), 10.19 (1H, s, OH-5), 12.95 (1H, s, OH-2′); ^{13}C NMR (125 MHz, DMSO): δC: 21.9 (C-7′), 52.1 (OCH_3-7), 55.9 (OCH_3, C-9′),55.9 (OCH_3-8), 103.1 (C-4),103.5 (C-5′), 107.1 (C-6), 110.1 (C-1′ and 3′), 125.8 (C-2), 127.9 (C-1), 147.8 (C-4′), 156.6 (C-3), 158.1 (C-5), 160.7 (C-6′),163.2 (C-6′),165.7 (C-7), and 199.3(C-8′) (Silva-Silva et al., 2022).

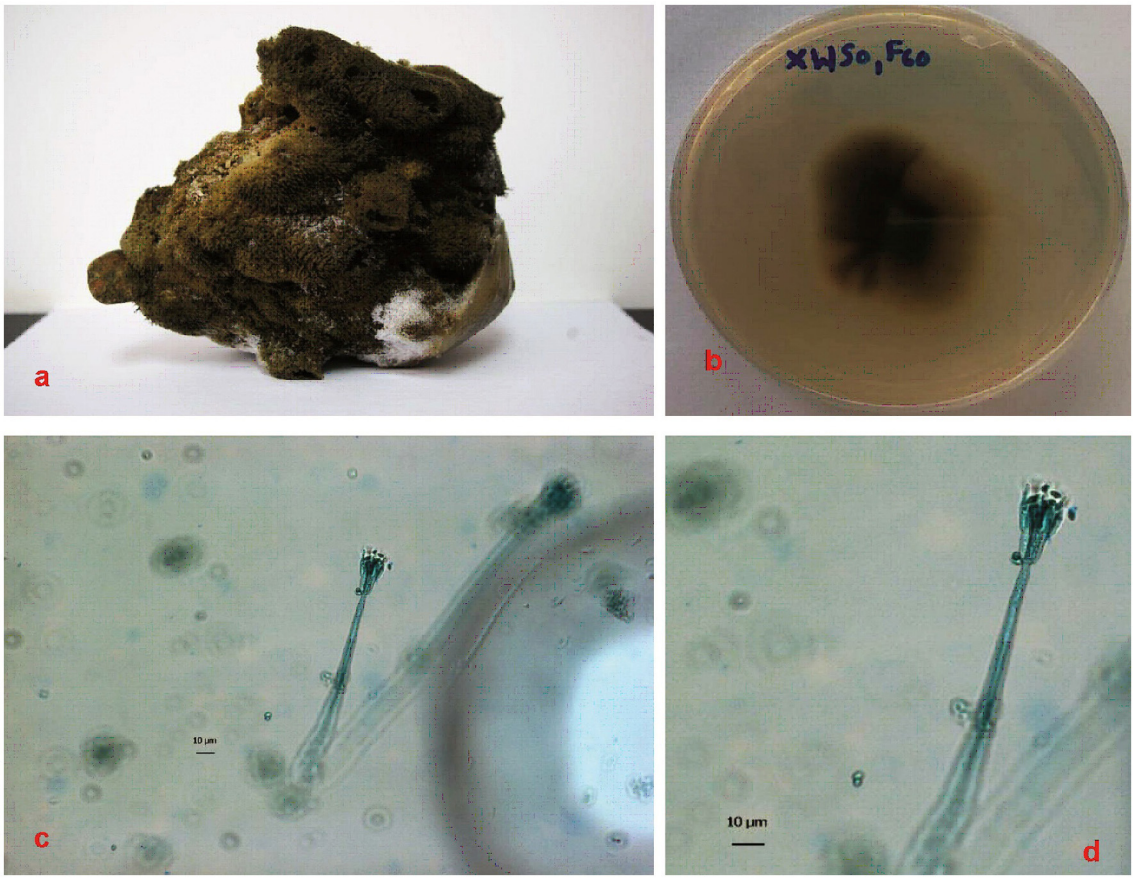

FIGURE 1
Sponge specimen and fungal colonies. **(a)**: Sponge specimen *S. officinalis*. **(b)**: Fungal colony of *P.verruculosum* (XWSO1 F60) in the MB agar plate. **(c, d)**: Hypha of the fungal colony after 2 weeks under confocal microscopy imaging. Bars in both c and d represent 10 µm.

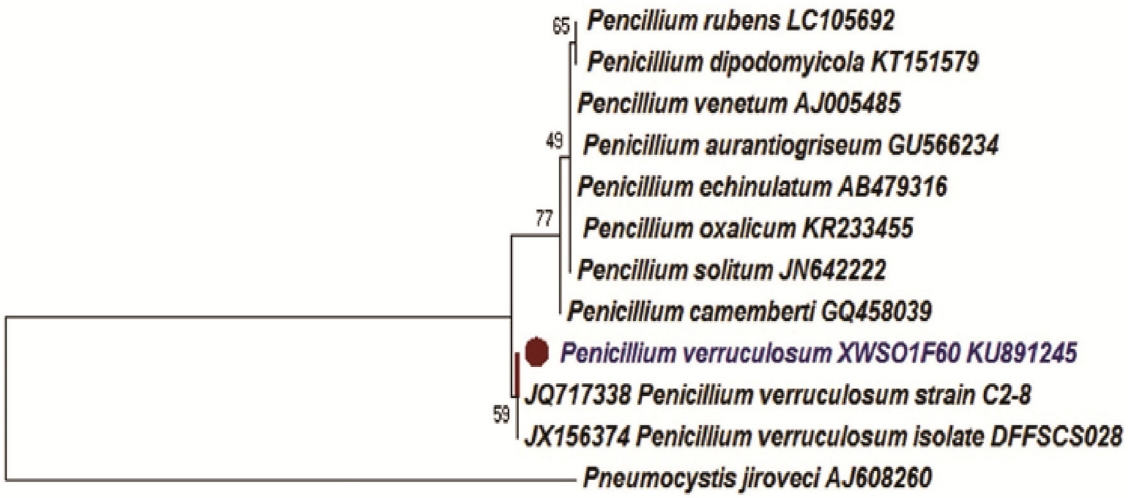

FIGURE 2
Phylogenetic Neighbor-Joining (NJ) tree inferred from ITS rDNA sequences. Bar represents 0.1 substitutions per site.

10.3389/fmicb.2023.1216928

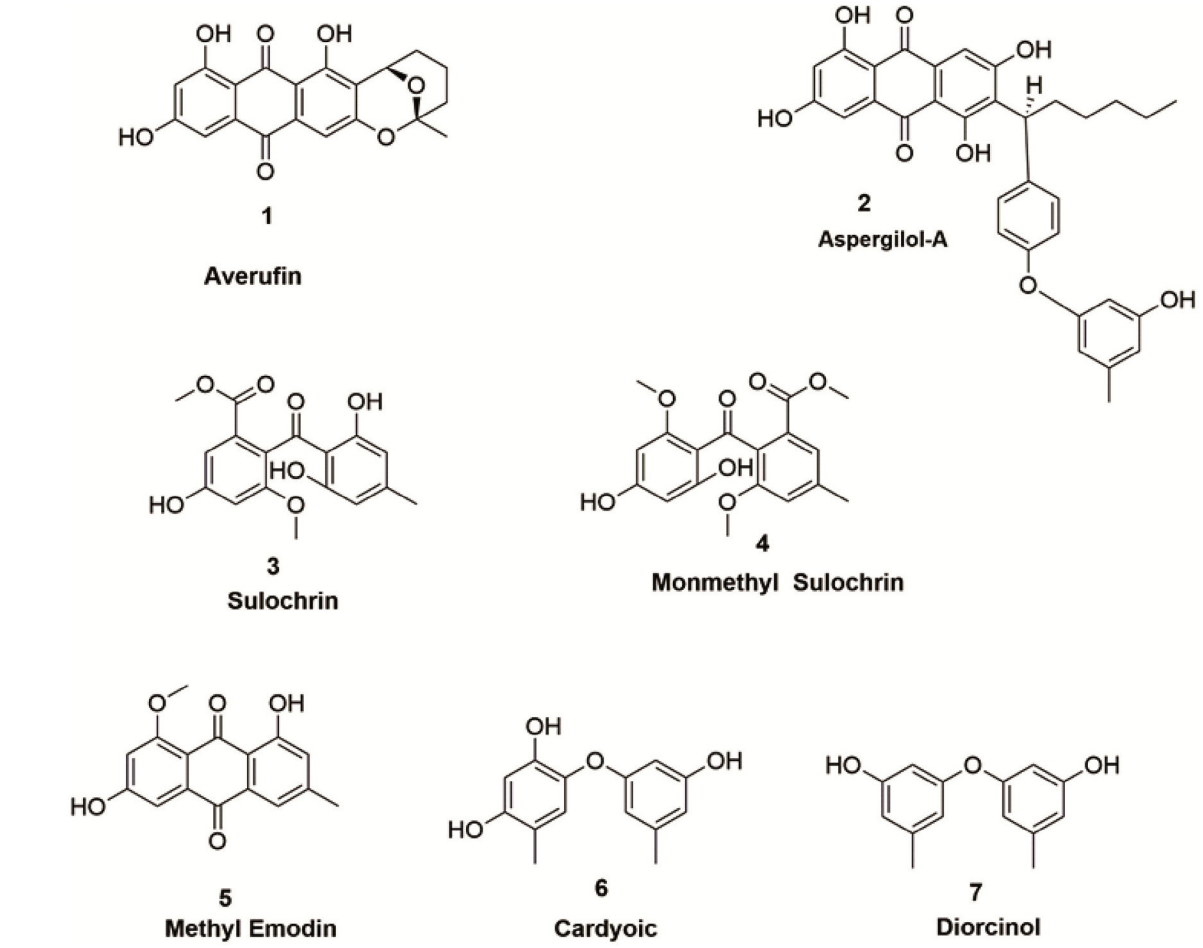

FIGURE 3
Metabolites isolated from *P.verruculosum* fungi.

TABLE 1 Anticancer activity of compounds from *P. verruculosum*.

Cpd	K562	A549	DU145	H1975	MCF-7	Huh-7	HL7702	HL60	HeLa	MOLT-4	MCF-10A
1	17.4 ± 0.01	76.1± 0.01	91.2± 0.01	8.64± 0.01	6.71± 0.01	3.13± 0.01	3.57± 0.01	1.005± 0.01*	8.11± 0.01	5.77± 0.01	≥50
5	16.3 ± 0.01	81.3± 0.01	101.4± 0.01	43.5± 0.01	54.3± 0.01	25.1± 0.01	67.2± 0.01	13.2± 0.01	24.9± 0.01	13.6± 0.01	≥50
Taxol	0.003 ± 0.01	0.024± 0.01	0.015± 0.01	0.014± 0.01	0.002± 0.01*	0.003± 0.01	0.003± 0.01	0.002± 0.01*	0.003± 0.01	0.003± 0.01	≥50
SI	1.22	1.87	3.11	1.24	1.78	2.47	3.89	13.47	3.24	2.47	69.41

Data are computed as standard deviation mean ± SD, n = 3, SI (selective index), ∗p ≤ 0.05 (one-way ANOVA).

3.2.5. Methyl emodin (5)

Orange powder: ^{1}H NMR (500MHz, DMSO):δH: 2.38 (3H, s, H3-3), 3.86 (3H, s, OCH_3-1), 6.68 (1H, br s, H-7), 7.08 (1H, s, H-2), 7.10 (1H, s, H-5), 7.39 (1H, s, H-4), 13.58 (1H, s, OH-8); ^{13}C NMR (125 MHz, DMSO): δC: 21.3 (3-CH_3), 56.9 (1-OCH_3), 105.1 (C-7), 108.7 (C-5), 110.6 (C-8a), 114.5 (C-9a), 118.7 (C-4), 123.9 (C-2), 132.1 (C- 10a), 136.6 (C-4a), 145.9 (C-3), 161.6 (C-6), 163.7 (C-1), 167.8 (C-8), 182.8 (C-10), and 185.3 (C-9) (Qian et al., 2011).

3.2.6. Citreorosein (6)

Yellow amorphous solid: ^{1}H NMR (500MHz, DMSO):δH: 4.60 (2H, br s, H-6),6.59 (1H, d, J = 2.0, H-2),7.12 (1H, d, J = 2.0, H-4), 7.24 (1H, s, H-7), 7.63 (1H, s, H-5), 12.06 (1H, d, J = 14, OH-1); ^{13}C NMR (125 MHz, DMSO): δC: 61.9 (CH_2OH),107.9 (C-2),108.9 (C-4), 108.9 (C-8a), 114.1 (C-9a), 117.0 (C-7),120.7 (C-5), 132.9 (C-4a), 135.1 (C-10a),152.8 (C-6), 161.5 (C-3), 164.3 (C-8), 165.5 (C-1), 181.3 (C-10), and 189.6 (C-9) (Ren et al., 2006).

10.3389/fmicb.2023.1216928

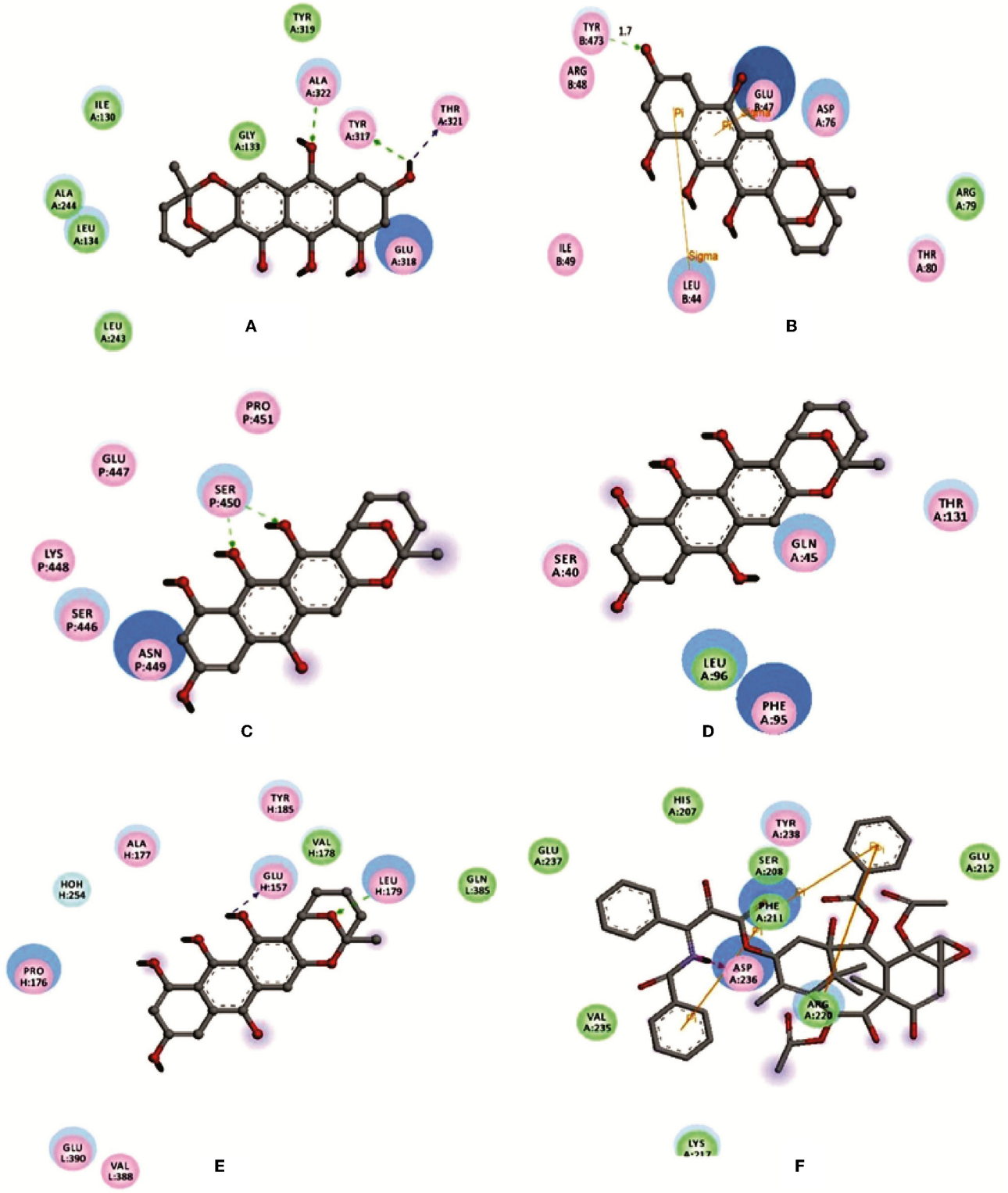

FIGURE 4
Depicting the molecular visualization of protein-ligand interactions. The interactions were visualized in Discovery Studio software. **(A)**: 1A8E and averufin. **(B)**: 1JFF and averufin. **(C)**: 2JOP and averufin. **(D)**: 3BKY_chain-H and averufin. **(E)**: 3BKY_chain-P and averufin. **(F)**: 1A8E and taxol. The dashed arrow shows the hydrogen bond.

TABLE 2 Molecular docking score against the target proteins.

Compound	1A8E (Kcal/mol)	2JOP (Kcal/mol)	3BKY (Chain P) (Kcal/mol)	3BKY (Chain H) (Kcal/mol)	1JFF (Kcal/mol)
Averufin	−9.0467	−8.28216	−6.2627	−7.69887	−10.2202
Taxol	−8.4532	−8.30715	−2.51873	−7.30745	−8.93775

TABLE 3 Lipinski rule-ADME validation for the compound averufin.

Compound	Molecular weight (g/mol)	Lipophilicity (MLogP)	H-bond donors	H-bond acceptors	Rule violations	Drug-likeness	Status
Averufin	368.34	2.98	3	7	1	Yes	Accepted

TABLE 4 Osiris pharmacokinetic rule for the compound averufin.

Compound	Mutagenic	Tumorigenic	Irritant	Reproductive toxicity	Drug Score	Status
Averufin	No	No	Slightly	No	0.15	Accepted

3.2.7. Diorcinol (7)

Brown oil: ^{1}H NMR (500MHz, CD3OD):δH: 2.23 (6H, s, H3-7 and 7′), 6.23 (2H, br s, H2-2 and 2′), 6.29 (2H, br s, H2-4 and 4′), 6.39 (2H, br s, H2-6, and 6′); ^{13}C NMR (125 MHz, CD3OD): δC: 21.5 (CH_3-5), 104.2 (C-2,), 111.7 (C-4 and C-6), 112.1 (C-4′and C-6′), 141.6 (C-5), 159.5 (C-1 and C-3), and 159.5 (C-1′,and C-3′) (Zhang et al., 2014).

3.3. Biological screening

3.3.1. Anticancer assay

Anticancer screening for all the seven compounds assessed using *in-vitro* methods revealed that compounds averufin (1) and methyl emodin (5) exhibit a significant anticancer effect against cancer cell lines compared to the others. Compound (1) shows strong anticancer activity toward HL60 cells with an IC_{50} value of 1.005 μM concentration, and compound (5) shows moderate activity (Table 1). The rest of the compounds did not show any positive anticancer effects (data not shown due to any efficient activity).

3.3.2. Antimicrobial, antiviral, and anti-tubercular assays

None of the tested compounds was recorded with any positive antimicrobial, anti-tuberculosis, or antiviral activity in the screening, except for anti-tuberculosis INH (Isoniazid), with a MIC value of 3.98μM, which was recorded. For antiviral, Tamiflu was used as the positive control with IC_{50} values of 15.2 and 17.6nM, respectively, and for antimicrobial, ciprofloxacin was used as the positive control for *S. aureus* and *E. coli* with MIC values of 2.96 and 0.19μM, respectively.

3.3.3. Molecular docking

Averufin (1) showed a better docking score when compared to the standard drug Taxol against all the target proteins, as evidenced by the protein-ligand interaction (Figure 4 and Table 2). The interacting amino acids present in the binding site and the hydrogen bonds are shown in Figure 4. The docking score ranged from −6.2627 to −10.2202 Kcal/mol. The best docking score of −9.0467 was observed against the 1A8E ligand, which corresponds to human transferring protein and is highly significant when compared to that of the Taxol drug. Since the protein 1JFF alpha-beta tubulin exerted a higher binding score of −10.2202 Kcal/mol, which was also significantly higher than the standard Taxol (−8.93775 Kcal/mol), the binding energy with 1A8E is very prominent. Similarly, averufin (1) showed quite a better docking hit against other target proteins. The docking study substantiates the *in-vitro* results.

3.3.4. *In-silico* pharmacokinetic ADME predictions

Pharmacokinetic ADME predictions of averufin revealed considerable results for plausible drug properties. As per Lipinski's rule of five compound averufin has three hydrogen bond donors and seven hydrogen bond acceptors. The molecular weight, log P-value, and molar refractivity are within the acceptable limit of 368.34 g/mol, 2.98, and 93.40, respectively (Table 3). The Osiris pharmacokinetic analysis (Table 4) revealed that compound (1) averufin has no mutagenic, tumorigenic, and reproductive toxicity, which strongly support the consideration of this compound for future pharmacological screening for *in-vivo* experiments as this compound has a good drug score. The boiled egg simulation shows that the compound averufin (1) is hydrophilic, which is a good hallmark of its palatability in gastrointestinal digestion (Figure 5). Above all, the oral bioavailability of averufin is marked as well,

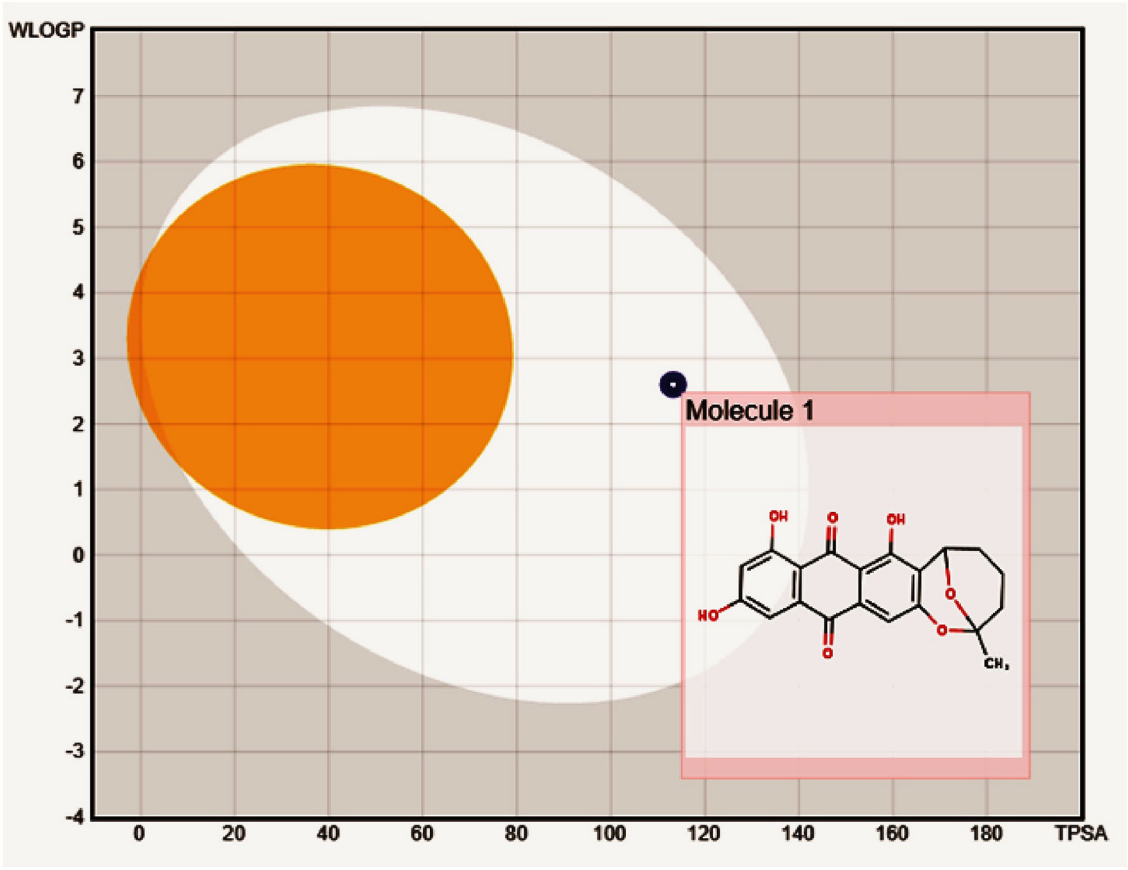

FIGURE 5
Boiled egg model to depict the gastrointestinal and blood-brain barrier solubility nature of compound averufin.

both by Veber's and Egan's rules. This analysis revealed that all the pharmacokinetic parameters of averufin are within the permissible range for human use, which strongly suggests that averufin could be a potential drug-like molecule.

3.3.5. Molecular dynamics study

Molecular dynamic results revealed the ligand-protein interaction stability over time. The root means square deviation (RMSD) analysis report states that the compound (1) averufin binds with the target protein (1A8E). At the arrival time of simulation, it displayed a steady state of around 0.15 ns to the completion until 100 ns, which is a hallmark for good drug target interaction stability without drug binding displacement from the 1A8E protein target domain (Figure 6A). The root means square fluctuation (RMSF) prediction for human transferrin protein (1A8E) flexibility is depicted in Figure 6B; it reveals that peaks indicate areas of the protein that fluctuate the most during the simulation. Typically, the protein tails (N- and C-terminal) fluctuate more than any other part of the protein. Secondary structure elements, such as alpha helices and beta strands, are usually more rigid than the unstructured part of the proteins and thus fluctuate less than the loop regions. Protein residues that interact with the ligand are marked with green-colored vertical bars, showing that the ligand interacts with protein maximum at 130–145 ns time scale (Figure 6C). The protein-ligand interaction studies show that the maximum interaction of ligand averufin of 71% takes place through its –OH functional groups that binds the target proteins with asparagine and glutamine amino acids, which was further confirmed from Figure 4.

4. Discussion

Marine-derived natural products have seemingly attracted the interest of pharmacologists worldwide in recent years. Sponge-derived fungi account for the majority of the novel compounds (28%) reported from marine isolates of fungi (Hong et al., 2007; Hawas and El-Beih, 2012). Secondary metabolites derived from fungi are widely categorized as flavonoids, quinones, alkaloids, terpenoids, polyketides, isocoumarin derivatives, steroids, phenolic acids, and peptides with intriguing bioactive properties (Hajjaj et al., 2000; Ouyang, 2006; Zhang et al., 2009; Tian et al., 2015a,b). In the present study, seven different metabolites were isolated from the sponge-derived fungi *P.verruculosum* strain. Compounds (1-7) are of polyketide, quinone, and phenone derivatives. All seven isolated compounds were subjected to different biological assays, which include anticancer, antimicrobial, antiviral, and anti-tuberculosis screening. Compound (1) averufin exerts strong anticancer activity

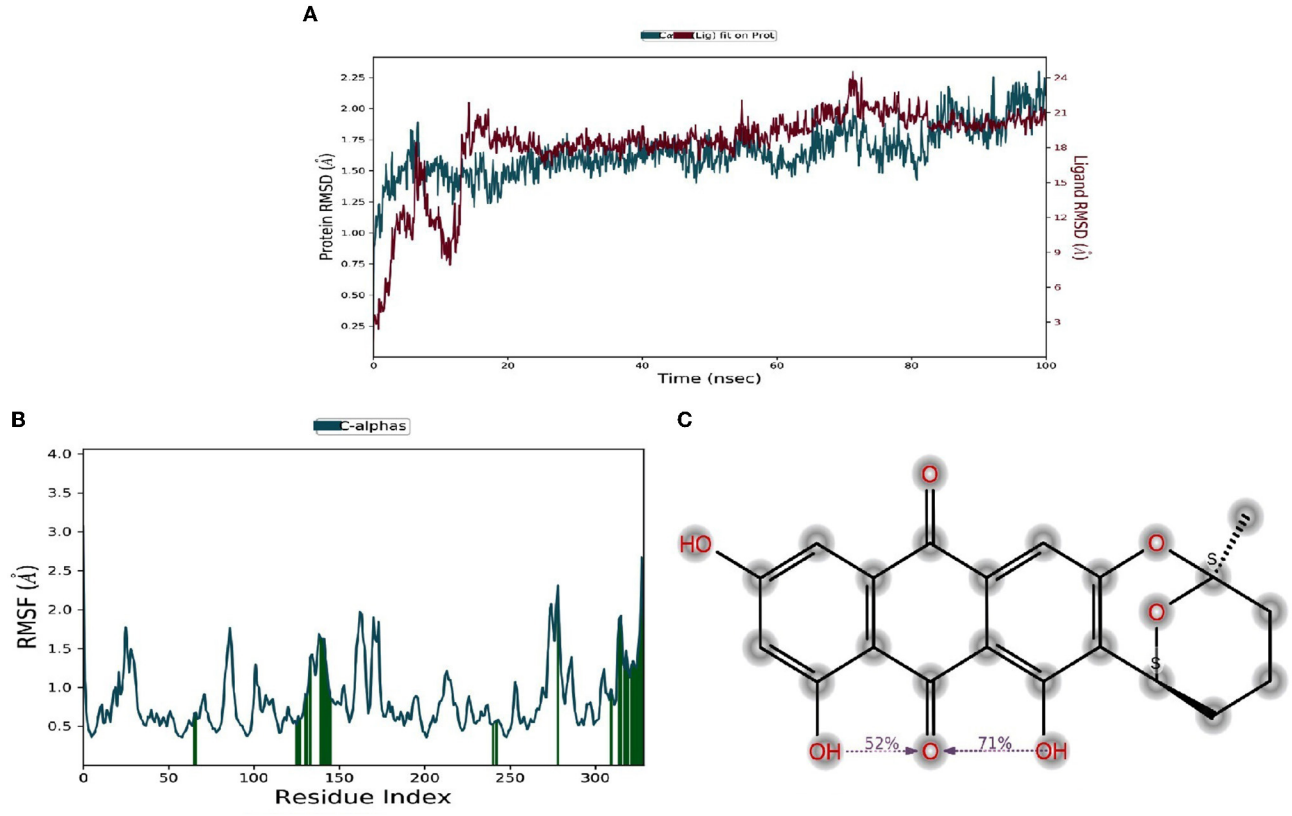

FIGURE 6
(A–C) Molecular dynamic studies of compound Averufin with HL-60 antigen 1A8E.

against HL60 (Human leukemic cell lines), with a strong IC_{50} value of 1.005µm concentration prominent at that of standard drug taxol. Reports have suggested that Averufin isolated from a marine-derived *Penicillium flavidorsum* SHK1-27 exerted a weak antitumor activity toward K562 cell lines with MIC values of 72.4 µmol/L (Hong et al., 2007). Compound (5), methyl emodin, exerts a weak anticancer effect against the tested cell lines. In a previous study, methyl-emodin tended to exert a moderate anticancer effect against the SGC-7901 cell line (Yang et al., 2009). Most of the compounds isolated herein have been reported from the *P.verruculosum* strain for the first time. Compound (2), a recently reported new compound from *Aspergillus versicolor* (Wu et al., 2016), is an interesting incidence and a first-time report from the *P.verruculosum* strain.

Molecular docking is a virtual technology that allows analyzing the precise drug-target interactions at the molecular level. With the advent of molecular docking studies, drug discovery and development have become convenient, especially for certain viral diseases like COVID-19 and Severe Acute Respiratory Syndrome (SARS) (Quimque et al., 2023). A plant-derived phenolic compound named Kobophenol-A binds with Spike protein receptors of both SARS-CoV-2 effectively, which were screened through virtual docking simulations, revealing that many natural products can be a potential drug target for many viral diseases (Gangadevi et al., 2021). Since compound (1) averufin exerts a strong anticancer effect on the HL60 cell line, the antigenic targets of HL60 cell lines 1AE, 1JFF, 2JOP, and 3BKY were docked with averufin and the standard drug taxol. ADME-Tox prediction helps assess the drug and non-drug properties with a high probability of success or failure based on the drug mimickers for a molecule. Averufin was recorded with good binding energy, and its pharmacokinetic ADME pharmacokinetic analysis of averufin revealed that it is oral bioavailability and drug score based on OSIRIS and Lipinski rule, which are good indicators of drug validation in prospect. *P.verruculosum,* an endophytic fungus, has been reported to produce intriguing secondary metabolites and polyketide compounds with prominent anticancer activity. Monascorubrine and monascin are the groups of polyketide compounds from *P. verruculosum* that show considerable cytotoxic activity toward KA3IT cancer cells (Shah et al., 2014). The dynamic molecular study of compound (1) averufin with target protein 1A8E confirms that the drug-target interaction is good without any displacement up to 100 ns. A previous study on sulfonamide-benzoxazoles, a synthetic chemical drug was docked with HL-60 antigens, revealed that the drug showed the same interaction with minimal saturation (Oksuzoglu et al., 2017). Understanding how polyketide structural variation is generated is key to identifying new products encoded in the vast number of emerging sequenced microbial genomes and developing new bioactive polyketides through rational pathways or enzyme engineering (Crawford et al., 2010). The results indicate that averufin, an aromatic polyketide, is a potent tumor inhibitor against HL60, a human myeloid leukemia

cell line, and it can be beneficial in the therapy of leukemic treatment in the future. The present study also highlights that sponge endophyte *P. verruculosum* is a promising source of natural bioactive compounds.

5. Conclusions

In this study, we have evaluated the different metabolites isolated from sponge-derived fungi *P.verruculosum*. All of its structural characterization by NMR spectral studies speculate the chemical diversity of the fungus. Experimental results have shown the biomedical importance of isolated metabolites. Some of the isolated compounds have been reported from this fungus for the first time. The *in-vitro* and *in-silico* experimental findings of the compound averufin as a potent anticancer agent against leukemic HL-60 cell lines and its target antigens would also be helpful for researchers to conduct further *in-vitro* and *in-vivo* experimental studies for future applications.

Data availability statement

The datasets presented in this study can be found in online repositories. The names of the repository/repositories and accession number(s) can be found in the article/Supplementary material.

Author contributions

KK and LS equally contributed to the experimental work. YL and RK performed experimental supervision. SS and ZJ performed molecular docking studies, molecular dynamics, and data interpretations. SE and KS conducted manuscript drafting and reviewing. NMA, NA, and MS performed data interpretation. All authors reviewed and approved the final version of the manuscript.

Funding

The authors express their gratitude to the Princess Nourah bint Abdulrahman University Researchers Supporting Project number (PNURSP2023R356), Princess Nourah bint Abdulrahman University, Riyadh, Saudi Arabia.

Conflict of interest

The authors declare that the research was conducted in the absence of any commercial or financial relationships that could be construed as a potential conflict of interest.

Publisher's note

All claims expressed in this article are solely those of the authors and do not necessarily represent those of their affiliated organizations, or those of the publisher, the editors and the reviewers. Any product that may be evaluated in this article, or claim that may be made by its manufacturer, is not guaranteed or endorsed by the publisher.

Supplementary material

The Supplementary Material for this article can be found online at: https://www.frontiersin.org/articles/10.3389/fmicb.2023.1216928/full#supplementary-material

References

Brogi, S., Quimque, M. T., Notarte, K. I., Africa, J. G., Hernandez, J. B., Tan, S. M., et al. (2022). Virtual combinatorial library screening of quinadoline b derivatives against SARS-CoV-2 RNA-dependent RNA polymerase. *Computation*. 10, 7. doi: 10.3390/computation10010007

Bugni, T. S., and Ireland, C. M. (2004). Marine-derived fungi: a chemically and biologically diverse group of microorganisms. *Nat.Prod. Rep*. 21, 143–163. doi: 10.1039/b301926h

Crawford, J. M. Townsend, C.A. (2010). New insights into the formation of fungal aromatic polyketides. *Nat. Rev. Microbio*. 8, 879–889. doi: 10.1038/nrmicro2465

de Leon, V. N. O., Manzano, J. A. H., Pilapil, D. Y. H., Fernandez, R. A. T., Ching, J. K. A. R., Quimque, M. T. J. (2021). Anti-HIV reverse transcriptase plant polyphenolic natural products with in-silico inhibitory properties on seven non-structural proteins vital in SARS-CoV-2 pathogenesis. *J. Genet. Eng. Biotechnol*. 19, 104. doi: 10.1186/s43141-021-00206-2

Duverna, R., Ablordeppey, S. Y., and Lamango, N. S. (2010). Biochemical and docking analysis of substrate interactions with poly isoprenylated methylated protein methyl esterase. *Curr. Cancer. Drug. Target*. 10, 634–648. doi: 10.2174/156800910791859443

Fang, W., Lin, X. P., Zhou, X. F., Wan, J. T., Lu, X., Yang, B., et al. (2014). Cytotoxic and antiviral nitrobenzoyl sesquiterpenoids from the marine-derived fungus *Aspergillus ochraceus* Jcma1f17. *Med. Chem. Comm*. 5, 701–705. doi: 10.1039/C3MD00371J

Gangadevi, S., Badavath, V. N., Thakur, A., Yin, N., Jonghe, D. e., Acevedo, S., et al. G. (2021). Kobophenol A inhibits binding of host ACE2 receptor with spike RBD domain of SARS-CoV-2, a lead compound for blocking COVID-19. *The Journal of physical chemistry letters*. 12, 1793–1802. doi: 10.1021/acs.jpclett.0c03119

Hajjaj, H., Blanc, P., Groussac, E., Uribelarrea, J. L., Goma, G., Loubiere, P., et al. (2000). Kinetic analysis of red pigment and citrinin by *Monascus rubber* as a function of organic acid accumulation. *Enz. Microb. Tech*. 27, 619–625. doi: 10.1016/S0141-0229(00)00260-X

Hawas, U. W., and El-Beih, A. A. El- Halawany. (2012). Bioactive anthraquinones from endophytic fungus *Aspergillus versicolor* isolated from red sea algae. *Arch. Pharm. Res*. 35, 1749–1756. doi: 10.1007/s12272-012-1006-x

Hong, R., Qun, Q., and Cheng, C. (2007). Anthraquinone derivatives produced by marine-derived *Penicillium flavidorsum* SHK1-27 and their antitumor activities. *Chin. J. Med. Chem*. 17, 148–154.

Huang, K., Yoshida, Y., Mikawa, K., Fujii, I., Ebizuka, Y., Sankawa, U., et al. (1996). Purification and characterization of sulochrin oxidase from *Penicillium frequentans*. *Bio. Pharm. Bull*. 19, 42–46. doi: 10.1248/bpb.19.42

Koopmans, M., Martens, D., and Wijffels, R. H. (2009). Towards commercial production of sponge medicines. *Mar.Drugs*.7, 787–802. doi: 10.3390/md7040787

Lagorce, D., Sperandio, O., Baell, J. B., Miteva, M. A., and Villoutreix, B. O. (2015). FAF-Drugs3: a web server for compound property calculation and chemical library design. *Nucleic Acids Res*. 43, 200–207. doi: 10.1093/nar/gkv353

Launder, T. M., Bray, R. A., Stempora, L., Chenggis, M. L., and Farhi, D. C. (1996). Lymphoid-associated antigen expression by acute myeloid leukemia. *Am J Clin Pathol*. 106, 185–91. doi: 10.1093/ajcp/106.2.185

Manzo, E., Ciavatta, M. L., Villani, G., Varcamonti, M., Sayem, S. A., Van Soest, R., et al. (2011). Bioactive terpenes from Spongia officinalis. *J. Nat. Products*, 74, 1241–1247. doi: 10.1021/np200226u

Mehbub, M. F., Lei, J., Franco, C., and Zhang, W. (2014). Marine sponge derived natural products between 2001 and 2010: Trends and opportunities for discovery of bioactives. *Mar. Drugs*, 12, 4539–4577. doi: 10.3390/md12084539

Notarte, K., Nakao, Y., Yaguchi, T., Bungihan, M., Suganuma, K., Delacruz, T., et al. (2017). Trypanocidal activity, cytotoxicity and histone modifications induced by malformin A1 isolated from the marine-derived fungus *Aspergillus tubingensis* IFM 63452. *Mycosphere*. 8, 111–120. doi: 10.5943/mycosphere/8/1/10

Notarte, K. I., Yaguchi, T., and Suganuma, K. (2018). Antibacterial, cytotoxic and trypanocidal activities of marine-derived fungi isolated from Philippine macroalgae and seagrasses. *Acta Bot. Croatica*, 77, 141–151. doi: 10.2478/botcro-2018-0016

Notarte, K. I. R., Quimque, M. T. J., Macaranas, I. T., Khan, A., Pastrana, A. M., Villaflores, O. B. (2023). Attenuation of lipopolysaccharide-induced inflammatory responses through inhibition of the nf-κb pathway and the increased NRF2 Level by a flavonol-enriched n-butanol fraction from *Uvaria alba. ACS Omega.,* 8, 5377–5392. doi: 10.1021/acsomega.2c06451

Oksuzoglu, E., Ertan-Bolelli, T., Can, H., Tarhan, M., and Ozturk, K. (2017). Antitumor activities on HL-60 human leukemia cell line, molecular docking, and quantum-chemical calculations of some sulfonamide-benzoxazoles. *Artif. Cells., Nanomed. Biotechnol.* 45, 1388–1396. doi: 10.1080/21691401.2016.1241796

Ouyang, M. A. (2006). A new adenosyl alkaloid from *Ostrea rivularis*. *Nat. Prod. Res*. 20, 79–83. doi: 10.1080/14786410500061207

Pawlik, J. R., McFall, G., and Zea, S. (2002). Does the odor from sponges of the genus *Ircinia* protect them from fish predators? *J. Chem. Ecol*. 28, 1103–1115. doi: 10.1023/A:1016221415028

Paz, Z., Komon, M., Zelazowska, I. S., Druzhinina, M. M., Aveskamp, A., Shnaiderman, S. A., et al. (2010). Diversity and potential antifungal properties of fungi associated with a Mediterranean sponge. *Fungal Diver*. 42, 17–26. doi: 10.1007/s13225-010-0020-x

Pecundo, M. H. dela Cruz, T. E. E., Chen, T., Notarte, K. I., Ren, H., Li, N. (2021). Diversity, phylogeny and antagonistic activity of fungal endophytes associated with endemic species of *Cycas* (cycadales) in China. *J. Fungi* 7, 572. doi: 10.3390/jof7070572

Qian, Z. J., Zhang, C., Li, Y. X., Je, J. Y., Kim, S. K., Jung, W. K., et al. (2011). Protective effects of emodin and chrysophanol isolated from marine fungus *aspergillus sp*. on ethanol-induced toxicity in HepG2/CYP2E1 cells. *Evid. Based. Compl. Alter. Med*. 452621. doi: 10.1155/2011/452621

Quimque, M. T., Notarte, K. I., Adviento, X. A., Cabunoc, M. H., Delos Reyes, V. N. (2023). Polyphenolic natural products active *in silico* against SARS-CoV-2 spike receptor binding domains and non-structural proteins - a review. *Comb. Chem. High Throughput Screen*. 26, 459–488. doi: 10.2174/1386207325666210917113207

Quimque, M. T., Notarte, K. I., Letada, A., Fernandez, R. A., and Pilapil, D. Y. 4th., Pueblos, K.R., Agbay, J.C., Dahse, H.M., Wenzel-Storjohann, A., Tasdemir, D., Khan, A., Wei, D.Q., Gose Macabeo, A.P. (2021a). Potential Cancer- and Alzheimer's Disease-Targeting Phosphodiesterase Inhibitors from *Uvaria alba*: Insights from In Vitro and Consensus Virtual Screening. *ACS Omega*. 6, 8403–8417. doi: 10.1021/acsomega.1c00137

Quimque, M. T. J., Notarte, K. I. R., Fernandez, R. A. T., Mendoza, M. A. O., Liman, R. A. D., Lim, J. A. K., et al. (2021b). Virtual screening-driven drug discovery of SARS-CoV2 enzyme inhibitors targeting viral attachment, replication, post-translational modification and host immunity evasion infection mechanisms. *J Biomol Struct Dyn*. 39, 4316–4333. doi: 10.1080/07391102.2020.1776639

Ramirez, C. S. P., and Notarte, K. I. R. (2020). Antibacterial activities of mangrove leaf endophytic fungi from Luzon Island, Philippines. *Stu. Fungi*, 5, 320–331. doi: 10.5943/sif/5/1/14

Rateb, M. E., and Ebel, E. (2011). Secondary metabolites of fungi from marine habitats. *Nat. Prod. Rep*. 28, 290–344. doi: 10.1039/c0np00061b

Ren, H., Tian, L., Gu, Q., and Zhu, W. (2006). Secalonic acid D: a cytotoxic constituent from marine lichen-derived fungus *Gliocladium* sp. T31. *Arch. Pharm. Res*. 29, 59–63. doi: 10.1007/BF02977469

Shah, S. G., Shier, W. T., Tahir, N., Hameed, A., Ahmad, S., Ali, N., et al. (2014). *Penicillium verruculosum* SG: A source of polyketide and bioactive compounds with varying cytotoxic activities against normal and cancer lines. *Arch.Microbio*. 196, 267–78. doi: 10.1007/s00203-013-0945-z

Shariftabrizi, A., Ahmadian, S., and Pazhang, Y. (2012). Dynamics of γ-tubulin cytoskeleton in HL-60 leukemia cells undergoing differentiation and apoptosis by all-trans retinoic acid. *Mol Med Rep*. 5, 545–51. doi: 10.3892/mmr.2011.635

Silva-Silva, J. V., Moreira, R. F., Watanabe, L. A., Hardoim, C. D. S. F., Taniwaki, D. J. (2022). Mono-methylsulochrin isolated from biomass extract of *Aspergillus* sp. against Leishmania amazonensis: in vitro biological evaluation and molecular docking. *Front. Cell. Inf. Microbio*. 25, 974910. doi: 10.3389/fcimb.2022.974910

Suay, F. Arenal, F.J., Asensio, A., Basilio, M.A., Cabello, M.T., Diez. (2000). Screening of basidiomycetes for antimicrobial activities. *Anton Van Leeuwen*. 78, 129–139. doi: 10.1023/A:1026552024021

Sun, J. F., Wu, Y., Bin, Y., and Liu, Y. (2015). Chemical Constituents of Marine Sponge *Halichondria sp* from South China Sea. *Chem.Nat.Comp*. 21, 975–977. doi: 10.1007/s10600-015-1467-5

Taetle, R., Rhyner, K., Castagnola, J., To, D., and Mendelsohn, J. (1985). Role of transferrin, Fe, and transferrin receptors in myeloid leukemia cell growth. Studies with an antitransferrin receptor monoclonal antibody. *J Clin Invest*. 75, 1061–7. doi: 10.1172/JCI111768

Thomas Edison, E., dela Cruz, T. E. E., Notarte, K. I. R., Apurillo, C. C. S., Tarman, K., and Bungihan, M. E. (2020). *Biomining Fungal Endophytes From Tropical Plants and Seaweeds for Drug Discovery, Biodiversity and Biomedicine*. London: Academic Press. p: 51–62.

Tian, Y., and Lin, J. Liu., Kumaravel, K., Ai, W., Ju, Z. (2015a). Ascomycotin A, a new citromycetin analogue produced by *Ascomycota sp*. Ind19F07 isolated from deep sea sediment. *Nat. Prod. Res*. 29, 820–826. doi: 10.1080/14786419.2014.988620

Tian, Y. X., Qin, X., Lin, X. P., Kumaravel, K., Zhou, X. F., Liu, J., et al. (2015b). Sydoxanthone C and acremolin B produced by deep sea derived fungus *Aspergillus sp* SCSIO Ind09F01. *J.Antibiotics*. 68, 703–706. doi: 10.1038/ja.2015.55

Unson, M. D., Holland, N. D., and Faulkner, D. J. A. (1994). Brominated secondary metabolite synthesized by the cyanobacterial symbiont of a marine sponge and accumulation of the crystalline metabolite in the sponge tissue. *Mar.Biol*. 119, 1–11. doi: 10.1007/BF00350100

Volkov, P. V., Rozhkova, A. M., Gusakov, A. V., and Sinitsyn, A. P. (2014). Homologous cloning, purification and characterization of highly active cellobiohydrolase I (Cel7A) from *Penicillium canescens*. *Prot.Expr. Purif*.103, 1–7. doi: 10.1016/j.pep.2014.08.011

Wang, J. F., Lin, X. P., Qin, C., Liao, J. T., Wan, T. Y., Zhang, J., et al. (2014). Antimicrobial and antiviral sesquiterpenoids from sponge-associated fungus, *Aspergillus sydowii* ZSDS1-F6. *J.Antibiotics*. 67, 581–583. doi: 10.1038/ja.2014.39

Wang, J. F., Wang, Z., Ju, Z. R., Wan, J. T., Liao, S. R., Lin, X. P., et al. (2015a). Cytotoxic Cytochalasins from Marine-Derived Fungus *Arthrinium arundinis*. *Planta Med*.81, 160–166. doi: 10.1055/s-0034-1383403

Wang, J. F., Wei, X. Y., Qin, X. C., Lin, X. P., Zhou, X. F., Liao, S. R., et al. (2015b). Arthpyrones A–C, Pyridone Alkaloids from a Sponge-Derived Fungus *Arthrinium arundinis* ZSDS1-F3. *Org. Letters*. 17, 656–659. doi: 10.1021/ol503646c

Wu, X. Q., Ding, H. F., Hu, X., Pan, J. H., Liao, Y. J., Gong, D. M., et al. (2018). Exploring inhibitory mechanism of gallocatechin gallate on a-amylase and a-glucosidase relevant to postprandial hyperglycemia. *J Fun Foods*, 48, 200–209. doi: 10.1016/j.jff.2018.07.022

Wu, Z., Wang, Y., Liu, D., Proksch, P., Yu, S., Lin, W., et al. (2016). Antioxidative phenolic compounds from a marine-derived fungus *Aspergillus versicolor*. *Tetrahedron*.72, 50–57. doi: 10.1016/j.tet.2015.10.038

Yang, B., Dong, J., Zhou, X., Yang, X., Lee, K. J., Wang, L., et al. (2009). Proline-containing dipeptides from a marine sponge of a *Callyspongia* species," *Helv. Chimi. Acta*. 92, 1112–1117. doi: 10.1002/hlca.200800422

Zhang, H., Liu, R., and Zhou, F. (2014). Antimicrobial Metabolites from the Endophytic Fungus *Aspergillus sp*. of *Eucommia ulmoides*. *Chem.Nat. Comp*. 50, 526–528. doi: 10.1007/s10600-014-1003-z

Zhang, Y., Mu, J., Feng, Y., Kang, Y., Zhang, J., Gu, P. J., et al. (2009). Broad-spectrum antimicrobial epiphytic and endophytic fungi from marine organisms: isolation, bioassay and taxonomy. *Mar. Drugs*. 7, 97–112. doi: 10.3390/md7020097

frontiers | Frontiers in Microbiology

TYPE Original Research
PUBLISHED 08 December 2023
DOI 10.3389/fmicb.2023.1259101

OPEN ACCESS

EDITED BY
Ajay Kumar,
Amity University, India

REVIEWED BY
Carolina Elena Girometta,
University of Pavia, Italy
Chenyang Huang,
Chinese Academy of Agricultural Sciences, China

*CORRESPONDENCE
Xiuqing Yang
✉ yangxq@qau.edu.cn

†These authors have contributed equally to this work

RECEIVED 15 July 2023
ACCEPTED 27 November 2023
PUBLISHED 08 December 2023

CITATION
Wang J, Liu M, Mao C, Li S, Zhou J, Fan Y, Guo L, Yu H and Yang X (2023) Comparative proteomics reveals the mechanism of cyclosporine production and mycelial growth in *Tolypocladium inflatum* affected by different carbon sources.
Front. Microbiol. 14:1259101.
doi: 10.3389/fmicb.2023.1259101

Comparative proteomics reveals the mechanism of cyclosporine production and mycelial growth in *Tolypocladium inflatum* affected by different carbon sources

Junqi Wang†, Meijie Liu†, Chengzhi Mao†, Sizhu Li, Jiabao Zhou, Yaqin Fan, Lizhong Guo, Hao Yu and Xiuqing Yang*

Shandong Provincial Key Laboratory of Applied Mycology, School of Life Sciences, Qingdao Agricultural University, Qingdao, Shandong Province, China

Cyclosporine A (CsA) is a secondary cyclopeptide metabolite produced by *Tolypocladium inflatum* that is widely used clinically as an immunosuppressant. CsA production and mycelial growth differed when *T. inflatum* was cultured in different carbon source media. During early fermentation, CsA was preferred to be produced in fructose medium, while the mycelium preferred to accumulate in sucrose medium. On the sixth day, the difference was most pronounced. In this study, high-throughput comparative proteomics methods were applied to analyze differences in protein expression of mycelial samples on day 6, revealing the proteins and mechanisms that positively regulate CsA production related to carbon metabolism. The differences included small molecule acid metabolism, lipid metabolism, organic catabolism, exocrine secretion, CsA substrate Bmt synthesis, and transcriptional regulation processes. The proteins involved in the regulation of mycelial growth related to carbon metabolism were also revealed and were associated with waste reoxidation processes or coenzyme metabolism, small molecule synthesis or metabolism, the stress response, genetic information or epigenetic changes, cell component assembly, cell wall integrity, membrane metabolism, vesicle transport, intramembrane localization, and the regulation of filamentous growth. This study provides a reliable reference for CsA production from high-efficiency fermentation. This study provides key information for obtaining more CsA high-yielding strains through metabolic engineering strategies.

KEYWORDS

***Tolypocladium inflatum*, carbon sources, fructose, sucrose, cyclosporine A, mycelium**

1 Introduction

The application of cyclosporine A (CsA) is another great discovery in the exploration of secondary fungal metabolites since the discovery of penicillin (Survase et al., 2011; Kjærbølling et al., 2019). CsA inhibits the mixed lymphocyte response and contrasts with other immunosuppressants and cytostatic drugs with its weak myelotoxicity (Borel et al., 1976). Thus, CsA has been widely used in bone marrow immunotherapy and organ transplantation to inhibit chronic inflammatory reactions, HIV, and hepatitis C virus (Survase et al., 2011).

CsA is a non-ribosomal peptide (NRP) secondary metabolite mainly derived from the Ascomycota fungus *Tolypocladium inflatum* W. Gams 1971 (Rossman et al., 2017). *Tolypocladium inflatum* is widely produced in the pharmaceutical industry but more efficient production methods are needed to optimize the procedure. Current research has focused on obtaining better strains using chemical mutagenesis and optimizing medium using high throughput contrast tests. *Tolypocladium* strain VCRC F21 NRRL No. 18950 produces a high level of CsA in composition-optimized fermentation media and has been exploited for industrial production (Balaraman and Mathew, 2006). Diethyl sulfate-based mutagenesis was performed on the fungal strain *Tolypocladium inflatum* MTCC-3538. Liquid chromatography-mass spectrometry (LC–MS)-based high throughput medium has been used to optimize one of the mutants in 20 different media combinations to increase the CsA yield (Abrol et al., 2022).

The carbon source provides energy for cell growth and metabolism and is a key factor affecting fungal growth and the synthesis of secondary metabolites (Li et al., 2015). It has been reported that *Fusarium proliferatum* (Matsush.) Nirenberg cultured with sucrose as the only carbon source increases the production of fumonisin but fumonisin production is inhibited when using fructose as the carbon source (Jian et al., 2019). Replacing glucose with fructose in the initial fermentation medium is more conducive to the production of pneumocandin B_0, the precursor of the antifungal drug caspofungin, and biomass accumulation (Zhang et al., 2020). Reduced growth, thinner hyphae, and visible injury were observed early during the cultivation of *Penicillium janczewskii* K.W. Zaleski in a fructose-containing medium, and the culture reached the maximum between days 12 and 15 (Pessoni et al., 2015). Some studies have attempted to replace CsA-producing strains with selected *Aspergillus terreus* Thom (FCBP58), and the CsA yield was effectively increased by optimizing the ratio of the carbon source to the nitrogen source in the medium (Tanseer and Anjum, 2011). However, few studies have analyzed how carbon sources affect the production of secondary metabolite CsA and its producing fungal mycelium growth.

Therefore, this aspect still needs further research. Some advancements in new technologies, like the various omics analyses, have become key tools to help us for these explorations and understand the molecular mechanisms that respond to changes in environmental conditions (Bi et al., 2018; Zhang et al., 2020). There are many successful studies here. The transcriptomic and proteomic analyses of the mycelium and fruiting bodies of *Cordyceps militaris* (L.) Fr. revealed differences in gene expression, including the cordycepin metabolism-related genes (Yin et al., 2012). The mechanism of the metabolic regulation and development of *Pleurotus ostreatus sensu* Stevenson fruiting bodies inhibited by a high CO_2 concentration was revealed using proteomics analysis (Lin et al., 2022). The global protein expression profile of white *Hypsizygus marmoreus* (Peck) H.E. Bigelow mycelium under heat stress has been studied using a label-free comparative proteomics technique, and the molecular mechanism of mushroom heat stress response was explained (Xu et al., 2021). Comparative proteomic analysis techniques combined with protein-to-protein interaction networks have been used to study the differences in the intracellular transcription mechanisms of carbon-de-inhibited and wild-type *Pichia pastoris* (Guillierm.) Phaff strains fed with three carbon sources. The cluster modules of the differentially expressed proteins (DEPs) associated with the carbon sources were obtained, and the co-expression relationships between the DEPs have been constructed (Shi et al., 2020; Wang et al., 2022).

In this study, fructose and sucrose were used as carbon sources during fermentation of *T. inflatum*. We determined the CsA yield between the two carbon sources and analyzed the differences in protein expression and metabolic pathways by proteomics analysis. The proteins regulating CsA synthesis related to carbon metabolism were explored. This study provides additional candidate genes or proteins for modification through metabolic engineering strategies and affords new ideas for obtaining more CsA high-yielding strains.

2 Materials and methods

2.1 Sample material

Fructose and sucrose were used as carbon sources to prepare the liquid media called fructose medium and sucrose medium. Here was the recipe: D-(−)-fructose (Shanghai Sangon Biotech Co., Ltd., EINECS number: 200–333-3)/sucrose (Shanghai Sangon Biotech Co., Ltd., EINECS number: 200–334-9) 30 g/L, $(NH_4)_2HPO_4$ 6 g/L, Yeast extract (Shanghai Sangon Biotech Co., Ltd., EINECS number: 232–387-9) 5 g/L, $CaCl_2{\cdot}2H_2O$ 1.32 g/L, $MgSO_4{\cdot}7H_2O$ 2.05 g/L, $FeSO_4{\cdot}7H_2O$ 27.4 mg/L, $ZnSO_4{\cdot}7H2O$ 17.8 mg/L, $CoCl_2{\cdot}6H_2O$ 27.5 mg/L, $CuSO_4{\cdot}5H_2O$ 3.1 mg/L, ddH_2O added to 1 L final volume. Adjusted pH to 5. The media were sterilized with moist heat at 115°C for 15 min (Yang et al., 2018).

Tolypocladium inflatum NRRL 8044 was grown on potato dextrose agar (BD Difco, Sparks, MD, United States) for 2 weeks. The impurities and mycelia were removed by filtrating through sterile degreasing cotton with a thickness of about 0.5 cm to obtain the spore suspension. The spore suspension was diluted to a final concentration of 10^8 spores/mL. A 100 μL aliquot of the diluted spore suspension was removed and inoculated into 50 mL of liquid medium/250 mL conical flask at 25°C and 150 rpm in a constant temperature oscillating incubator for 3 days. The seed suspension was obtained after the incubation. Eight mL of the seed suspension was removed and inoculated into 250 mL of liquid medium/500 mL conical flask at 25°C at 150 rpm shaking for 9 days. Three biological replicates were used for each group.

The mycelia could be weighted and collected beginning on day 4. At the same time every day, 15 mL of culture broth including the fermentation product was removed and the mycelia were collected and placed in liquid nitrogen or stored at −80°C to determine hydrogen peroxide content, CsA production, total protein, and RNA.

2.2 Determination of CsA content

The Agilent 1,100 high-performance liquid chromatograph (Agilent Technologies Inc., Shanghai, China) was used to detect CsA, with a diode array UV detector. The separation was performed using the yuexu xtimate C18 column (particle size: 5 μm; column length: 4.6 × 250 mm); the sample size was 10 μL, and the detection wavelength was 210 nm. The parameter settings were column temperature of 40°C, mobile phase: A: water, B: acetonitrile (CAN), at a flow rate of 1 mL/min. The elution

procedure was 0–28 min, 65–71.7% B; 28–34 min, and 71.7–65% B. The peak corresponding to CsA appeared at about 21 min (Yang et al., 2018).

The standard curve to determine the absolute weight of CsA was y = 2972.1 x - 286.44, R2 = 0.9985, where x is the absolute weight of CsA, unit: μg; y was the integrated peak area, and the units are mAU·s. The CsA standard was 98% pure (Aladdin).

2.3 Determination of accumulated biomass

A 5 mL aliquot of the fermentation products was thoroughly dehydrated at low temperature in a freeze-drying machine (Scientz-18 N/A, Ningbo Scientz Biotechnology Co., Ltd., Ningbo, China). The products were weighed to dryness to determine dry weight (DW).

2.4 Total protein acquisition and mass spectrometry detection

The proteome was detected using label-free LC–MS/MS Quantitative Proteomics Analysis technology (Benagen Co., Ltd., Wuhan, China). All protein extraction and digestion methods and the MS detection for total proteins were described in a previous study (Yang et al., 2021).

2.5 Protein identification and DEP screening

The total protein sequences from the raw files were screened out with a false discovery rate (FDR) < 0.05 for mapping to the *T. inflatum* genomic database (Bushley et al., 2013). Raw data were normalized by Proteome Discovery software suite version 2.0 (Thermo Fisher Scientific, San Jose, CA, United States). Firstly, missing values were supplemented by the k proximity method. Then, median standardization was executed on intensity data. After that, EdgeR was used to screen DEPs with $|\log_2 (\text{fold change})| > 1$ and value of $p<0.05$. The protein expression difference of different samples was shown by a volcano plot constructed by TB tools.

2.6 Functional annotation of the DEPs

The DEPs were annotated and functionally enriched using Uniprot and Pfam. We also performed GO and KEGG analyses to annotate the DEPs. TBtools was used for the enrichment analyses.

The GO tool (http://geneontology.org; accessed on May 2023) was used and different terms were enriched. All terms were divided into three classes cellular components (CC), molecular functions (MF), and biological processes (BP).

The DEPs mapping to the KEGG pathways were retrieved by blasting against the KEGG database (https://www.genome.jp/kegg/pathway.html; accessed on May 2023). The pathways were attributed to several classes, such as Metabolism (A09100), Brite hierarchies (A09180), Genetic information processing (A09120), and Cellular processes (A09140).

2.7 Co-expression analysis of the DEPs

The String (search tool for the retrieval of interacting genes/proteins) database was used to accurately identify and annotate all co-expressed DEPs.[1] The network of related DEPs in each sample was constructed using Cytoscape. The minimum required interaction score of confidence was 0.4. Proteins with high connectivity in the network were identified as hub DEPs and were believed to play core roles in co-regulating life processes. The DEPs that closely contacted the hubs were hub-surrounded DEPs, which assisted in determining the functionality of the hubs.

2.8 The proteomic data were validated by quantitative real-time PCR analysis

Total RNA and cDNA were prepared according to the description of the previous job (Yu et al., 2018). The threshold cycle values were normalized by the expression level of the 18S rRNA gene (Liu et al., 2018). RT-qPCR reactions were performed in a volume of 15 μL on a LightCycler® 96 Real-Time PCR System (F. Hoffmann-La Roche Ltd., Basel, Switzerland) with ChamQ Universal SYBR qPCR Master Mix (Sparkjade, Shandong, China) according to the manufacturer's instruction. Expression levels were calculated according to the $2^{-\Delta\Delta CT}$ method.

3 Results and discussion

3.1 Changes in CsA yield and mycelium in fructose medium and sucrose medium, respectively

CsA and mycelium production increased over time, and their production rates were different every day. The maximum CsA production rate in fructose medium was 73.38 μg CyA/5 mL fermentation broth/day (μg/5 mL/day) on day 6, and the rate of increase was the fastest. Compared with the rate on day 5 (17.60 μg/5 mL/day), the rate of increase was 316.93% [=(73.38–17.60)/17.60] (Figures 1A,B). However, mycelium production increased slowly in the fructose medium on day 6 at a production rate of 2.72 mg DW mycelium/5 mL fermentation broth (mg DW/5 mL) (Figures 1C,D).

However, the CsA yield and production rate in sucrose medium were much lower than those in fructose medium. On day 6, the CsA production rate was 18.71 μg/5 mL/day, which was 1/3.92 of that in fructose medium (Figures 1A,B). However, the mycelium production rate reached a maximum of 10.58 mg DW/5 mL on day 6, which was 3.89 times higher than the mycelium production rate in fructose medium (Figures 1C,D). CsA production, CsA production rate, mycelium production, and mycelium production rate were recorded (Supplementary Table S1).

It was known that the production of CsA and the accumulation of mycelium had different priorities in these two different media

1 https://cn.string-db.org/cgi/

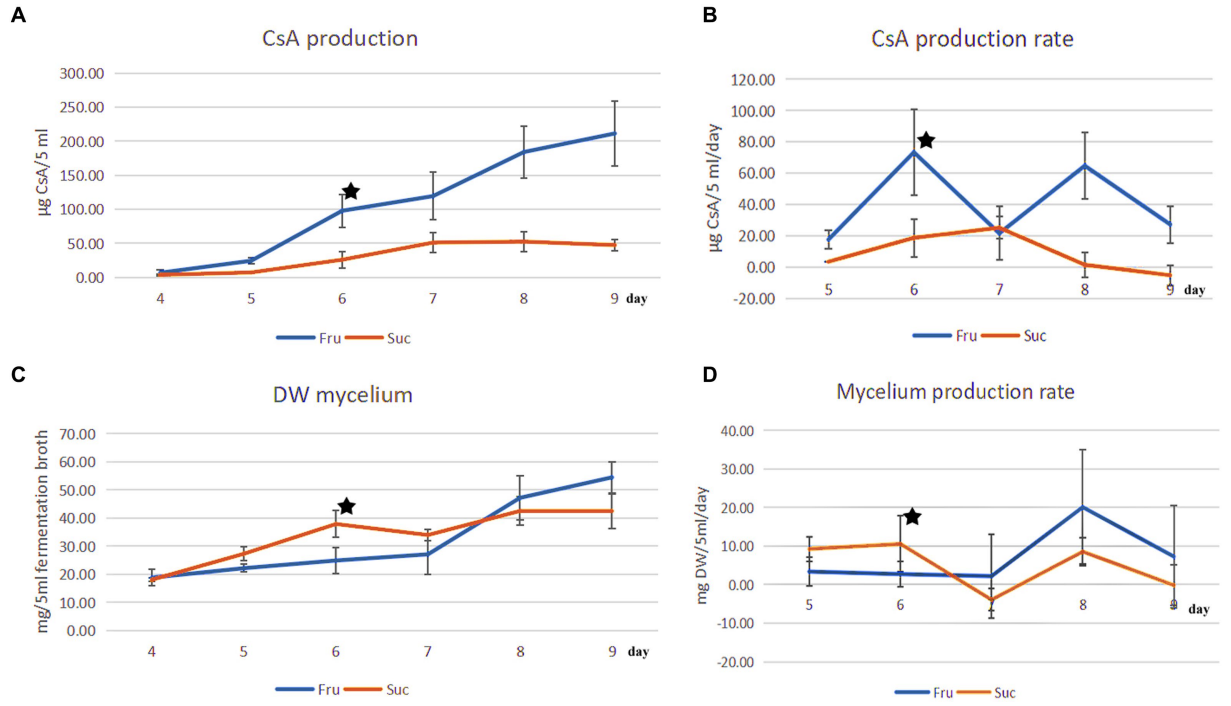

FIGURE 1
Comparison of CsA production and mycelial production from different carbon sources. **(A)** The change in the CsA yield from days 4 to 9 was cultured separately in fructose and sucrose media. **(B)** The CsA production rate from days 5 to 9. **(C)** The change in mycelial production corresponded to the change in CsA yield. **(D)** The mycelial production rate corresponded to the CsA production rate. ★: There were different priorities in CsA production and mycelium production on the 6th day.

according to the above results. On day 6, there was a higher priority for the production of CsA in the fructose medium, at this point fructose became a better carbon source for promoting CsA production, and the relatively high expression protein in the fructose fermentation product was more likely to be positive regulatory for the production of cyclosporine. However, mycelium preferentially accumulated in the sucrose medium on day 6, so sucrose was a better carbon source suitable for mycelium growth and the highly expressed protein in the sucrose fermentation was more likely to be a positive regulatory protein promoting mycelial growth (Figure 2).

3.2 Label-free LC–MS/MS technology was used to enable the high-throughput proteomic analysis of the samples separately cultured in fructose medium and sucrose medium

To screen the positively regulating proteins related to carbon metabolism of CsA synthesis and mycelial growth, fresh mycelium obtained on day 6 was selected as the test sample according to the results and named "Fru" and "Suc." The extracted total proteins were detected by label-free LC–MS/MS technology. A total of 3,227 proteins were identified and were median standardized (Supplementary Table S2). Principal component analysis indicated large differences between the groups and high similarities within the groups, indicating that the data were valid and could be used for further analysis (Figure 3A).

3.3 Screening of the DEPs

The DEPs were screened to compare the expression of Fru with Suc. A total of 244 DEPs were obtained and annotated (Supplementary Table S3-Total), including 74 highly expressed DEPs in the Fru (Supplementary Table S3-Fru) and 170 highly expressed DEPs in the Suc (Supplementary Table S3-Suc). The volcano plot shows the different effects of protein expression between the two groups and the distribution of the DEPs in each group. The different DEPs are circled and marked in yellow in the DEP list (Supplementary Table S3-Fru, Suc), and they may play a role in the trait formation of each group (Figure 3B). Four of the highly expressed DEPs, which are marked in green in the DEPs list (Supplementary Table S3-Fru), have been verified to be enzymes from the CsA biosynthetic gene cluster (Yang et al., 2018), including non-ribosomal peptide synthetase (NRPS, SimA, TINF00159), polyketide synthase (PKS, SimG, TINF00267), aminotransferase (SimJ, TINF00351), and ABC transporter (SimD, TINF00536). None of the CsA biosynthetic gene cluster proteins were highly expressed in Suc. These results further demonstrate that our analysis was accurate.

3.4 Functional analysis for the highly expressed DEPs in the Fru

Eighteen terms ($p < 0.05$) were significantly enriched in the GO analysis, including the BP terms of small molecules, such as carboxylic acid, oxoacid, organic acid, metabolic processes, lipid metabolic

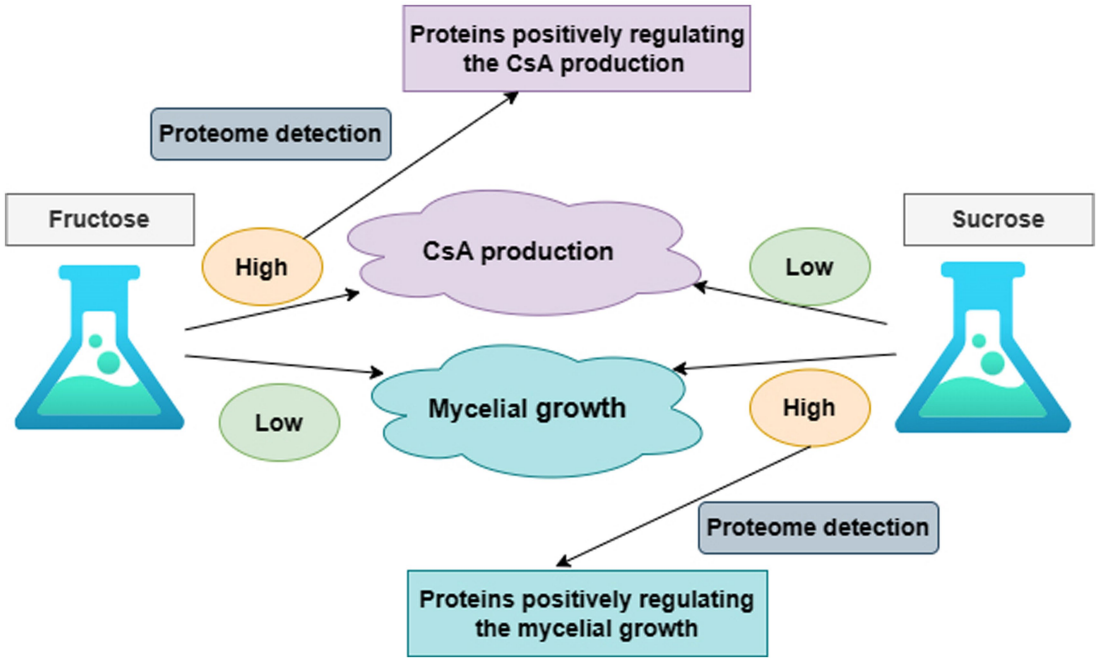

FIGURE 2
The overall research idea to illustrate the correlation between CsA production, mycelium growth, and protein expression.

processes ($p < 0.01$), cellular/organic substance catabolic processes, organonitrogen compound catabolic processes, (organic substance) and metabolic processes, including the CC terms of cell periphery, endoplasmic reticulum, and obsolete cytoplasmic part and the MF term of catalytic activity ($p < 0.01$). The DEPs annotations, expression ratios, and p-values are listed (Figure 4A; Supplementary Table S4-1).

Five pathways ($p < 0.05$) were enriched in the KEGG pathway enrichment analysis. Three pathways were involved in metabolism, including amino acid metabolism ($p < 0.01$), lipid metabolism, and carbohydrate metabolism. The exosome pathway belonged to the Brite hierarchy. The last pathway was transport and catabolism, which belonged to the CP. The detailed KEGG information is listed (Figure 5A; Supplementary Table S5-1).

Nineteen highly expressed DEPs were functionally related to Fru and connected in the network with the help of a co-expression analysis (Figure 6A). Twelve of these DEPs were related to small molecules, such as monocarboxylic acid, lipid, amino acid, and carbohydrate, metabolic processes (GO: 0044281, 0032787, 0006629, 0044255, 0019752, 0043436, 0006082, 0071704; KEGG: B 09103, B 09105, B 09101). The hub DEPs were aldehyde dehydrogenase (TINF03264), long-chain-fatty-acid-CoA ligase 1 (TINF02972), 2,4-dienoyl-CoA reductase [(3E)-enoyl-CoA-producing] (TINF06393), and malate synthase (TINF00525). Among them, polyketide synthase (TINF00267) was a major enzyme in the CsA gene cluster. The TINF02972 hub positively regulates CsA synthesis because it has a direct co-expression relationship with TINF00267. Ten of the DEPs were related to organic substances, particularly organonitrogen compounds, catabolic processes (GO: 1901575, 0009056, and 1,901,565), and transport and catabolism (KEGG: B 09141). The hub DEPs were TINF06393, TINF00525, TINF03264, and catalase (TINF06528). Notably, almost all DEPs involved in this network belonged to the obsolete cytoplasmic part (GO:0044444) or exosome (KEGG: 04147), indicating that these proteins were less relevant to primary metabolism, and more relevant to secondary metabolism, further reminding us that these proteins are related to the synthesis, metabolism, and transportation of secondary CsA metabolites. The DEPs involved in the network are listed and the hub DEPs are marked in red (Table 1).

Many studies have improved the CsA yield. These mostly rely on the traditional method of mutagenesis and screening of high-yielding strains, but results using this method are random and counterproductive (Domratcheva et al., 2018). Although filamentous fungi could undergo some natural mutations as they grow, such as low-frequency gene recombination could be produced by parasexuality, some recombinants could be obtained for screening strains with a higher yield of secondary metabolites to a certain extent, but this evolutionary speed is not as fast as bacteria, which is far from meeting the needs of production (Meyer, 2008). CsA is a secondary cyclopeptide metabolite (Zhang et al., 2017) composed of 11 amino acids (Molnár et al., 2010). CsA synthesis requires the unusual amino acid (4*R*)-4-[(*E*) -2-butenyl]-4-methyl-*L*-threonine (Bmt) as a substrate (Kirihata et al., 1995), and MeBmt (partially methylated Bmt) was marked out (Figure 7). However, CsA chemical synthetic methods are mostly limited by the difficulty of obtaining Bmt, because Bmt does not exist in natural medium, and its yield is very low in Bmt-producing fungi. In addition, Bmt is difficult to isolate and purify from complex products. Some researchers have been working to obtain MeBmt through a chemical synthesis approach (Rolt et al., 2019). However, this method involves many steps, many intermediate products, and a low final yield, and is difficult to put into industrial production.

The full biosynthetic mechanism of CsA has been analyzed at the genetic level. The CsA biosynthetic gene cluster has been suggested to include 12 genes encoding enzymes, including NRPS (SimA,

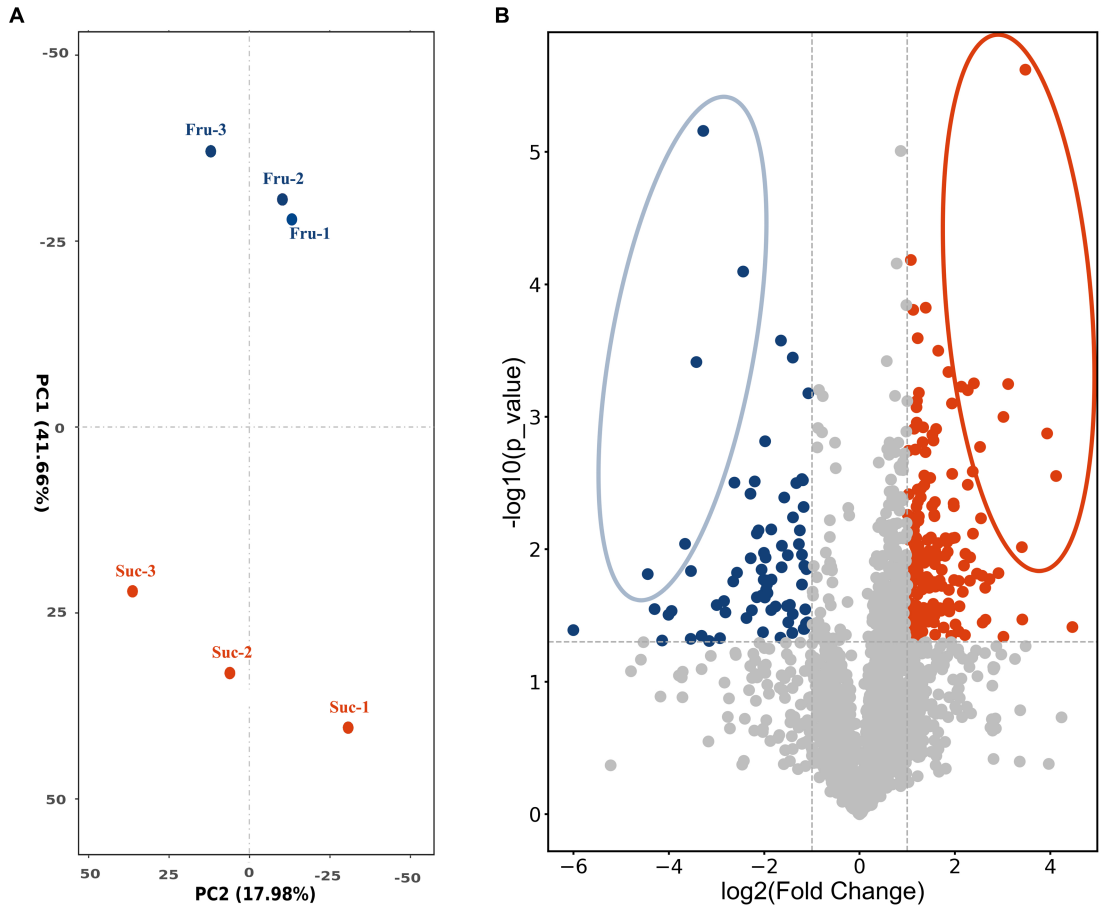

FIGURE 3
PCA analysis and volcano plot. **(A)** PCA plot shows the clustering of the samples based on their similarities. **(B)** The volcano plot shows the differential expression of the proteins in Fru and Suc. Each dot represents one protein. The horizontal coordinate measures the difference, and the vertical coordinates measure the significance of the difference. The highly expressed DEPs are blue in the Fru and red in the Suc. DEPs with relatively large and significant differences are circled.

TINF00159) responsible for assembling the 11 amino acid substrates of CsA and PKS (SimG, TINF00267) to mediate Bmt production (Yang et al., 2018). Many attempts have been made to obtain high-yielding engineered strains by expressing important secondary metabolites genes or gene clusters in a heterologous host that are produced at low levels by the original strain (Lan et al., 2019). However, NRPS and PKS are usually abundant in filamentous fungi, so cloning and processing large DNA fragments or complete gene clusters to achieve their hetero-expression is a challenge (Nielsen et al., 2019). Mining more genes or proteins that positively regulate CsA synthesis from several perspectives will indicate the direction to obtain engineered strains with higher CsA yields and provide more space for genetic manipulation.

In addition to these proteins analyzed, other proteins may play vital roles in the regulation of CsA synthesis. It has been confirmed that cytochrome P450 (SimI, TINF00470) and aminotransferase (SimJ, TINF00351) are involved in Bmt synthesis (Yang et al., 2018). Two DEPs highly expressed in Fru were functionally similar. Copper radical oxidase (TINF06995) is a biocatalyst for the selective oxidation of primary alcohols to aldehydes and has a wide range of specificities for aliphatic compounds, which have a similar function to TINF00470 (Cleveland et al., 2021). The other DEP was an aminotransferase (putative, TINF08869), which was the same as TINF00351.

Overexpressing the basic leucine zipper (bZIP) transcription regulator (SimL, TINF00394), which directly regulates the expression of the CsA gene cluster, improves CsA production (Yang et al., 2018). Interestingly, three highly expressed DEPs regulated DNA transcription in Fru. The Myb transcription factor (TINF04891), which can be activated by bZip transcription factors, participated in transducing the aerial stimulus signal. Both factors jointly activate a C(2)H(2) zinc finger transcription factor, which plays a central role in fungal growth and virulence (Garzia et al., 2010; Lee et al., 2021). TINF04891 may participate in the regulation of CsA biosynthesis. Another protein containing the critical features of the tristetraprolin zinc finger domain has been linked to the control of pheromone signal transduction and the coordination of mitosis (Cuthbertson et al., 2008). The CCCH zinc finger DNA binding protein (TINF00841) may regulate the CsA biosynthetic process. The transcriptional activator ALCR, which is a transcriptional activator in the ethanol utilization pathway of filamentous fungi, is a DNA-binding protein with a helix-turn-helix structure (Kulmburg et al., 1992). The helix-turn-helix domain-containing protein (TINF02756) may also be a transcriptional activator of CsA biosynthesis.

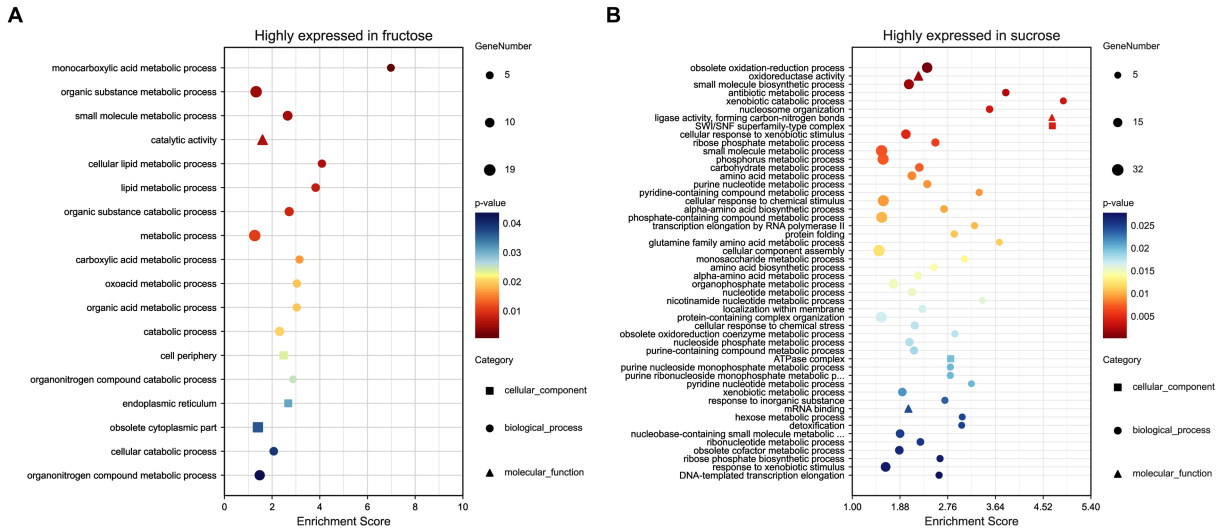

FIGURE 4
(A) GO analysis of the highly expressed DEPs in the Fru. **(B)** GO analysis of the highly expressed DEPs in the Suc. The GO terms were distributed into three classes, biological process (●), molecular function (▲), and cellular component (■). The larger the graph, the more DEPs were involved. *p*-values ranged from 0 to 0.05, indicating warmer colors and more significant differences. The enrichment score (ES) is the maximum statistical value accumulated by the degree of association between each protein in the protein set and the phenotype, representing the degree of association between the whole protein set and the phenotype.

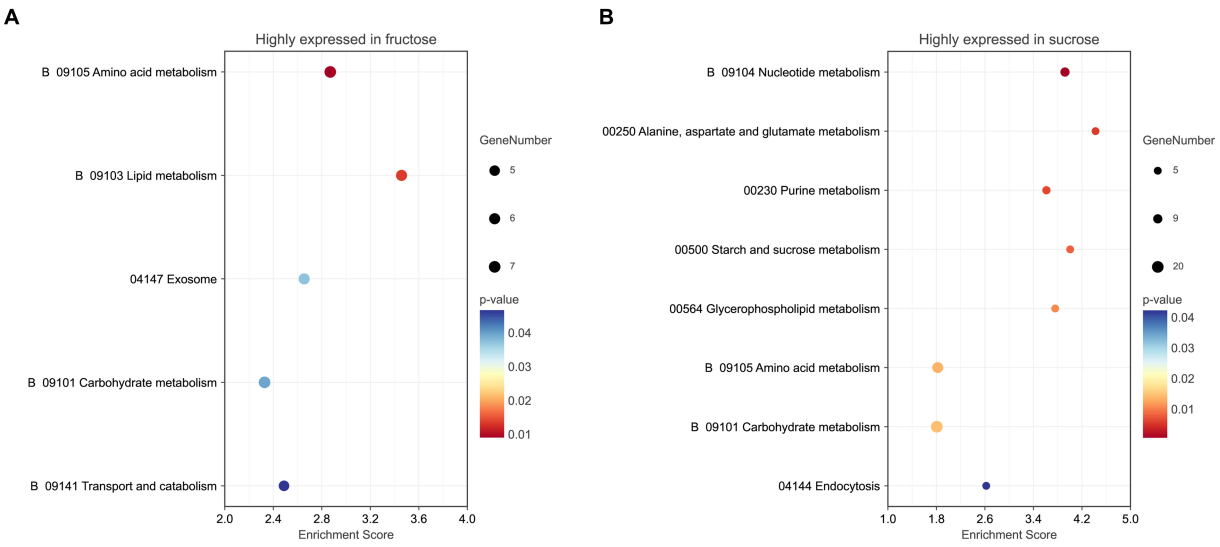

FIGURE 5
(A) KEGG pathway analysis of the highly expressed DEPs in the Fru. **(B)** KEGG pathway analysis of the highly expressed DEPs in the Suc. The color of the graph represents the value of *p* ranging from 0 to 0.05. The size of the graph represents the number of the included DEPs.

The ABC transporter (SimD, TINF00536) in the CsA gene cluster may facilitate the production of more CsA and increase tolerance to the fungus by transferring CsA to reduce its concentration (Yang et al., 2018). The WSC domain-containing protein (TINF08949) may have a similar function as SimD because it localizes in the vacuoles and cell wall/membrane of the filamentous fungus *Beauveria bassiana* and, hence, has been linked to cell membrane- and vacuole-related cellular events (Tong et al., 2019). The short-chain dehydrogenase/reductase SDR (TINF06213, TINF03230) could also enhance fungal tolerance to secondary metabolites by the non-toxic transformation of secondary metabolites (Xing et al., 2021). It may also participate in CsA transformation.

3.5 Highly expressed DEPs in Suc

Industrial fermentation to produce secondary metabolites often requires a segmented culture of engineered fungi. More secondary metabolites are produced when the mycelium reaches a particular

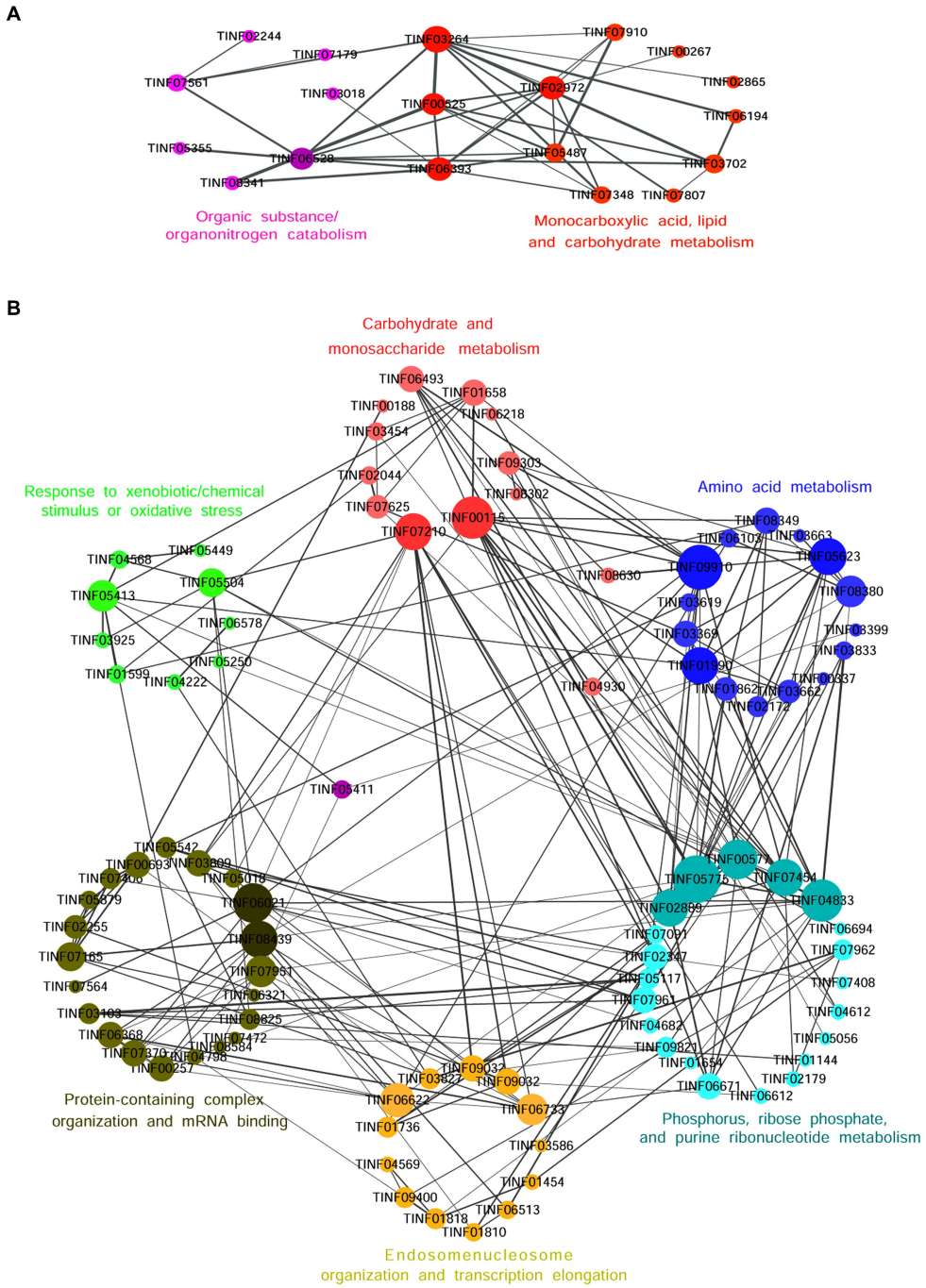

FIGURE 6
The co-expression network diagrams of the functionally related DEPs in the Fru **(A)** and the Suc **(B)**. Circles represent one DEP and size indicates the connectivity value of the proteins. The hub DEPs with high connectivity values are marked in deeper colors. The straight lines represent edges and the width of a straight line indicates the weighted value. The larger the weighted value between two DEPs, the closer their relationship.

abundance. A previous study was aimed at optimizing the culture medium for biomass production and phenolic compounds using *Ganoderma lucidum*. The culture was optimized in two stages. After the maximum biomass production was reached under optimal conditions, more phenolic compounds were obtained (Zárate-Chaves et al., 2013). We analyzed the highly expressed DEPs in Suc medium, which are mostly involved in the regulation of *T. inflatum* mycelial growth.

Seventy-four terms ($p < 0.05$) were significantly enriched in the GO analysis, including the BP terms of obsolete oxidation–reduction processes and obsolete oxidoreduction coenzyme metabolic processes, small molecules, such as antibiotic and pyridine-containing compounds, biosynthetic or metabolic processes ($p < 0.01$), cellular response to xenobiotic/chemical stimulus/stress, response to inorganic substance/oxidative stress and detoxification, xenobiotic catabolic/metabolic processes, obsolete cofactor metabolic

TABLE 1 The highly expressed DEPs of Fru in a network.

Classification	Protein id	Functional annotation	Connective degree
Monocarboxylic acid,lipid and carbohydrate metabolism	TINF03264	Aldehyde dehydrogenase	10
	TINF02972	Long-chain-fatty-acid-CoA ligase 1	8
	TINF06393	2,4-dienoyl-CoA reductase [(3E)-enoyl-CoA-producing]	8
	TINF00525	Malate synthase	7
	TINF03702	glycerol kinase	5
	TINF05487	Acyl-CoA dehydrogenase	5
	TINF07348	methylmalonate-semialdehyde dehydrogenase (CoA acylating)	4
	TINF07910	Oxidoreductase, 2-nitropropane dioxygenase family, putative	4
	TINF06194	Aldolase	2
	TINF07807	Oxidoreductase	2
	TINF02865	Amidase family protein	1
	TINF00267	Polyketide synthase, putative	1
Organic substance/ organonitrogen catabolism	TINF03264	Aldehyde dehydrogenase	10
	TINF06393	2,4-dienoyl-CoA reductase [(3E)-enoyl-CoA-producing]	8
	TINF00525	Malate synthase	7
	TINF06528	Catalase	7
	TINF07561	Glutathione transferase (Gto1), putative	4
	TINF08341	Allantoicase	2
	TINF02244	Glutathione hydrolase	1
	TINF03018	Short chain dehydrogenase/reductase	1
	TINF05355	Phosphorylcholine phosphatase	1
	TINF07179	Alpha-mannosidase	1

The hub proteins were marked in yellow.

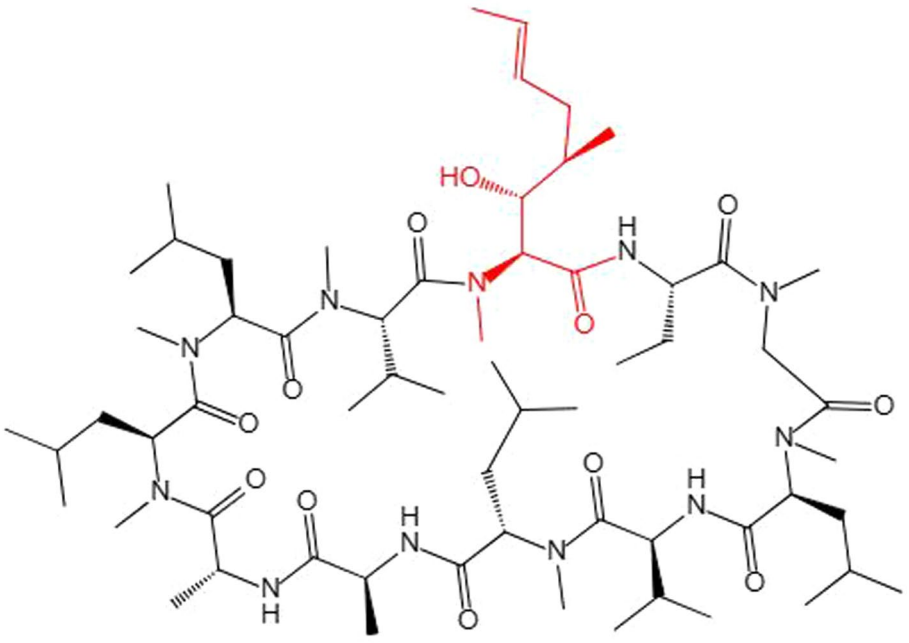

FIGURE 7
The chemical structure of CsA. MeBmt is red.

processes, ribose phosphate metabolic processes, phosphorus metabolic processes, nucleotide metabolic processes, nucleosome organization ($p < 0.01$), DNA conformational changes, transcription elongation, amino acid biosynthetic/metabolic processes, carbohydrate catabolic/biosynthetic processes, cellular component assembly/organization, localization within membranes, negative regulation of cellular component organization, and the regulation of filamentous growth. Additionally including the MF terms oxidoreductase activity ($p < 0.01$), ligase activity, forming carbon-nitrogen bonds ($p < 0.01$), mRNA binding, unfolded protein/protein binding, isomerase activity, including the CC terms SWI/SNF superfamily-type complex ($p < 0.01$), ATPase complex, cytosol, and endosome (Figure 4B; Supplementary Table S4-2).

Eight KEGG pathways ($p < 0.05$) were enriched. Seven pathways were involved in metabolism, including nucleotide metabolism ($p < 0.01$), amino acid metabolism, alanine, aspartate, and glutamate metabolism ($p < 0.01$), purine metabolism ($p < 0.01$), carbohydrates, such as starch and sucrose, metabolism, glycerophospholipid metabolism, and endocytosis in CP (Figure 5B; Supplementary Table S5-2).

Ninety-three DEPs were connected to a network (Figure 6B; Table 2). Thirteen were related to carbohydrate (GO: 0005975, 0016051, 0016052; KEGG: B 09101), monosaccharide (GO: 0005996), hexose (GO: 0019318), or starch and sucrose (KEGG: 00500) metabolic processes. The hub DEPs were phosphoglycerate kinase (TINF00115) and SNF2-family ATP-dependent chromatin remodeling factor snf21 (TINF07210). Six DEPs were related to carbon metabolism, TINF00115, ribose-phosphate diphosphokinase (TINF04682), serine/threonine-protein kinase cot-1 (TINF06493), dihydrolipoyl dehydrogenase (TINF09910), glycerol-3-phosphate dehydrogenase [NAD(+)] (TINF01599), and phosphoenolpyruvate carboxykinase (ATP) (TINF09303), (Supplementary Figure S1). Fifteen participated with amino acids, such as alanine, aspartate, and glutamate, metabolic processes (GO: 0006520, 0008652, 1,901,605, 1,901,607; KEGG: B 09105, 00250). The hub DEPs were TINF09910, glutamine synthetase (TINF01990), and glutamate dehydrogenase (TINF05623). Nine DEPs were related to amino acid biosynthesis, including TINF01990, TINF04682, TINF00115, TINF06493, asparagine synthetase (TINF01862), aconitate hydratase, mitochondrial (TINF03619), glutamate-5-semialdehyde dehydrogenase (TINF03662), imidazole glycerol phosphate synthase hisHF (TINF03833), and threonine synthase (TINF08349) (Supplementary Figure S2). Interestingly, TINF04682, TINF00115, and TINF06493 were closely related to carbon metabolism and amino acid biosynthesis. Twenty-one DEPs participated in phosphorus (GO: 0006793, 0006796; KEGG: 00564), ribose phosphate (GO: 0009123, 0009259, 0046390, 0019693, 0009161; KEGG: B 09104), and purine ribonucleotide (GO: 0009150, 0009126, 0009167, 0009199; KEGG: 00230) metabolic processes. The hub DEPs were adenylosuccinate lyase (TINF00577), GMP synthase [glutamine-hydrolyzing] (TINF04833), phospho ribosylformyl glycinamidine synthase (TINF02889), CTP synthase (TINF05775), and glycerol-3-phosphate dehydrogenase [NAD(+)] (TINF07454). Thirteen DEPs were components of the endosome (GO: 0005768) or enzymes contributing to transcription elongation (GO: 0006354, 0006368), nucleosome organization (GO: 0034728), and protein-DNA complex subunit organization (GO: 0071824). The hub DEPs were FK506-binding protein (TINF06622) and protein arginine N-methyltransferase 1 (TINF06733). Interestingly, another three DEPs from the network were associated with nuclear changes or transcription. The nuclear movement protein nudC (TINF04353) is required for nuclear migration during vegetative growth and development (Xiang et al., 1995). The polybromo-1 (putative, TINF04750) coordinates key features common to all remodeling complexes, including chromatin localization, recruitment of protein subunits, and changes in chromatin architecture (Thompson, 2009). The C2H2 transcription factor RfeC (TINF01322) has broad regulatory roles in various fungal growth and developmental processes, conidiation, and the abiotic stress response in eukaryotes (Chen et al., 2020). Twenty-two DEPs were related to protein-containing complex organization or assembly (GO: 0043933, 0065003) and mRNA binding (GO: 0003729). The hub DEPs were the eukaryotic translation initiation factor subunit eIF-4F, putative (TINF06021), nucleolar protein 58 (TINF08439), and WD repeat-containing protein 36 (TINF07951). TINF07951 and TINF08439 were related to ribosome biogenesis, and elongation factor 2 (TINF08620) was related to ribosome function (Supplementary Figure S3). Eleven DEPs were related to response to xenobiotic stimulus/inorganic substance/chemical stimulus (GO: 0009410, 0010035, 0042221, 0051716, 0070887, 0071466), xenobiotic catabolic processes (GO: 0042178), response to oxidative stress (GO: 0034599, 0055114), and detoxification (GO: 0098754). The hub DEPs were TINF07951, glutathione peroxidase (TINF05413), and mitochondrial protein import protein MAS5 (TINF05504). In addition, three highly expressed proteins from the network were associated with oxidative stress. Survival factor 1 (TINF07979) was involved in coping with reactive oxygen species, which promote survival under conditions of oxidative stress in *S. cerevisiae* (Yu et al., 2019). The non-specific serine/threonine protein kinase (TINF06713) is involved in energy flux and protein synthesis. Deleting this protein increases the sensitivity of yeast cells to oxidative stress (H2O2 treatment) and partially inhibits cell growth (Huang et al., 2014). Thioredoxin (TINF01860) is an enzyme comprising the thioredoxin system, which participates in resistance to oxidative stress (Missall and Lodge, 2005). Another two DEPs from the network participate in signal transduction in response to various abiotic stressors. Elongation factor 2 (TINF08620) could potentially be phosphorylated by the Rck2 kinase in response to environmental stress (Bartish et al., 2007). The AMP-activated protein kinase glycogen-binding domain-containing protein (TINF02240) is activated under conditions of nutrient or metabolic stress (Wiatrowski et al., 2004). Mitogen-activated protein kinases (MAPKs) are a group of serine–threonine protein kinases that are activated by different extracellular stimuli, such as cytokines, neurotransmitters, hormones, cellular stress, and cell adhesion. TINF01599, TINF06713, TINF07454, and the phosphotransmitter protein Ypd1 (putative, TINF01654) participated in the MAPK signaling pathway (Supplementary Figure S4).

The cell walls of filamentous fungi contain chitin, protein, mannan, and amorphous glucan. Six highly expressed DEPs related to fungal cell walls occurred. Four of these DEPs were involved in the formation of cell wall components and maintaining cell wall integrity. The beta-flanking protein (TINF04729) was a conserved genomic neighbor localized within a recently identified metabolic cell wall gene cluster in genomes of *Aspergillus* spp., which may participate in cell wall biosynthesis (Guerriero et al., 2016). The carbohydrate-binding WSC (TINF05352) was not recognized in substrates but attaches the enzyme to plant and/or fungal cell walls, and may

10.3389/fmicb.2023.1259101

TABLE 2 The highly expressed DEPs of Suc in a network.

Classification	Protein id	Functional annotation	Connective degree
Phosphorus,ribose phosphate,and purine ribonucleotide metabolism	TINF05775	CTP synthase	14
	TINF04833	GMP synthase [glutamine-hydrolyzing]	12
	TINF00577	Adenylosuccinate lyase	11
	TINF02889	phosphoribosylformylglycinamidine synthase	10
	TINF07454	Glycerol-3-phosphate dehydrogenase [NAD(+)]	10
	TINF06671	Phosphoribosylaminoimidazole carboxylase	6
	TINF07961	Cytochrome b-c1 complex subunit Rieske, mitochondrial	6
	TINF02347	Histone chaperone	6
	TINF05117	Cytochrome c oxidase subunit 6, mitochondrial	4
	TINF07962	GTPase-activating protein	4
	TINF09821	1-acyl-sn-glycerol-3-phosphate acyltransferase	4
	TINF07091	DUF1750 domain protein	3
	TINF04612	UDP-N-acetylglucosamine pyrophosphorylase	2
	TINF06612	RNA polymerase II transcription elongation factor Ctr9, putative	2
	TINF02179	choline-phosphate cytidylyltransferase	2
	TINF04682	ribose-phosphate diphosphokinase	2
	TINF06694	Hsp90 chaperone protein kinase-targeting subunit	1
	TINF07408	Protein phosphatase PP2A regulatory subunit	1
	TINF01144	V-type proton ATPase subunit F	1
	TINF05056	Kynurenine formamidase	1
	TINF01654	Phosphotransmitter protein Ypd1, putative	1
Endosome, nucleosome，organization and transcription elongation	TINF06622	FK506-binding protein	9
	TINF06733	Protein arginine N-methyltransferase 1	8
	TINF04310	SWI-SNF complex subunit (BAF60b), putative	6
	TINF09032	Ran-specific GTPase-activating protein 1, putative	6
	TINF09400	Protein transport protein BOS1	4
	TINF01736	Transcription regulator BDF1, putative	4
	TINF01818	SNARE protein Snc2, putative	4
	TINF03827	Guanyl-nucleotide exchange factor (Sec7), putative	4
	TINF01810	Histone H1-binding protein	3
	TINF06513	DNA replication licensing factor MCM7	3
	TINF04569	t-SNARE	2
	TINF01454	Zinc finger protein gcs1	2
	TINF03586	Leukotriene A4 hydrolase	1
Protein-containing complex organization and mRNA binding	TINF06021	Eukaryotic translation initiation factor subunit eIF-4F, putative	11
	TINF08439	Nucleolar protein 58	10
	TINF07951	WD repeat containing protein 36	8
	TINF07165	Small nuclear ribonucleoprotein SmB, putative	7
	TINF06368	Nucleolin protein Nsr1, putative	6
	TINF00257	U3 small nucleolar RNA associated protein	6
	TINF00693	Pre-mRNA processing splicing factor, putative	6
	TINF07370	Protein PUF6, putative	6
	TINF03809	Replication protein A subunit	6
	TINF02255	mRNA splicing factor (Prp17)	5
	TINF03103	Cytochrome c oxidase polypeptide VIb	4
	TINF07406	Splicing factor U2AF subunit	4
	TINF05542	Mitochondrial export translocase Oxa1, putative	4
	TINF08825	Mitochondrial outer membrane translocase complex, subunit Tom22	4
	TINF05879	Pre-mRNA splicing factor CWC21	3
	TINF05018	Nuclear cohesin complex subunit (Psc3), putative	3

(Continued)

TABLE 2 (Continued)

Classification	Protein id	Functional annotation	Connective degree
	TINF04798	Endoplasmic reticulum transmembrane protein	2
	TINF06321	C2H2-type domain-containing protein	1
	TINF08584	Uncharacterized protein	1
	TINF07472	Proteasome component	1
	TINF07564	Topisomerase II associated protein	1
Response to xenobiotic/chemical stimulus or oxidative stress	TINF05413	Glutathione peroxidase	8
	TINF05504	Mitochondrial protein import protein MAS5	7
	TINF01599	Catalase	3
	TINF04568	Oxidoreductin	3
	TINF04222	Zinc homeostasis factor 1	2
	TINF03925	Monothiol glutaredoxin-5	2
	TINF05449	Protein disulfide-isomerase tigA	1
	TINF05250	Lysine decarboxylase-like protein	1
	TINF06578	Serine/threonine-protein kinase cot-1	1
Carbohydrate and monosaccharide metabolism	TINF00115	Phosphoglycerate kinase	12
	TINF07210	SNF2-family ATP dependent chromatin remodeling factor snf21	10
	TINF01658	1,4-alpha-glucan-branching enzyme	6
	TINF06493	Ribulose-phosphate 3-epimerase	6
	TINF07625	Alpha,alpha-trehalose phosphate synthase subunit TPS3	5
	TINF09303	Phosphoenolpyruvate carboxykinase (ATP)	5
	TINF03454	Glycogenin	3
	TINF02044	Trehalase	3
	TINF00188	TINF00188	1
	TINF08302	nitric oxide dioxygenase	1
	TINF06218	UDP-glucose 4-epimerase	1
Amino acid metabolism	TINF09910	Dihydrolipoyl dehydrogenase	13
	TINF05623	Glutamate dehydrogenase	10
	TINF01990	Glutamine synthetase	10
	TINF08380	leucine--tRNA ligase	8
	TINF03369	Glutamate decarboxylase	6
	TINF08349	threonine synthase	6
	TINF01862	Asparagine synthetase	5
	TINF03662	glutamate-5-semialdehyde dehydrogenase	5
	TINF02172	Arg-6 protein	4
	TINF03619	Aconitate hydratase, mitochondrial	3
	TINF06103	Multisynthetase complex auxiliary component p43	3
	TINF03833	Imidazole glycerol phosphate synthase hisHF	3
	TINF03399	Alcohol dehydrogenase, putative	1
	TINF03663	Methionine aminopeptidase 2	1
	TINF00337	Sulfate adenylyltransferase	1

The hub proteins were marked in yellow.

be potentially involved in β-glucan remodeling to maintain cell wall integrity and participate in the stress response (Wawra et al., 2019). The oxidoreductase, 2OG-Fe(II) oxygenase family (putative, TINF05005) may affect the composition of the secondary cell wall (Fang et al., 2012). The sphingolipid long-chain base-responsive protein PIL1 (TINF07009) inhibits protein kinases involved in signaling pathways for cell wall integrity (Delom et al., 2006). The other two DEPs were components of the cell wall and related to different cell wall functions. The chitin-binding, domain 3 (TINF05053) has been predicted to be localized in the cell wall (Zhan and Guo, 2015). Cyanovirin-N (TINF06073) in filamentous ascomycetes is a nonsecretory monodomain protein and a multidomain protein bearing functionally related modules, such as peptidoglycans and chitin-binding domain LysM, in the cell wall (Percudani et al., 2005).

Lipid molecules, such as cholesterol and ergosterol, are found in eukaryotic cell membranes. Eight DEPs were related to membrane and transport. Four of these DEPs were involved in the formation of the plasma membrane. Squalene monooxygenase (TINF07977) is an important enzyme involved in the synthesis of

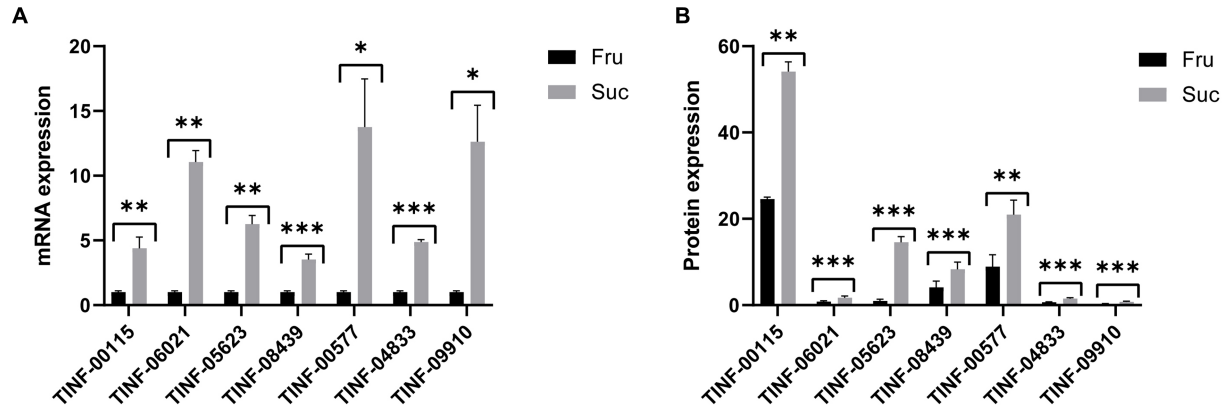

FIGURE 8
Quantitative real-time PCR validation of the proteomic results. **(A)** The mRNA expression of the seven hub DEPs. **(B)** The protein expression of the seven hub DEPs. ***: p-value <0.001, **: p-value <0.01, *: p-value <0.05. The protein expression changes are consistent with those of their mRNAs.

ergosterol, cholesterol, and phytosterols (Zare et al., 2014). The BAR domain protein (TINF01359) is a membrane-shaping protein, which determines organelle biogenesis, membrane trafficking, cell division, and cell migration (Frost et al., 2009). The ankyrin repeats domain-containing protein (TINF00399) is localized on the cytoplasmic membrane during transient expression in onion epidermal cells (Zhang et al., 2010). The oxysterol binding protein (TINF02166) is an important non-vesicular trafficking protein involved in the transportation of lipids in eukaryotic cells, and may also participate in membrane formation (Qiu and Zeng, 2019). Another four DEPs were involved in the formation of membrane organelles, such as vacuoles and vesicles, as well as transportation processes. Carboxypeptidase (TINF00103) has been used as a marker enzyme for investigations on the intracellular transport of vacuolar proteins and vacuolar biogenesis in *S. cerevisiae* (Ohsumi et al., 2001). The hsc70 cochaperone (SGT) (putative, TINF09583) bends membranes based on their ability to oligomerize. This activity promotes endosomal microautophagy and the turnover of specific synaptic proteins (Uytterhoeven et al., 2015). The apolipoprotein/apolipoprotein (TINF08525) is involved in phagocytosis, and possibly pattern recognition (Whitten et al., 2004). The vesicle-fusing ATPase (TINF02607) serves a dual role in vacuolar integrity to regulate vacuole fusion and fission reactions in yeast (Qiu, 2012).

Five DEPs were related to mycelial growth and development. The cipC-like antibiotic response protein (putative, TINF04883) was exclusively found in the hyphal morphotype, which enables invasive growth of *Aspergillus fumigatus* during infection (Bauer et al., 2010). The protein kinase activator (Mob2) (putative, TINF07215) is crucial for normal hyphal development (Gutiérrez-Escribano et al., 2011). Two DEPs targeting the endoplasmic reticulum (ER), the short-chain dehydrogenase/reductase family protein (TINF05550), and signal recognition particle subunit SRP72 (TINF01479) are related to cell death, defense responses, and protein transport (Brown et al., 1994; Zheng et al., 2022). The glia maturation factor beta (TINF07923) is a regulator of the actin cytoskeleton with a unique role in remodeling the actin network architecture, and it has roles in controlling actin filament spatial organization and the dynamics underlying cell motility, endocytosis, and other biological processes (Goode et al., 2018).

3.6 Quantitative real-time polymerase chain reaction (PCR) validation of DEP expression

Gene expression is largely consistent with protein expression. We used RT-qPCR to determine the gene expression levels (mRNA content) of seven key DEPs, including the hub DEPs in the pathways of carbohydrate and monosaccharide metabolism, protein-containing complex organization and mRNA binding, amino acid metabolism, (ribose) and phosphorus and purine ribonucleotide metabolism to verify the accuracy of our proteomics results. The primers for RT-qPCR analysis are listed in Supplementary Table S6-1. The results showed that the changes in gene expression (Supplementary Table S6-2) were consistent with changes in protein expression (Supplementary Table S6-3), indicating the reliability of our proteomic results and the accuracy of the DEP screening (Figure 8).

4 Conclusion

CsA production and the accumulation of mycelia differed in Fru and Suc media. The difference was most obvious on day 6 of culture when CsA was produced in the Fru medium and mycelium preferentially grew in the Suc medium. The mycelium proteome in these two groups was determined and compared. The highly expressed mycelial proteins cultured in Fru medium were involved in the regulation of CsA production, metabolism, and transportation. These DEPs participated in the processes of small molecules, such as carboxylic acid, oxic acid, and organic acid metabolism; lipid metabolism; catabolic processes of organic substances, particularly organo-nitrogen compounds; CsA transport and exocrine-derived functions of the ER, exosomes, and obsolete cytoplasmic parts; regulating the synthesis of the CsA substrate Bmt; functions of transcriptional regulators. The highly expressed DEPs in the Suc medium were involved in the regulation of mycelial growth. They were mainly involved in the processes of the abandoned REDOX or coenzyme metabolism; small molecules, such as antibiotics, pyridine-containing compounds, amino acids, carbohydrates, biosynthesis or metabolism; response to stress, such as exogenous stimuli/inorganic/chemical stimuli, exogenous catabolism, oxidative stress, and detoxification; genetic information or epigenetic changes, such as changes in nuclear

organization and DNA conformation, nucleotide (phosphorylated) metabolism; cell component assembly/organization; cell wall integrity; membrane metabolism and vesicle transport, intramembrane localization, and regulation of filamentous growth.

Data availability statement

The datasets presented in this study can be found in online repositories. The names of the repository/repositories and accession number(s) can be found in the article/Supplementary material.

Author contributions

JW: Conceptualization, Data curation, Formal analysis, Investigation, Supervision, Validation, Visualization, Writing – original draft. ML: Conceptualization, Data curation, Formal analysis, Investigation, Supervision, Validation, Visualization, Writing – original draft. CM: Conceptualization, Data curation, Formal analysis, Investigation, Validation, Visualization, Writing – review & editing. SL: Data curation, Formal analysis, Investigation, Validation, Visualization, Writing – review & editing. JZ: Data curation, Formal analysis, Visualization, Writing – review & editing. YF: Conceptualization, Methodology, Writing – review & editing. LG: Conceptualization, Methodology, Writing – review & editing. HY: Conceptualization, Methodology, Writing – review & editing. XY: Conceptualization, Data curation, Formal analysis, Funding acquisition, Investigation, Methodology, Project administration, Resources, Supervision, Validation, Visualization, Writing – original draft, Writing – review & editing.

Funding

The author(s) declare financial support was received for the research, authorship, and/or publication of this article. This research was financially supported by the National Natural Science Foundation of China (Grant No. 32000041) and the Shandong Provincial Natural Science Foundation, China (ZR2020QC005) the Qingdao Agricultural University Scientific Research Foundation (6631120076).

Acknowledgments

Thanks to Chengshu Wang, Center for Excellence in Molecular Plant Sciences, Chinese Academy of Sciences, for providing research materials.

Conflict of interest

The authors declare that the research was conducted in the absence of any commercial or financial relationships that could be construed as a potential conflict of interest.

Publisher's note

Supplementary material

The Supplementary material for this article can be found online at: https://www.frontiersin.org/articles/10.3389/fmicb.2023.1259101/full#supplementary-material

References

Abrol, V., Kushwaha, M., Mallubhotla, S., and Jaglan, S. (2022). Chemical mutagenesis and high throughput media optimization in *Tolypocladium inflatum* MTCC-3538 leads to enhanced production of cyclosporine A. *3 Biotech* 12:158. doi: 10.1007/s13205-022-03219-x

Balaraman, K., and Mathew, N. (2006). Optimization of media composition for the production of cyclosporin a by *Tolypocladium* species. *Indian J. Med. Res.* 123, 525–530. Available at: https://pubmed.ncbi.nlm.nih.gov/16783043/.

Bartish, G., Moradi, H., and Nygård, O. (2007). Amino acids Thr56 and Thr58 are not essential for elongation factor 2 function in yeast. *FEBS J.* 274, 5285–5297. doi: 10.1111/j.1742-4658.2007.06054.x

Bauer, B., Schwienbacher, M., Broniszewska, M., Israel, L., Heesemann, J., and Ebel, F. (2010). Characterisation of the CipC-like protein AFUA_5G09330 of the opportunistic human pathogenic mould *Aspergillus fumigatus*. *Mycoses* 53, 296–304. doi: 10.1111/j.1439-0507.2009.01718.x

Bi, Z. Q., Ren, L. J., Hu, X. C., Sun, X. M., Zhu, S. Y., Ji, X. J., et al. (2018). Transcriptome and gene expression analysis of docosahexaenoic acid producer *Schizochytrium sp.* under different oxygen supply conditions. *Biotechnol. Biofuels* 11:249. doi: 10.1186/s13068-018-1250-5

Borel, J. F., Feurer, C., Gubler, H. U., and Stähelin, H. (1976). Biological effects of cyclosporin a: a new antilymphocytic agent. *Agents Actions* 6, 468–475. doi: 10.1007/BF01973261

Brown, J. D., Hann, B. C., Medzihradszky, K. F., Niwa, M., Burlingame, A. L., and Walter, P. (1994). Subunits of the *Saccharomyces cerevisiae* signal recognition particle required for its functional expression. *EMBO J.* 13, 4390–4400. doi: 10.1002/j.1460-2075.1994.tb06759.x

Bushley, K. E., Raja, R., Jaiswal, P., Cumbie, J. S., Nonogaki, M., Boyd, A. E., et al. (2013). The genome of *Tolypocladium inflatum*: evolution, organization, and expression of the cyclosporin biosynthetic gene cluster. *PLoS Genet.* 9:e1003496. doi: 10.1371/journal.pgen.1003496

Chen, L., Zhao, J., and Xia, H. (2020). FpCzf14 is a putative C_2H_2 transcription factor regulating conidiation in *fusarium pseudograminearum*. *Phytopathol. Res.* 2:33. doi: 10.1186/s42483-020-00074-7

Cleveland, M., Lafond, M., Xia, F. R., Chung, R., Mulyk, P., Hein, J. E., et al. (2021). Two *fusarium* copper radical oxidases with high activity on aryl alcohols. *Biotechnol. Biofuels* 14:138. doi: 10.1186/s13068-021-01984-0

Cuthbertson, B. J., Liao, Y., Birnbaumer, L., and Blackshear, P. J. (2008). Characterization of zfs1 as an mRNA-binding and -destabilizing protein in *Schizosaccharomyces pombe*. *J. Biol. Chem.* 283, 2586–2594. doi: 10.1074/jbc.M707154200

Delom, F., Szponarski, W., Sommerer, N., Boyer, J. C., Bruneau, J. M., Rossignol, M., et al. (2006). The plasma membrane proteome of *Saccharomyces cerevisiae* and its response to the antifungal calcofluor. *Proteomics* 6, 3029–3039. doi: 10.1002/pmic.200500762

Domratcheva, A. G., Zhgun, A. A., Novak, N. V., and Dzhavakhiya, V. V. (2018). The influence of chemical mutagenesis on the properties of the cyclosporine a high-producer strain *Tolypocladium inflatum* VKM F-3630D. *Appl. Biochem. Microbiol.* 54, 53–57. doi: 10.1134/S0003683818010027

Fang, L., Zhao, F., Cong, Y., Sang, X., Du, Q., Wang, D., et al. (2012). Rolling-leaf14 is a 2OG-Fe (II) oxygenase family protein that modulates rice leaf rolling by affecting

secondary cell wall formation in leaves. *Plant Biotechnol. J.* 10, 524–532. doi: 10.1111/j.1467-7652.2012.00679.x

Frost, A., Unger, V. M., and De Camilli, P. (2009). The BAR domain superfamily: membrane-molding macromolecules. *Cells* 137, 191–196. doi: 10.1016/j.cell.2009.04.010

Garzia, A., Etxebeste, O., Herrero-García, E., Ugalde, U., and Espeso, E. A. (2010). The concerted action of bZip and cMyb transcription factors FlbB and FlbD induces brlA expression and asexual development in *aspergillus nidulans*. *Mol. Microbiol.* 75, 1314–1324. doi: 10.1111/j.1365-2958.2010.07063.x

Goode, B. L., Sweeney, M. O., and Eskin, J. A. (2018). GMF as an actin network remodeling factor. *Trends Cell Biol.* 28, 749–760. doi: 10.1016/j.tcb.2018.04.008

Guerriero, G., Silvestrini, L., Obersriebnig, M., Hausman, J. F., Strauss, J., and Ezcurra, I. (2016). A WDR gene is a conserved member of a chitin synthase gene cluster and influences the cell wall in *aspergillus nidulans*. *Int. J. Mol. Sci.* 17:1031. doi: 10.3390/ijms17071031

Gutiérrez-Escribano, P., González-Novo, A., Suárez, M. B., Li, C. R., Wang, Y., de Aldana, C. R., et al. (2011). CDK-dependent phosphorylation of Mob2 is essential for hyphal development in *Candida albicans*. *Mol. Biol. Cell* 22, 2458–2469. doi: 10.1091/mbc.E11-03-0205

Huang, M., Xu, Q., Mitsui, K., and Xu, Z. (2014). PSK1 regulates expression of SOD1 involved in oxidative stress tolerance in yeast. *FEMS Microbiol. Lett.* 350, 154–160. doi: 10.1111/1574-6968.12329

Jian, Q., Li, T., Wang, Y., Zhang, Y., Zhao, Z., Zhang, X., et al. (2019). New insights into fumonisin production and virulence of *fusarium proliferatum* underlying different carbon sources. *Food Res. Int.* 116, 397–407. doi: 10.1016/j.foodres.2018.08.053

Kirihata, M., Nakao, Y., Fukuari, M., and Ichimoto, I. (1995). Synthesis and structural confirmation of (2S,3R,4R,6E)-2-acetylamino-3-hydroxy-4-methyl-6-octenoic acid, a new amino acid produced by neocosmospora vasinfecta. *Biosci. Biotechnol. Biochem.* 59, 2228–2230. doi: 10.1271/bbb.59.2228

Kjærbølling, I., Mortensen, U. H., Vesth, T., and Andersen, M. R. (2019). Strategies to establish the link between biosynthetic gene clusters and secondary metabolites. *Fungal Genet. Biol.* 130, 107–121. doi: 10.1016/j.fgb.2019.06.001

Kulmburg, P., Sequeval, D., Lenouvel, F., Mathieu, M., and Felenbok, B. (1992). Identification of the promoter region involved in the autoregulation of the transcriptional activator ALCR in *aspergillus nidulans*. *Mol. Cell. Biol.* 12, 1932–1939. doi: 10.1128/mcb.12.5.1932-1939.1992

Lan, X., Yuan, W., Wang, M., and Xiao, H. (2019). Efficient biosynthesis of antitumor ganoderic acid HLDOA using a dual tunable system for optimizing the expression of CYP5150L8 and a *Ganoderma* P450 reductase. *Biotechnol. Bioeng.* 116, 3301–3311. doi: 10.1002/bit.27154

Lee, S., Völz, R., Song, H., Harris, W., and Lee, Y. H. (2021). Characterization of the MYB genes reveals insights into their evolutionary conservation, structural diversity, and functional roles in *Magnaporthe oryzae*. *Front. Microbiol.* 12:721530. doi: 10.3389/fmicb.2021.721530

Li, T., Fan, Y., Nambou, K., Hu, F., Imanaka, T., Wei, L., et al. (2015). Improvement of ansamitocin P-3 production by *Actinosynnema mirum* with fructose as the sole carbon source. *Appl. Biochem. Biotechnol.* 175, 2845–2856. doi: 10.1007/s12010-014-1445-6

Lin, R., Zhang, L., Yang, X., Li, Q., Zhang, C., Guo, L., et al. (2022). Responses of the mushroom *Pleurotus ostreatus* under different CO_2 concentration by comparative proteomic analyses. *J. Fungi* 8:652. doi: 10.3390/jof8070652

Liu, Y., Cerejeira Matos, R., Heino, T. I., and Hietakangas, V. (2018). PWP1 promotes nutrient-responsive expression of 5S ribosomal RNA. *Biol. Open* 7:bio037911. doi: 10.1242/bio.037911

Meyer, V. (2008). Genetic engineering of filamentous fungi--progress, obstacles and future trends. *Biotechnol. Adv.* 26, 177–185. doi: 10.1016/j.biotechadv.2007.12.001

Missall, T. A., and Lodge, J. K. (2005). Thioredoxin reductase is essential for viability in the fungal pathogen *Cryptococcus neoformans*. *Eukaryot. Cell* 4, 487–489. doi: 10.1128/EC.4.2.487-489.2005

Molnár, I., Gibson, D. M., and Krasnoff, S. B. (2010). Secondary metabolites from entomopathogenic Hypocrealean fungi. *Nat. Prod. Rep.* 27, 1241–1275. doi: 10.1039/c001459c

Nielsen, M. R., Wollenberg, R. D., Westphal, K. R., Sondergaard, T. E., Wimmer, R., Gardiner, D. M., et al. (2019). Heterologous expression of intact biosynthetic gene clusters in *fusarium graminearum*. *Fungal Genet. Biol.* 132:103248. doi: 10.1016/j.fgb.2019.103248

Ohsumi, K., Matsuda, Y., Nakajima, H., and Kitamoto, K. (2001). Cloning and characterization of the cpyA gene encoding intracellular carboxypeptidase from *aspergillus nidulans*. *Biosci. Biotechnol. Biochem.* 65, 1175–1180. doi: 10.1271/bbb.65.1175

Percudani, R., Montanini, B., and Ottonello, S. (2005). The anti-HIV cyanovirin-N domain is evolutionarily conserved and occurs as a protein module in eukaryotes. *Proteins* 60, 670–678. doi: 10.1002/prot.20543

Pessoni, R. A., Tersarotto, C. C., Mateus, C. A., Zerlin, J. K., Simões, K., de Cássia, L., et al. (2015). Fructose affecting morphology and inducing β-fructofuranosidases in *Penicillium janczewskii*. *Springerplus* 4:487. doi: 10.1186/s40064-015-1298-7

Qiu, Q. S. (2012). V-ATPase, ScNhx1p and yeast vacuole fusion. *J. Genet. Genomics* 39, 167–171. doi: 10.1016/j.jgg.2012.02.001

Qiu, S., and Zeng, B. (2019). Advances in understanding of the oxysterol-binding protein homologous in yeast and filamentous fungi. *Int. Microbiol.* 22, 169–179. doi: 10.1007/s10123-019-00056-6

Rolt, A., O'Neill, P. M., Liang, T. J., and Stachulski, A. V. (2019). Synthesis of MeBmt and related derivatives via syn-selective ATH-DKR. *RSC Adv.* 9, 40336–40339. doi: 10.1039/c9ra08256e

Rossman, A. Y., Allen, W. C., Castlebury, L. A., Spatafora, J., Romero, A. I., and Verkley, G. (2017). (2517–2519) proposals to conserve the names *Balansia claviceps* against *Ephelis mexicana*, *Claviceps paspali* against *Ustilagopsis deliquescens*, and *Tolypocladium inflatum* against *Cordyceps subsessilis* (Ascomycota: Sordariomycetes: Hypocreales). *Taxon* 66, 749–750. doi: 10.12705/663.18

Shi, L., Wang, J., Wang, X., Zhang, Y., Song, Z., Cai, M., et al. (2020). Transcriptional regulatory networks of methanol-independent protein expression in *Pichia pastoris* under the AOX1 promoter with trans-acting elements engineering. *Bioresour. Bioprocess.* 7, 1–12. doi: 10.1186/s40643-020-00306-w

Survase, S. A., Kagliwal, L. D., Annapure, U. S., and Singhal, R. S. (2011). Cyclosporin A--a review on fermentative production, downstream processing and pharmacological applications. *Biotechnol. Adv.* 29, 418–435. doi: 10.1016/j.biotechadv.2011.03.004

Tanseer, S., and Anjum, T. (2011). Modification of c and n sources for enhanced production of cyclosporin 'a' by *aspergillus Terreus*. *Braz. J. Microbiol.* 42, 1374–1383. doi: 10.1590/S1517-838220110004000019

Thompson, M. (2009). Polybromo-1: the chromatin targeting subunit of the PBAF complex. *Biochimie* 91, 309–319. doi: 10.1016/j.biochi.2008.10.019

Tong, S. M., Wang, D. Y., Gao, B. J., Ying, S. H., and Feng, M. G. (2019). The DUF1996 and WSC domain-containing protein Wsc1I acts as a novel sensor of multiple stress cues in *Beauveria bassiana*. *Cell. Microbiol.* 21:e13100. doi: 10.1111/cmi.13100

Uytterhoeven, V., Lauwers, E., Maes, I., Miskiewicz, K., Melo, M. N., Swerts, J., et al. (2015). Hsc70-4 deforms membranes to promote synaptic protein turnover by endosomal microautophagy. *Neuron* 88, 735–748. doi: 10.1016/j.neuron.2015.10.012

Wang, S., Wu, R., Lu, J., Jiang, Y., Huang, T., and Cai, Y. D. (2022). Protein-protein interaction networks as miners of biological discovery. *Proteomics* 22:e2100190. doi: 10.1002/pmic.202100190

Wawra, S., Fesel, P., Widmer, H., Neumann, U., Lahrmann, U., Becker, S., et al. (2019). FGB1 and WSC3 are in planta-induced β-glucan-binding fungal lectins with different functions. *New Phytol.* 222, 1493–1506. doi: 10.1111/nph.15711

Whitten, M. M., Tew, I. F., Lee, B. L., and Ratcliffe, N. A. (2004). A novel role for an insect apolipoprotein (apolipophorin III) in beta-1,3-glucan pattern recognition and cellular encapsulation reactions. *J. Immunol.* 172, 2177–2185. doi: 10.4049/jimmunol.172.4.2177

Wiatrowski, H. A., Van Denderen, B. J., Berkey, C. D., Kemp, B. E., Stapleton, D., and Carlson, M. (2004). Mutations in the gal83 glycogen-binding domain activate the snf1/gal83 kinase pathway by a glycogen-independent mechanism. *Mol. Cell. Biol.* 24, 352–361. doi: 10.1128/MCB.24.1.352-361.2004

Xiang, X., Osmani, A. H., Osmani, S. A., Xin, M., and Morris, N. R. (1995). NudF, a nuclear migration gene in *aspergillus nidulans*, is similar to the human LIS-1 gene required for neuronal migration. *Mol. Biol. Cell* 6, 297–310. doi: 10.1091/mbc.6.3.297

Xing, M., Chen, Y., Li, B., and Tian, S. (2021). Characterization of a short-chain dehydrogenase/reductase and its function in patulin biodegradation in apple juice. *Food Chem.* 348:129046. doi: 10.1016/j.foodchem.2021.129046

Xu, L., Guo, L., and Yu, H. (2021). Label-free comparative proteomics analysis revealed heat stress responsive mechanism in *Hypsizygus marmoreus*. *Front. Microbiol.* 11:541967. doi: 10.3389/fmicb.2020.541967

Yang, X., Feng, P., Yin, Y., Bushley, K., Spatafora, J. W., and Wang, C. (2018). Cyclosporine biosynthesis in *Tolypocladium inflatum* benefits fungal adaptation to the environment. *MBio* 9, e01211–e01218. doi: 10.1128/mBio.01211-18

Yang, X., Lin, R., Xu, K., Guo, L., and Yu, H. (2021). Comparative proteomic analysis within the developmental stages of the mushroom white *Hypsizygus marmoreus*. *J. Fungi* 7:1064. doi: 10.3390/jof7121064

Yin, Y., Yu, G., Chen, Y., Jiang, S., Wang, M., Jin, Y., et al. (2012). Genome-wide transcriptome and proteome analysis on different developmental stages of *Cordyceps militaris*. *Public Libr. Sci.* 7:e51853. doi: 10.1371/journal.pone.0051853

Yu, Y., Du, J., Wang, Y., Zhang, M., Huang, Z., Cai, J., et al. (2019). Survival factor 1 contributes the oxidative stress response and is required for full virulence of *Sclerotinia sclerotiorum*. *Mol. Plant Pathol.* 20, 895–906. doi: 10.1111/mpp.12801

Yu, H., Zhao, S., Lu, W., Wang, W., and Guo, L. (2018). A novel gene, encoding 3-aminobenzoate 6-monooxygenase, involved in 3-aminobenzoate degradation in *Comamonas sp*. strain QT12. *Appl. Microbiol. Biotechnol.* 102, 4843–4852. doi: 10.1007/s00253-018-9015-4

Zárate-Chaves, C. A., Romero-Rodríguez, M. C., Niño-Arias, F. C., Robles-Camargo, J., Linares-Linares, M., Rodríguez-Bocanegra, M. X., et al. (2013). Optimizing a culture medium for biomass and phenolic compounds production using *Ganoderma lucidum*. *Braz. J. Microbiol.* 44, 215–223. doi: 10.1590/S1517-83822013005000032

Zare, B., Sepehrizadeh, Z., Faramarzi, M. A., Soltany-Rezaee-Rad, M., Rezaie, S., and Shahverdi, A. R. (2014). Antifungal activity of biogenic tellurium nanoparticles against *Candida albicans* and its effects on squalene monooxygenase gene expression. *Biotechnol. Appl. Biochem.* 61, 395–400. doi: 10.1002/bab.1180

Zhan, Y., and Guo, S. (2015). Three-dimensional (3D) structure prediction and function analysis of the chitin-binding domain 3 protein HD73_3189 from *Bacillus thuringiensis* HD73. *Biomed. Mater. Eng.* 26 Suppl 1, S2019–S2024. doi: 10.3233/BME-151506

Zhang, K., Huang, B., Yuan, K., Ji, X., Song, P., Ding, Q., et al. (2020). Comparative transcriptomics analysis of the responses of the filamentous fungus *Glarea lozoyensis* to different carbon sources. *Front. Microbiol.* 11:190. doi: 10.3389/fmicb.2020.0019005

Zhang, X., Li, D., Zhang, H., Wang, X., Zheng, Z., and Song, F. (2010). Molecular characterization of rice OsBIANK1, encoding a plasma membrane-anchored ankyrin repeat protein, and its inducible expression in defense responses. *Mol. Biol. Rep.* 37, 653–660. doi: 10.1007/s11033-009-9507-5

Zhang, Y. J., Yang, X. Q., Zhang, S., Humber, R. A., and Xu, J. (2017). Genomic analyses reveal low mitochondrial and high nuclear diversity in the cyclosporin-producing fungus *Tolypocladium inflatum*. *Appl. Microbiol. Biotechnol.* 101, 8517–8531. doi: 10.1007/s00253-017-8574-0

Zheng, Y., Zhu, Y., Mao, X., Jiang, M., Wei, Y., Lian, L., et al. (2022). SDR7-6, a short-chain alcohol dehydrogenase/reductase family protein, regulates light-dependent cell death and defence responses in rice. *Mol. Plant Pathol.* 23, 78–91. doi: 10.1111/mpp.13144

frontiers | Frontiers in Microbiology

TYPE Original Research
PUBLISHED 16 Januray 2024
DOI 10.3389/fmicb.2023.1302236

OPEN ACCESS

EDITED BY
Ragini Bodade,
Savitribai Phule Pune University, India

REVIEWED BY
Julian Ferreras,
CONICET Institute of Subtropical Biology (IBS), Argentina
Rohit Sharma,
IES University, India

*CORRESPONDENCE
Tae-Jin Oh
✉ tjoh3782@sunmoon.ac.kr

RECEIVED 26 September 2023
ACCEPTED 21 December 2023
PUBLISHED 16 Januray 2024

CITATION
Kim B, Han S-R, Lee H and Oh T-J (2024) Insights into group-specific pattern of secondary metabolite gene cluster in *Burkholderia* genus.
Front. Microbiol. 14:1302236.
doi: 10.3389/fmicb.2023.1302236

Insights into group-specific pattern of secondary metabolite gene cluster in *Burkholderia* genus

Byeollee Kim[1], So-Ra Han[2], Hyun Lee[2,3] and Tae-Jin Oh[1,2,4]*

[1]Department of Life Science and Biochemical Engineering, Graduate School, SunMoon University, Asan, Republic of Korea, [2]Genome-Based BioIT Convergence Institute, Asan, Republic of Korea, [3]Division of Computer Science and Engineering, SunMoon University, Asan, Republic of Korea, [4]Department of Pharmaceutical Engineering and Biotechnology, SunMoon University, Asan, Republic of Korea

Burkholderia is a versatile strain that has expanded into several genera. It has been steadily reported that the genome features of *Burkholderia* exhibit activities ranging from plant growth promotion to pathogenicity across various isolation areas. The objective of this study was to investigate the secondary metabolite patterns of 366 *Burkholderia* species through comparative genomics. Samples were selected based on assembly quality assessment and similarity below 80% in average nucleotide identity. Duplicate samples were excluded. Samples were divided into two groups using FastANI analysis. Group A included *B. pseudomallei* complex. Group B included *B. cepacia* complex. The limitations of MLST were proposed. The detection of genes was performed, including environmental and virulence-related genes. In the pan-genome analysis, each complex possessed a similar pattern of cluster for orthologous groups. Group A (n = 185) had 14,066 cloud genes, 2,465 shell genes, 682 soft-core genes, and 2,553 strict-core genes. Group B (n = 181) had 39,867 cloud genes, 4,986 shell genes, 324 soft-core genes, 222 core genes, and 2,949 strict-core genes. AntiSMASH was employed to analyze the biosynthetic gene cluster (BGC). The results were then utilized for network analysis using BiG-SCAPE and CORASON. Principal component analysis was conducted and a table was constructed using the results obtained from antiSMASH. The results were divided into Group A and Group B. We expected the various species to show similar patterns of secondary metabolite gene clusters. For in-depth analysis, a network analysis of secondary metabolite gene clusters was conducted, exemplified by BiG-SCAPE analysis. Depending on the species and complex, *Burkholderia* possessed several kinds of siderophore. Among them, ornibactin was possessed in most *Burkholderia* and was clustered into 4,062 clans. There was a similar pattern of gene clusters depending on the species. NRPS_04014 belonged to siderophore BGCs including ornibactin and indigoidine. However, it was observed that each family included a similar species. This suggests that, besides siderophores being species-specific, the ornibactin gene cluster itself might also be species-specific. The results suggest that siderophores are associated with environmental adaptation, possessing a similar pattern of siderophore gene clusters among species, which could provide another perspective on species-specific environmental adaptation mechanisms.

KEYWORDS

***Burkholderia* genus, comparative genomics, biosynthetic gene cluster, pattern analysis, network analysis**

1 Introduction

Burkholderia classified in the phylum *Proteobacteria* have been isolated from various sources worldwide (Radua et al., 2000; Levy et al., 2008; Hall et al., 2015; Peddayelachagiri et al., 2016), including cystic fibrosis patients (Medina-Pascual et al., 2015) and environmental sources such as soil (Hall et al., 2015), rice (Luo et al., 2007), and lichen (Han et al., 2016). The genus *Burkholderia* was named in 1992. It initially consisted of seven pathogenic strains affecting humans, animals, and plants (Yabuuchi et al., 1992). It has been categorized into two major groups: *Burkholderia cepacia* complex (BCC) and environmental *Burkholderia* (Compant et al., 2008; Sousa et al., 2011). However, some studies have focused on the beneficial effects of *Burkholderia* in plants, leading to its reclassification into new genera such as *Paraburkholderia* or *Caballeronia* (Kaur et al., 2017). Expansion of the *Burkholderia* genus is ongoing (Euzéby, 1997; Estrada-de Los Santos et al., 2018). The multi-genus complex that includes *Paraburkholderia* and *Caballeronia* is referred to as *B. sensu lato* which encompasses *Robbsia*, *Pararobbsia*, *Burkholderia*, *Trinickia*, and *Mycetohabitans*. Species reclassified within *Burkholderia* now fall under *B. sensu lato*, which also includes *Burkholderia*. *B. sensu stricto* encompasses BCC, *Burkholderia pseudomallei* complex (BPC), and rice pathogenic *Burkholderia*.

Recent reports of *Burkholderia* have highlighted the use of genome-based classification (Jin et al., 2020), genomic diversity analysis (Gee et al., 2021), and pan-genome analysis (Lee et al., 2021). After the report on the genome-based classification of BCC, the taxonomic position of the inherent Taxon K has been reevaluated (Vanlaere et al., 2009). Recent reports have focused on the reclassification and comparison analysis of genomics due to the registration of various genomes in databases. It is possible to study genome-based classification as well as secondary metabolites (Bach et al., 2022a) and evolutionary comparisons (Yu et al., 2006).

In the multi-genus complex known as *Burkholderia sensu lato*, antimicrobial compounds have been reported (Petrova and Mahenthiralingam, 2022; Rodríguez-Cisneros et al., 2023). This study primarily compiles the antimicrobial compounds identified in *Burkholderia*. Research in the field of discovery has progressed, including studies of new antimicrobial secondary metabolites associated with *Burkholderia*, and antimicrobial secondary metabolites are related to taxonomy (Depoorter et al., 2016; Deng et al., 2023). In *Burkholderia*, a wide range of natural products have been reported, including antimicrobial compounds and metabolites related to biocontrol and agriculture (Sulochana et al., 2014; Esmaeel et al., 2016, 2018; Kunakom and Eustáquio, 2019). For example, the antimicrobial compound bactobolin has been identified in *Burkholderia thailandensis* E264 (Seyedsayamdost et al., 2010). In addition, siderophores known for their roles in plant growth promotion have been detected in pathogenic *Burkholderia*.

Despite ongoing genomic and metabolite studies on *Burkholderia*, studies on *B. sensu stricto* have been limited and treated as a secondary aspect within the broader context of *B. sensu lato* study. In this study, we aimed to understand the characteristics of BCC and BPC complexes within *B. sensu stricto*. Different from previous studies focusing on the prevalence of BGCs according to individual genera within *B. sensu lato* (Mullins and Mahenthiralingam, 2021), we conducted a more detailed analysis of BGCs within *Burkholderia*, considering species variations. Furthermore, we aimed to uncover the interrelationships among different species and metabolites through network analysis.

2 Materials and methods

2.1 Preparation of *Burkholderia* genome

Complete genome sequences of 458 *Burkholderia* available in the NCBI genome database were downloaded on 17 February 2023 (Benson et al., 2017). Duplicated assemblies were removed prior to analysis. Information about strain isolation was searched in the database at NCBI (Barrett et al., 2012) and ENA (Cummins et al., 2022). Samples were categorized into three groups: none (unknown sample), PATH (pathological sample), and ENV (environmental sample) based on isolation information. We confirmed validated *Burkholderia* species in the LPSN database (Parte et al., 2020). The assembly quality of these genomes was determined using CheckM (Parks et al., 2015) and QUAST v5.2.0 (Gurevich et al., 2013) with default parameters. Assemblies were selected based on criteria of at least 90% completeness, less than 10% contamination, and a calculated value of completeness minus 5 times contamination greater than 50%. For further analysis, all genomes were annotated with prokka using default parameters (Seemann, 2014).

2.2 Phylogenomic analysis

Average Nucleotide Identity (ANI) was analyzed using FastANI (Jain et al., 2018) with default settings (K-mer size = 16, threads count for parallel execution = 1, fragment length default = 3,000). We analyzed multiple genomes using a genome list with command options of "—ql" and "--al." For visualization, we used "-matrix" command. For subsequent analysis, genomes with over 80% similarity were selected using FastANI. We visualized ANI results as a heatmap using ggplot2 package in R (Wickham, 2016). Referring to the study of Wallner et al. (2019), we analyzed genes listed as environmental-related genes (*nthAB*, *oxd*, *lipA*, *faeB*, *prnA-D*, and *uxaAB*) and human virulence genes (*clab*, *adhA*, *esnR*, *amil*, *ccil*, *cciR*, *opcl*, *kdgR*, *baiE*, *taruX*, *xsc*, *telA*, *terCEF*, *narG-J*, *narLM*, *narX*, and *lxa*) using blastp (Camacho et al., 2009).

2.3 Pan-genome analysis

Pan-genome and core-genome were analyzed using PEPPAN (Zhou et al., 2020). Prokka results in ".gff" file format were compiled for pan-genome analysis. PEPPAN uses a reference-based approach to generate an alignment for each gene group, which is then used to reconstruct a neighbor-joining gene tree using RapidNJ. In the case of PEPPAN results, ".gff" files were created as results. We generated them using "PEPPAN_parser." Results of the "PEPPAN_parser" displayed summaries, curve information, and gene presence-absence. We used curve information for visualization with a law model (Tettelin et al., 2008). All these processes were performed for group A and group B separately. The pan-genome value, referred to as gamma, was calculated using the Heaps' law model (Lü et al., 2010). Values of pan-genome and core-genome were calculated as alpha using the Power law model (Tettelin et al., 2008). We analyzed orthologues of core-genes and pan-genes using the web version of EGGNOG-mapper v2.1.9 (Cantalapiedra et al., 2021). Clusters of Orthologous Groups (COGs) results were visualized and preprocessed using R. We excluded no-detected COGs and duplicated COGs.

2.4 Secondary metabolite gene cluster analysis

Gene cluster analysis was conducted using the local version of antiSMASH (Blin et al., 2019) with command options of "--mibig." To visualize the results of antiSMASH, we conducted PCA based on BGC composition. We measured covariance and used scaled data for PCA analysis. These analyses obtained eigenvalues and eigenvectors using scikit-learn in Python. We visualized PCA data using Matplotlib (Hunter, 2007).

2.5 Network analysis in BGCs

Advanced analysis was performed using antiSMASH with the "--cc-mibig" command for comparison with the MIBiG database (Terlouw et al., 2023). For a more detailed analysis of BGCs, output results from antiSMASH were subjected to network and phylogeny analyses using BiG-SCAPE and CORASON (Navarro-Muñoz et al., 2020). We collected genes involved in BGCs already known and present in antiSMASH results. These genes were confirmed using blastp. We extracted the results of antiSMASH and information about similar gene clusters in MIBiG using Python. Gene clusters found to be similar to reference gene clusters were labeled in the network analysis. BiG-SCAPE offers advantages for conducting large-scale analyses and predicting domains using the pfam database (Mistry et al., 2021) and hmmscan from HMMER (Mistry et al., 2013). The process starts with calculating sequence similarity, followed by measuring pairwise distances between BGCs using sequence similarity. Network analysis was visualized using Cytoscape v3.10.0 (Shannon et al., 2003). Gene cluster visualization and comparison were conducted using Easyfig v2.2.5 (Sullivan et al., 2011).

2.6 Statistical analysis

Statistical analysis for the basic genome was performed using QUAST and tabulated. We conducted a Kruskal-Wallis test and *post hoc* Dunn test for multiple comparisons between species. Results were visualized using ggplot2. Pan-genome analysis was conducted using Heaps' law and Power law model for each Gamma value and Kappa value to check significant differences using PEPPAN. To compare genome features, we performed statistical analysis using Mann–Whitney in R. For group comparisons, we used the Mann–Whitney test. Data were visualized using the ggbetweenstats package in R.

3 Results and discussion

3.1 Curation and reclassification of genomic dataset

To ensure data integrity, we implemented two exclusion criteria. Firstly, we removed duplicated samples sourced from NCBI. Additionally, we excluded samples that did not meet the criteria after assessing their completeness and contamination using CheckM. To accurately analyze species of *Burkholderia*, the frequent occurrence of genus expansion, as reported in *Burkholderia*, was considered (Lin et al., 2020). We excluded samples with an ANI value below 83%, following the recommendation provided in the reference of fastANI. We excluded samples based on fastANI analysis, where species with ANI values below 83% were considered inter-species. This distinction was explained by Konstantinidis and Tiedje (2005), who confirmed that an ANI value above 94% corresponded to a DNA–DNA hybridization of around 70%. Excluded samples based on these results were documented in Supplementary Table 1. Species displaying ANI values lower than 83% included *B. glumae*, *B. gladioli*, and *B. plantarii* known to be plant pathogens belonging to *B. sensu stricto* (Kim et al., 2021; Bach et al., 2022b). *B. glumae*, *B. gladioli*, and *B. plantarii* are known as rice pathogenic bacteria belonging to *B. sensu stricto*. According to Bach et al. (2022b), *B. sensu stricto* shared a low number of conserved genes with *Burkholderia* spp. and BCC.

A total of 366 assembly samples were processed for a subsequent study, and samples were well divided by BCC and BPC. A total of 366 strains were validated by *Burkholderia* in the LPSN database. These samples were confirmed as contigs, total length, GC contents, and N50 using QUAST. We computed statistics for each species. The results are summarized in Table 1. The information for all samples is also included in Supplementary Table 2. The average values were 2.7 contigs, with a 7.18 Gb total length, and 67.43% GC content with a mean and average N50 length of 3.62 Gb. We confirmed 30 types of species, which contained BCC and BPC (Vanlaere et al., 2008; Price et al., 2013; Beukes et al., 2017; Tuanyok et al., 2017; Depoorter et al., 2020; Hall et al., 2022; Morales-Ruíz et al., 2022). The total length and GC contents were compared for species using the Kruskal-Wallis test in R (value of $p < 2.2e-16$; Figure 1). Genome sizes of *Burkholderia* were observed to range from a minimum of 5.2 Gb to a maximum of 9.4 Gb. GC contents ranged from 66% to 69%. Statistically significant variations of genome features were also detected among the species. In the *post hoc* Dunn test, if the value of p was less than or equal to alpha/2 (where alpha = 0.05), the null hypothesis was rejected. We visualized the length of the genome and GC content of species showing significant differences, along with their corresponding p-values as shown in Figure 1.

3.2 Phylogenomic analysis for BCC and BPC

We calculated pairwise ANI for 366 *Burkholderia* species (Figure 2A). Based on ANI analysis results, the 366 *Burkholderia* species were divided into two groups denoted as group A and group B. Group A included *B. humptydooensis*, *B. mallei*, *B. mayonis*, *B. oklahomensis*, *B. pseudomallei*, *B. savannae*, *B.* sp., and *B. thailandensis*. The group B were contained *B. aenigmatica*, *B. ambifaria*, *B. anthina*, *B. arboris*, *B. cenocepacia*, *B. cepacia*, *B. contaminans*, *B. diffusa*, *B. dolosa*, *B. lata*, *B. latens*, *B. metallica*, *B. multivorans*, *B. orbicola*, *B. pseudomultivorans*, *B. pyrrocinia*, *B. seminalis*, *B.* sp. *B. stabilis*, *B. stagnalis*, *B. territorii*, *B. ubonensis*, and *B. vietnamiensis*. The high similarity observed between *B. pseudomallei* and *B. mallei* in ANI results was consistent with merging results reported by Wallner et al. (2019). To determine differences between groups, the Mann–Whitney test was used for comparisons of contigs, length, GC contents, and N50 (Figure 2). Group B contained BCC such as *B. cepacia*, *B. multivorans*, *B. cenocepacia*, and *B. stabilis* (Lipuma, 2005). *Burkholderia* species with similarities over 99% were reclassified as similar species (Supplementary Table 3).

10.3389/fmicb.2023.1302236

TABLE 1 The overview of genomic features of *Burkholderia* species analyzed in this study.

Species*	Complex	Groups	Contig	Total length	GC contents	N50
Aenigmatica (*n* = 1)	*B. cepacia* complex	B	4.00 ± 0	9,449,413 ± 0	65.76 ± 0	3,713,971 ± 0
Ambifaria (*n* = 8)	*B. cepacia* complex	B	4.00 ± 1.22	7365060.75 ± 408939.05	66.66 ± 0.12	2829706.75 ± 253148.89
Anthina (*n* = 2)	*B. cepacia* complex	B	3.50 ± 1.50	7456936.50 ± 1000436.50	66.32 ± 0.04	3,275,428 ± 189,422
Arboris (*n* = 1)	*B. cepacia* complex	B	3.00 ± 0	8,573,812 ± 0	66.81 ± 0	3,525,317 ± 0
Cenocepacia (*n* = 27)	*B. cepacia* complex	B	3.40 ± 0.95	7745151.70 ± 476253.71	66.97 ± 0.24	3534080.51 ± 1286195.86
Cepacia (*n* = 20)	*B. cepacia* complex	B	3.10 ± 0.88	8189106.85 ± 659640.25	66.72 ± 0.17	3646257.55 ± 735245.99
Contaminans (*n* = 14)	*B. cepacia* complex	B	4.71 ± 1.22	8689272.71 ± 352361.14	66.23 ± 0.19	3238472.92 ± 61459.58
Diffusa (*n* = 1)	*B. cepacia* complex	B	3.00 ± 0	6,857,833 ± 0	66.47 ± 0	2,619,120 ± 0
Dolosa (*n* = 5)	*B. cepacia* complex	B	3.00 ± 0	6366878.2 ± 85622.97	66.99 ± 0.03	3407799.8 ± 1529.98
Humptydooensis (*n* = 1)	*B. pseudomallei* complex	A	3.00 ± 0	7,286,661 ± 0	67.14 ± 0	4,068,027 ± 0
Lata (*n* = 3)	*B. cepacia* complex	B	3.00 ± 0	8606041.66 ± 183289.35	66.32 ± 0.13	3560107.33 ± 131784.60
Latens (*n* = 3)	*B. cepacia* complex	B	3.66 ± 0.47	6289637 ± 424512.37	66.33 ± 0.04	3297008.66 ± 46764.47
Mallei (*n* = 27)	*B. pseudomallei* complex	A	1.96 ± 0.18	5702122.44 ± 137978.69	68.45 ± 0.03	3606983.29 ± 402520.32
Mayonis (*n* = 2)	*B. pseudomallei* complex	A	2.00 ± 0	6974222 ± 383308	66.36 ± 0.10	4,139,371 ± 300,571
Metallica (*n* = 1)	*B. cepacia* complex	B	3.00 ± 0	7,424,240 ± 0	67.09 ± 0	2,967,116 ± 0
Multivorans (*n* = 50)	*B. cepacia* complex	B	3.30 ± 0.64	6518391.70 ± 277268.32	67.12 ± 0.14	3356319.24 ± 238452.50
Oklahomensis (*n* = 3)	*B. pseudomallei* complex	A	2.00 ± 0	7257963.33 ± 87095.28	66.97 ± 0.06	4172494.66 ± 28808.71
Orbicola (*n* = 1)	*B. cepacia* complex	B	3.00 ± 0	7,971,389 ± 0	66.60 ± 0	3,213,911 ± 0
Pseudomallei (*n* = 128)	*B. pseudomallei* complex	A	2.11 ± 0.36	7226784.58 ± 150066.83	68.09 ± 0.15	4026508.67 ± 87456.08
Pseudomultivorans (*n* = 1)	*B. cepacia* complex	B	3.00 ± 0	7,956,789 ± 0	67.30 ± 0	4849929 ± 0
Pyrrocinia (*n* = 5)	*B. cepacia* complex	B	3.20 ± 0.40	7963581.20 ± 323,679.78	66.42 ± 0.10	3190692.6 ± 154980.73
Savannae (*n* = 2)	*B. pseudomallei* complex	A	3.00 ± 0	7,254,364 ± 173,191	67.18 ± 0.13	4,153,083 ± 75,195
Seminalis (*n* = 2)	*B. cepacia* complex	B	3.00 ± 0	7,835,640 ± 186,696	67.16 ± 0.13	3,031,317 ± 18,819
Burkholderia sp. (*n* = 18)	-	B	3.44 ± 0.76	7607546.66 ± 607,666.25	66.68 ± 0.46	3127340.5 ± 532685.47
Stabilis (*n* = 2)	*B. cepacia* complex	B	3.00 ± 0	8124525.50 ± 403,421.50	66.56 ± 0.14	3241054.5 ± 77825.5
Stagnalis (*n* = 1)	*B. cepacia* complex	B	3.00 ± 0	7,583,807 ± 0	67.65 ± 0	3,001,569 ± 0
Territorii (*n* = 1)	*B. cepacia* complex	B	3.00 ± 0	6,902,370 ± 0	66.73 ± 0	2,466,714 ± 0
Thailandensis (*n* = 19)	*B. pseudomallei* complex	A	2.15 ± 0.36	6746841.73 ± 128903.21	67.63 ± 0.10	3844628.42 ± 80,387.98
Ubonensis (*n* = 7)	*B. cepacia* complex	B	3.42 ± 0.49	7486224.85 ± 453586.04	67.11 ± 0.21	3105116.71 ± 511667.56
Vietnamiensis (*n* = 10)	*B. cepacia* complex	B	4.00 ± 1.48	7011401.40 ± 472445.79	66.85 ± 0.39	2609459.4 ± 992678.91

It is represented average values and standard deviations of genome features. The number of samples for each species is indicated by notation (such as *n* = 1).

We visualized the data using Minimum Spanning Tree analysis based on curated MLST genes for *Burkholderia*, which included *aptD*, *gltB*, *gyrB*, *recA*, *lepA*, *phaC*, and *trpB* known in BCC, as well as *ace*, *gltB*, *gmhD*, *lepA*, *lipA*, *narK*, and *ndh* known in *B. mallei* and *B. pseudomallei*. However, no notable peculiarities or distinctive patterns were identified (Supplementary Figure 1). Following the findings of Mullins et al. (2019), who concluded the possibility of expandability due to the limitations of curated genes, we collected genes and visualized their presence using BLAST analysis (Supplementary Table 4). However, selected genes did not separate each isolation, species, or group. Genes obtained from the Uniprot database included virulence-related genes (such as adhA, kdgR, narG, narH, narX, telA, terC, xsc, and amiI) and environmental-related genes including oxd, PrnA, prnC, PrnD, and uxaA. We constructed a

10.3389/fmicb.2023.1302236

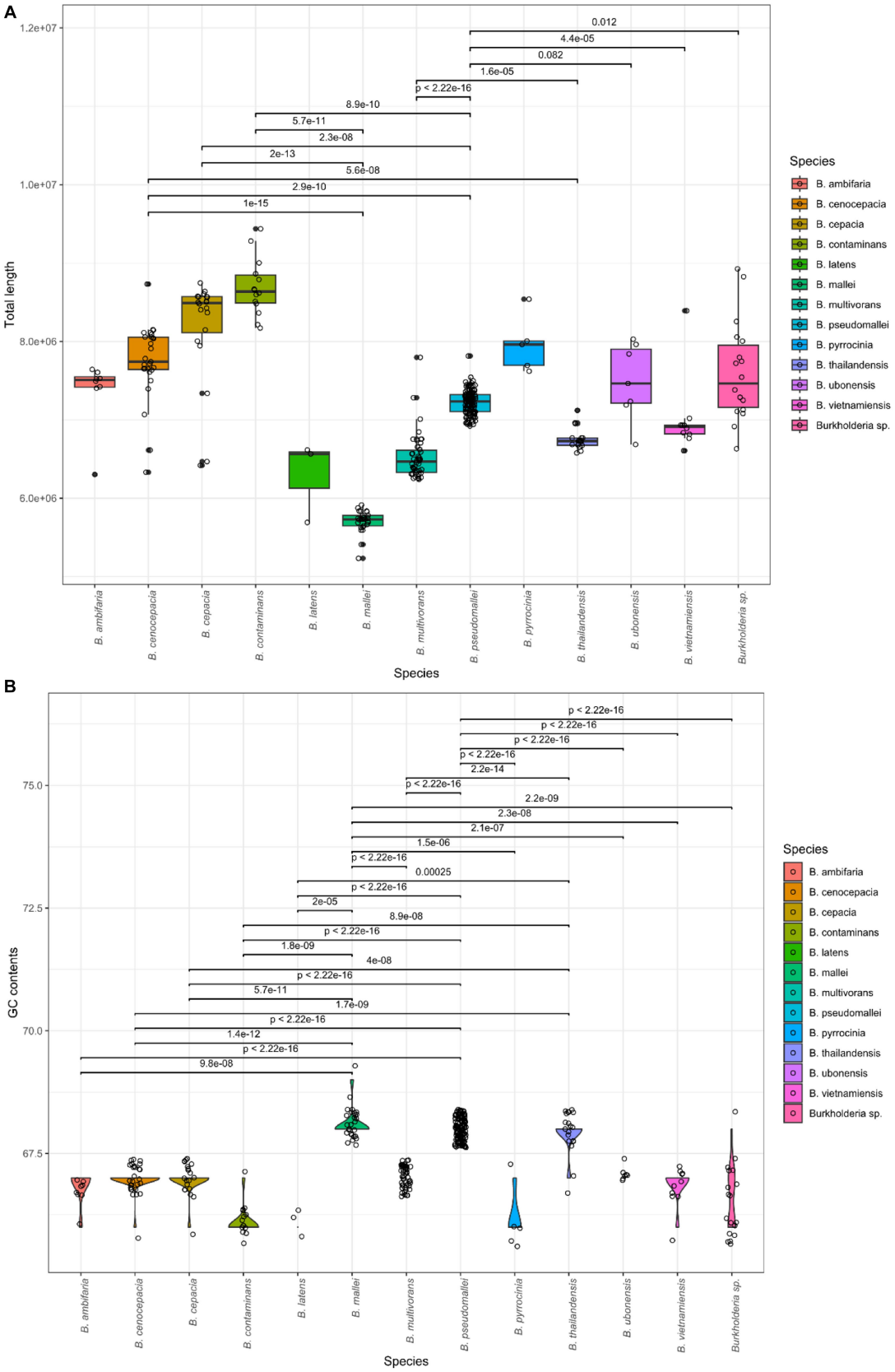

FIGURE 1
Comparison of genomic features in *Burkholderia* spp. **(A)** Average total length per species. **(B)** Average GC content per species.

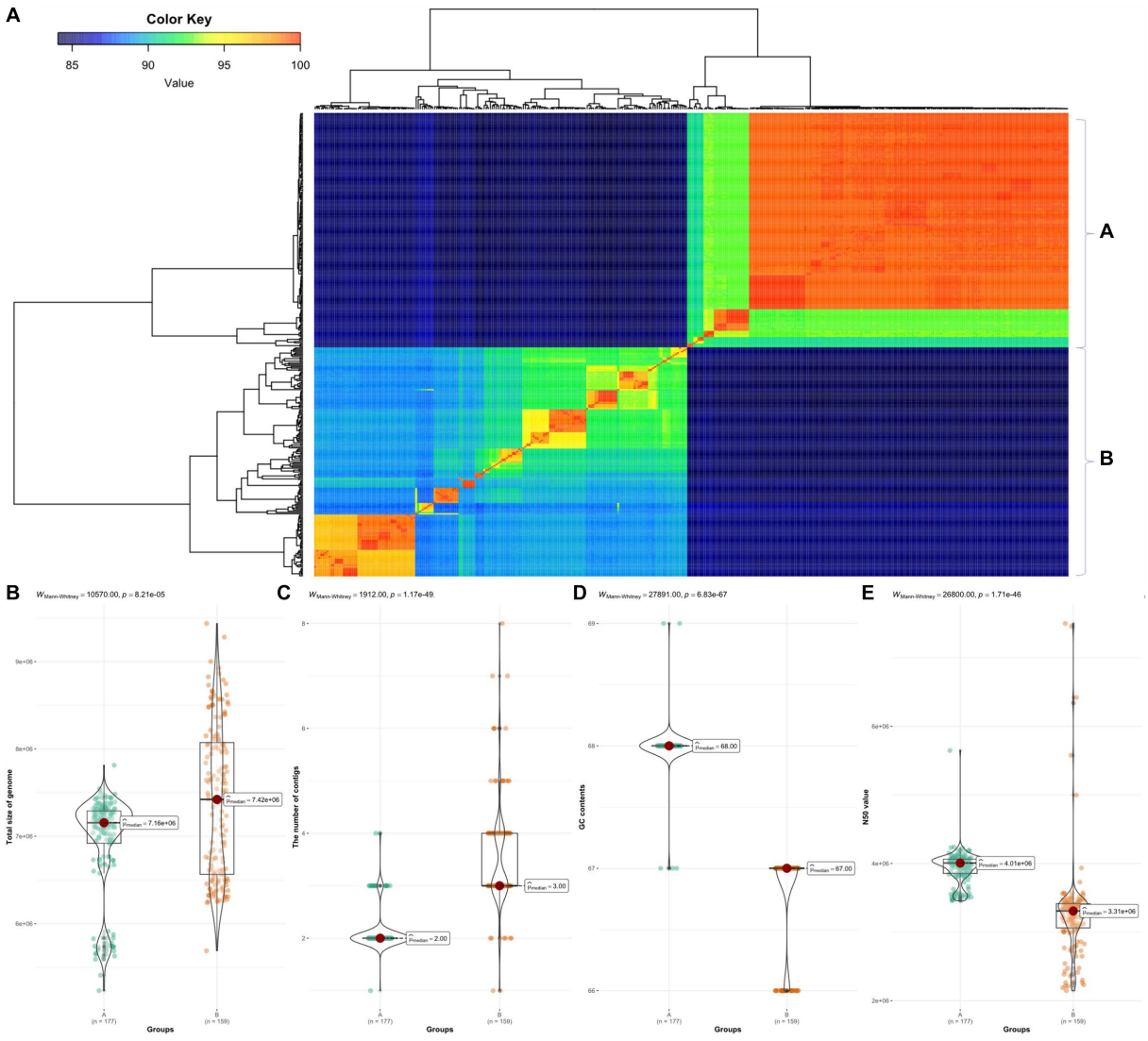

FIGURE 2
ANI in 366 *Burkholderia* spp. **(A)** ANI results using fastANI visualized using ggplot2. We divided samples into groups A and B. **(B)** Comparison of total length between group A and group B. **(C)** Comparison of contigs between group A and group B. **(D)** Comparison of GC contents between group A and group B. **(E)** Comparison of N50 between group A and group B. All comparisons were visualized using ggbetweenstats package in R.

database with these acquired genes and confirmed them using blastp. Results did not match the separation information recorded in NCBI or ENA. However, it was important to note that confirmed genes varied by species, indicating that these genes could serve as additional factors for confirming species, addressing limitations of MLST with only BCC, *B. mallei*, and *B. pseudomallei* available in pubMLST. The distinction between pathogenic and non-pathogenic strains can be confirmed by the presence of virulence factors. Taxonomic analysis may not serve as a clear indicator of their pathogenic potential. In comparative genomics studies, it remains a challenge to determine a suitable indicator for phenotypic characteristic analysis (Eberl and Vandamme, 2016). Investigating pathogenicity and non-pathogenicity is not straightforward.

While we cannot specifically discriminate individual species, our results suggest that for group B, which comprises species belonging to BCC, it would be possible to determine whether the target species is part of the BCC or not. Genomes of *Burkholderia* used in this study displayed significant similarity in cases where samples were obtained from the same hospital, which led to time-consuming analyses. Therefore, we propose that *Burkholderia* is the most valuable sample for making a pangenome graph (Hickey et al., 2023). By clustering samples and excluding similar regions, it would be possible to create a pangenome graph for comparison not only within *Burkholderia*, but also for a broader range of *B. sensu lato* and other related microorganisms.

3.3 Pan-genome analysis for each group of *Burkholderia*

We compared genomic patterns among 366 species of *Burkholderia* which were collected from NCBI. Prokka analysis was performed using species of *Burkholderia*, while pan-genome and core-genome analyses were performed using PEPPAN with the

Prokka output (Figure 3). In group A ($n = 185$) we observed, 14,066 cloud genes, 2,465 shell genes, 682 soft-core genes, and 2,553 strict-core genes (Figure 3A). The pan-genome results of group A of *Burkholderia* showed 18.53% of total core genes. Group A was confirmed to have 5,770 genes per genome with 20,292 pan-genes and 2,553 core-genes. In group A, Heaps' law showed a Gamma value of 0.289 ± 0.002 and a Kappa value of 4493.245 ± 46.171. In the Power law model, an Alpha value of 0.638 ± 0.013 and a Kappa value of 964.425 ± 32.586 were observed. The power law model for core genomes showed an Alpha value of 0.149 ± 0.001 and a Kappa value of 5591.983 ± 20.623. In the results for group B ($n = 181$), 39,867 cloud genes, 4,986 shell genes, 324 soft-core genes, 222 core genes, and 2,949 strict-core genes were observed (Figure 3B). Ran-genome results for group B of *Burkholderia* showed 7.22% of total core genes. In group B, Heaps' law showed a Gamma value of 0.389 ± 0.001 and a Kappa value of 6444.550 ± 30.636. In the Power law model, an Alpha value of 0.629 ± 0.003 and a Kappa value of 2719.814 ± 21.208 were observed. The power law model for core genomes showed an Alpha value of 0.099 ± 0.007 and a Kappa value of 4795.235 ± 131.235. Strict core genes showed 100% similarity, while core genes showed similarities ranging from over 99% to less than 100%. Soft-core genes showed similarities ranging from over 95% to less than 99%. Genes with similarities ranging from 0% to 15% were classified as cloud genes. Those with similarities ranging from 15% to 95% were categorized as shell genes. Pangenomes in both groups showed Alpha values under one. The pan-genome analysis of *Burkholderia* began in 2009, where 56 species of *Burkholderia* were found to possess 4,000 genes, with a core-genome consisting of 1,000 genes (Ussery et al., 2009). Subsequently, Bochkareva et al. (2018) analyzed 127 *Burkholderia* species using the micropan tool in the R environment. They conducted an analysis employing the binomial mixture model and Chao's lower bound. In this study, we attempted to conduct pan-genome analysis using the micropan tool, similar to previous research methods. However, we were unable to complete the analysis due to insufficient computer performance. Because of the large number of samples, we divided our samples into group A and group B based on ANI results. For pan-genome analysis, we utilized PEPPAN, which employs representative genes obtained through clustering to expedite the analysis process. When comparing our research findings to those of Bach et al. (2022a), we observed

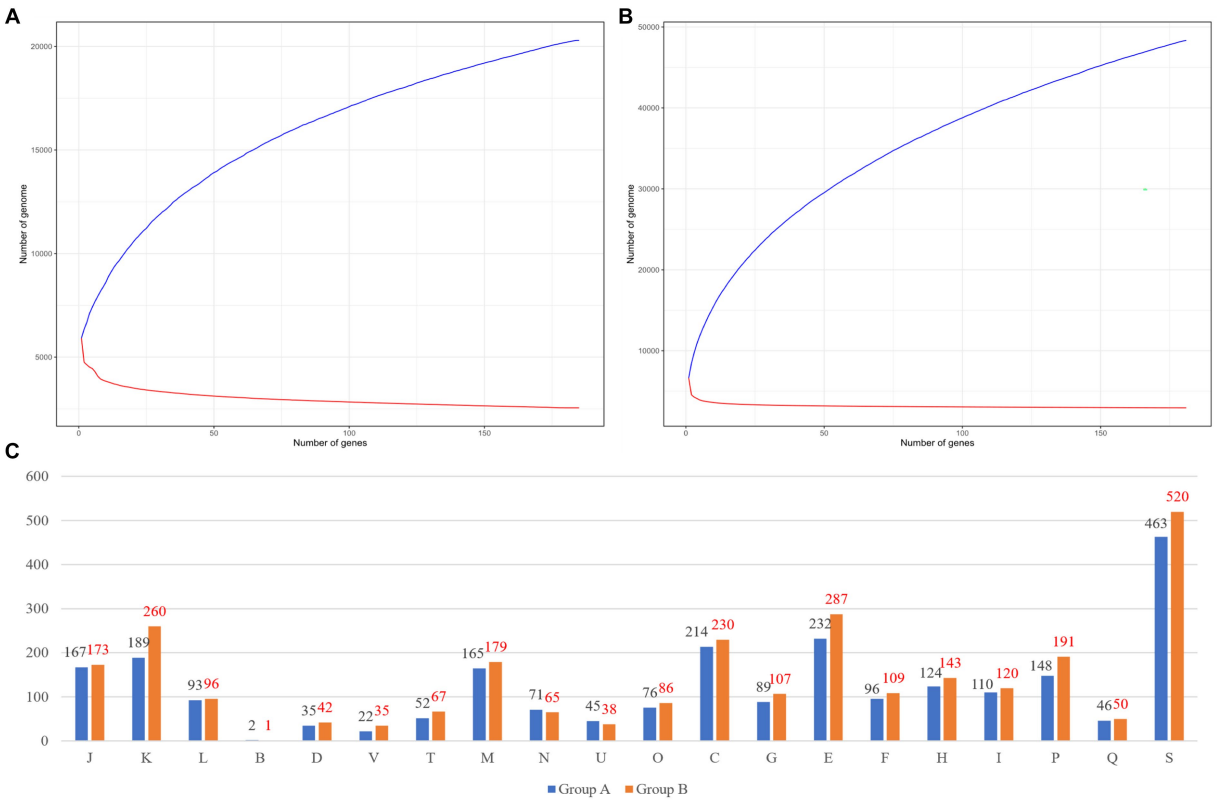

FIGURE 3
Pan-genome results of each group. **(A)** Group A's pan-genome and core-genome results. **(B)** Group B's pan-genome and core-genome results. **(C)** Differences between group A and group B. The number of COGs in group A is indicated by a black color and the number of COGs in group B is indicated by a red color. COGs categories are as follows: J, translation, ribosomal structure and biogenesis; (A), RNA processing and modification; (K), transcription; (L), replication, recombination, and repair; (B), chromatin structure and dynamics; D, cell cycle control, cell division, and chromosome partitioning; Y, nuclear structure; V, defense mechanisms; T, signal transduction mechanisms; (M), cell wall/membrane/envelope biogenesis; (N), cell motility; (Z), cytoskeleton; (W), extracellular structures; (U), intracellular trafficking, secretion, and vesicular transport; O, posttranslational modification, protein turnover, and chaperones; (X), mobilome, prophages, and transposons; C, energy production and conversion; G, carbohydrate transport and metabolism; E, amino acid transport and metabolism; F, nucleotide transport and metabolism; H, coenzyme transport and metabolism; I, lipid transport and metabolism; P, inorganic ion transport and metabolism; Q, secondary metabolites biosynthesis, transport, and catabolism; R, general function prediction only; and S, function unknown.

that group B, which included BCC, showed a slightly higher number of 2,949 strict core genes compared to ROARY results.

Ortholog analyses of core genes in group A and group B were performed using eggNOG. We visualized COGs. We analyzed functional annotations for 2,553 core-genes from group A. We visualized the results of COGs with both group A and group B (Figure 3C). Most differences were shown in V (37%) and K (27%), respectively. Pan-genome analyses have been steadily conducted for diverse *Burkholderia* species based on genomics of *B. contaminans* (Kim et al., 2023) or *B. cepacia* (Ahmad and Azam, 2020; which showed similar results with ours) and BCC classification (Jin et al., 2020). Recently, Bach et al. (2022b) reported a pan-genome focused study that analyzed not only BCC but also *B. sensu lato* and *B. sensu stricto*. Through pan-genome analysis, Lood et al. (2021) confirmed patient diversity using genomics. The present study has identified unique attributes exclusive to *Burkholderia* using a pattern analysis of BGCs based on a comparison between BCC and BPC of *Burkholderia*. Our results provide unique insights and can be used to perform further genome analysis for pathogenic *Burkholderia*.

3.4 Analysis of BGC

Using antiSMASH, this study detected and categorized 6,666 BGCs belonging to 113 kinds of BGCs and 30 classes including polyketide synthase (PKS), terpene, and siderophore. We analyzed BGCs using PCA (Figure 4A). During the process of visualizing PCA results, we examined both environmental and pathological samples. However, no significant differences were observed. Instead, PCA results revealed a more distinct separation based on species and groups (data not shown).

When visualizing the results of PCA for each species, we observed distinct clusters corresponding to *B. pseudomallei* and *B. mallei*. *B. pseudomallei* was the most frequently analyzed species with 128 samples, which might have influenced PCA results, showing a distinct clustering. Despite the high similarity observed between *B. pseudomallei* and *B. mallei* in ANI results, they exhibited clear separation in the PCA analysis (Supplementary Figure 2). Investigation of 366 *Burkholderia* strains revealed an average of 17 BGCs per strain. *B. latens* AU0505 was found to possess 7 BGCs, while *B. pseudomallei* 1710b, *B. pseudomallei* BSR, *B. pseudomallei* 406e, and *B. mayonis* BDU8 were found to harbor 26 BGCs each. In this study, we calculated the number of BGCs in each species. BCC and BPC showed higher numbers of candidate BGCs than previously known BGCs (Mullins and Mahenthiralingam, 2021; Figure 4B). We found three novel BGCs from *B. cenocepacia* J2315, *B. pseudomallei* 3,000,047,530, and *B. pyrrocinia* MS455. A study on genomic diversity and metabolic capabilities of *B. sensu lato*, has found that *Burkholderia* possesses a more diverse set of BGCs than other genera (Mullins and Mahenthiralingam, 2021; Petrova and Mahenthiralingam, 2022). Alam et al. (2021) have also confirmed genome mining of BGCs in *Burkholderia* including *B. latens*, *B. cenocepacia*, *B. cepacia*, *B. ambifaria*, and *B. lata*. Our study showed similar patterns of BGC possession and confirmed novel species recently assigned to BCC and BPC.

Based on these results, we hypothesized that there would be distinct metabolite patterns depending on the species of *Burkholderia*. BiG-SCAPE results were then subjected to network analysis, categorizing antiSMASH outcomes into NRPS, terpene, PKSI, RiPPs, PKSother, PKS-NRPS hybrids, and others (Figure 5; Supplementary Table 5). A total of 192 types of BGCs were found and compared with the MiBIG database (Supplementary Tables 6, 7). Two types of alkaloids, 48 types of NRPS (including one kind of NRPS-alkaloid and 13 kinds of NRPS-polyketide BGCs), 30 kinds of polyketide, 28 kinds of RiPP, 12 kinds of saccharide, 17 kinds of terpene, and 55 BGCs of others were found. We confirmed the most popular 667 terpene-related BGCs known as carotenoids-related BGCs from *Myxococcus xanthus*. We found 44 novel BGCs in distinct samples. These novel BGCs contained 13 other BGCs classes and followed polyketide. For each BGC, known compounds were compiled and core gene information was organized to detect gene clusters (Table 2; Liu and Cheng, 2014; Kunakom and Eustáquio, 2019) and undertake a more detailed analysis, described below.

3.5 Pattern analysis for NRPS and PKS

The NRPS network yielded 2,345 BGCs with 138,894 links and 118 families, including 28 singletons. Many compounds have been reported in *Burkholderia*. The following compounds were identified in NRPS gene clusters: valdiazen, glidopeptin A, rhizomide A, occidiofungins, fragin, sulfazecin, and icosalide A/B. PKSI network yielded 459 BGCs with 22,730 links, and 30 families, including 7 singletons. PKSother network showed 642 BGCs, 33,515 links, 48 families, and 15 singletons. The network of PKS-NRPS hybrids yielded 524 BGCs with 29,440 links and 31 families, including 6 singletons. PKS-NRPS hybrid BGCs could be categorized as follows based on their gene cluster types: NRPS-T1PKS, PKS-NRPS, and transAT-PKS. Network analysis was visualized with reference gene clusters (Figure 6). We found 44 types of BGCs, and BGCs were known from *Burkholderia, Paraburkholderia,* and *Pseudomonas*. In the network analysis, we visualized the node as the sample species and the edge as the link between samples. Each node color indicates a species. We visualized the reference for BGC from the MiBIG database in each dependent network. We grouped each clan based on the results of BiG-SCAPE. In the results of network analysis, some BGCs were calculated in the part of PKS-NRPS hybrid, NRPS, and PKSother. We visualized the main clans in NRPS, PKS-NRPS hybrid, PKSI, and PKSother. We also visualized BGCs known as *Burkholderia*-related species such as *Paraburkholderia* and *Pseudomonas*. Although network analyses of BGCs through genome mining and broader global analyses have been reported in previous studies, only *B. ambifaria* has been found to focus on the secondary metabolite (Mullins et al., 2019).

Clan members within NRPS_05113 were confirmed to include BGC0002071, BGC0001758, BGC0001131, and BGC0001128, which are known to generate virginiafactin, rhizomide A, ambactin, and luminmide, respectively. The similarity between each BGC was visualized using Easyfig. Reference BGCs identified in each network were compared and visualized as shown in Figure 6. The representative compounds identified in each clan are also indicated. Although the comparison of BGCs between BCC and the BPC was based on gene cluster similarity analysis and network analysis, a greater diversity of BGCs was observed than anticipated. Similar BGCs were also identified in other plant species, fungi, and beyond *Burkholderia*. These unique BGC-specific features across different species have

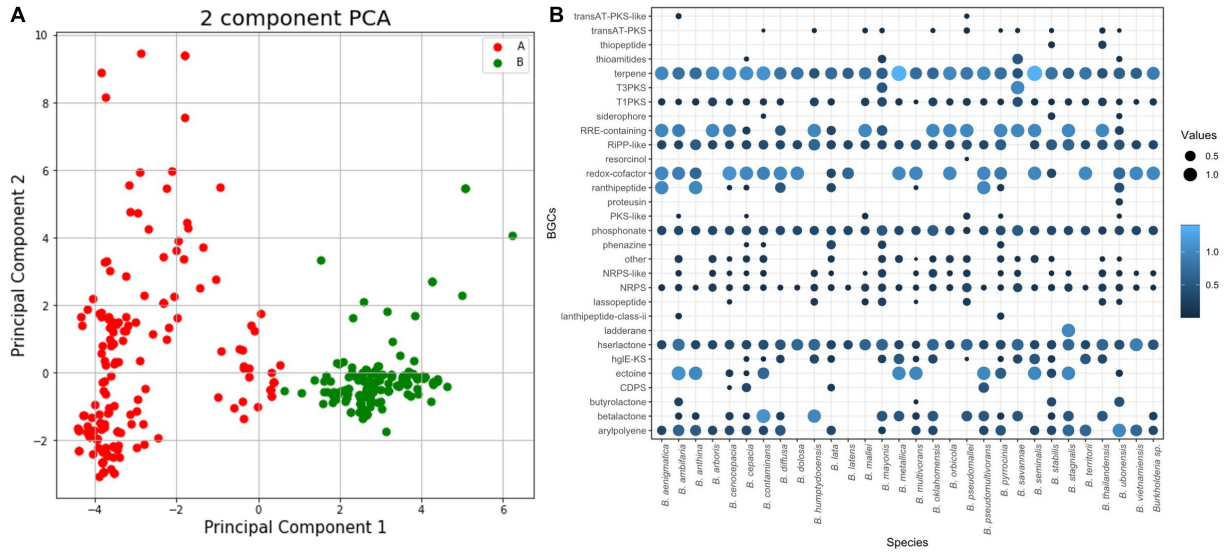

FIGURE 4
BGC analysis for 366 *Burkholderia* spp. **(A)** AntiSMASH results of *Burkholderia* spp. We visualized BGCs in each species and combined similar BGCs in one group. **(B)** PCA analysis using antiSMASH results matrix and color by groups.

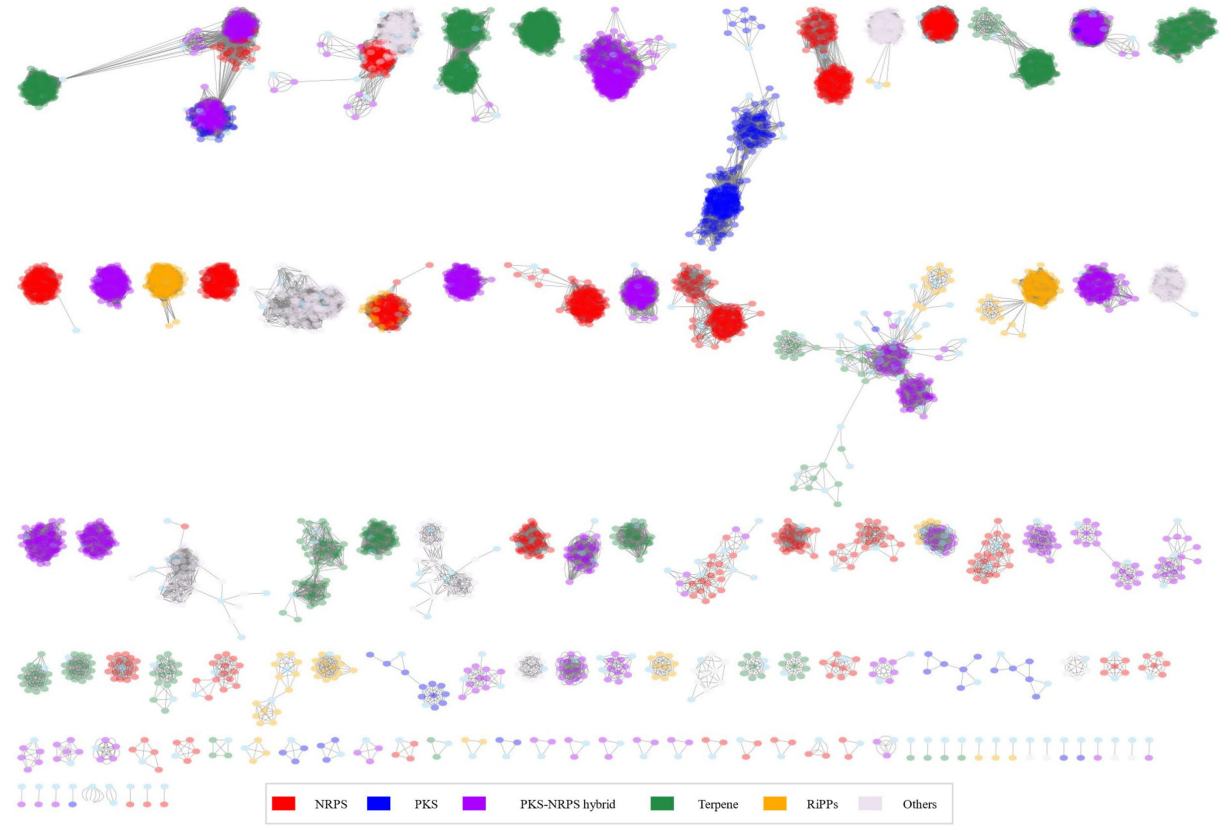

FIGURE 5
Network analysis for 366 *Burkholderia* spp.

expanded the scope of *Burkholderia* research, enabling more extensive investigations. Most clans revealed that *B. pseudomallei* was the main species excluding NRPS_04014. The NRPS_04014 clan contained ornibactin and indigoidine-related BGCs. Ornibactin was known as a siderophore from *B. cenocepacia*. In 44 types of BGCs, we confirmed several types of siderophore. Siderophore-related BGCs were

TABLE 2 Secondary metabolites reported from *Burkholderia*.

BGCs classification	Compounds	Genes	References
NRPS	Fragin	*hamA-G*	Jenul et al. (2018)
NRPS	Glidopeptin A	*glpCDE*	Wang et al. (2018)
NRPS	Sulfazecin	*sulC-K, sulM*	Li et al. (2017)
NRPS	Valdiazen	*hamACDEG*	Liu and Cheng (2014)
PKS-NRPS	Bactobolin	*btaKNOML*	Esmaeel et al. (2018)
PKS-NRPS	Burkholdin	*bksABCDEFG*	Esmaeel et al. (2018)
PKS-NRPS	fk228	*depABCDE*	Gong et al. (2023)
PKS-NRPS	Glidobactin A	*glbFC*	Esmaeel et al. (2018)
PKS-NRPS	Malleilactone	*malAF*	Esmaeel et al. (2018)
PKS-NRPS	Occidiofungins	*ocfA-N*	Gu et al. (2011)
PKS-NRPS	Spiruchostatin	*spiABC1DE1C2E2*	Gong et al. (2023)
PKS-NRPS	Spliceostatins	*fr9CDEFGHI*	Eustáquio et al. (2014)
PKS-NRPS	Thailandamides	*thaA-R*	Ishida et al. (2010)
PKS-NRPS	Thailandepsins/Burkholdacs	*tdpABC1DE1C2E2*	Esmaeel et al. (2018)
PKS-NRPS	Thailanstatins	*tstCDEFGHI*	Esmaeel et al. (2018)
trans-AT-PKS	Thailandene A-C	*orgA-M*	Park et al. (2020)
RiPP	Capistruin	*capABCD*	Knappe et al. (2009)
RiPP	Cepacin A-B	*ccnA-P*	Mullins et al. (2019)
RiPP	Rhamnolipids	*rhlABC*	Dubeau et al. (2009)
RiPP	Ubonodin (lasso peptide)	*uboABCD*	Cheung-Lee et al. (2020)
Other	Hydrogen cyanide	*hcnABC*	Ryall et al. (2008)
Other	Phenazines (PCA/phencomycins)	*phzABCDEFIR*	Hendry et al. (2021)
Other	Phenylpyrrole (pyrrolnitrin)	*prnABCD*	Hammer et al. (1999)
Other	Quinolone (burkholone, pseudane)	*hhqABCDEFG, hmqABCDEFG, pqsABCDE*	Prothiwa et al. (2021)
Other	Tropolonea	*troR1, troK, troR2*	Wang et al. (2016)

confirmed. Ornibactin are known to possess *Pseudomonas* and siderophore-like compounds (Anthoni et al., 1995).

3.6 Identification of siderophore and pattern analysis for BCC and BPC

We predicted that complex and/or species would have different types of siderophore-related BGCs. To test our hypothesis, we performed additional analysis. Siderophores have been reported to exist in BCC. A comparative transcriptome study of *B. pseudomallei* reported on the induction of siderophores that were able to adapt and survive in the host (Ghazali et al., 2023). However, in antiSMASH results, species belonging to group B did not show the presence of siderophore-related clans. Since *Burkholderia* are known to produce various siderophores that might not be detected by antiSMASH, we conducted further analysis using the results of MiBIG similarity to explore siderophore gene clusters (Table 3). In *Burkholderia*, the following types of siderophores have been reported: ornibactin, malleobactin, cepaciachelin, pyochelin, and cepabactin (Butt and Thomas, 2017). For ornibactin biosynthesis, NRPS genes such as *orbI* and *orbJ* are known, and we used them to search for the corresponding BGCs (Agnoli et al., 2006). Pyochelin biosynthesis involves *pchE* and *pchF* known as NRPS (Quadri et al., 1999). We used these genes to search for the corresponding BGCs with malleobactin related genes as well (Alice et al., 2006). To find cepaciachelin, we collected genes such as *cphA*, *cphB*, and *cphC* (Esmaeel et al., 2016). Cepabactin-related genes have not been described. Malleonitrone is a compound formed by the combination of malleobactins and pyochelin (Trottmann et al., 2019). Other siderophores, burkholdac A and pseudomonine, were identified in group A, which belonged to the BPC, but not in group B. Burkholdac A was exclusively found in *B. savannae* and *B. thailandensis*, while pseudomonine was detected in *B. humptydooensis*, *B. mayonis*, *B. pseudomallei*, and *B. thailandensis* only. Siderophores are known to be species-specific. Our investigation revealed that species within the same complex in *Burkholderia* commonly possessed siderophore-related BGCs (Sandy and Butler, 2009). Alongside siderophores, compounds related to terpenes and RiPPs have been reported. Additionally, certain strains known as plant pathogens, such as *B. glumae*, have been reported to contain a variety of secondary metabolites. For instance, toxoflavin (Kim

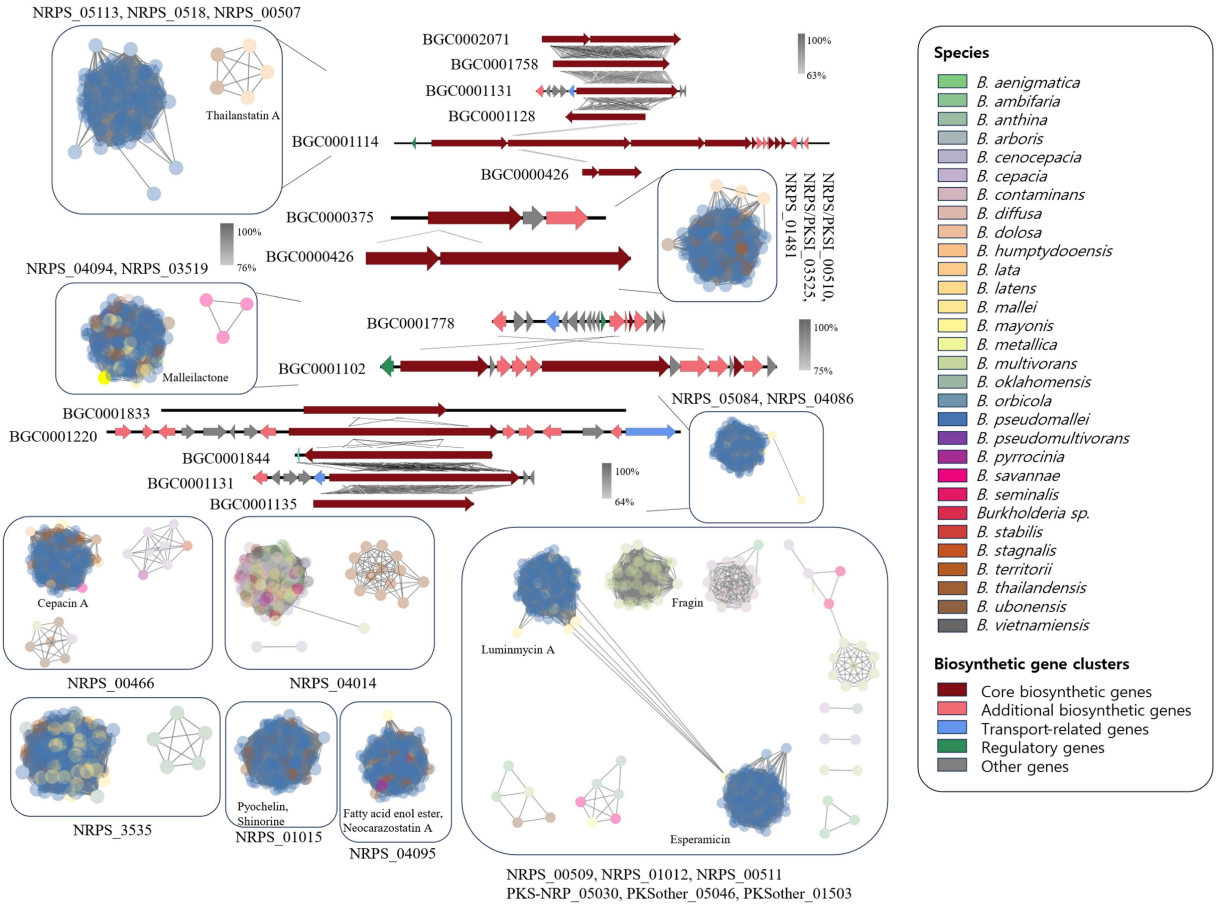

FIGURE 6
Network analysis of NRPS and PKS related clan and visualization of reference BGCs.

et al., 2004), gladiofungin A (gladiostatin; Niehs et al., 2020), and gladiolin from *B. gladioli* (Song et al., 2017) have been identified. Furthermore, compounds such as enacyloxin, which has not been confirmed due to limited known genes, have been reported in *B. ambifaria*. They are believed to contain PKS-related modules (Mahenthiralingam et al., 2011).

This study utilized ClusterBlast to extract similar gene clusters. We structured them into a table using Python. Among confirmed siderophore-related compounds, we identified nine, namely malleilactone, pyrrolnitrin, cepacin A, malleobactin, burkholdac A, ornibactin, enterobactin, pseudomonine, pyochelin, quinolobactin, and pyocyanine. Among these, ornibactin was the most commonly found across various species. The NRPS_4602 clan, which harbored the ornibactin BGC, encompassed gene clusters for ornibactin, pyocyanine, indigoidine, burkholderic acid, anabaenopeptin, burkholdac A, depudecin, and fellutamide B. We visualized ornibactin BGCs within this clan using CORASON (Figure 7). Within the NRPS_4602 clan, ornibactin BGCs were distributed across families FAM_1520, FAM_2544, FAM_2559, FAM_4014, FAM_4564, FAM_4602, and FAM_5592. Each family's gene clusters exhibited similarity, further confirming their species-specific nature.

In the case of FAM_1520, it mainly corresponded to ornibactin BGCs identified in *B. vietnamiensis*, while FAM_2544 was primarily associated with *B. ubonensis*. For all other families, we visualized gene clusters as shown in Figure 7 and Supplementary Figures 2, 3. The observed similarity in gene clusters within the same species suggested their potential utility in distinguishing between BCC and BPC. Previous studies on siderophores have been limited to a small number of *Burkholderia* strains (Esmaeel et al., 2016). Our research presents a new direction for the genome mining of the secondary metabolism, with an expanded sample size and an analytical approach.

4 Conclusion

To date, *Burkholderia* has been known for its diversity in species, but more recent reclassification efforts have associated all complexes within the *Burkholderia* genus as having pathogenic characteristics. In this study, we aimed to analyze features of *Burkholderia* through ANI analysis and reference genes, categorizing them into BCC and BPC for analysis. Through PCA analysis based on antiSMASH results, BCC and BPC were revealed to be distinct. This indicates that each complex is likely to possess a different pattern of BGCs. The network analysis, BiG-SCAPE analysis, and comparative analysis using the MiBIG database revealed that BGCs differed by complex. Through network analysis and visualization of siderophores specific to

TABLE 3 Pattern of siderophore in each *Burkholderia* species.

Species/number of samples		Malleilactone	Pyrrolnitrin	Cepacin A	Burkholdac A	Ornibactin	Enterobactin	Pseudomonine	Pyochelin	Pyocyanine
B. aenigmatica	($n = 1$)	0	0	0	0	1	0	0	0	0
B. ambifaria	($n = 8$)	0	0	0	0	11	0	0	1	0
B. anthina	($n = 2$)	0	0	0	0	3	0	0	0	0
B. arboris	($n = 1$)	0	0	0	0	1	0	0	1	0
B. cenocepacia	($n = 27$)	0	1	0	0	29	2	0	24	0
B. cepacia	($n = 20$)	0	1	0	0	20	0	0	17	3
B. contaminans	($n = 14$)	1	0	0	0	15	0	0	9	0
B. diffusa	($n = 1$)	0	0	0	0	2	0	0	0	0
B. dolosa	($n = 5$)	0	0	0	0	5	0	0	0	0
B. humptydooensis	($n = 1$)	0	0	0	0	0	0	3	0	0
B. lata	($n = 3$)	0	0	0	0	3	0	0	2	0
B. latens	($n = 3$)	0	0	0	0	3	0	0	0	0
B. mallei	($n = 27$)	14	0	0	0	0	0	0	0	0
B. mayonis	($n = 2$)	2	0	0	0	0	0	2	0	0
B. metallica	($n = 1$)	0	0	0	0	1	0	0	0	0
B. multivorans	($n = 50$)	1	0	0	0	49	0	0	0	0
B. oklahomensis	($n = 3$)	3	0	2	0	0	0	0	0	0
B. orbicola	($n = 1$)	0	0	0	0	1	0	0	1	0
B. pseudomallei	($n = 128$)	117	7	120	0	1	0	1	126	0
B. pseudomultivorans	($n = 1$)	0	0	0	0	1	0	0	0	0
B. pyrrocinia	($n = 5$)	0	2	0	0	7	0	0	0	0
B. savannae	($n = 2$)	3	2	0	3	3	0	0	0	0
B. seminalis	($n = 2$)	0	0	0	0	2	0	0	2	0
Burkholderia sp.	($n = 18$)	0	0	0	0	2	0	0	0	0
B. stabilis	($n = 2$)	0	0	0	0	3	0	0	3	0
B. stagnalis	($n = 1$)	0	0	0	0	1	0	0	0	0
B. territorii	($n = 1$)	0	0	0	0	1	0	0	0	0
B. thailandensis	($n = 19$)	17	0	5	3	0	0	12	17	0
B. ubonensis	($n = 7$)	2	3	0	0	7	0	0	0	1
B. vietnamiensis	($n = 10$)	0	0	0	0	11	0	0	0	0

10.3389/fmicb.2023.1302236

10.3389/fmicb.2023.1302236

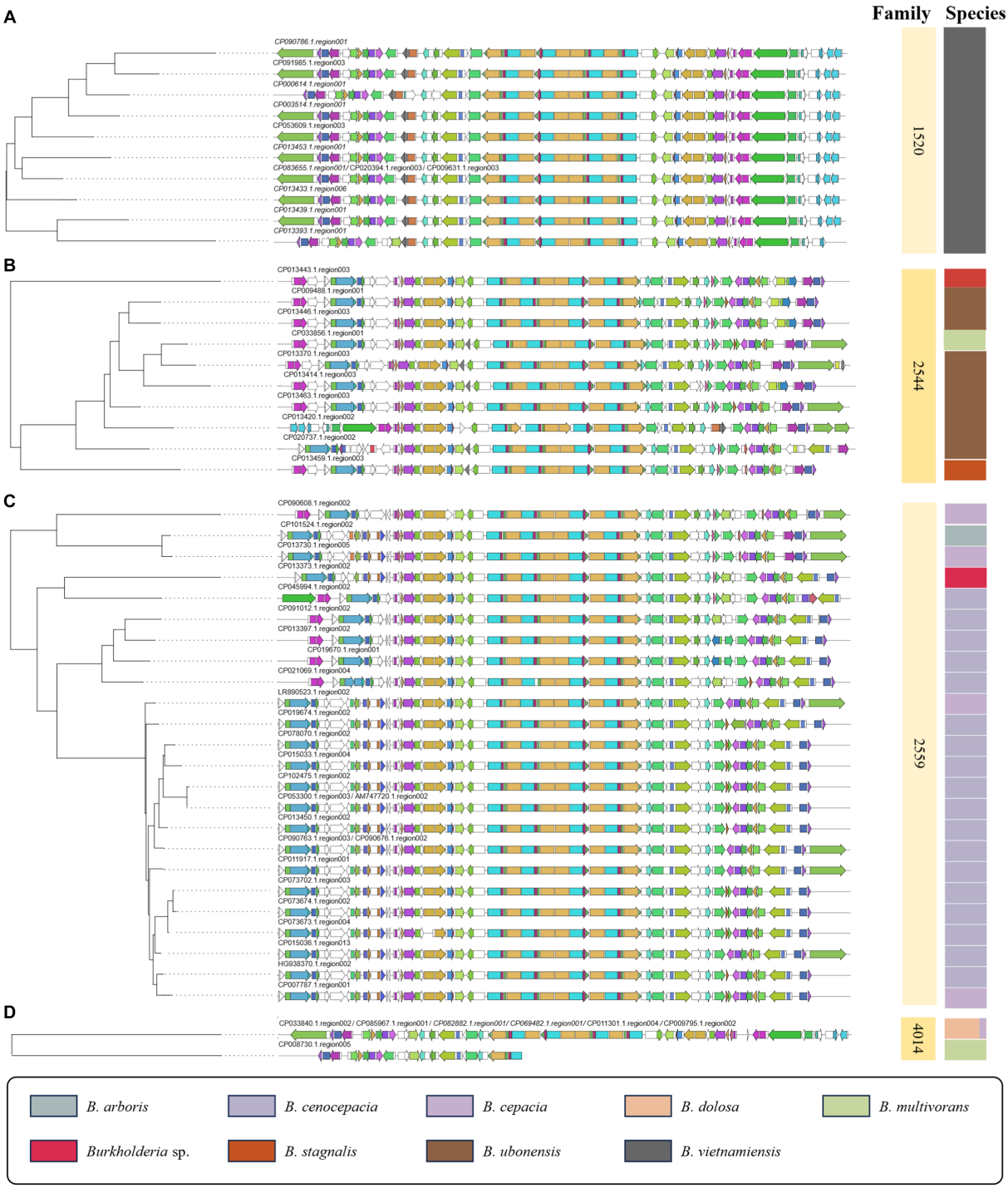

FIGURE 7
Visualization of ornibactin-related biosynthetic genes in NRPS_4602 clan. **(A)** The phylogeny of 1520 family. **(B)** The phylogeny of 2544 family. **(C)** The phylogeny of 2559 family. **(D)** The phylogeny of 4014 family.

each species, we also demonstrated unique siderophore patterns for each species and/or complex. Furthermore, this study explored known BGCs reported not only in *Burkholderia*, but also in *Pseudomonas* and *Paraburkholderia*. By visualizing the gene cluster of ornibactin, the siderophore found in the highest number of species, we anticipate that pattern analysis could be further advanced from a broader perspective. This research became possible due to the increasing number of *Burkholderia* genomes and the identification of various BGCs in *Burkholderia*. However, identifying novel BGCs remains challenging. We could only confirm that results for just three BGCs were not detected from the known MiBIG database. This study serves as a comprehensive investigation into NRPS and PKS. It contributes to future research on secondary metabolites in *Burkholderia*.

Author contributions

BK: Conceptualization, Data curation, Formal analysis, Investigation, Methodology, Project administration, Software, Validation, Writing – original draft, Writing – review & editing. S-RH: Data curation, Methodology, Software, Writing – original draft, Writing – review & editing. HL: Formal analysis, Methodology, Software, Writing – original draft, Writing – review & editing. T-JO: Conceptualization, Funding acquisition, Investigation, Project administration, Resources, Supervision, Validation, Writing – original draft, Writing – review & editing.

Funding

The author(s) declare financial support was received for the research, authorship, and/or publication of this article. This work was supported by the Technology Innovation Program (20018705, entitled "Development of masking and commercialization of biodegradable technology in an urban residential environment using rancid odor-reducing microorganisms and its fragrances") funded by the Ministry of Trade, Industry and Energy (MOTIE, Republic of Korea). This research was also supported by a project entitled "Development of potential antibiotic compounds using polar organism resources (20200610)" funded by the Ministry of Oceans and Fisheries, Republic of Korea.

Conflict of interest

The authors declare that the research was conducted in the absence of any commercial or financial relationships that could be construed as a potential conflict of interest.

Publisher's note

Supplementary material

The Supplementary material for this article can be found online at: https://www.frontiersin.org/articles/10.3389/fmicb.2023.1302236/full#supplementary-material

References

Agnoli, K., Lowe, C. A., Farmer, K. L., Husnain, S. I., and Thomas, M. S. (2006). The ornibactin biosynthesis and transport genes of *Burkholderia cenocepacia* are regulated by an extracytoplasmic function sigma factor which is a part of the Fur regulon. *J. Bacteriol.* 188, 3631–3644. doi: 10.1128/JB.188.10.3631-3644.2006

Ahmad, F., and Azam, S. S. (2020). From pan-genome to protein dynamics: a computational hierarchical quest to identify drug target in multi-drug resistant *Burkholderia cepacia*. *J. Mol. Liq.* 317:113904. doi: 10.1016/j.molliq.2020.113904

Alam, K., Islam, M. M., Gong, K., Abbasi, M. N., Li, R., Zhang, Y., et al. (2021). In silico genome mining of potential novel biosynthetic gene clusters for drug discovery from *Burkholderia* bacteria. *Comput. Biol. Med.* 140:105046. doi: 10.1016/j.compbiomed.2021.105046

Alice, A. F., López, C. S., Lowe, C. A., Ledesma, M. A., and Crosa, J. H. (2006). Genetic and transcriptional analysis of the siderophore malleobactin biosynthesis and transport genes in the human pathogen *Burkholderia pseudomallei* K96243. *J. Bacteriol.* 188, 1551–1566. doi: 10.1128/JB.188.4.1551-1566.2006

Anthoni, U., Christophersen, C., Nielsen, P. H., Gram, L., and Petersen, B. O. (1995). Pseudomonine, an isoxazolidone with siderophoric activity from *Pseudomonas fluorescens* AH2 isolated from Lake Victorian Nile perch. *J. Nat. Prod.* 58, 1786–1789. doi: 10.1021/np50125a026

Bach, E., Passaglia, L. M. P., Jiao, J., and Gross, H. (2022a). *Burkholderia* in the genomic era: from taxonomy to the discovery of new antimicrobial secondary metabolites. *Crit. Rev. Microbiol.* 48, 121–160. doi: 10.1080/1040841X.2021.1946009

Bach, E., Sant'Anna, F. H., Seger, G. D. D. S., and Passaglia, L. M. P. (2022b). Pangenome inventory of *Burkholderia sensu lato, Burkholderia sensu stricto*, and the *Burkholderia cepacia* complex reveals the uniqueness of *Burkholderia catarinensis*. *Genomics* 114, 398–408. doi: 10.1016/j.ygeno.2021.11.011

Barrett, T., Clark, K., Gevorgyan, R., Gorelenkov, V., Gribov, E., Karsch-Mizrachi, I., et al. (2012). BioProject and BioSample databases at NCBI: facilitating capture and organization of metadata. *Nucleic Acids Res.* 40, D57–D63. doi: 10.1093/nar/gkr1163

Benson, D. A., Cavanaugh, M., Clark, K., Karsch-Mizrachi, I., Lipman, D. J., Ostell, J., et al. (2017). GenBank. *Nucleic Acids Res.* 45, D37–D42. doi: 10.1093/nar/gkw1070

Beukes, C. W., Palmer, M., Manyaka, P., Chan, W. Y., Avontuur, J. R., van Zyl, E., et al. (2017). Genome data provides high support for generic boundaries in *Burkholderia sensu lato*. *Front. Microbiol.* 8:1154. doi: 10.3389/fmicb.2017.01154

Blin, K., Shaw, S., Steinke, K., Villebro, R., Ziemert, N., Lee, S. Y., et al. (2019). antiSMASH 5.0: updates to the secondary metabolite genome mining pipeline. *Nucleic Acids Res.* 47, W81–W87. doi: 10.1093/nar/gkz310

Bochkareva, O. O., Moroz, E. V., Davydov, I. I., and Gelfand, M. S. (2018). Genome rearrangements and selection in multi-chromosome bacteria *Burkholderia* spp. *BMC Genomics* 19:965. doi: 10.1186/s12864-018-5245-1

Butt, A. T., and Thomas, M. S. (2017). Iron acquisition mechanisms and their role in the virulence of *Burkholderia* species. *Front. Cell. Infect. Microbiol.* 7:460. doi: 10.3389/fcimb.2017.00460

Camacho, C., Coulouris, G., Avagyan, V., Ma, N., Papadopoulos, J., Bealer, K., et al. (2009). BLAST+: architecture and applications. *BMC Bioinformatics.* 10:421. doi: 10.1186/1471-2105-10-421

Cantalapiedra, C. P., Hernández-Plaza, A., Letunic, I., Bork, P., and Huerta-Cepas, J. (2021). eggNOG-mapper v2: functional annotation, orthology assignments, and domain prediction at the metagenomic scale. *Mol. Biol. Evol.* 38, 5825–5829. doi: 10.1093/molbev/msab293

Cheung-Lee, W. L., Parry, M. E., Zong, C., Cartagena, A. J., Darst, S. A., Connell, N. D., et al. (2020). Discovery of ubonodin, an antimicrobial lasso peptide active against members of the *Burkholderia cepacia* complex. *ChemBioChem* 21, 1335–1340. doi: 10.1002/cbic.201900707

Compant, S., Nowak, J., Coenye, T., Clément, C., and Ait Barka, E. (2008). Diversity and occurrence of *Burkholderia* spp. in the natural environment. *FEMS Microbiol. Rev.* 32, 607–626. doi: 10.1111/j.1574-6976.2008.00113.x

Cummins, C., Ahamed, A., Aslam, R., Burgin, J., Devraj, R., Edbali, O., et al. (2022). The European nucleotide archive in 2021. *Nucleic Acids Res.* 50, D106–D110. doi: 10.1093/nar/gkab1051

Deng, P., Jia, J., Foxfire, A., Baird, S. M., Smith, L. J., and Lu, S. E. (2023). A polyketide synthetase gene cluster is responsible for antibacterial activity of *Burkholderia contaminans* MS14. *Phytopathology* 113, 11–20. doi: 10.1094/PHYTO-03-22-0106-R

Depoorter, E., Bull, M. J., Peeters, C., Coenye, T., Vandamme, P., and Mahenthiralingam, E. (2016). *Burkholderia*: an update on taxonomy and biotechnological potential as antibiotic producers. *Appl. Microbiol. Biotechnol.* 100, 5215–5229. doi: 10.1007/s00253-016-7520-x

Depoorter, E., De Canck, E., Peeters, C., Wieme, A. D., Cnockaert, M., Zlosnik, J. E. A., et al. (2020). *Burkholderia cepacia* complex taxon K: where to split? *Front. Microbiol.* 11:1594. doi: 10.3389/fmicb.2020.01594

Dubeau, D., Déziel, E., Woods, D. E., and Lépine, F. (2009). *Burkholderia thailandensis* harbors two identical *rhl* gene clusters responsible for the biosynthesis of rhamnolipids. *BMC Microbiol.* 9:263. doi: 10.1186/1471-2180-9-263

Eberl, L., and Vandamme, P. (2016). Members of the genus Burkholderia: good and bad guys. *F1000Res* 5:F1000. doi: 10.12688/f1000research.8221.1

Esmaeel, Q., Pupin, M., Jacques, P., and Leclère, V. (2018). Nonribosomal peptides and polyketides of *Burkholderia*: new compounds potentially implicated in biocontrol and pharmaceuticals. *Environ. Sci. Pollut. Res. Int.* 25, 29794–29807. doi: 10.1007/s11356-017-9166-3

Esmaeel, Q., Pupin, M., Kieu, N. P., Chataigné, G., Béchet, M., Deravel, J., et al. (2016). *Burkholderia* genome mining for nonribosomal peptide synthetases reveals a great potential for novel siderophores and lipopeptides synthesis. *Microbiology* 5, 512–526. doi: 10.1002/mbo3.347

Estrada-de Los Santos, P., Palmer, M., Chávez-Ramírez, B., Beukes, C., Steenkamp, E. T., Briscoe, L., et al. (2018). Whole genome analyses suggests that *Burkholderia sensu lato* contains two additional novel genera (*Mycetohabitans ge*n. Nov., and *Trinickia gen*. Nov.): implications for the evolution of diazotrophy and nodulation in the *Burkholderiaceae*. *Genes* 9:389. doi: 10.3390/genes9080389

Eustáquio, A. S., Janso, J. E., Ratnayake, A. S., O'Donnell, C. J., and Koehn, F. E. (2014). Spliceostatin hemiketal biosynthesis in *Burkholderia* spp. is catalyzed by an iron/α-ketoglutarate-dependent dioxygenase. *Proc. Natl. Acad. Sci. U. S. A.* 111, E3376–E3385. doi: 10.1073/pnas.1408300111

Euzéby, J. P. (1997). List of bacterial names with standing in nomenclature: a folder available on the internet. *Int. J. Syst. Evol. Microbiol.* 47, 590–592. doi: 10.1099/00207713-47-2-590

Gee, J. E., Gulvik, C. A., Castelo-Branco, D. S. C. M., Sidrim, J. J. C., Rocha, M. F. G., Cordeiro, R. A., et al. (2021). Genomic diversity of *Burkholderia pseudomallei* in Ceara, Brazil. *mSphere.* 6, e01259–e01220. doi: 10.1128/mSphere.01259-20

Ghazali, A. K., Firdaus-Raih, M., Uthaya Kumar, A., Lee, W. K., Hoh, C. C., and Nathan, S. (2023). Transitioning from soil to host: comparative transcriptome analysis reveals the *Burkholderia pseudomallei* response to different niches. *Microbiol Spectr.* 11:e0383522. doi: 10.1128/spectrum.03835-22

Gong, K., Wang, M., Duan, Q., Li, G., Yong, D., Ren, C., et al. (2023). High-yield production of FK228 and new derivatives in a *Burkholderia* chassis. *Metab. Eng.* 75, 131–142. doi: 10.1016/j.ymben.2022.12.002

Gu, G., Smith, L., Liu, A., and Lu, S. E. (2011). Genetic and biochemical map for the biosynthesis of occidiofungin, an antifungal produced by *Burkholderia contaminans* strain MS14. *Appl. Environ. Microbiol.* 77, 6189–6198. doi: 10.1128/AEM.00377-11

Gurevich, A., Saveliev, V., Vyahhi, N., and Tesler, G. (2013). QUAST: quality assessment tool for genome assemblies. *Bioinformatics* 29, 1072–1075. doi: 10.1093/bioinformatics/btt086

Hall, C. M., Baker, A. L., Sahl, J. W., Mayo, M., Scholz, H. C., Kaestli, M., et al. (2022). Expanding the *Burkholderia pseudomallei* complex with the addition of two novel species: *Burkholderia mayonis* sp. nov. and *Burkholderia savannae* sp. nov. *Appl. Environ. Microbiol.* 88:e0158321. doi: 10.1128/AEM.01583-21

Hall, C. M., Busch, J. D., Shippy, K., Allender, C. J., Kaestli, M., Mayo, M., et al. (2015). Diverse *Burkholderia* species isolated from soils in the southern United States with no evidence of *B. pseudomallei*. *PloS One* 10:e0143254. doi: 10.1371/journal.pone.0143254

Hammer, P. E., Burd, W., Hill, D. S., Ligon, J. M., and van Pée, K. (1999). Conservation of the pyrrolnitrin biosynthetic gene cluster among six pyrrolnitrin-producing strains. *FEMS Microbiol. Lett.* 180, 39–44. doi: 10.1111/j.1574-6968.1999.tb08775.x

Han, S. R., Yu, S. C., Ahn, D. H., Park, H., and Oh, T. J. (2016). Complete genome sequence of *Burkholderia* sp. strain PAMC28687, a potential octopine-utilizing bacterium isolated from Antarctica lichen. *J. Biotechnol.* 226, 16–17. doi: 10.1016/j.jbiotec.2016.03.043

Hendry, S., Steinke, S., Wittstein, K., Stadler, M., Harmrolfs, K., Adewunmi, Y., et al. (2021). Functional analysis of phenazine biosynthesis genes in *Burkholderia* spp. *Appl. Environ. Microbiol.* 87, e02348–e02320. doi: 10.1128/AEM.02348-20

Hickey, G., Monlong, J., Ebler, J., Novak, A. M., Eizenga, J. M., and Gao, Y. (2023). Pangenome graph construction from genome alignments with Minigraph-Cactus. *Nat. Biotechnol.* doi: 10.1038/s41587-023-01793-w

Hunter, J. D. (2007). Matplotlib: a 2D graphics environment. *Comput Sci Eng.* 9, 90–95. doi: 10.1109/MCSE.2007.55

Ishida, K., Lincke, T., Behnken, S., and Hertweck, C. (2010). Induced biosynthesis of cryptic polyketide metabolites in a *Burkholderia thailandensis* quorum sensing mutant. *J. Am. Chem. Soc.* 132, 13966–13968. doi: 10.1021/ja105003g

Jain, C., Rodriguez-R, L. M., Phillippy, A. M., Konstantinidis, K. T., and Aluru, S. (2018). High throughput ANI analysis of 90K prokaryotic genomes reveals clear species boundaries. *Nat. Commun.* 9:5114. doi: 10.1038/s41467-018-07641-9

Jenul, C., Sieber, S., Daeppen, C., Mathew, A., Lardi, M., Pessi, G., et al. (2018). Biosynthesis of fragin is controlled by a novel quorum sensing signal. *Nat. Commun.* 9:1297. doi: 10.1038/s41467-018-03690-2

Jin, Y., Zhou, J., Zhou, J., Hu, M., Zhang, Q., Kong, N., et al. (2020). Genome-based classification of *Burkholderia cepacia* complex provides new insight into its taxonomic status. *Biol. Direct* 15:6. doi: 10.1186/s13062-020-0258-5

Kaur, C., Selvakumar, G., and Ganeshamurthy, A. N. (2017). "*Burkholderia* to *Paraburkholderia*: the journey of a plant-beneficial-environmental bacterium" in *Recent Advances in Applied Microbiology*. ed. P. Shukla (Springer Nature Singapore).

Kim, E., Jung, H. I., Park, S. H., Kim, H. Y., and Kim, S. K. (2023). Comprehensive genome analysis of *Burkholderia contaminans* SK875, a quorum-sensing strain isolated from the swine. *AMB Exp* 13:30. doi: 10.1186/s13568-023-01537-8

Kim, J., Kim, J. G., Kang, Y., Jang, J. Y., Jog, G. J., Lim, J. Y., et al. (2004). Quorum sensing and the LysR-type transcriptional activator ToxR regulate toxoflavin biosynthesis and transport in *Burkholderia glumae*. *Mol. Microbiol.* 54, 921–934. doi: 10.1111/j.1365-2958.2004.04338.x

Kim, N., Mannaa, M., Kim, J., Ra, J. E., Kim, S. M., Lee, C., et al. (2021). The in vitro and in planta interspecies interactions among rice-pathogenic *Burkholderia* species. *Plant Dis.* 105, 134–143. doi: 10.1094/PDIS-06-20-1252-RE

Knappe, T. A., Linne, U., Robbel, L., and Marahiel, M. A. (2009). Insights into the biosynthesis and stability of the lasso peptide capistruin. *Chem. Biol.* 16, 1290–1298. doi: 10.1016/j.chembiol.2009.11.009

Konstantinidis, K. T., and Tiedje, J. M. (2005). Genomic insights that advance the species definition for prokaryotes. *Proc. Natl. Acad. Sci. U. S. A.* 102, 2567–2572. doi: 10.1073/pnas.0409727102

Kunakom, S., and Eustáquio, A. S. (2019). *Burkholderia* as a source of natural products. *J. Nat. Prod.* 82, 2018–2037. doi: 10.1021/acs.jnatprod.8b01068

Lee, H. H., Park, J., Jung, H., and Seo, Y. S. (2021). Pan-genome analysis reveals host-specific functional divergences in *Burkholderia gladioli*. *Microorganisms.* 9:1123. doi: 10.3390/microorganisms9061123

Levy, A., Merritt, A. J., Aravena-Roman, M., Hodge, M. M., and Inglis, T. J. (2008). Expanded range of *Burkholderia* species in Australia. *Am. J. Trop. Med. Hyg.* 78, 599–604. doi: 10.4269/ajtmh.2008.78.599

Li, R., Oliver, R. A., and Townsend, C. A. (2017). Identification and characterization of the sulfazecin monobactam biosynthetic gene cluster. *Cell Chem Biol.* 24, 24–34. doi: 10.1016/j.chembiol.2016.11.010

Lin, Q. H., Lv, Y. Y., Gao, Z. H., and Qiu, L. H. (2020). *Pararobbsia silviterrae* gen. Nov., sp. nov., isolated from forest soil and reclassification of *Burkholderia alpina* as *Pararobbsia alpina* comb. nov. *Int. J. Syst. Evol. Microbiol.* 70, 1412–1420. doi: 10.1099/ijsem.0.003932

Lipuma, J. J. (2005). Update on the *Burkholderia cepacia* complex. *Curr. Opin. Pulm. Med.* 11, 528–533. doi: 10.1097/01.mcp.0000181475.85187.ed

Liu, X., and Cheng, Y. Q. (2014). Genome-guided discovery of diverse natural products from *Burkholderia* sp. *J. Ind. Microbiol. Biotechnol.* 41, 275–284. doi: 10.1007/s10295-013-1376-1

Lood, C., Peeters, C., Lamy-Besnier, Q., Wagemans, J., De Vos, D., Proesmans, M., et al. (2021). Genomics of an endemic cystic fibrosis *Burkholderia multivorans* strain reveals low within-patient evolution but high between-patient diversity. *PLoS Pathog.* 17:e1009418. doi: 10.1371/journal.ppat.1009418

Lü, L., Zhang, Z. K., and Zhou, T. (2010). Zipf's law leads to Heaps' law: analyzing their relation in finite-size systems. *PloS One* 5:e14139. doi: 10.1371/journal.pone.0014139

Luo, J., Xie, G., Li, B., and Lihui, X. (2007). First report of *Burkholderia glumae* isolated from symptomless rice seeds in China. *Plant Dis.* 91:1363. doi: 10.1094/PDIS-91-10-1363B

Mahenthiralingam, E., Song, L., Sass, A., White, J., Wilmot, C., Marchbank, A., et al. (2011). Enacyloxins are products of an unusual hybrid modular polyketide synthase encoded by a cryptic *Burkholderia ambifaria* genomic island. *Chem. Biol.* 18, 665–677. doi: 10.1016/j.chembiol.2011.01.020

Medina-Pascual, M. J., Valdezate, S., Carrasco, G., Villalón, P., Garrido, N., and Saéz-Nieto, J. A. (2015). Increase in isolation of *Burkholderia contaminans* from Spanish patients with cystic fibrosis. *Clin. Microbiol. Infect.* 21, 150–156. doi: 10.1016/j.cmi.2014.07.014

Mistry, J., Chuguransky, S., Williams, L., Qureshi, M., Salazar, G. A., Sonnhammer, E. L. L., et al. (2021). Pfam: the protein families database in 2021. *Nucleic Acids Res.* 49, D412–D419. doi: 10.1093/nar/gkaa913

Mistry, J., Finn, R. D., Eddy, S. R., Bateman, A., and Punta, M. (2013). Challenges in homology search: HMMER3 and convergent evolution of coiled-coil regions. *Nucleic Acids Res.* 41:e121. doi: 10.1093/nar/gkt263

Morales-Ruíz, L. M., Rodríguez-Cisneros, M., Kerber-Díaz, J. C., Rojas-Rojas, F. U., Ibarra, J. A., Santos, E.-d. L., et al. (2022). *Burkholderia orbicola* sp. nov., a novel species within the *Burkholderia cepacia* complex. *Arch. Microbiol.* 204:178. doi: 10.1007/s00203-022-02778-0

Mullins, A. J., and Mahenthiralingam, E. (2021). The hidden genomic diversity, specialized metabolite capacity, and revised taxonomy of *Burkholderia sensu lato*. *Front. Microbiol.* 12:726847. doi: 10.3389/fmicb.2021.726847

Mullins, A. J., Murray, J. A. H., Bull, M. J., Jenner, M., Jones, C., Webster, G., et al. (2019). Genome mining identifies cepacin as a plant-protective metabolite of the biopesticidal bacterium *Burkholderia ambifaria*. *Nat. Microbiol.* 4, 996–1005. doi: 10.1038/s41564-019-0383-z

Navarro-Muñoz, J. C., Selem-Mojica, N., Mullowney, M. W., Kautsar, S. A., Tryon, J. H., Parkinson, E. I., et al. (2020). A computational framework to explore large-scale biosynthetic diversity. *Nat. Chem. Biol.* 16, 60–68. doi: 10.1038/s41589-019-0400-9

Niehs, S. P., Kumpfmüller, J., Dose, B., Little, R. F., Ishida, K., Flórez, L. V., et al. (2020). Insect-associated bacteria assemble the antifungal butenolide gladiofungin by non-canonical polyketide chain termination. *Angew. Chem. Int. Ed. Engl.* 59, 23122–23126. doi: 10.1002/anie.202005711

Park, J. D., Moon, K., Miller, C., Rose, J., Xu, F., Ebmeier, C. C., et al. (2020). Thailandenes, cryptic polyene natural products isolated from *Burkholderia thailandensis* using phenotype-guided transposon mutagenesis. *ACS Chem. Biol.* 15, 1195–1203. doi: 10.1021/acschembio.9b00883

Parks, D. H., Imelfort, M., Skennerton, C. T., Hugenholtz, P., and Tyson, G. W. (2015). CheckM: assessing the quality of microbial genomes recovered from isolates, single cells, and metagenomes. *Genome Res.* 25, 1043–1055. doi: 10.1101/gr.186072.114

Parte, A. C., Sardà Carbasse, J., Meier-Kolthoff, J. P., Reimer, L. C., and Göker, M. (2020). List of prokaryotic names with standing in nomenclature (LPSN) moves to the DSMZ. *Int. J. Syst. Evol. Microbiol.* 70, 5607–5612. doi: 10.1099/ijsem.0.004332

Peddayelachagiri, B. V., Paul, S., Nagaraj, S., Gogoi, M., Sripathy, M. H., and Batra, H. V. (2016). Prevalence and identification of *Burkholderia pseudomallei* and near-neighbor species in the Malabar coastal region of India. *PLoS Negl. Trop. Dis.* 10:e0004956. doi: 10.1371/journal.pntd.0004956

Petrova, Y. D., and Mahenthiralingam, E. (2022). Discovery, mode of action and secretion of *Burkholderia sensu lato* key antimicrobial specialised metabolites. *Cell Surf.* 8:100081. doi: 10.1016/j.tcsw.2022.100081

Price, E. P., Sarovich, D. S., Webb, J. R., Ginther, J. L., Mayo, M., Cook, J. M., et al. (2013). Accurate and rapid identification of the *Burkholderia pseudomallei* near-neighbour, *Burkholderia ubonensis*, using real-time PCR. *PloS One* 8:e71647. doi: 10.1371/journal.pone.0071647

Prothiwa, M., Filz, V., Oehler, S., and Böttcher, T. (2021). Inhibiting quinolone biosynthesis of *Burkholderia*. *Chem. Sci.* 12, 6908–6912. doi: 10.1039/d0sc06167k

Quadri, L. E., Keating, T. A., Patel, H. M., and Walsh, C. T. (1999). Assembly of the *Pseudomonas aeruginosa* nonribosomal peptide siderophore pyochelin: in vitro reconstitution of aryl-4,2-bisthiazoline synthetase activity from PchD, PchE, and PchF. *Biochemistry* 38, 14941–14954. doi: 10.1021/bi991787c

Radua, S., Ling, O. W., Srimontree, S., Lulitanond, A., Hin, W. F., Yuherman, L., et al. (2000). Characterization of *Burkholderia pseudomallei* isolated in Thailand and Malaysia. *Diagn. Microbiol. Infect. Dis.* 38, 141–145. doi: 10.1016/s0732-8893(00)00189-9

Rodríguez-Cisneros, M., Morales-Ruíz, L. M., Salazar-Gómez, A., Rojas-Rojas, F. U., and Santos, E.-d. L. (2023). Compilation of the antimicrobial compounds produced by *Burkholderia sensu stricto*. *Molecules* 28:1646. doi: 10.3390/molecules28041646

Ryall, B., Lee, X., Zlosnik, J. E., Hoshino, S., and Williams, H. D. (2008). Bacteria of the *Burkholderia cepacia* complex are cyanogenic under biofilm and colonial growth conditions. *BMC Microbiol.* 8:108. doi: 10.1186/1471-2180-8-108

Sandy, M., and Butler, A. (2009). Microbial iron acquisition: marine and terrestrial siderophores. *Chem. Rev.* 109, 4580–4595. doi: 10.1021/cr9002787

Seemann, T. (2014). Prokka: rapid prokaryotic genome annotation. *Bioinformatics* 30, 2068–2069. doi: 10.1093/bioinformatics/btu153

Seyedsayamdost, M. R., Chandler, J. R., Blodgett, J. A., Lima, P. S., Duerkop, B. A., Oinuma, K., et al. (2010). Quorum-sensing-regulated bactobolin production by *Burkholderia thailandensis* E264. *Org. Lett.* 12, 716–719. doi: 10.1021/ol902751x

Shannon, P., Markiel, A., Ozier, O., Baliga, N. S., Wang, J. T., Ramage, D., et al. (2003). Cytoscape: a software environment for integrated models of biomolecular interaction networks. *Genome Res.* 13, 2498–2504. doi: 10.1101/gr.1239303

Song, L., Jenner, M., Masschelein, J., Jones, C., Bull, M. J., Harris, S. R., et al. (2017). Discovery and biosynthesis of gladiolin: a *Burkholderia gladioli* antibiotic with promising activity against *Mycobacterium tuberculosis*. *J. Am. Chem. Soc.* 139, 7974–7981. doi: 10.1021/jacs.7b03382

Sousa, S. A., Ramos, C. G., and Leitão, J. H. (2011). *Burkholderia cepacia* complex: emerging multihost pathogens equipped with a wide range of virulence factors and determinants. *Int J Microbiol.* 2011:607575. doi: 10.1155/2011/607575

Sullivan, M. J., Petty, N. K., and Beatson, S. A. (2011). Easyfig: a genome comparison visualizer. *Bioinformatics* 27, 1009–1010. doi: 10.1093/bioinformatics/btr039

Sulochana, M. B., Jayachandra, S. Y., Kumar, S. A., Parameshwar, A. B., Reddy, K. M., and Dayanand, A. (2014). Siderophore as a potential plant growth-promoting agent produced by *Pseudomonas aeruginosa* JAS-25. *Appl. Biochem. Biotechnol.* 174, 297–308. doi: 10.1007/s12010-014-1039-3

Terlouw, B. R., Blin, K., Navarro-Muñoz, J. C., Avalon, N. E., Chevrette, M. G., Egbert, S., et al. (2023). MIBiG 3.0: a community-driven effort to annotate experimentally validated biosynthetic gene clusters. *Nucleic Acids Res.* 51, D603–D610. doi: 10.1093/nar/gkac1049

Tettelin, H., Riley, D., Cattuto, C., and Medini, D. (2008). Comparative genomics: the bacterial pan-genome. *Curr. Opin. Microbiol.* 11, 472–477. doi: 10.1016/j.mib.2008.09.006

Trottmann, F., Franke, J., Ishida, K., García-Altares, M., and Hertweck, C. (2019). A pair of bacterial siderophores releases and traps an intercellular signal molecule: an unusual case of natural nitrone bioconjugation. *Angew. Chem. Int. Ed. Engl.* 58, 200–204. doi: 10.1002/anie.201811131

Tuanyok, A., Mayo, M., Scholz, H., Hall, C. M., Allender, C. J., Kaestli, M., et al. (2017). *Burkholderia humptydooensis* sp. nov., a new species related to *Burkholderia thailandensis* and the fifth member of the *Burkholderia pseudomallei* complex. *Appl. Environ. Microbiol.* 83, e02802–e02816. doi: 10.1128/AEM.02802-16

Ussery, D. W., Kiil, K., Lagesen, K., Sicheritz-Pontén, T., Bohlin, J., and Wassenaar, T. M. (2009). The genus *Burkholderia*: analysis of 56 genomic sequences. *Genome Dyn.* 6, 140–157. doi: 10.1159/000235768

Vanlaere, E., Baldwin, A., Gevers, D., Henry, D., De Brandt, E., LiPuma, J. J., et al. (2009). Taxon K, a complex within the *Burkholderia cepacia* complex, comprises at least two novel species, *Burkholderia contaminans* sp. nov. and *Burkholderia lata* sp. nov. *Int. J. Syst. Evol. Microbiol.* 59, 102–111. doi: 10.1099/ijs.0.001123-0

Vanlaere, E., Lipuma, J. J., Baldwin, A., Henry, D., De Brandt, E., Mahenthiralingam, E., et al. (2008). *Burkholderia latens* sp. nov., *Burkholderia diffusa* sp. nov., *Burkholderia arboris* sp. nov., *Burkholderia seminalis* sp. nov. and *Burkholderia metallica* sp. nov., novel species within the *Burkholderia cepacia* complex. *Int. J. Syst. Evol. Microbiol.* 58, 1580–1590. doi: 10.1099/ijs.0.65634-0

Wallner, A., King, E., Ngonkeu, E. L. M., Moulin, L., and Béna, G. (2019). Genomic analyses of *Burkholderia cenocepacia* reveal multiple species with differential host-adaptation to plants and humans. *BMC Genomics* 20:803. doi: 10.1186/s12864-019-6186-z

Wang, M., Tachibana, S., Murai, Y., Li, L., Lau, S. Y., Cao, M., et al. (2016). Indole-3-acetic acid produced by *Burkholderia heleia* acts as a phenylacetic acid antagonist to disrupt tropolone biosynthesis in *Burkholderia plantarii*. *Sci. Rep.* 6:22596. doi: 10.1038/srep22596

Wang, X., Zhou, H., Chen, H., Jing, X., Zheng, W., Li, R., et al. (2018). Discovery of recombinases enables genome mining of cryptic biosynthetic gene clusters in *Burkholderiales* species. *Proc. Natl. Acad. Sci. U. S. A.* 115, E4255–E4263. doi: 10.1073/pnas.1720941115

Wickham, H. (2016). *ggplot2: Elegant graphics for data analysis*. Springer-Verlag New York.

Yabuuchi, E., Kosako, Y., Oyaizu, H., Yano, I., Hotta, H., Hashimoto, Y., et al. (1992). Proposal of *Burkholderia* gen. Nov. and transfer of seven species of the genus *Pseudomonas* homology group II to the new genus, with the type species *Burkholderia cepacia* (Palleroni and Holmes 1981) comb. nov. *Microbiol. Immunol.* 36, 1251–1275. doi: 10.1111/j.1348-0421.1992.tb02129.x

Yu, Y., Kim, H. S., Chua, H. H., Lin, C. H., Sim, S. H., Lin, D., et al. (2006). Genomic patterns of pathogen evolution revealed by comparison of *Burkholderia pseudomallei*, the causative agent of melioidosis, to avirulent *Burkholderia thailandensis*. *BMC Microbiol.* 6:46. doi: 10.1186/1471-2180-6-46

Zhou, Z., Charlesworth, J., and Achtman, M. (2020). Accurate reconstruction of bacterial pan- and core genomes with PEPPAN. *Genome Res.* 30, 1667–1679. doi: 10.1101/gr.260828.120

frontiers | Frontiers in Microbiology

TYPE Original Research
PUBLISHED 29 January 2024
DOI 10.3389/fmicb.2024.1278439

OPEN ACCESS

EDITED BY
Ajay Kumar,
Amity University, India

REVIEWED BY
Alireza Seidavi,
Islamic Azad University, Rasht Branch, Iran
Atte Johannes Von Wright,
University of Eastern Finland, Finland

*CORRESPONDENCE
Fatima Muccee
✉ fatima.sbb@pu.edu.pk

RECEIVED 16 August 2023
ACCEPTED 08 January 2024
PUBLISHED 29 January 2024

CITATION
Shahbaz F, Muccee F, Shahab A, Safi SZ, Alomar SY and Qadeer A (2024) Isolation and *in vitro* assessment of chicken gut microbes for probiotic potential.
Front. Microbiol. 15:1278439.
doi: 10.3389/fmicb.2024.1278439

Isolation and *in vitro* assessment of chicken gut microbes for probiotic potential

Fatima Shahbaz[1], Fatima Muccee[1]*, Aansa Shahab[1], Sher Zaman Safi[2], Suliman Yousef Alomar[3] and Abdul Qadeer[4]

[1]School of Biochemistry and Biotechnology, University of the Punjab, Lahore, Pakistan, [2]Faculty of Medicine, MAHSA University, Kuala Lumpur, Malaysia, [3]Department of Zoology, College of Science, King Saud University, Riyadh, Saudi Arabia, [4]Department of Cell Biology, School of Life Sciences, Central South University, Changsha, China

Poultry production occupies an important place in the economy of any country. High broiler production in recent years has badly affected its profitability due to bad feed quality, excessive use of chemotherapeutic agents, emergence of diverse pathogens, and the deficiencies in management practices during rearing cycle. Microbiological improvement of the meat quality using potential probiotics can be beneficial for broiler farming. Present study was initiated to isolate chicken gastrointestinal tract (GIT) bacteria with probiotic potential. To isolate probiotics from chicken gut, alimentary canal of chickens of known sizes and ages was suspended in ringers soln. Under shaking conditions for overnight followed by serial dilutions of ringers soln. Bacterial isolates were analyzed via growth curve analysis, biochemical testing using RapID™ NF Plus Panel kit, molecular characterization, antimicrobial activity assay, antibiotic sensitivity assay, GIT adherence assay, bile salt and gastric acid resistant assay, and cholesterol assimilation assay. Four bacteria isolated in present study were identified as *Limosilactobacillus antri* strain PUPro1, *Lactobacillus delbrueckii* strain PUPro2, *Lacticaseibacillus casei* strain PUPro3, and *Ligilactobacillus salivarius* strain PUPro4. *L. delbrueckii* strain PUPro2 grew extremely fast. All isolates exhibited exceptional resistance to increasing concentrations of NaCl and bile salts with value of p >0.5. *L. delbrueckii* strain PUPro2 adhered to chicken ileum epithelial cells and demonstrated the highest viable counts of 320 colony forming units (CFUs). Antagonistic action was found in all isolates against *P. aeruginosa*, *B. subtilis*, *B. proteus*, and *S. aureus*, with value of p >0.5. Antibiotic susceptibility testing showed sensitivity to all the antibiotics used. Cholesterol assimilation was detected in all bacteria, with values ranging from 216.12 to 192.2 mg/dL. All isolates exhibited γ-hemolysis. In future, these bacteria might be tested for their impact on broilers meat quality and growth and can be recommended for their use as supplements for broilers diet with positive impact on poultry production.

KEYWORDS

probiotics, bile salts, gut, chicken, poultry, hemolysis, adhesion

1 Introduction

In Pakistan, poultry is a dynamic livestock sector which has contributed to employment opportunities to 1.5 million people in last few years due to its massive development, i.e., at the rate of 7.5%. It contributes 40% to the total annual meat production, 5.76% to agricultural sector, and 12.6% to overall GDP of Pakistan (Akbar et al., 2023). At present, Pakistan poultry turnover is 1,190 billion rupees (Alam et al., 2023). In global poultry industry, current filet yield of 16 and 22% has been recorded by the slow and fast growing chickens, respectively (Baéza et al., 2022). Poultry goods production in Pakistan during last 3 years is described in detail in Supplementary Table S1 (Henchion et al., 2021).

However, this industry has been on the brink of collapse in Pakistan as in seven tehsils of Rawalpindi and District Mansehra due to limitations associated with broilers farming (Saman et al., 2023). These limitations include high cost of broilers feed, mortality due to diseases, improper nutrition, lack of disease control programs, poor hatching conditions, improper sanitation, and poor immunity in chickens. Additionally, farmers use antibiotics to reduce enteric illnesses and increase feed conversion ratio (FCR) and body weight gain (BWG) to meet increased demand for poultry products (Desiere et al., 2018; Ogbuewu et al., 2022). As a consequence, broiler meat is saturated with carcinogenic hormones and antibiotic growth promoters (AGPs). As antibiotic abuse has virtually outlawed them, so breeders are under pressure to find more ecologically benign ways to promote the broilers growth (Arsène et al., 2021). Poor waste management practices at poultry farms expose broilers during rearing procedures to deep litter producing a filthy environment where young chicks are more likely to die immediately after delivery (Yan et al., 2021).

To compensate these losses, chicken gut microbiome is being targeted by the veterinarians and microbiologists. Replacing the gut bacteria with potential probiotics has been reported to be an emerging alternative to AGPs (Dowarah et al., 2018; Reuben et al., 2019; Melese et al., 2023). Probiotics are the live microorganisms which improve host health when given in sufficient amounts (Reid et al., 2019). Probiotics, employed in poultry industry, are the inhabitants of chicken gut in most of the cases. They improve serum calcium (Ca) and phosphorus (P) availability thus strengthening the tibial bone (Rizzoli and Biver, 2020). They boost amino acid levels in broiler chickens, improving their flavor (Yadav et al., 2018). Probiotic-fed broilers have been observed to exhibit the reduced midsection fat and increased breast muscle (Zhang et al., 2020). Metabolites of probiotics have also been found to be associated with health promotion activities such as tryptamine, short chain fatty acids (SCFAs), tryptophan, vitamins, and bacteriocins play role in immune system homeostasis, cell to cell communication, and microbiota cross talk, provide resistance to pathogens gut colonization, promote integrity, structure, and function of gut, and activate toll-like receptors (TLRs) on binding with enterocytes leading to cytokine expression (Agus et al., 2018; Khan et al., 2020; Liu et al., 2022; He et al., 2023; Li et al., 2023). In addition to this, metabolites such as lauric acid, pantothenate acid, L-glutamic acid, and N-acetyl-L-aspartic acid have been reported to positively regulate the lipid metabolism in broilers (Wu et al., 2021; Zhang et al., 2021). Probiotic supplements, at an approximate amount of 0.5 g/kg, are reported to improve meat texture and pH in broilers (Mohammed et al., 2021).

The probiotics reported so far in literature include *L. monocytogenes*, *E. faecalis*, *S. enteritidis*, *S. typhimurium*, *Bifidobacterium*, *Roseburia*, *Akkermansia*, *Propionibacterium*, *Faecalibacterium*, *L. reuteri* I2, *Pediococcus acidilactici* I5, *P. acidilactici* C3, *P. acidilactici* I8, *P. acidilactici* I13, *L. acidophilus*, *L. plantarum*, *L. brevis*, *L. salivarius* and *L. fermentum* and *Enterococcus faecium* C14, *Brevibacillus laterosporus* S62, *B. coagulans*, *B. licheniformis*, and *E. coli* (Sanders et al., 2019; Sorescu et al., 2021; Tang et al., 2021; Gupta et al., 2023; Li et al., 2023). Among these, *B. subtilis* supplementation reduced broiler belly fat in a project (Liu et al., 2020). *Lactobacillus* sp. boosted chicken feed protein and crude protein retention (Wu et al., 2019). *E. faecium* NCIMB 11181 supplementation increased FCR (Wu et al., 2019; Yang et al., 2023). *Limosilactobacillus fermentum* PC-76 and PC-10 were found to be anti-*Salmonella gallinarum* (Mehmood et al., 2023).

Under natural circumstances, young chickens are well protected through feeding on parent feces which contain efficient microflora for protection against pathogenic microbes, but the chickens being reared under commercial settings are usually deprived of such beneficial microbes due to cleanliness maintained at the hatching place, i.e., incubators. Shell contamination of pathogens and the gastric secretion of HCl at eighteenth day of incubation exacerbate the composition of gut microflora. Therefore, the post-birth probiotic feed supplementation is crucial in chickens (Lutful, 2009; Ivanova and Denisenko, 2019). Although literature reports various chicken gut-associated bacteria with different probiotic potentials, however, in majority of the cases, a single bacterium does not exhibit wide range of probiotic characteristics simultaneously and cannot be recommended as a sole nutritional tool. They can only be used in combination with other bacteria. Present study has been initiated to isolate and characterize the GIT inhabiting bacteria which might exhibit maximum potential of exerting probiotic effects on chicken health as a single bacterium. For this purpose, we selected the 10 broilers with improved performance and hypothesized that we might find wholesome probiotic bacteria from their guts. These bacteria might be administered via broiler feed as a sole zootechnical tool for the wholesomeness of meat, better FCR, high-quality egg production, healthy weight gain, effective establishment of intestinal microflora, immune system modulation, and pathogen resistance.

2 Materials and methods

2.1 Sample collection and preparation

Healthy broiler chickens ($n = 10$) at 21 days of age were purchased from a butcher and slaughtered. The chickens were washed twice with distilled water followed by 70% ethanol, before the GIT sampling. Followed this, gut was aseptically removed and washed with 0.9% NaCl. Washed gut was minced in 225 mL of ringer solution and mixed well for an hour (Musikasang et al., 2009; Shamsudin et al., 2019).

2.2 Isolation and culturing of probiotics

De Man–Rogosa–Sharpe agar (MRS) (Merck KGaA, 64271 Darmstadt, EMD Millipore Corporation, Germany) and Mueller Hinton agar (MHA) (M0203, FLINN SCIENTIFIC) were used for

isolation and characterization of probiotics, respectively. MRS was prepared and poured into petri plates and allowed to get solidified (Kumar and Kumar, 2015; Soemarie et al., 2022; Gupta et al., 2023). The original sample (200 µL) and its six serial dilutions (10^{-6} to 10^{-1}) were poured on solidified agar plates. Plates were incubated at 37°C. Bacterial colonies obtained after 24 h were enumerated to determine CFUs/ml using the formula:

CFUs / ml of ringers soln. =
(No. of colonies × dilution factor) / volume of culture

The isolated bacteria were preserved in the form of glycerol stocks for later use (Fadanka et al., 2022).

2.3 Molecular characterization by 16S rRNA gene sequence analysis

Using an organic extraction method, DNA was isolated from bacterial pellet (Gupta, 2019). Agarose (RXP 10121, RxBiosciences, Rockville) gels assessed DNA quality. Forty-five min after activation at 90 volts, the Gel Documentation System (4,191,354, BIO-RAD) revealed DNA bands under UV light (Green and Sambrook, 2019). Using particular primers F1 and R1 (Supplementary Table S2), 16S rDNA was amplified by polymerase chain reaction (PCR) equipment (MyGeneTM Series Thermal Cycler) (Beckers et al., 2016). The 12.5 µL master mix, 1 µL forward primer, 1 µL reverse primer, 2 µL template, 8 µL injection water, and 0.5 µL Taq polymerase were added to 20 µL PCR reaction mixture. PCR conditions used are as follows: initial denaturation at 94°C for 10–15 min, followed by 38 cycles of denaturation at 94°C for 30–40 s, annealing at 94°C for 30–40 s, extension at 72°C for 30 s, and final extension at 72°C for 10 min. The results of the PCR amplification were verified by gel electrophoresis. After inspecting the gel in UV light, the Gel Documentation System captured an image of it (Lorenz, 2012). PCR products were shipped to Macrogen, Inc., Korea, for DNA sequence analysis using Sanger chain termination method (Young, 2018).

2.4 Bioinformatics analysis

Sequencing results were downloaded in FASTA format. Basic Local Alignment Search Tool (BLAST) program[1] from the National Center for Biotechnology Information (NCBI)[2] was used to align and scan these sequences against bacterial database. Clustal Omega[3] multiple sequence alignment was performed using NCBI consensus sequences of isolates and related bacteria. Phylogenetic tree was constructed using MEGA 11,[4] after aligning the gaps. The neighbor joining statistical approach, maximum likelihood substitution method, and 1,000-repeat Bootstrap analysis were used to build phylogenetic trees (Sievers and Higgins, 2014).

1 https://blast.ncbi.nlm.nih.gov
2 https://www.ncbi.nlm.gov
3 https://www.ebi.ac.uk
4 https://www.megasoftware.net

2.5 Submission of DNA sequences to GenBank

Sequences of four isolates have been deposited in the publically accessible NCBI GenBank database. DNA sequences and their corresponding accession codes are listed in Supplementary Table S3.

2.5.1 Growth analysis

Bacterial growth was monitored by measuring the optical density of the cultures at 600 nm (OD^{600}) at different time intervals (0, 3, 6, 9, 24, 27, 30, 51, 54, 57 h) using a UV–visible spectrophotometer (BioTek Equipment, Inc.). A growth curve was obtained by plotting the OD^{600} versus time. Growth assay was performed in triplicates using synchronized cultures.

2.6 Biochemical characterization by RapID™ NF plus panel system

For this biochemical study, we used the Remel RapID™ NF Plus Panel kit (Thermo Scientific™) qualitative micromethod (Maloney et al., 2014). RapID™ NF Plus Panel kit screened the isolates for the presence of arginine dihydrolase (ADH), aliphatic thiol (TRD), triglyceride (EST), p-nitrophenyl-phosphoesterase (PHS), p-nitrophenyl-N-acetyl-β-D-glucosaminidase (NAG), p-nitrophenyl-D-α glucosidase (α-Glu), p-nitrophenyl-β-D-glucosidase (β-Glu), p-nitrophenyl-β-D-galactosidase (ONPG), urea hydrolysis test (URE), glucose fermentation test (GLU), proline β-naphthylamidase test (PRO), pyrrolidonyl β-naphthylamidase test (PYR), γ-glutamyl β-naphthylamidase test (GGT), tryptophan β-naphthylamidase (TRY), N-benzyl-arginine naphthylamidase test (BANA), tryptophan fermentation test (IND), and nitrate utilization test (NO_3).

2.7 Assays of probiotics

All the assays performed to assess the probiotic potential of present study bacteria were carried out in triplicates. This helped to validate the observed results. Synchronized cultures were used as inoculum in triplicate experiments.

2.7.1 NaCl tolerance assay

To test salt tolerance of present study bacteria, NaCl (ONLINESCIENCEMALL, Clay Palmerdale Road, Pinson, United States) concentrations of 0.2, 2, and 5% were selected. To get synchronized cultures, fresh overnight grown cultures (100 µL) were inoculated to MRS broth supplemented with different NaCl concentration. The OD^{600} was measured at 0 h. Following this, bacteria were cultured in shaking incubator (Bio-Techne, China) at 150 rpm and 37°C until the log phase was achieved. After that, bacterial growth was assessed by measuring OD^{600} at the end of exponential phase (Rocha-Ramírez et al., 2021).

2.7.2 HCl tolerance assay

Present study bacterial isolates were grown for overnight at 37°C under shaking conditions. Cultures were centrifuged using centrifuge machine (HERMLE, Z380) at 6,000 rpm, 4°C, and

10 min to get the pellet. MRS medium of three different pH values, i.e., 2, 3, and 5, was prepared in three separate tubes, each tube containing 2 mL medium. The pH was adjusted with HCl (AQUABOND Inc.). Each of these tubes were inoculated with pelleted bacterial cells and incubated for 3 h at shaker at 37°C. The OD^{600} was measured at 0 h (before incubation) and 3 h (after incubation) to measure the tolerance of bacteria against different pH values (Nawaz et al., 2017).

2.7.3 Bile salt tolerance assay

Bile salt tolerance was tested at 0.3% concentration of bile salt (Research Products International, United States). MRS broth without bile salts was used as control. Experimental solution was made by adding 0.3 g bile salts to 100 mL MRS broth. Both MRS broth and control were inoculated with 100 µL fresh overnight cultures. It was then cultured at 37°C and 250 rpm until the log phase was achieved. Using a spectrophotometer, OD^{600} was measured at 0 h and at log phase to test the bile salt tolerance in bacteria (Xu et al., 2020).

2.7.4 Cell adhesion assay

The chicken gut was kept at 4°C for 30 min in phosphate buffer saline (PBS) (G-Biosciences, United States) to release surface mucus and was cut into four 1 cm pieces of disinfected ileum. Each component was added in probiotic cell suspension at 37°C for different time intervals, i.e., 0, 30, 60, and 90 min. Ileum was collected and macerated to remove non-adherent bacteria, seeded on MHA agar plates, and incubated for 24 h at 37°C. CFUs in each plate were counted (Reuben et al., 2019).

2.7.5 Growth in the presence of pathogens

Isolates were tested against different pathogens, i.e., *Pseudomonas aeruginosa*, *Bacillus subtilis*, *Bacillus proteus*, and *Staphylococcus aureus*. The pathogen glycerol stocks (60 µL) and overnight grown cultures of probiotics (60 µL) were used as inoculum and added to MRS broth (5 mL). Control comprised of MRS broth inoculated with overnight grown probiotic culture (60 µL). Cultures were incubated under shaking conditions for 24 h at 37°C and 150 rpm. Growth of probiotics in the presence of pathogens was assessed by measuring OD^{600} (Cizeikiene and Jagelaviciute, 2021).

2.7.6 Antibiotic sensitivity profiling

The disk diffusion method was used to determine the antibiotic sensitivity profile of all isolates by measuring the inhibitory zone for each antibiotic. Tested antibiotics included amoxicillin (DMS Chemical Pharmaceutical Inc., Ltd, China), azithromycin (Jenpharm Life Sciences, Pakistan), cefadroxil (Wellona Pharma, India), velosef (GlaxoSmithKline, London), kanamycin (Kanto Chemical Co., Inc., Tokyo, Japan), and augmentin (MEDSAFE, New Zealand) (Jomehzadeh et al., 2020). Three concentrations of each of these antibiotics were consulted, i.e., 5, 10, and 15 µL.

2.7.7 Hemolytic assay

Autoclaved blood agar (Millipore, India) was poured into petri plates. After solidification, overnight bacterial cultures were streaked. These plates were incubated at 37°C for 24 h, and hemolytic activities were estimated. The presence of a clear, colorless, or light-yellow zone surrounding the colonies will show total red blood cell (RBC) lysis, i.e., β-hemolysis. A greenish to brownish discoloration of the media will reflect reduction of hemoglobin, i.e., α-hemolysis, and no change in media color will reflect the ϒ-hemolysis (Kumari VB et al., 2023).

2.7.8 Cholesterol assay

Cholesterol breakdown characteristics were evaluated by CHOD-PAP method using cholesterol liquicolor kit (PATHOZYME DIAGNOSTICS, India). The probiotic culture cuvette received 10 µL of cholesterol standard (STD). The standard was mixed with culture and incubated at 20–25°C for 5 min. Blank cuvette contained 10 µL STD. OD was measured at 500 nm. Cholesterol concentration was measured as follows:

$$C^{STD} = 553 \times \Delta A\,(\text{mg/dl}) \text{ or, } C = 14.3 \times \Delta A\,(\text{mmol/l})$$

$$\text{Cholesterol concentration}\,(\text{mg/dl}) = 200 \times \Delta A_{\text{sample}} / \Delta A_{\text{STD}}$$

$$\text{Cholesterol concentration}\,(\text{mmol/l}) = 5.17 \times \Delta A_{\text{sample}} / \Delta A_{\text{STD}}$$

2.8 Statistical analysis

After each test, the findings were summarized as a mean ± SD as triplicates of each experiment were conducted separately. One-way ANOVA statistical tests were run using SPSS version 18.0. Threshold for statistical significance was set at $p \leq 0.05$.

3 Results

3.1 Isolation of probiotics

Probiotics were isolated from chicken intestines using MRS broth. Clear bacterial colonies appeared on the plates after 24 h of incubation at 37°C.

3.2 Molecular characterization

Present study bacteria were identified using molecular analysis (Supplementary Figure S1). Sequences of 16S rRNA gene have been deposited in GenBank database, and accession numbers were assigned (Supplementary Table S3).

3.3 Phylogeny analysis

Phylogenetic analysis revealed the close relation of *L. delbrueckii* strain PUPro2 with *L. delbrueckii* strain sample AAA with bootstrap value of 100. *L. antri* strain PUPro1 and *L. panis* strain DSM 6035 both originated from the shared clade of *L. antri* strain DSM 106038 and *L. antri* strain Kx146A4. *L. casei* strain PUPro3 originated from the same branch point as that of

L. casei strain TA001 with strong bootstrap value of 100 showing their close relatedness. *L. salivarius* strain PUPro4 was closely related to *Lactobacillus* species OTU343 through strong bootstrap value of 100 (Figure 1).

3.4 Growth analysis

All bacterial isolates were fast growing. *L. antri* strain PUPro1 entered the logarithmic phase at 24 h and exited after 57 h. *L. delbrueckii* strain PUPro2 grew logarithmically from 3 to 24 h. *L. salivarius* strain PUPro4 exhibited log phase of 9–24 h. *L. casei* strain PUPro3 grew logarithmically between 6 and 24 h (Figure 2; Supplementary Tables S4, S5).

3.5 Biochemical characterization

All isolates were tested positive for TRD and EST tests. Only *L. antri* strain PUPro1 was positive for PHS. All isolates fermented glucose except *L. delbrueckii* strain PUPro2 and *L. casei* strain PUPro3. All isolates were nitrate-reducing and NO^{3-}positive. All the isolates showed negative results for ADH, NAG, α-GLU, β-GLU, PRO, PYR, GGT, TRY, BANA, IND, and ONPG assays (Supplementary Figure S2; Supplementary Table S6).

3.6 Assays of probiotics

3.6.1 NaCl tolerance assay

Each isolate survived at 0.2, 2, and 5% concentration of NaCl, and OD^{600} dropped slightly as NaCl increased from 0.2 to 2 and 5% (Figure 3). *L. salivarius* strain PUPro4 had the highest tolerance at 0.2 and 2% NaCl with $OD^{600} = 0.984$ and 0.929, respectively, while *L. casei* strain PUPro3 had the lowest OD^{600}. *L. salivarius* strain PUPro4, with an OD^{600} of 0.922, was the most tolerant to 5% NaCl. Least tolerance was observed in case of *L. antri* strain PUPro1 with 0.714 (Table 1). Statistics showed value of $p > 0.05$.

3.6.2 HCl tolerance assay

Present study bacteria were analyzed for resistance against HCl via incubation in media of three different pH values, i.e., 2, 3, and 5. All the four isolates showed maximum tolerance to HCl at pH value of 3. Highest growth measured in terms of $O.D^{600}$ at pH 3 was 1.60 ± 0.003, 1.56 ± 0.04, 1.54 ± 0.004, and 1.44 ± 0.001 for *L. casei*

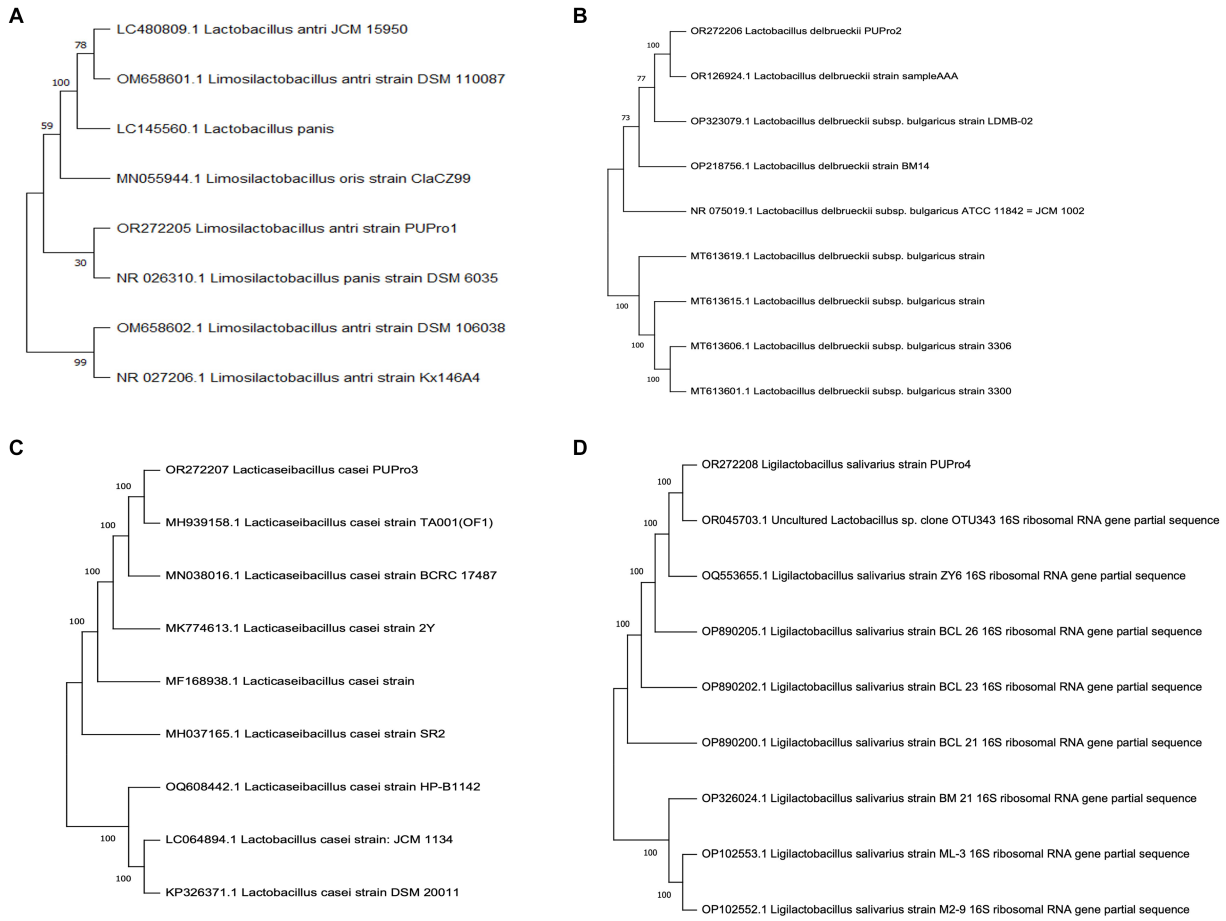

FIGURE 1
Phylogenetic trees constructed for present study bacteria using MEGA11. **(A)** *Limosilactobacillus antri* strain PUPro1. **(B)** *Lactobacillus delbrueckii* strain PUPro2. **(C)** *Lacticaseibacillus casei* strain PUPro3. **(D)** *Ligilactobacillus salivarius* strain PUPro4.

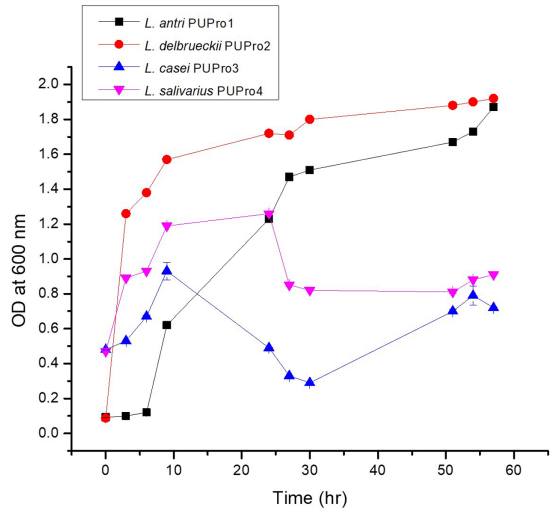

FIGURE 2
Growth curve analysis of present study bacterial isolates performed measuring OD^{600}.

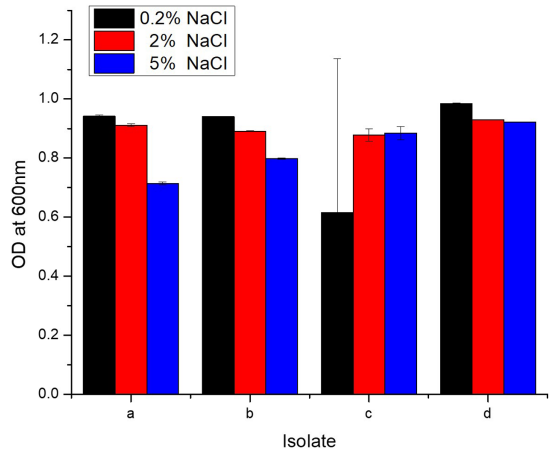

FIGURE 3
NaCl resistance potential of present study bacteria performed measuring OD^{600} at different NaCl concentrations. (a) *L. antri* strain PUPro1, (b) *L. delbrueckii* strain PUPro2, (c) *L. casei* strain PUPro3, (d) *L. salivarius* strain PUPro4.

strain PUPro3, *L. delbrueckii* strain PUPro2, *L. antri* strain PUPro1, and *L. salivarius* strain PUPro4, respectively (Figure 4; Supplementary Table S7). These results showed that these bacteria are capable of surviving the acidity of stomach before reaching the host chicken intestine.

3.6.3 Bile salt tolerance assay

In bile salt tolerance test, all isolates performed well. After 24 h incubation at 37°C, the isolates with bile salts showed a marked increase in the OD^{600} value (Figure 5). *L. casei* strain PUPro3 exhibited the greatest OD^{600}, i.e., 0.973 in the presence of bile salts, while *L. delbrueckii* strain PUPro2 had the lowest value of 0.851 (Table 2). Statistical analysis revealed significant results with value of p greater than 0.05.

TABLE 1 Survival of present study bacterial strains at 0.2, 2, and 5% NaCl concentration estimated through measuring OD^{600} in the presence of bile salts.

Isolate	OD (600 nm) at different of concentration NaCl after 24 h															
	0.2% NaCl						2% NaCl						5% NaCl			
	1st	2nd	3rd	Mean	SD	*p*-value	1st	2nd	3rd	Mean	SD	*p*-value	1st	2nd	3rd	Mean	SD	*p*-value
L. antri strain PUPro1	0.947	0.939	0.941	0.942	±0.004	0.437	0.916	0.904	0.913	0.911	±0.005	0.749	0.711	0.723	0.708	0.714	±0.005	0.999
L. delbrueckii strain PUPro2	0.942	0.943	0.941	0.940	±0.001		0.888	0.893	0.889	0.891	±0.002		0.7999	0.794	0.801	0.798	±0.002	
L. casei strain PUPro3	0.013	0.919	0.913	0.615	±0.521		0.894	0.895	0.845	0.878	±0.022		0.883	0.889	0.880	0.884	±0.022	
L. salivarius strain PUPro4	0.980	0.987	0.985	0.984	±0.003		0.930	0.928	0.929	0.929	±0.0004		0.918	0.923	0.925	0.922	±0.0004	

3.6.4 Cell adhesion assay

All isolates adhered to chicken ileum epithelial cells, and the number of CFUs increased as incubation time raised from 0 to 90 min (Supplementary Figure S3; Figure 6). Incubation for 0 min yielded zero CFU. *L. delbrueckii* strain PUPro2 adhered chicken ileum epithelial cells best and had the highest CFUs, i.e., 102.33, 261.33, and 312.67 after 30, 60, and 90 min of incubation, respectively. Least tendency of adherence was observed in case of *L. casei* strain PUPro3 (Table 3). The results were significant with $p > 0.05$.

3.6.5 Growth in the presence of pathogens

All isolates showed excellent tolerance against pathogens. *L. delbrueckii* strain PUPro2 had the highest tolerance against *Pseudomonas aeruginosa* with OD^{600} of 1.226, whereas *L. casei* strain PUPro3 had the lowest resistance with $OD^{600} = 1.017$ (Supplementary Table S8). *L. casei* strain PUPro3 exhibited highest resistance against *B. subtilis* with $OD^{600} = 1.394$, while *L. delbrueckii* strain PUPro2 showed least tolerance with OD^{600} of 1.127 (Supplementary Table S9). *L. casei* strain PUPro3 had highest OD^{600} value of 1.033 against *B. proteus* (Supplementary Table S10). *L. salivarius* strain PUPro4 had the highest OD^{600} (1.321) against *Staphylococcus aureus*, while in case of *L. casei* strain PUPro3, the value was 0.861 (Supplementary Table S11). Statistical analysis demonstrated the *p*-value of above 0.05 (Figure 7).

3.6.6 Antibiotic sensitivity profiling

All isolates were antibiotic-sensitive and exhibited zones of inhibition (Figure 8). In case of amoxicillin, cefadroxil, and kanamycin, highest zones of inhibition were observed in *L. casei* strain PUPro3, i.e., 34.33, 24.33, and 30.33 mm, respectively, while for azithromycin in *L. antri* strain PUPro1 (28.67 mm). For velosef and

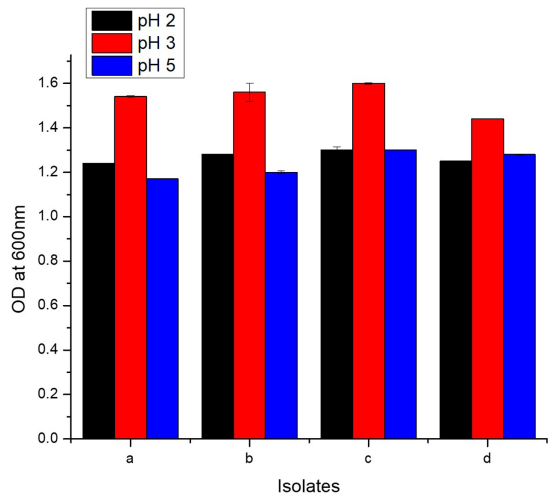

FIGURE 4
Comparison of HCl resistance potential of present study bacteria performed via measuring OD^{600} at different pH values. (a) *Limosilactobacillus antri* strain PUPro1. (b) *Lactobacillus delbrueckii* strain PUPro2. (c) *Lacticaseibacillus casei* strain PUPro3. (d)*Ligilactobacillus salivarius* strain PUPro4.

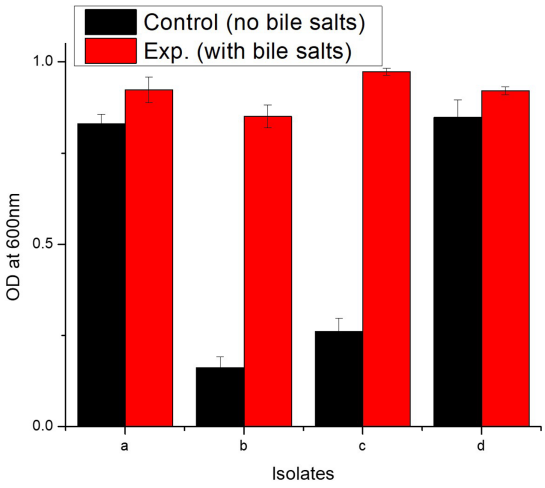

FIGURE 5
Characterization of probiotics reported in present study using bile salt tolerance assay and antimicrobial assay. (a) Comparison of OD^{600} of isolates in the absence and presence of bile salts. (b) Graphical representation of antimicrobial resistance of probiotic isolates against *Pseudomonas aeruginosa*, *Bacillus subtilis*, *Bacillus proteus*, and *Staphylococcus aureus*. (a) *L. antri* strain PUPro1, (b) *L. delbrueckii* strain PUPro2, (c) *L. casei* strain PUPro3, (d) *L. salivarius* strain PUPro4.

TABLE 2 Bile salt resistance estimated in present study bacterial strains through measurement of OD^{600} in the presence and absence of bile salts.

Isolates	OD of control at log phase (600 nm)						OD with bile salts at log phase (600 nm)					
	1st	2nd	3rd	Mean	SD	*p*-value	1st	2nd	3rd	Mean	SD	*p*-value
L. antri strain PUPro1	0.81	0.861	0.820	0.83	± 0.027	0.996	0.92	0.961	0.89	0.923	± 0.035	0.987
L. delbrueckii strain PUPro2	0.192	0.132	0.160	0.161	± 0.030		0.851	0.82	0.883	0.851	± 0.031	
L. casei strain PUPro3	0.273	0.22	0.291	0.261	± 0.036		0.985	0.964	0.972	0.973	± 0.010	
L. salivarius strain PUPro4	0.871	0.881	0.792	0.848	± 0.048		0.921	0.933	0.911	0.921	± 0.011	

10.3389/fmicb.2024.1278439

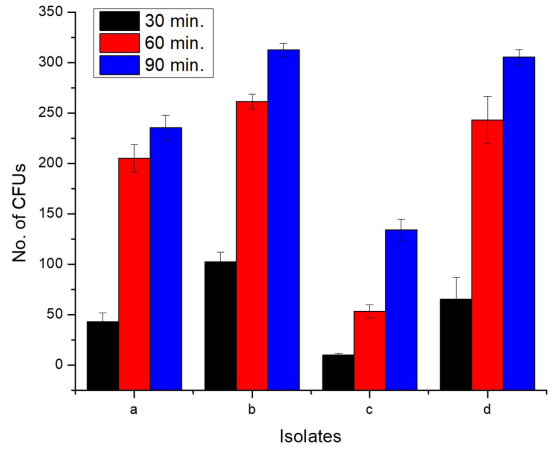

FIGURE 6
Comparison of CFUs of present study bacteria formed at different time intervals during cell adhesion assay indicating their ileum adhering tendency. (a) *Limosilactobacillus antri* strain PUPro1. (b) *Lactobacillus delbrueckii* strain PUPro2. (c) *Lacticaseibacillus casei* strain PUPro3. (d) *Ligilactobacillus salivarius* strain PUPro4.

augmentin, largest zones were observed in *L. salivarius* strain PUPro4, i.e., 33.67 and 39.33 mm (Supplementary Table S12). Significant $p > 0.05$ were obtained for all the antibiotics.

3.6.7 Hemolytic assay

Since there was no change in color of media, so all isolates were found to show ϒ-hemolysis (Supplementary Table S13). No zones were observed around the colonies (Supplementary Figure S4), indicating no RBC lysis, making these isolates the safest and best.

3.6.8 Cholesterol assay

Among the four present study bacteria, *L. casei* strain PUPro3 significantly degraded cholesterol from 216.12 to 192.2 mg/dL. *L. antri* strain PUPro1 showed the lowest cholesterol assimilation, i.e., 208 mg/dL (Figure 8).

4 Discussion

Poultry serves as major source of animal protein in the form of meat and eggs all over the world. In 2018, per person consumption of broiler meat has been estimated to be 14 kg globally and 48 kg in USA (Thorp, 2021). In Pakistan, both the private and public sectors have increased their poultry investment from 1.28 billion $ in 2015 to 4.47 billion $ in 2018 (Aslam et al., 2020). Protein production from animal agriculture in a sustainable way is becoming crucial need because the global food demand is expected to increase by 35 to 56% between 2010 and 2050 (Van Dijk et al., 2021; Castro et al., 2023), but these days poultry industry is suffering from major challenges which can be overcome through direct-fed microbial (DFM) probiotics which might equip chickens with beneficial properties such as tolerance to heat stress, reduction in foodborne illnesses, competitive exclusion of pathogens, enhanced immunity, and prebiotics with positive physiological impact (Abd El-Hack et al., 2020; Ebeid et al., 2021).

TABLE 3 Analysis of intestinal adhesion potential of present study isolates through determination of colony forming units (CFUs) at 0, 30, 60, and 90 min in cell adhesion assay.

Isolates	No. of CFUs at 0 min incubation						No. of CFUs at 30 min incubation						No. of CFU at 60 min Incubation						No. of CFU at 90 min Incubation					
	1st	2nd	3rd	Mean	SD	*p*-value	1st	2nd	3rd	Mean	SD	*p*-value	1st	2nd	3rd	Mean	SD	*p*-value	1st	2nd	3rd	Mean	SD	*p*-value
L. antri strain PUPro1	0	0	0	0	0	0.00	33	49	47	43	± 8.717	0.82	201	220	194	205	± 13.453	0.956	222	246	238	235.33	± 12.220	0.988
L. delbrueckii strain PUPro2	0	0	0	0	0		93	102	112	102.33	± 9.504		261	269	254	261.33	± 7.505		307	311	320	312.67	± 6.658	
L. casei strain PUPro3	0	0	0	0	0		12	8	9	9.66	± 2.08		47	53	60	53.33	± 6.506		139	122	141	134	± 10.440	
L. salivarius strain PUPro4	0	0	0	0	0		49	57	90	65.33	± 21.73		249	263	217	243	± 23.579		311	297	309	305.67	± 7.571	

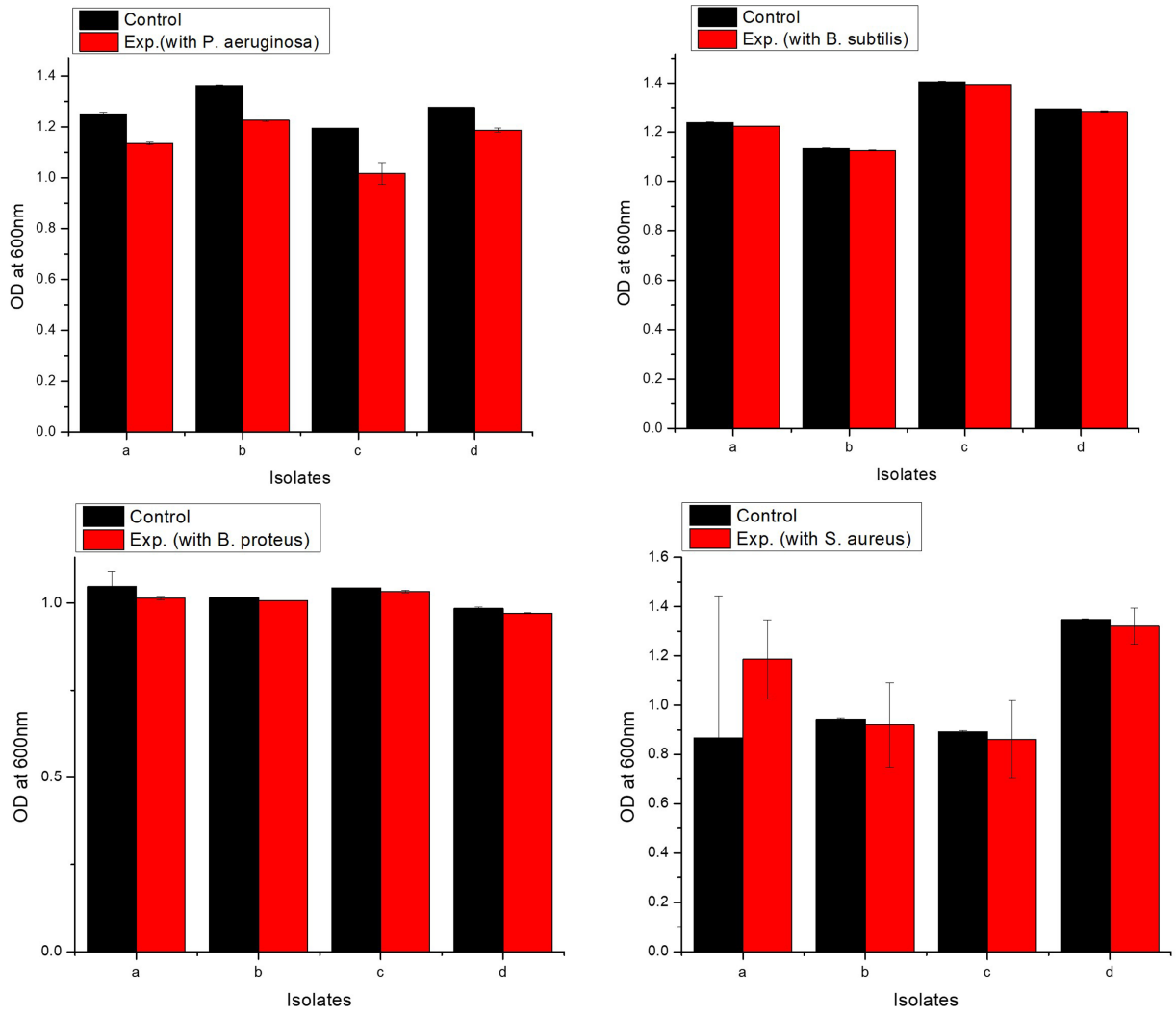

FIGURE 7
Analysis of resistance against pathogenic bacteria in present study isolates. Control comprised of medium and bacterium, while experimental tube contained medium, bacterium, and pathogen. (a) *L. antri* strain PUPro1, (b) *L. delbrueckii* strain PUPro2, (c) *L. casei* strain PUPro3, (d) *L. salivarius* strain PUPro4.

Keeping in view the role of probiotics in overcoming the challenges of poultry industry, present project was initiated to isolate bacteria from broiler chicken GIT and their *in vitro* assessment for probiotic potential. Bacteria qualifying the *in vitro* assessment assays, as described in methodology of this study, might contribute to upgrade the economic status of Pakistan associated with poultry performance by providing hygienic and proper broilers diet in cost effective way. These might serve for the production of disease-resistant broilers with reduce cooking, pressing, and shear losses. They may also enhance bone mass, meat quality (amino acids, fat content, protein content, texture), and FCR (Pourakbari et al., 2016; Fekadie et al., 2022).

In addition to abovementioned benefits, the prebiotics derived from these probiotics also positively regulate the chicken metabolism in variety of ways, e.g., compound probiotics have been observed to contribute to growth performance of broilers exposed to heat stress, through increased rate of arginine, amino sugar, alanine, aspartate and glutamate, and beta alanine biosynthesis (Zhang et al., 2023). Metabolomics has also confirmed the formation of same metabolites in chicken intestine as formed in the presence of antibiotics, i.e., amino acids, sugars, organic acids, disaccharides, and trisaccharides, confirming their use as alternative to antibiotics (Li et al., 2023). Among the probiotics reported in the literature, *Lactobacillus* have been found to have strong involvement in the regulation of gut metabolites which in turn improves homoeostasis in chickens. In a study, chickens were fed on *L. acidophilus* supplemented diet which positively affected the amino acid and lipid metabolism along with increased production of immunoglobulin G (IgG) (Chen et al., 2023). Another study has reported enhanced concentration of acetate in broiler chickens fed with diet supplemented with *L. salivarius*. When this probiotic was combined with phytobiotics, it reduced extended-spectrum beta-lactamase (ESBL) producing *E. coli* (Ren et al., 2019). In a study,

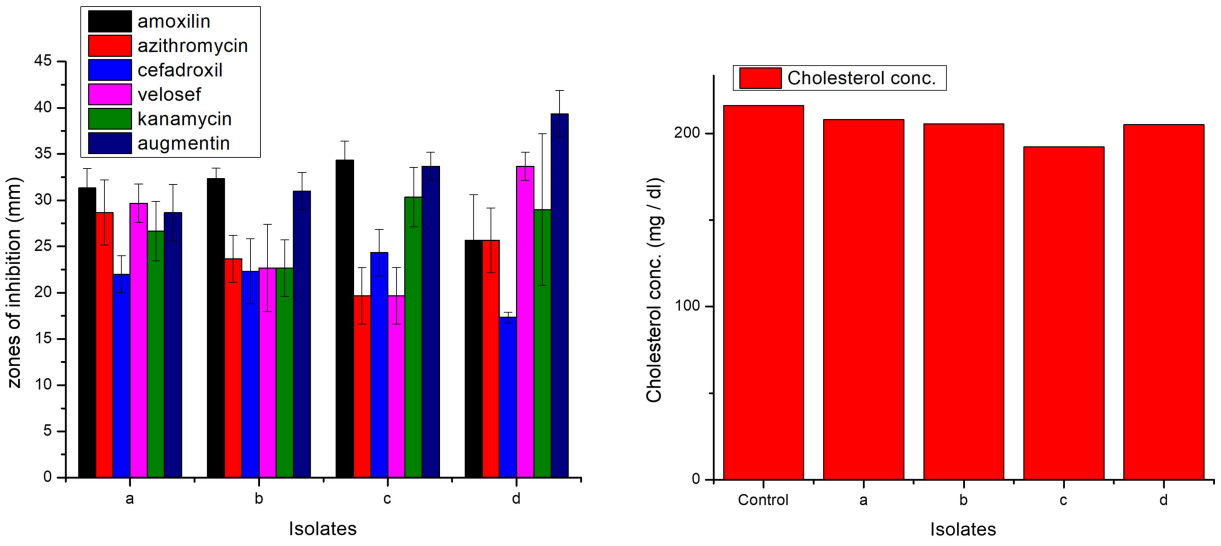

FIGURE 8
Comparison of zones of inhibition exhibited by present study bacteria against different antibiotics and comparison of cholesterol degradation potential of present study bacteria evaluated by CHOD-PAP method using cholesterol liquicolor kit. (a) *L. antri* strain PUPro1, (b) *L. delbrueckii* strain PUPro2, (c) *L. casei* strain PUPro3, (d) *L. salivarius* strain PUPro4.

broilers fed with *L. plantarum*-derived metabolites considerably increased height of villi and growth (Gao et al., 2017). Dietary supplementation with *L. plantarum* along with fructooligosaccharide (FOS) showed increased levels of short chain fatty acids (SCFAs), IgA, and IgG and efficient growth performance in *E. coli* O78 challenged broilers (Ding et al., 2019). Another study has reported increased expression of genes involved in sulfur and nitrogen metabolism, flagella assembly and chemotaxis, and vitamin and cofactor synthesis, in lincomycin exposed broilers, supplemented with *L. plantarum* P-8 (Gao et al., 2017). Literature has also reported efficient role of *L. plantarum*-derived postbiotics in enhancing carcass yield, immunity, intestinal microbial composition, and growth performance of broilers exposed to heat stress (Humam et al., 2019).

In addition to above health benefits, probiotics through interfering the metabolic pathways of host chickens enable them to withstand heat and oxidative stresses. Probiotics, in intestinal epithelial cells, activate the heat shock proteins (HSPs), glutathione S-transferase (GST), and glutathione (GSH) and inactivates iNOS, COX-2, NF-KB, and toll-like receptor-4 (TLR-4) when there is high reactive oxygen species (ROS) accumulation. ROS are produced in intestine under oxidative stress. Activation of GST by probiotics results in production of GSH which serves as an antioxidant and removes ROS. Inhibition of iNOS by probiotics inhibits synthesis of nitric oxide synthase (NOS) resulting in decreased nitric oxide (NO) thus reducing ROS. Inhibition of COX-2, NF-KB, and TLR-4 reduces heat shock-induced inflammation in intestinal epithelium thus protecting the digestive system from permanent damage. To reduce the heat-induced epithelium disruption, probiotics accelerate the production of mucous and tight junction-adherent junction (TJ-AJ) pathway which seals intracellular space between neighboring cells (Abd El-Hack et al., 2020).

Keeping in view, these beneficial effects of probiotics, we attempted to isolate bacteria from chicken GIT. Four fast growing isolates were processed for detailed *in vitro* characterization. These isolates were identified to be *L. antri*, *L. delbrueckii*, *L. casei*, and *L. salivarius*, respectively. As all of these had different species and also showed variations during characterization, so were designated as different strains, i.e., PUPro1, PUPro2, PUPro3, and PUPro4, respectively. Our study is consistent with the previous one because most of the broilers have been reported to have *Lactobacilli* as gut flora (Boonkumklao et al., 2006). *L. casei, L. johnsonii, L. acidophilus, L. crispatus, L. salivarius,* and *L. aviaries* are the most reported *Lactobacillus* species in poultry (Sanders and Klaenhammer, 2001; Tharmaraj and Shah, 2003; Neville and O'Toole, 2010; Pieniz et al., 2014).

All isolates were found fast growing. Log phases comprising of 24–57 h, 3–51 h, 6–24 h, and 9–24 h were observed in *L. antri* strain PUPro1, *L. delbrueckii* strain PUPro2, *L. casei* strain PUPro3, and *L. salivarius* strain PUPro4, respectively. These findings are in line with previously reported chicken gut-associated bacteria which exhibited a rapid growth (Vinderola et al., 2002; Śliżewska and Chlebicz-Wójcik, 2020).

Literature describes various biochemical features of probiotics (Bansal et al., 2019; Samedi and Charles, 2019; Abid et al., 2022), but this is the first study to use the RapID™ NF Plus Panel for biochemical testing. The ability of a bacterium to use arginine as a carbon source can be tested biochemically by ADH test (Kwon et al., 2005). In present analysis, none of the isolates tested positive for ADH. All isolates were positive in EST and GLU test results. In the EST test, lipid break down releases fatty acids which drop the pH and change the color (MacFaddin, 2000). With the exception of *L. antri* strain PUPro1, all of the probiotic strains tested positive for PHS assay (Gilardi et al., 1975). None of the isolates showed positive results for GGT, NAG, α-GLU, β-GLU, PRO, BANA, IND, TRY, PYR, ONPG, and URE tests that detects the presence of glutamyl aminopeptidase, p-nitrophenyl-N-acetyl-*β*-D-glucosaminidase, ρ-nitrophenyl-D-glucosidase, ρ-nitrophenyl-β-D-glucosidase, proline aminopeptidase,

N-benzyl-arginine aminopeptidase, potential of tryptophan to indole conversion, tryptophan aminopeptidase, pyrrolidonyl aminopeptidase, ρ-nitrophenyl-β-D-galactosidase, and urea hydrolysis potential, respectively (Westley et al., 1967; Mulczyk and Szewczuk, 1970; Gilardi et al., 1975; Kilian and Bülo, 1976; Nagatsu et al., 1976; Humble et al., 1977; Holt et al., 1984; Kwon et al., 2005). *L. antri* strain PUPro1 and *L. salivarius* strain PUPro4 tested positive for NO_3 test that identifies nitrate reductase activity (Mulczyk and Szewczuk, 1970).

All the isolates were found to be resistant to NaCl at 0.2, 2, and 5% concentration. *L. salivarius* strain PUPro4 was the most resistant, with OD^{600} of 0.984, 0.929, and 0.922 for 0.2, 2, and 5% NaCl concentration, respectively. A previous study indicated that LAB from milk and milk products, meats, chicken dung, and other sources can grow in 1–10% NaCl treatments (Hoque et al., 2010; Shehata et al., 2016). Our findings are consistent with the literature and imply that present study bacteria can survive higher concentrations of NaCl and stress in vitro (Ye et al., 2020).

Probiotic strains must bind to host intestinal cells for better colonization (Collado et al., 2007). Probiotics' antimicrobial and cholesterol-lowering benefits require strong colon epithelial cell attachment (Shokryazdan et al., 2014). In this study, all isolates adhered to chicken ileum epithelial cells with increased viability over 90 min *L. casei* strain PUPro3, with a maximum CFUs count of 134, showed the lowest adhesion ability. Our findings are consistent with those of literature that observed rumen LAB isolates' adherence increased with incubation period (Setyawardani et al., 2014; Jose et al., 2015).

Stay of probiotics in different parts of chicken GIT varies as per the pH values of these parts. Generally, pH varies between 2 and 6.5, i.e., pH values for crop, proventriculus, gizzard, small intestine, and large intestine have been reported to be 4.8, 4.4, 2.6, 6.2, and 6.3, respectively (Svihus, 2014). Keeping in view these values, acidity tolerance of present study bacteria was estimated at three pH values, i.e., 2, 3, and 5. Maximum survival during interval of 3 h was observed in *L. delbrueckii* strain PUPro2 (pH = 2), in *L. antri* strain PUPro1, *L. delbrueckii* strain PUPro2 and *L. casei* strain PUPro3 (pH = 3), and in *L. casei* strain PUPro3 (pH = 6). No survival was observed in *L. antri* strain PUPro1 at pH = 6. These results were according to the previous research study reporting good survival of *L. salivarius* and *L. fermentum* at pH = 2.5 for 3 h (Hutari et al., 2011). Other studies have also reported survival of probiotics at the same pH (Reuben et al., 2019; Salehizadeh et al., 2020; Gupta et al., 2023). These findings confirmed the survival of present study bacteria in chicken gut during passage through stomach.

Hydrophobic bile salts play crucial roles in digestive system including fat emulsification and resistance against antimicrobials. So, when taken orally, probiotics must survive the severe environment of small intestine (Olejnik et al., 2005). In chicken gut, bile salt concentration varies, i.e., 0.0085% (caecum), 0.17% (duodenum), and 0.7% (jejunum). Typical 0.3% bile salt level has been considered in many probiotic bile salt tolerance studies (Shokryazdan et al., 2014; García-Hernández et al., 2016). The current study's isolates survived in 0.3% bile salts and exhibited enhanced growth after 24 h. In this study, *L. casei* strain PUPro3 had the highest OD value of 0.973 in the presence of bile salts. Present finding is in accordance with previous literature reporting tolerance to 0.3% concentration of bile salts (Shin et al., 2008; Salehizadeh et al., 2020). Our findings also support prior research that revealed bile salts increased probiotic proliferation (Reuben et al., 2019).

The chicken industry loses a lot of revenue due to zoonotic and foodborne disease illnesses (Nallala et al., 2017). Potential probiotics need to have antimicrobial activity against such pathogens. All of the present study isolates were highly antagonistic to four distinct pathogens: *Pseudomonas aeruginosa, Bacillus subtilis, Bacillus proteus*, and *Staphylococcus aureus*. Antimicrobial activity against *P. aeruginosa*, *B. subtilis*, *B. proteus*, and *S. aureus* was highest for *L. delbrueckii* strain PUPro2, *L. casei* strain PUPro3, *L. casei* strain PUPro3, and *L. salivarius* strain PUPro4. This finding is consistent with previous study. Our results are also supported by the observation that chicken-derived probiotics have a broad-spectrum antagonistic impact against a wide range of infections (García-Hernández et al., 2016; Oyewole et al., 2018).

Antibiotic-resistant genes in probiotic could cause gut infections, so antibiotic profiling of isolated bacteria was crucial (Nallala et al., 2017). All isolates were ecologically benign and showed unique inhibitory zones against augmentin, azithromycin, amoxicillin, kanamycin, cefadroxil, and velosef. The obtained inhibitory zones had diameters between 17.33 mm and 39.33 mm. The literature reports antibiotic susceptibility in chicken probiotic cultures against antibiotics such as penicillin, ampicillin, chloramphenicol, ceftriaxone, and novobiocin supporting our findings (Gueimonde Fernández et al., 2013; Anandharaj and Sivasankari, 2014; Puniya et al., 2016; Dowarah et al., 2018). However, contrary to our findings, the literature also reports resistance against kanamycin, aminoglycosides and glycopeptides, streptomycin, gentamicin, and vancomycin in *Lactobacilli* (Jose et al., 2015; Zavišić et al., 2023).

According to FAO guidelines, probiotic microbial strains should not pose any host safety risks (Borras et al., 2021). Hemolytic activity destroys the protective epithelial layer, allowing infections to penetrate easily. Non-pathogenic strains must be non-hemolytic (De Vuyst et al., 2003). None of the isolates tested in this study produced the toxic chemical hemolysin, and all were non-hemolytic. Non-hemolytic LAB strains have been reported in the literature, which is in line with our findings (Chang et al., 2013; Oloyede and Afolabi, 2013; Oyewole et al., 2018).

Hypercholesterolemia or high blood cholesterol is a primary cause of deaths caused by heart diseases in poultry which can be decreased by lowering serum cholesterol (Shehata et al., 2016). Cholesterol lowering potential of isolates was measured using a cholesterol liquicolor kit. All of the isolated bacteria showed degradation potential toward cholesterol. The *L. casei* strain PUPro3 was the most effective at degrading cholesterol, reducing cholesterol levels from 216.12 to 192.2 mg/dL. *L. antri* strain PUP1 degraded cholesterol at a rate of just 208 mg/dL. These results are consistent with the literature (Miremadi et al., 2014; Shehata et al., 2016).

5 Conclusion

Probiotic strains separated from their natural host are more likely to establish themselves in the GIT and exert their therapeutic benefits. Present study is significant because the bacteria isolated might have potential as antibiotic substitutes and broiler productivity boosters. To further test and confirm their possible effect on broilers meat quality,

they can be cultured for the estimation of CFU production followed by their immobilization in approximate quantity on any suitable substrate. This will enhance their shelf life. Afterward, these probiotics can be fed to broilers through feed supplementation. In addition to this, probiotic metabolomics and its integration with proteomics might also prove helpful in getting insight into their possible contributions to sustainable poultry production.

Data availability statement

The datasets presented in this study can be found in online repositories. The names of the repository/repositories and accession number(s) can be found in the article/Supplementary material.

Author contributions

FS: Data curation, Writing – original draft. FM: Conceptualization, Writing – original draft. AS: Formal analysis, Writing – original draft. SS: Writing – original draft. SA: Formal analysis, Writing – original draft. AQ: Writing – review & editing.

Funding

The authors declare that financial support was received for the research work and publication of this article from King Saud University, Riyadh, Saudi Arabia.

Acknowledgments

The authors would like to thank the Researchers Supporting Project number (RSP2024R35), King Saud University, Riyadh, Saudi Arabia.

Conflict of interest

The authors declare that the research was conducted in the absence of any commercial or financial relationships that could be construed as a potential conflict of interest.

Publisher's note

All claims expressed in this article are solely those of the authors and do not necessarily represent those of their affiliated organizations, or those of the publisher, the editors and the reviewers. Any product that may be evaluated in this article, or claim that may be made by its manufacturer, is not guaranteed or endorsed by the publisher.

Supplementary material

The Supplementary material for this article can be found online at: https://www.frontiersin.org/articles/10.3389/fmicb.2024.1278439/full#supplementary-material

References

Abd El-Hack, M. E., El-Saadony, M. T., Shafi, M. E., Qattan, S. Y. A., Batiha, G. E., Khafaga, A. F., et al. (2020). Probiotics in poultry feed: a comprehensive review. *J. Anim. Physiol. Anim. Nutr.* 104, 1835–1850. doi: 10.1111/jpn.13454

Abid, S., Farid, A., Abid, R., Rehman, M. U., Alsanie, W. F., Alhomrani, M., et al. (2022). Identification, biochemical characterization, and safety attributes of locally isolated *Lactobacillus fermentum* from *Bubalus bubalis* (buffalo) milk as a probiotic. *Microorganisms* 10:954. doi: 10.3390/microorganisms10050954

Agus, A., Planchais, J., and Sokol, H. (2018). Gut microbiota regulation of tryptophan metabolism in health and disease. *Cell Host Microbe* 23, 716–724. doi: 10.1016/j.chom.2018.05.003

Akbar, M., Akbar, A., Yaqoob, H. S., Hussain, A., Svobodová, L., and Yasmin, F. (2023). Islamic finance education: current state and challenges for Pakistan. *Cogent. Econ. Finance* 11:2164665. doi: 10.1080/23322039.2022.2164665

Alam, W., Khan, S., Sultan, A., Ahmad, N., Tanweer, A. J., Abbas, G., et al. (2023). Effect of dietary supplementation of animal blood plasma powder on production performance, dressed weight and immune response of broiler. *Pak. J. Sci.* 75, 419–426. doi: 10.57041/pjs.v75i02.8

Anandharaj, M., and Sivasankari, B. (2014). Isolation of potential probiotic *Lactobacillus oris* HMI68 from mother's milk with cholesterol-reducing property. *J. Biosci. Bioeng.* 118, 153–159. doi: 10.1016/j.jbiosc.2014.01.015

Arsène, M. M., Davares, A. K., Andreevna, S. L., Vladimirovich, E. A., Carime, B. Z., Marouf, R., et al. (2021). The use of probiotics in animal feeding for safe production and as potential alternatives to antibiotics. *Vet. World.* 14:319. doi: 10.14202/vetworld.2021.319-328

Aslam, H. B., Alarcon, P., Yaqub, T., Iqbal, M., and Häsler, B. (2020). A value chain approach to characterize the chicken sub-sector in Pakistan. *Front. Vet. Sci.* 7:361. doi: 10.3389/fvets.2020.00361

Baéza, E., Guillier, L., and Petracci, M. (2022). Production factors affecting poultry carcass and meat quality attributes. *Animal* 16:100331. doi: 10.1016/j.animal.2021.100331

Bansal, P., Kumar, R., Singh, J., and Dhanda, S. (2019). Next generation sequencing, biochemical characterization, metabolic pathway analysis of novel probiotic *Pediococcus acidilactici* NCDC 252 and it's evolutionary relationship with other lactic acid bacteria. *Mol. Biol. Rep.* 46, 5883–5895. doi: 10.1007/s11033-019-05022-z

Beckers, B., Op De Beeck, M., Thijs, S., Truyens, S., Weyens, N., Boerjan, W., et al. (2016). Performance of 16s rDNA primer pairs in the study of rhizosphere and endosphere bacterial microbiomes in metabarcoding studies. *Front. Microbiol.* 7:650. doi: 10.3389/fmicb.2016.00650

Boonkumklao, P., Kongthong, P., and Assavanig, A. (2006). Acid and bile tolerance of *Lactobacillus thermotolerans*, a novel species isolated from chicken feces. *Agric. Nat. Resour.* 40, 13–17.

Borras, L., Valiño, E., Elías, A., Martínez, J., Sanabria, A., and Becerra, M. (2021). Effect of fibrous materials inclusion on the solid-state fermentation of post harvested wastes of *Solanum tuberosum*. *Cuba. J. Agric. Sci.* 55, 31–42.

Castro, F. L. S., Chai, L., Arango, J., Owens, C. M., Smith, P. A., Reichelt, S., et al. (2023). Poultry industry paradigms: connecting the dots. *J. Appl. Poult. Res.* 32:100310. doi: 10.1016/j.japr.2022.100310

Chang, S. M., Tsai, C. L., Wee, W. C., and Yan, T. R. (2013). Isolation and functional study of potentially probiotic lactobacilli from Taiwan traditional paocai. *Afr. J. Microbiol. Res.* 7, 683–691. doi: 10.5897/AJMR12.2196

Chen, X., Chen, W., Ci, W., Zheng, Y., Han, X., Huang, J., et al. (2023). Effects of dietary supplementation with *Lactobacillus acidophilus* and *Bacillus subtilis* on mucosal immunity and intestinal barrier are associated with its modulation of gut metabolites and microbiota in late-phase laying hens. *Probiot.Antimicrob. Proteins* 15, 912–924. doi: 10.1007/s12602-022-09923-7

Cizeikiene, D., and Jagelaviciute, J. (2021). Investigation of antibacterial activity and probiotic properties of strains belonging to *Lactobacillus* and *Bifidobacterium* genera for their potential application in functional food and feed products. *Probiot. Antimicrob. Proteins* 13, 1387–1403. doi: 10.1007/s12602-021-09777-5

Collado, M. C., Meriluoto, J., and Salminen, S. (2007). In vitro analysis of probiotic strain combinations to inhibit pathogen adhesion to human intestinal mucus. *Food Res. Int.* 40, 629–636. doi: 10.1016/j.foodres.2006.11.007

De Vuyst, L., Moreno, M. F., and Revets, H. (2003). Screening for enterocins and detection of hemolysin and vancomycin resistance in enterococci of different origins. *Int. J. Food Microbiol.* 84, 299–318. doi: 10.1016/S0168-1605(02)00425-7

Desiere, S., Hung, Y., Verbeke, W., and D'Haese, M. (2018). Assessing current and future meat and fish consumption in sub-Sahara Africa: learnings from FAO food balance sheets and LSMS household survey data. *Glob. Food Sec.* 16, 116–126. doi: 10.1016/j.gfs.2017.12.004

Ding, S., Wang, Y., Yan, W., Li, A., Jiang, H., and Fang, J. (2019). Effects of *Lactobacillus plantarum* 15-1 and fructooligosaccharides on the response of broilers to pathogenic *Escherichia coli* O78 challenge. *PLoS One* 14:e0212079. doi: 10.1371/journal.pone.0223971

Dowarah, R., Verma, A. K., Agarwal, N., Singh, P., and Singh, B. R. (2018). Selection and characterization of probiotic lactic acid bacteria and its impact on growth, nutrient digestibility, health and antioxidant status in weaned piglets. *PLoS One* 13:e0192978. doi: 10.1371/journal.pone.0192978

Ebeid, T. A., Al-Homidan, I. H., and Fathi, M. M. (2021). Physiological and immunological benefits of probiotics and their impacts in poultry productivity. *World Poultry Sci. J.* 77, 883–899. doi: 10.1080/00439339.2021.1960239

Fadanka, S., Minette, S., and Mowoh, N. (2022). *Preparation of Bacteria glycerol stocks*. Available at: https://www.protocols.io/view/preparation-of-bacteria-glycerol-stocks-b85iry4e.

Fekadie, A., Abera, A., and Yitbarek, C. (2022). Effective microbes (EM) supplementation effect on feed intake digestibility and live weight changes of Washera sheep fed wheat straw. *Iran. J. Appl. Anim. Sci.* 4, 713–722.

Gao, P., Hou, Q., Kwok, L. Y., Huo, D., Feng, S., and Zhang, H. (2017). Effect of feeding *Lactobacillus plantarum* P-8 on the faecal microbiota of broiler chickens exposed to lincomycin. *Sci. Bull.* 62, 105–113. doi: 10.1016/j.scib.2017.01.001

García-Hernández, Y., Pérez-Sánchez, T., Boucourt, R., Balcázar, J. L., Nicoli, J. R., Moreira-Silva, J., et al. (2016). Isolation, characterization and evaluation of probiotic lactic acid bacteria for potential use in animal production. *Res. Vet. Sci.* 108, 125–132. doi: 10.1016/j.rvsc.2016.08.009

Gilardi, G., Hirschl, S., and Mandel, M. (1975). Characteristics of yellow-pigmented nonfermentative bacilli (groups Ve-1 and Ve-2) encountered in clinical bacteriology. *J. Clin. Microbiol.* 1, 384–389. doi: 10.1128/jcm.1.4.384-389.1975

Green, M. R., and Sambrook, J. (2019). Analysis of DNA by agarose gel electrophoresis. *Cold Spring Harbor Protoc* 2019:pdb.top100388. doi: 10.1101/pdb.top100388

Gueimonde Fernández, M., Sánchez García, B., De Los, G., Reyes-Gavilán, C., and Margolles Barros, A. (2013). Antibiotic resistance in probiotic bacteria. *Front. Microbiol.*:202:4. doi: 10.3389/fmicb.2013.00202

Gupta, N. (2019). DNA extraction and polymerase chain reaction. *J. Cytol.* 36, 116–117. doi: 10.4103/JOC.JOC_110_18

Gupta, M., Raut, R., Manandhar, S., Chaudhary, A., Shrestha, U., Dangol, S., et al. (2023). Identification and characterization of probiotics isolated from indigenous chicken (*Gallus domesticus*) of Nepal. *PLoS One* 18:e0280412. doi: 10.1371/journal.pone.0280412

He, Y., Li, J., Wang, F., Na, W., and Tan, Z. (2023). Dynamic changes in the gut microbiota and metabolites during the growth of Hainan Wenchang chickens. *Animals* 13:348. doi: 10.3390/ani13030348

Henchion, M., Moloney, A. P., Hyland, J., Zimmermann, J., and Mccarthy, S. (2021). Trends for meat, milk and egg consumption for the next decades and the role played by livestock systems in the global production of proteins. *Animal* 15:100287. doi: 10.1016/j.animal.2021.100287

Holt, J. G., Krieg, N., Sneath, P., Staley, J., and Williams, S. (1984). *Bergey's manual of systematic bacteriology*. The Williams and Wilkins Co., Baltimore.

Hoque, M., Akter, F., Hossain, K., Rahman, M., Billah, M., and Islam, K. (2010). Isolation, identification and analysis of probiotic properties of *Lactobacillus* spp. from selective regional yoghurts. *World J. Dairy Food Sci.* 5, 39–46.

Humam, A. M., Loh, T. C., Foo, H. L., Samsudin, A. A., Mustapha, N. M., Zulkifli, I., et al. (2019). Effects of feeding different postbiotics produced by *Lactobacillus plantarum* on growth performance, carcass yield, intestinal morphology, gut microbiota composition, immune status, and growth gene expression in broilers under heat stress. *Animals* 9:644. doi: 10.3390/ani9090644

Humble, M., King, A., and Phillips, I. (1977). API ZYM: a simple rapid system for the detection of bacterial enzymes. *J. Clin. Pathol.* 30, 275–277. doi: 10.1136/jcp.30.3.275

Hutari, A., Jaseem, W. S., Hamid, A. A., and Yusoff, W. M. W. (2011). Screening of *Lactobacillus* strains against *Salmonella* both isolated from Malaysian free-range chicken intestine for use as probiotic. *Sains Malays* 40, 1115–1122.

Ivanova, N. N., and Denisenko, L. I. (2019). "The role of probiotics in the poultry industry" in *Urgent issues of agricultural science, production and education*, 209–212. Available at: https://www.elibrary.ru/item.asp?id=37404056

Jomehzadeh, N., Javaherizadeh, H., Amin, M., Saki, M., Al-Ouqaili, M. T., Hamidi, H., et al. (2020). Isolation and identification of potential probiotic Lactobacillus species from feces of infants in Southwest Iran. *Int. J. Infect. Dis.* 96, 524–530. doi: 10.1016/j.ijid.2020.05.034

Jose, N. M., Bunt, C. R., and Hussain, M. A. (2015). Comparison of microbiological and probiotic characteristics of lactobacilli isolates from dairy food products and animal rumen contents. *Microorganisms* 3, 198–212. doi: 10.3390/microorganisms3020198

Khan, S., Moore, R. J., Stanley, D., and Chousalkar, K. K. (2020). The gut microbiota of laying hens and its manipulation with prebiotics and probiotics to enhance gut health and food safety. *Appl. Environ. Microbiol.* 86, e00600–e00620. doi: 10.1128/AEM.00600-20

Kilian, M., and Bülo, P. (1976). Rapid diagnosis of *Enterobacteriaceae*: I. Detection of bacterial glycosidases. *Acta Pathol. Microbiol. Scand. Sect. B Microbiol.* 84, 245–251.

Kumar, A., and Kumar, D. (2015). Characterization of *Lactobacillus* isolated from dairy samples for probiotic properties. *Anaerobe* 33, 117–123. doi: 10.1016/j.anaerobe.2015.03.004

Kumari Vb, C., Huligere, S. S., Alotaibi, G., Al Mouslem, A. K., Bahauddin, A. A., Shivanandappa, T. B., et al. (2023). Antidiabetic activity of potential probiotics *limosilactobacillus* spp., *levilactobacillus* spp., and *lacticaseibacillus* spp. isolated from fermented sugarcane juice: a comprehensive in vitro and in silico study. *Nutrients* 15:1882. doi: 10.3390/nu15081882

Kwon, K. K., Lee, H.-S., Yang, S. H., and Kim, S. J. (2005). *Kordiimonas gwangyangensis* gen. Nov., sp. nov., a marine bacterium isolated from marine sediments that forms a distinct phyletic lineage (*Kordiimonadales* Ord. Nov.) in the '*Alphaproteobacteria*'. *Int. J. Syst. Evol. Microbiol.* 55, 2033–2037. doi: 10.1099/ijs.0.63684-0

Li, Y., Zhang, J. L., Deng, J. J., Chen, Z., Liu, S., Liu, J., et al. (2023). *Integrative analysis of the microbiome and metabolome of broiler intestine: insights into the mechanisms of probiotic action as an antibiotic substitute*. doi: 10.21203/rs.3.rs-3456870/v1

Liu, J., Wang, J., Zhou, Y., Han, H., Liu, W., Li, D., et al. (2022). Integrated omics analysis reveals differences in gut microbiota and gut-host metabolite profiles between obese and lean chickens. *Poultry Sci.* 101:102165. doi: 10.1016/j.psj.2022.102165

Liu, Q., Yu, Z., Tian, F., Zhao, J., Zhang, H., Zhai, Q., et al. (2020). Surface components and metabolites of probiotics for regulation of intestinal epithelial barrier. *Microb. Cell Factories* 19, 1–11. doi: 10.1186/s12934-020-1289-4

Lorenz, T. C. (2012). Polymerase chain reaction: basic protocol plus troubleshooting and optimization strategies. *J. Vis. Exp.*:63:e3998. doi: 10.3791/3998

Lutful, K. S. M. (2009). The role of probiotics in the poultry industry. *Int. J. Mol. Sci.* 10, 3531–3546. doi: 10.3390/ijms10083531

MacFaddin, J. (2000). *Biochemical tests for identification of medical bacteria*. Lippincott Williams & Wilkins Philadelphia, PA.

Maloney, S., Engler, C., and Norton, R. (2014). Evaluation of the Remel RapID NF plus rapid biochemical method for identification of *Burkholderia pseudomallei*. *J. Clin. Microbiol.* 52, 2175–2176. doi: 10.1128/JCM.00025-14

Mehmood, A., Nawaz, M., Rabbani, M., and Mushtaq, M. H. (2023). In vitro characterization of probiotic potential of *Limosilactobacillus fermentum* against *Salmonella gallinarum* causing fowl typhoid. *Animals* 13:1284. doi: 10.3390/ani13081284

Melese, K., Alemu, T., and Desalegn, A. (2023). Isolation, characterization and *in-vitro* evaluation of potential probiotic lactic acid bacteria isolated from chicken gut. [Preprint]. doi: 10.21203/rs.3.rs-2697471/v1

Miremadi, F., Ayyash, M., Sherkat, F., and Sojanovska, L. (2014). Cholesterol reduction mechanisms and fatty acid composition of cellular membranes of probiotic *lactobacilli* and *Bifidobacteria*. *J. Funct. Foods* 9, 295–305. doi: 10.1016/j.jff.2014.05.002

Mohammed, A., Zaki, R., Negm, E., Mahmoud, M., and Cheng, H. (2021). Effects of dietary supplementation of a probiotic (*Bacillus subtilis*) on bone mass and meat quality of broiler chickens. *Poult. Sci.* 100:100906. doi: 10.1016/j.psj.2020.11.073

Mulczyk, M., and Szewczuk, A. (1970). Pyrrolidonyl peptidase in bacteria: a new colrimetric test for differentiation of enterobacteriaceae. *J. Gen. Microbiol.* 61, 9–13.

Musikasang, H., Tani, A., Kittikun, A.-H., and Maneerat, S. (2009). Probiotic potential of lactic acid bacteria isolated from chicken gastrointestinal digestive tract. *World J. Microbiol. Biotechnol.* 25, 1337–1345. doi: 10.1007/s11274-009-0020-8

Nagatsu, T., Hino, M., Fuyamada, H., Hayakawa, T., Sakakibara, S., Nakagawa, Y., et al. (1976). New chromogenic substrates for X-prolyl dipeptidyl-aminopeptidase. *Anal. Biochem.* 74, 466–476. doi: 10.1016/0003-2697(76)90227-X

Nallala, V., Sadishkumar, V., and Jeevaratnam, K. (2017). Molecular characterization of antimicrobial *Lactobacillus* isolates and evaluation of their probiotic characteristics in vitro for use in poultry. *Food Biotechnol.* 31, 20–41. doi: 10.1080/08905436.2016.1269289

Nawaz, A. S. N., Jagadeesh, K. S., and Krishnaraj, P. U. (2017). Isolation and screening of lactic acid bacteria for acidic pH and bile tolerance. *Int. J. Curr. Microbiol. Appl. Sci.* 6, 3975–3980. doi: 10.20546/ijcmas.2017.607.411

Neville, B., and O'Toole, P. (2010). Probiotic properties of *Lactobacillus salivarius* and closely related Lactobacillus species. *Future Microbiol.* 5, 759–774. doi: 10.2217/fmb.10.35

Ogbuewu, I. P., Mabelebele, M., Sebola, N. A., and Mbajiorgu, C. (2022). *Bacillus* probiotics as alternatives to in-feed antibiotics and its influence on growth, serum chemistry, antioxidant status, intestinal histomorphology, and lesion scores in disease-challenged broiler chickens. *Front. Vet. Sci.* 9:876725. doi: 10.3389/fvets.2022.876725

Olejnik, A., Lewandowska, M., Obarska, M., and Grajek, W. (2005). Tolerance of *Lactobacillus* and *Bifidobacterium* strains to low pH, bile salts and digestive enzymes. *Food Sci. Technol.* 8:5.

Oloyede, A., and Afolabi, O. (2013). Phenotypic characterization and in vitro screening of lactic acid bacteria from goat milk for probiotic USE. *J. Agric. Sci. Environ.* 13, 50–61. doi: 10.51406/jagse.v13i1.1210

Oyewole, O. F., Maria, C. O., Tope, P. S., and FunmI, O. O. (2018). In vitro study of potential probiotic lactic acid bacteria isolated from the gut of chickens in Abeokuta, Nigeria. *Alex. J. Vet. Sci* 58. doi: 10.5455/ajvs.290499

Pieniz, S., Andreazza, R., Anghinoni, T., Camargo, F., and Brandelli, A. (2014). Probiotic potential, antimicrobial and antioxidant activities of *Enterococcus durans* strain LAB18s. *Food Control* 37, 251–256. doi: 10.1016/j.foodcont.2013.09.055

Pourakbari, M., Seidavi, A., Asadpour, L., and Martínez, A. (2016). Probiotic level effects on growth performance, carcass traits, blood parameters, cecal microbiota, and immune response of broilers. *An. Acad. Bras. Ciênc.* 88, 1011–1021. doi: 10.1590/0001-3765201620150071

Puniya, M., Ravinder Kumar, M., Panwar, H., Kumar, N., and Ramneek, A. K. P. (2016). Screening of lactic acid bacteria of different origin for their probiotic potential. *J. Food Process. Technol.* 7:545.

Reid, G., Gadir, A. A., and Dhir, R. (2019). Probiotics: reiterating what they are and what they are not. *Front. Microbiol.* 10:424. doi: 10.3389/fmicb.2019.00424

Ren, H., Vahjen, W., Dadi, T., Saliu, E. M., Boroojeni, F. G., and Zentek, J. (2019). Synergistic effects of probiotics and phytobiotics on the intestinal microbiota in young broiler chicken. *Microorganisms* 7:684. doi: 10.3390/microorganisms7120684

Reuben, R. C., Roy, P. C., Sarkar, S. L., Alam, R.-U., and Jahid, I. K. (2019). Isolation, characterization, and assessment of lactic acid bacteria toward their selection as poultry probiotics. *BMC Microbiol.* 19, 1–20. doi: 10.1186/s12866-019-1626-0

Rizzoli, R., and Biver, E. (2020). Are probiotics the new calcium and vitamin D for bone health? *Curr. Osteoporos. Rep.* 18, 273–284. doi: 10.1007/s11914-020-00591-6

Rocha-Ramírez, L. M., Hernández-Chiñas, U., Moreno-Guerrero, S. S., Ramírez-Pacheco, A., and Eslava, C. A. (2021). Probiotic properties and immunomodulatory activity of *Lactobacillus* strains isolated from dairy products. *Microorganisms* 9:825. doi: 10.3390/microorganisms9040825

Salehizadeh, M., Modarressi, M. H., Mousavi, S. N., and Ebrahimi, M. T. (2020). Evaluation of lactic acid bacteria isolated from poultry feces as potential probiotic and its in vitro competitive activity against *Salmonella typhimurium*. *Vet. Res. Forum* 11, 67–75. doi: 10.30466/vrf.2018.84395.2110

Saman, A., Chaudhry, M., Ijaz, M., Shaukat, W., Zaheer, M. U., Mateus, A., et al. (2023). Assessment of knowledge, perception, practices and drivers of antimicrobial resistance and antimicrobial usage among veterinarians in Pakistan. *Prev. Vet. Med.* 212:105836. doi: 10.1016/j.prevetmed.2022.105836

Samedi, L., and Charles, A. L. (2019). Isolation and characterization of potential probiotic lactobacilli from leaves of food plants for possible additives in pellet feeding. *Ann. Agric. Sci.* 64, 55–62. doi: 10.1016/j.aoas.2019.05.004

Sanders, M., and Klaenhammer, T. (2001). Invited review: the scientific basis of *Lactobacillus acidophilus* NCFM functionality as a probiotic. *J. Dairy Sci.* 84, 319–331. doi: 10.3168/jds.S0022-0302(01)74481-5

Sanders, M. E., Merenstein, D. J., Reid, G., Gibson, G. R., and Rastall, R. A. (2019). Probiotics and prebiotics in intestinal health and disease: from biology to the clinic. *Nat. Rev. Gastroenterol. Hepatol.* 16, 605–616. doi: 10.1038/s41575-019-0173-3

Setyawardani, T., Rahayu, W., Maheswari, R., and Palupi, N. (2014). Antimicrobial activity and adhesion ability of indigenous lactic acid bacteria isolated from goat milk. *Int. J. Food Res.* 21.

Shamsudin, W. N. F., San Loo, S., Ho, Y. W., Abdullah, N., Saad, W. Z., and Wan, K. L. (2019). Probiotic properties of *Lactobacillus* isolates from chicken intestines. *J. Biochem. Microbiol. Biotechnol.* 7, 8–13. doi: 10.54987/jobimb.v7i2.476

Shehata, M., El-Sohaimy, S., El-Sahn, M. A., and Youssef, M. (2016). Screening of isolated potential probiotic lactic acid bacteria for cholesterol lowering property and bile salt hydrolase activity. *Anna. Agric. Sci.* 61, 65–75. doi: 10.1016/j.aoas.2016.03.001

Shin, M., Han, S., Ji, A., Kim, K., and Lee, W. (2008). Isolation and characterization of bacteriocin-producing bacteria from the gastrointestinal tract of broiler chickens for probiotic use. *J. Appl. Microbiol.* 105, 2203–2212. doi: 10.1111/j.1365-2672.2008.03935.x

Shokryazdan, P., Kalavathy, R., Sieo, C., Alitheen, N., Liang, J., Jahromi, M., et al. (2014). Isolation and characterization of Lactobacillus strains as potential probiotics for chickens. *Pertanika J. Trop. Agric. Sci* 37, 141–157. doi: 10.1155/2014/927268

Sievers, F., and Higgins, D. G. (2014). Clustal omega, accurate alignment of very large numbers of sequences. *Methods Mol. Biol.* 1079, 105–116. doi: 10.1007/978-1-62703-646-7_6

Śliżewska, K., and Chlebicz-Wójcik, A. (2020). Growth kinetics of probiotic Lactobacillus strains in the alternative, cost-efficient semi-solid fermentation medium. *Biology* 9:423. doi: 10.3390/biology9120423

Soemarie, Y. B., Milanda, T., and Barliana, M. I. (2022). Isolation, characterization, and identification candidate of probiotic bacteria isolated from Wadi Papuyu (*Anabas testudineus* Bloch.) a fermented fish product from Central Kalimantan, Indonesia. *Int. J. Food Sci.* 2022:4241531. doi: 10.1155/2022/4241531

Sorescu, I., Dumitru, M., and Ciurescu, G. (2021). *Lactobacillus* spp. strains isolation, identification, preservation and quantitative determinations from gut content of 45-day-old chickens broilers. *Braz. J. Poultry Sci.* 23, 1–7. doi: 10.1590/1806-9061-2020-1378

Svihus, B. (2014). Function of the digestive system. *J. Appl. Poult. Res.* 23, 306–314. doi: 10.3382/japr.2014-00937

Tang, X., Liu, X., and Liu, H. (2021). Effects of dietary probiotic (*Bacillus subtilis*) supplementation on carcass traits, meat quality, amino acid, and fatty acid profile of broiler chickens. *Front. Vet. Sci.* 8:767802. doi: 10.3389/fvets.2021.767802

Tharmaraj, N., and Shah, N. (2003). Selective enumeration of *Lactobacillus delbrueckii* ssp. *bulgaricus*, *Streptococcus thermophilus*, *Lactobacillus acidophilus*, *Bifidobacteria*, *Lactobacillus casei*, *Lactobacillus rhamnosus*, and *Propionibacteria*. *J. Dairy Sci.* 86, 2288–2296. doi: 10.3168/jds.S0022-0302(03)73821-1

Thorp, B. (2021). *The poultry industry: poultry health: a guide for professionals*. CABI, Wallingford.

Van Dijk, M., Morley, T., Rau, M. L., and Saghai, Y. (2021). A meta-analysis of projected global food demand and population at risk of hunger for the period 2010–2050. *Nature Food* 2, 494–501. doi: 10.1038/s43016-021-00322-9

Vinderola, C. G., Mocchiutti, P., and Reinheimer, J. A. (2002). Interactions among lactic acid starter and probiotic bacteria used for fermented dairy products. *J. Dairy Sci.* 85, 721–729. doi: 10.3168/jds.S0022-0302(02)74129-5

Westley, J., Anderson, P., Close, V., Halpern, B., and Lederberg, E. (1967). Aminopeptidase profiles of various bacteria. *Appl. Microbiol.* 15, 822–825. doi: 10.1128/am.15.4.822-825.1967

Wu, Y., Zhang, H., Zhang, R., Cao, G., Li, Q., Zhang, B., et al. (2021). Serum metabolome and gut microbiome alterations in broiler chickens supplemented with lauric acid. *Poultry Sci.* 100:101315. doi: 10.1016/j.psj.2021.101315

Wu, Y., Zhen, W., Geng, Y., Wang, Z., and Guo, Y. (2019). Effects of dietary *Enterococcus faecium* NCIMB 11181 supplementation on growth performance and cellular and humoral immune responses in broiler chickens. *Poult. Sci.* 98, 150–163. doi: 10.3382/ps/pey368

Xu, Y., Zhou, T., Tang, H., Li, X., Chen, Y., Zhang, L., et al. (2020). Probiotic potential and amylolytic properties of lactic acid bacteria isolated from Chinese fermented cereal foods. *Food Control* 111:107057. doi: 10.1016/j.foodcont.2019.107057

Yadav, M., Dubey, M., Yadav, M., and Shankar, K. S. (2018). Effect of supplementation of probiotic (*Bacillus subtilis*) on growth performance and carcass traits of broiler chickens. *Int. J. Curr. Microbiol. Appl. Sci.* 7, 3440–4849. doi: 10.20546/ijcmas.2018.708.510

Yan, L., Lv, Z., An, S., Xing, K., Wang, Z., Lv, M., et al. (2021). Effects of rearing system and narasin on growth performance, gastrointestinal development, and gut microbiota of broilers. *Poult. Sci.* 100:100840. doi: 10.1016/j.psj.2020.10.073

Yang, S., Yang, Y., Long, X., Zhang, F., and Wang, Z. (2023). Integrated analysis of the effects of cecal microbiota and serum metabolome on market weights of Chinese native chickens. *Animals* 13:3034. doi: 10.3390/ani13193034

Ye, K., Li, P., and Gu, Q. (2020). Complete genome sequence analysis of a strain *Lactobacillus pentosus* ZFM94 and its probiotic characteristics. *Genomics* 112, 3142–3149. doi: 10.1016/j.ygeno.2020.05.015

Young, J. (2018). Sanger sequencing–a hands-on simulation. *Genet. Soc. Am. Peer Rev. Educ. Port.* 2018:3. doi: 10.1534/gsaprep.2018.003

Zavišić, G., Popović, M., Stojkov, S., Medić, D., Gusman, V., Jovanović Lješković, N., et al. (2023). Antibiotic resistance and probiotics: knowledge gaps, market overview and preliminary screening. *Antibiotics* 12:1281. doi: 10.3390/antibiotics12081281

Zhang, T., Ding, H., Chen, L., Lin, Y., Gong, Y., Pan, Z., et al. (2021). Antibiotic-induced dysbiosis of microbiota promotes chicken lipogenesis by altering metabolomics in the cecum. *Meta* 11:487. doi: 10.3390/metabo11080487

Zhang, M., Liu, L., Chen, D., Zhang, X., Zhou, C., Gan, Q., et al. (2020). Functional microRNA screening for dietary vitamin E regulation of abdominal fat deposition in broilers. *Br. Poult. Sci.* 61, 344–349. doi: 10.1080/00071668.2020.1736265

Zhang, L., Wang, Y., Jia, H., Liu, X., Zhang, R., and Guan, J. (2023). Transcriptome and metabolome analyses reveal the regulatory effects of compound probiotics on cecal metabolism in heat-stressed broilers. *Poultry Sci.* 102:102323. doi: 10.1016/j.psj.2022.102323

frontiers | Frontiers in Microbiology

TYPE Original Research
PUBLISHED 19 February 2024
DOI 10.3389/fmicb.2024.1347601

OPEN ACCESS

EDITED BY
Vijay K. Sharma,
Agricultural Research Organization (ARO), Israel

REVIEWED BY
Fengyu Du,
Qingdao Agricultural University, China
Pundrik Jaiswal,
National Institutes of Health (NIH), United States

*CORRESPONDENCE
Pei-Ji Zhao
✉ pjzhao@ynu.edu.cn

†These authors have contributed equally to this work

RECEIVED 01 December 2023
ACCEPTED 01 February 2024
PUBLISHED 19 February 2024

CITATION
Li S-S, Qu S-L, Xie J, Li D and Zhao P-J (2024) Secondary metabolites and their bioactivities from *Paecilomyces gunnii* YMF1.00003. *Front. Microbiol.* 15:1347601. doi: 10.3389/fmicb.2024.1347601

Secondary metabolites and their bioactivities from *Paecilomyces gunnii* YMF1.00003

Su-Su Li[1,2†], Shuai-Ling Qu[1†], Juan Xie[1], Dong Li[1] and Pei-Ji Zhao[1*]

[1]State key Laboratory for Conservation and Utilization of Bio-Resources in Yunnan, School of Life Sciences, Yunnan University, Kunming, Yunnan, China, [2]The Maternal and Child Health Hospital of Qianxinan, Xingyi, Guizhou, China

Four new polyketides (**1**–**4**) and seven known compounds (**5**–**11**) including three polyketides and four sterols were isolated from the fermented extracts of *Paecilomyces gunnii* YMF1.00003. The new chemical structures were determined through the analysis of the nuclear magnetic resonance and high-resolution electrospray ionization mass spectrometry, and their configurations were subsequently confirmed by nuclear overhauser effect spectroscopy, the calculated electronic circular dichroism (ECD) spectra, and quantum chemical calculations of the NMR data (qcc NMR). Based on the results of pre-activity screening and compound structure target prediction, certain metabolites were assayed to evaluate their cytotoxic and protein kinase Cα inhibitory activities. Results indicated that 3β-hydroxy-7α-methoxy-5α,6α-epoxy-8(14),22*E*-dien-ergosta (**8**) exhibited potent cytotoxic activity, with half-maximal inhibitory concentration values of 3.00 ± 0.27 to 15.69 ± 0.61 μM against five tumor cells, respectively. The new compound gunniiol A (**1**) showed weak cytotoxic activity at a concentration of 40 μM. At a concentration of 20 μg/mL, compounds **1**, **6**, and **7** exhibited protein kinase Cα inhibition by 43.63, 40.93, and 57.66%, respectively. This study is the first to report steroids demonstrating good cytotoxicity and polyketides exhibiting inhibitory activity against protein kinase Cα from the extracts of *P. gunnii*.

KEYWORDS

***Paecilomyces gunnii*, polyketides, cytotoxic activity, protein kinase Cα inhibitory activity, calculated electronic circular dichroism**

1 Introduction

Cordyceps, a fungus known for parasitizing insects, fungi, and plants (Qu et al., 2022), gained historical recognition during the Qing Dynasty, with *Cordyceps sinensis* emerging as the most well-known species documented in Bencao Beiyao. An in-depth study of its pharmacological properties revealed immunomodulatory functions and a significant impact on antitumor effects, organ transplantation, and heart disease (Kuo et al., 1996). *Cordyceps gunnii*, a well-known fungus in the *Cordyceps* genus, exhibits diverse bioactivities.

Paecilomyces gunnii, an anamorph of *C. gunnii*, produces metabolites that exhibit various pharmacological activities. Three new metabolites, gunnilactams A-C, were isolated from the deep fermentation broth of *P. gunnii*, and gunnilactam A showed cytotoxic activity against C42B cells (human prostate cancer) with a half-maximal inhibitory concentration (IC_{50}) of

5.4 μM (Zheng et al., 2017). Following the performance of activity-guided procedures and liquid chromatography–mass spectrometry (LC-MS), paecilomycones A–C were identified from *P. gunnii*, exhibiting strong tyrosinase inhibitory activity with IC_{50} values of 0.11, 0.17, and 0.14 μM, respectively (Lu et al., 2014). In addition, a new selenopolysaccharide (SeCPS-II), consisting of α-L-rhamnose, α-D-mannose, α-D-glucose, and β-D-galactose with a molecular weight of 4.12×10^3 kDa, was obtained from *C. gunnii* and showed weak inhibition of SeCPS-II on SKOV-3 cells (Sun et al., 2018). The identified active compounds exhibited potential for various applications, and further in-depth research on them holds significant value in the fields of pharmacology and medicine. In a previous study, we examined the metabolome and the activity of extracts derived from the *P. gunnii* YMF1.00003 strain. Results showed significant variations in the activities of fermentation product extracts under various culture conditions. The extract obtained from the wheat bran medium (WGA) exhibited notable inhibitory activity against the tested cell lines, resembling the effects observed in the extract from the stroma and host complex of *C. gunnii* (Qu et al., 2022). In this study, we aimed to examine the chemical structures of four new polyketides and seven known compounds isolated from *P. gunnii* YMF1.00003 cultivated in two types of media (Figure 1). Based on the results of a previous study (Qu et al., 2022), extensive literature research, and the prediction of compound structure targets, we conducted assays on select compounds to assess their cytotoxic activity and protein kinase Cα inhibitory activity.

2 Materials and methods

2.1 General experimental procedures

Electrospray ionization mass spectra (ESI-MS) and high-resolution electrospray ionization mass spectra (HR-ESI-MS) were acquired using a high-resolution Q Exactive Focus Mass Spectrometer (Thermo Fisher Scientific, Bremen, Germany). Optical rotation measurements were conducted using a Jasco DIP-370 digital polarimeter (JASCO, Tokyo, Japan). Ultraviolet (UV) spectra were recorded using a Shimadzu UV-2401PC spectrophotometer. Nuclear magnetic resonance (NMR) spectra were recorded using an Avance III-600 spectrometer (Bruker BioSpin, Rheinstetten, Germany) using tetramethylsilane as an internal standard. Column chromatography was performed using silica gel (200–300 mesh), GF254 (Qingdao Marine Chemical Inc., Qingdao, China), and Sephadex LH-20 (Amersham Pharmacia, United Kingdom). Semipreparative high-performance liquid chromatography (HPLC) was performed using an LC3000 system (Beijing Chuangxintongheng Science and Technology Co., Ltd., Beijing, China). Precoated silica gel GF254 plates (Qingdao

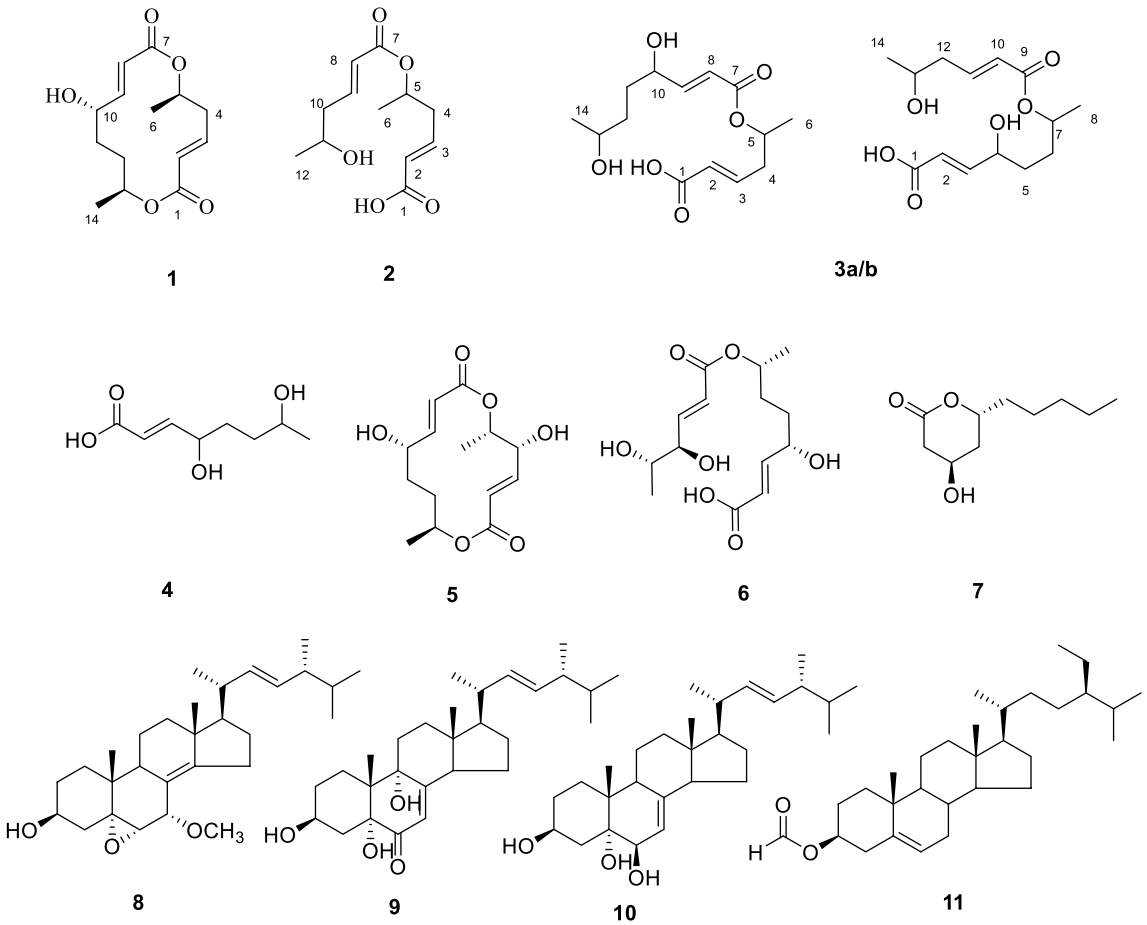

FIGURE 1
Structures derived from the *Paecilomyces gunnii* YMF1.00003.

Marine Chemical Factory, Qingdao, China) were used for thin-layer chromatography (TLC) analysis.

2.2 Microbial strain, media, and cultivation

The *P. gunnii* YMF1.00003 strain was officially deposited at the State Key Laboratory for the Conservation and Utilization of Bio-Resources, Yunnan University, Kunming, China. *Paecilomyces gunnii* YMF1.00003 was fermented in two different media. During the pre-experiment, the solid and liquid forms of four different media (PDB, modified Sabouraud medium, Rice, and Oats) were used to determine the most suitable medium for the production of YMF1.00003 metabolites. Based on the amount of extracts and results of TLC analysis, the modified Sabouraud medium demonstrated a substantial amount of YMF1.00003 extracts, with a more diverse range of compounds. Consequently, the modified Sabouraud agar medium was selected for subsequent fermentation. The strain was cultured in 9-cm dishes with modified Sand's solid medium (comprising 5.0 g of tryptone, 1.0 g of yeast extract, 60.0 g of glucose, 0.25 g of K_2HPO_4, 0.25 g of $MgSO_4$, 0.25 g of KCl, 15.0 g of agar, and 1 L of water) at 28°C for 21 days and 30 L. The cultures were extracted using organic reagents (ethyl acetate/methanol/glacial acetic acid = 80:15:5, *v/v/v*; Pu et al., 2021; Liu et al., 2022) to obtain 23.9 g of crude extract and subsequently designated as the MSA fraction. In addition, the strain was cultured on a modified wheat bran medium (comprising 30.0 g of wheat bran, 20.0 g of glucose, 1.5 g of KH_2PO_4, 1.5 g of $MgSO_4$, 0.5 g of $MnSO_4$•H_2O, 0.5 g of $ZnSO_4$•$7H_2O$, 0.5 g of $CuSO_4$•$5H_2O$, 8.0 g of $(NH_4)_2SO_4$, 15 g of agar, and 1 L of water) at 28°C for 50 days. Subsequently, 30 g of crude extract was obtained and designated as the WB fraction.

2.3 Isolation and purification

After mixing with silica 60 RP-C18, the MSA fraction (23.9 g) was placed on an RP-C18 column (50 g) and eluted with H_2O/MeOH (100:0 → 0:100, *v/v*) to obtain 12 fractions (Fr.1–Fr.12). Fr.9 (1.617 g) was separated with a Sephadex LH-20 column (chloroform–methanol, 1:1) to obtain nine fractions (Fr.9.1-9). Fr.9.3 (1.254 g) was separated using a silica gel column (200–300 mesh) and eluted with petroleum ether/acetone (100:1 → 6:4, *v/v*) to obtain five fractions (Fr.9.3.1-5). Fr.9.3.2 (135 mg) was loaded on a silica gel column eluting with chloroform/acetone (100:1 → 6:4, *v/v*) and then purified by Sephadex LH-20 (acetone) to obtain compound **8** (3 mg). Fr.9.3.4 (180 mg) was subjected to Sephadex LH-20 chromatography (chloroform–methanol, 1:1) to obtain four fractions (Fr.9.3.4.1-4). Fr.9.3.4.3 (132 mg) underwent separation on a silica gel column eluted with chloroform/acetone (100:1 → 8:2, *v/v*) and was subsequently purified by a Sephadex LH-20 (acetone) to obtain compound **9** (2 mg). Fr.9.3.5 (113 mg) was loaded on a Sephadex LH-20 (acetone) and purified on a silica gel column via elution with chloroform/methanol (100:1 → 8:2, *v/v*) to obtain compound **10** (8 mg). Fr.5 (259 mg) was subjected to Sephadex LH-20 (chloroform–methanol, 1:1) chromatography to obtain five fractions (Fr.5.1-5). Fr.5.4 (54 mg) was further separated using a silica gel column via elution with chloroform/acetone (100:1 → 6:4, *v/v*) and purified by Sephadex LH-20 chromatography (acetone) to obtain compound **2** (7 mg). Fr.5.5 (80 mg) was subjected to silica gel column chromatography and eluted with chloroform/acetone (100:0 → 8:2, *v/v*) and purified by Sephadex LH-20 chromatography (methanol) to obtain compound **7** (5 mg). Fr.4 (1.6 g) was loaded on a Sephadex LH-20 column (chloroform–methanol, 1:1) to obtain seven fractions (Fr.4.1-7). Fr.4.5 (637 mg) was further separated using Sephadex LH-20 (methanol) to obtain four fractions (Fr.4.5.1-4). Fr.4.5.2 (439 mg) was subjected to semi-preparative HPLC with gradient elution of MeOH–H_2O (30:70 → 35:65 and 40:60 → 100:0) for 50 min to obtain five fractions (Fr.4.5.2.1-5). Fr.4.5.2.3 (120 mg) was separated using a Sephadex LH-20 column (methanol) to obtain three fractions (Fr.4.5.2.3.1-3). Fr.4.5.2.3.3 (108 mg) was further separated using a silica gel column via elution with chloroform/acetone (100:1 → 0:100, *v/v*) to obtain eight fractions (Fr.4.5.2.3.3.1-8). Fr.4.5.2.3.3.6 (51 mg) was separated using a Sephadex LH-20 column (methanol) to obtain compound **6** (28 mg). Fr.4.5.2.5 (64 mg) was separated using a Sephadex LH-20 column (methanol) to obtain two fractions (Fr.4.5.2.5.1-2). Fr.4.5.2.5.2 (59 mg) was further separated using a column of silica gel via elution with chloroform/acetone (100:1 → 0:100, *v/v*) and purified by Sephadex LH-20 (methanol) to obtain compound **3a/b** (5 mg). Fr.3 (2.135 g) was separated using a Sephadex LH-20 column (chloroform–methanol, 1:1) to obtain five fractions (Fr.3.1-5). Fr.3-5 (1.232 g) was separated using a Sephadex LH-20 column (chloroform–methanol, 1:1) to obtain four fractions (Fr.3.5.1-4). Fr.3.5.4 (1.081 g) was subjected to semi-preparative RP-C18 HPLC with a gradient elution of MeOH:H_2O (10:90 → 45:55 and 60:40 → 100:0) for 40 min to obtain three fractions (Fr.3.5.4.1-3). Fr.3.5.4.3 (34 mg) was further separated using a silica gel column via elution with chloroform/acetone (50:1 → 0:100, *v/v*) to obtain four fractions (Fr.3.5.4.3.1-4). Fr.3.5.4.3.2 (8 mg) was separated using a Sephadex LH-20 column (methanol) to obtain compound **4** (5 mg).

The WB fraction (30.0 g) was placed on an RP-C18 column (60 g) and eluted with H_2O/MeOH mixtures (100:0 → 0:100, *v/v*) to obtain 15 fractions (Fr.1-15). Fr.15 (878 mg) was separated using a silica gel column via elution with petroleum ether/ethyl acetate (300:1 → 6:4, *v/v*) to obtain five fractions (Fr.15.1-5). Fr.15.2 (153 mg) was separated using a silica gel column via elution with petroleum ether/ethyl acetate (100:1 → 8:2, *v/v*) and then purified with a silica gel column via elution with petroleum ether/ethyl acetate (200:1 → 8:2, *v/v*) to obtain compound **11** (1 mg). Fr.15.4 (123 mg) was separated using a silica gel column via elution with chloroform/acetone (10:1 → 6:4, *v/v*) and then purified by Sephadex LH-20 (acetone) to obtain compound **8** (2 mg). Fr.6 (385 mg) was loaded on a Sephadex LH-20 column (methanol) to obtain six fractions (Fr.6.1-6). Fr.6.3 (108 mg) was subjected to a silica gel column (100:1 → 7:3, *v/v*) and purified by Sephadex LH-20 (methanol) to obtain compound **1** (6 mg). Fr.4 (1.15 g) was subjected to Sephadex LH-20 column (chloroform–methanol, 1:1) to obtain five fractions (Fr.4.1-5). Fr.4.1 (715 mg) was loaded on a silica gel column via elution with chloroform/acetone (100:1 → 8:2, *v/v*) to obtain four fractions (Fr.4.1-4). Fr.4.1.3 (83 mg) was subjected to a Sephadex LH-20 column (methanol) and purified by a silica gel column via elution with chloroform/acetone (100:1 → 8:2, *v/v*) to obtain compound **5** (15 mg).

2.4 Spectroscopic data

Gunniol A (**1**), colorless solid; $[\alpha]_D^{23} = 75.5$ ($c = 0.10$, MeOH); UV (MeOH) λ_{max} (log ε) nm: 204 (4.46); ^{1}H-NMR ($CDCl_3$, 600 MHz) and ^{13}C-NMR ($CDCl_3$, 150 MHz), see Table 1; ESI-MS *m/z*: 291 $[M+Na]^+$; HR-ESI-MS *m/z*: 291.1190 ($[M+Na]^+$, calcd. 291.1203).

10.3389/fmicb.2024.1347601

TABLE 1 The NMR data of gunniiols A (1) and B (2).

Position	Gunniiol A (1)			Gunniiol B (2)		
	^{1}H	^{13}C	HMBC	^{1}H	^{13}C	HMBC
1	-	165.5, s	-	-	170.6, s	-
2	5.79 (1H, d, 15.7)	126.3, d	C-3, C-4, C-1	5.89 (1H, d, 15.5)	123.8, d	C-1, C-4
3	6.71 (1H, ddd, 5.2, 10.7, 15.7)	143.4, d	C-1, C-4	6.97 (1H, m)	146.2, d	C-1, C-2, C-4, C-5
4	2.55 (1H, dt, 12.9, 3.8)	40.4, t	C-2, C-3, C-5	2.52 (2H, brs)	38.5, t	C-2, C-3, C-6, C-5
	2.29 (1H, dt, 10.7, 12.9)		C-2, C-3, C-5,C-6			
5	5.23 (1H, m)	68.5, d	-	5.11 (1H, m)	69.0, d	-
6	1.36 (3H, d, 6.3)	20.6, d	C-4, C-5	1.29 (3H, d, 6.3)	19.9, q	C-4, C-5
7	-	165.7, s	-	-	165.7, s	-
8	5.90 (1H, dd, 1.7, 15.7)	121.2, d	C-7, C-9, C-10	5.89 (1H, d, 15.5)	123.6, d	C-7, C-10
9	6.82 (1H, dd, 4.6, 15.9)	150.5, d	C-7, C-8, C-10	6.94 (1H, m)	145.5, d	C-7, C-10, C-11
10	4.60 (1H, brs)	70.3, d	-	2.36 (2H, t, 6.9)	41.8, t	C-8, C-9, C-11, C-12
11	1.96 (1H, m)	29.2, t	C-9, C-10, C-12	3.99 (1H, m)	66.8, d	-
	1.77 (1H, m)		C-9, C-12, C-13			
12	1.69 (1H, m)	26.3, t	C-10, C-11, C-14	1.23 (3H, d, 6.2)	23.2, q	C-10, C-11
	1.52 (1H, m)		-			
13	5.18 (1H, m)	69.2, d	C-11, C-14	-	-	-
14	1.19 (3H, d, 6.7)	17.7, d	C-12, C-13	-	-	-

TABLE 2 The NMR data of gunniiol C (3a/b).

Position		Gunniiol C (a/b)				
	^{1}H	^{13}C	HMBC	^{1}H	^{13}C	HMBC
1	-	167.8, s	-	-	167.8, s	-
2	5.89 (1H, d, 15.7)	124.5, d	C-1, C-4	6.00 (1H, d, 15.7)	120.8, d	C-1, C-4
3	6.83 (1H, m)	144.2, d	C-4, C-5	6.95 (1H, dd, 4.9, 15.7)	152.7, d	C-1, C-4
4	2.50 (2H, brt, 6.5)	39.3, t	C-2, C-3, C-5,C-6	4.23 (1H, m)	71.7, d	-
5	5.08 (1H, tq, 6.2, 6.3)	70.9, d	-	1.54 (2H, m)	33.5, t	C-4, C-6, C-7
6	1.28 (3H, d, 6.3)	20.3, q	C-4, C-5	1.63 (1H, m)	32.9, t	C-5, C-7
				1.71 (1H, m)		C-5, C-7
7	-	167.8, s	-	4.96 (1H, tq, 6.2, 6.1)	72.2, d	-
8	5.98 (1H, d, 15.7)	120.8, d	C-7, C-10	1.24 (3H, d, 6.2)	20.0, q	C-6, C-7
9	6.95 (1H, dd, 4.9, 15.7)	152.7, d	C-7, C-10	-	167.6, s	-
10	4.23 (1H, dt, 5.8, 4.9)	71.5, d	-	5.89 (1H, d, 15.6)	124.5, d	C-9, C-12
11	1.54 (2H, m, overlap)	33.9, t	C-10, C-12, C-13	7.00 (1H, dd, 7.4, 15.6)	147.3, d	C-9, C-12′
12	1.54 (2H, m, overlap)	35.9, t	C-10, C-11, C-13	2.34 (2H, m)	42.6, t	C-10, C-11, C-13, C-14
13	3.73 (1H, q, 6.4)	68.3, d	-	3.89 (1H, tq, 6.2, 6.2)	67.5, d	-
14	1.15 (3H, d, 6.2)	23.5, q	C-12, C-13	1.18 (3H, d, 6.2)	23.5, q	C-12, C-13

Gunniiol B (**2**), colorless oil; $[\alpha]_D^{23} = 22.5$ ($c = 0.10$, MeOH); UV (MeOH) λ_{max} (log ε) nm: 197 (4.57); ^{1}H-NMR ($CDCl_3$, 600 MHz) and ^{13}C-NMR ($CDCl_3$, 150 MHz), see Table 1; ESI-MS *m/z*: 265 $[M + Na]^+$; HR-ESI-MS *m/z*: 265.1040 ($[M + Na]^+$, calcd. 265.1046).

Gunniiol C (**3a/b**), colorless oil; ^{1}H-NMR (CD_3OD, 600 MHz) and ^{13}C-NMR (CD_3OD, 150 MHz), see Table 2; ESI-MS *m/z*: 287 $[M + H]^+$, 309 $[M + Na]^+$; HR-ESI-MS *m/z*: 309.1300 ($[M + Na]^+$, calcd. 309.1309).

(*E*)-4,7-dihydroxyoct-2-enoic acid (**4**), colorless solid; $[\alpha]_D^{23} = 19.4$ ($c = 0.10$, MeOH); UV (MeOH) λ_{max} (log ε) nm: 198 (4.33); ^{1}H-NMR (CD_3OD, 600 MHz) and ^{13}C-NMR (CD_3OD, 150 MHz), see Table 3; ESI-MS *m/z*: 173 $[M - H]^-$; HR-ESI-MS *m/z*: 173.0808 ($[M - H]^-$, calcd. 173.0808).

TABLE 3 The NMR data of compound 4.

Position	^{1}H	^{13}C	HMBC	COSY
1	-	170.2, s	-	-
2	5.98 (1H, d, 15.6)	121.3, d	C-1, C-4	H-3
3	6.89 (1H, dd, 15.6, 5.2)	152.3, d	C-1, C-4	H-2, H-4
4	4.23 (1H, m)	71.7, d	-	H-3, H-5
5	1.54 (1H, m)	34.0, t	C-7	H-4, H-6
	1.70 (1H, m)		C-6, C-7	
6	1.54 (1H, m)	35.9, t	C-7	H-5, H-7
	1.47 (1H, m)		C-5, C-7, C-8	
7	3.73 (1H, dq, 6.2, 6.2)	68.6, d	-	H-6, H-8
8	1.16 (3H, d, 6.2)	23.5, q	C-6, C-7	H-7

Clonostachydiol (**5**), colorless solid; ESI-MS *m/z*: 307 $[M+Na]^+$; ^{1}H-NMR (600 MHz, CD_3OD) δ: 6.83 (1H, dd, J = 15.6, 4.0 Hz), 6.76 (1H, d, J = 15.6, 3.2 Hz), 6.14 (1H, t, J = 15.6, 1.6 Hz), 5.85 (1H, dd, J = 15.6, 1.6 Hz), 5.25 (1H, dq, J = 6.4, 2.0 Hz), 5.14 (1H, m), 4.57 (1H, m), 4.41 (1H, m), 1.95 (1H, m), 1.75 (1H, m), 1.64 (1H, m), 1.51 (1H, m), 1.41 (3H, d, J = 6.3 Hz), and 1.20 (3H, d, J = 6.6 Hz); ^{13}C-NMR (150 MHz, CD_3OD) δ: 167.3 (s), 167.0 (s), 153.5 (d), 148.4 (d), 125.1 (d), 121.7 (d), 77.2 (d), 73.0 (d), 71.2 (d), 70.6 (d), 29.7 (t), 27.1 (t), 17.9 (q), and 17.8 (q).

7*R*-[[4R,5S-dihydroxy-1-oxo-2*E*-hexen-1-yl]oxy]-4*S*-hydroxy-2*E*-octenoic acid (**6**), colorless oil; ESI-MS *m/z*: 325 $[M+Na]^+$; ^{1}H-NMR (600 MHz, CD_3OD) δ: 5.99 (1H, d, J = 15.9 Hz, H-2), 6.91 (1H, dd, J = 4.8, 15.9 Hz, H-3), 4.25 (1H, m, H-4), 1.56 (1H, m, H-5a), 1.67 (2H, m, H-5b/6a), 1.75 (1H, m, H-6b), 5.00 (1H, m, H-7), 1.26 (3H, d, J = 6.4 Hz, H-8), 6.08 (1H, d, J = 15.9 Hz, H-2′), 7.07 (1H, dd, J = 4.8, 15.9 Hz, H-3′), 4.07 (1H, t, J = 4.8 Hz, H-4′), 3.72 (1H, t, J = 6.4 Hz, H-5′), and 1.18 (3H, d, J = 6.5 Hz, H-5b/H-6′); ^{13}C-NMR (150 MHz, CD_3OD) δ: 170.3 (s, C-1), 121.6 (d, C-2), 152.1 (d, C-3), 71.4 (d, C-4), 32.9 (t, C-5), 33.2 (t, C-6), 72.5 (d, C-7), 20.4 (q, C-8), 167.9 (s, C-1′), 122.7 (d, C-2′), 149.5 (d, C-3′), 76.2 (d, C-4′), 71.3 (d, C-5′), and 19.1 (q, C-6′).

(3*R*,5*R*)-3-hydroxy-5-decanolide (**7**), colorless oil; ESI-MS *m/z*: 209 $[M+Na]^+$; ^{1}H-NMR (600 MHz, $CDCl_3$) δ: 4.72 (1H, dm, J = 11.2 Hz, H-5), 4.44–4.48 (1H, m, H-3), 2.78 (1H, dd, J = 17.7, 5.2 Hz, H-2a), 2.66 (1H, ddd, J = 17.7, 3.8, 1.6 Hz, H-2b), 1.99 (1H, dm, J = 14.7 Hz, H-4a), 1.78 (1H, ddd, J = 14.7, 11.2, 3.8 Hz, H-4b), 1.72–1.78 (2H, m, H-6), 1.30–1.34 (6H, m, H-7/8/9), and 0.93 (3H, t, J = 6.5 Hz, H-10); ^{13}C-NMR (150 MHz, $CDCl_3$) δ: 170.7 (s, C-1), 38.8 (t, C-2), 62.9 (d, C-3), 36.2 (t, C-4), 76.1 (d, C-5), 34.8 (t, C-6), 24.8 (t, C-7), 31.8 (t, C-8), 22.8 (t, C-9), and 14.2 (q, C-10).

3β-hydroxy-7α-methoxy-5α,6α-epoxy-8(14),22*E*-dien-ergosta (**8**), colorless oil; ESI-MS *m/z*: 443 $[M+H]^+$, 465 $[M+Na]^+$; ^{1}H-NMR (600 MHz, $CDCl_3$,) δ: 3.96 (1H, tt, J = 11.3, 4.7 Hz, H-3), 3.24 (1H, d, J = 2.7 Hz, H-6), 4.20 (1H, d, J = 2.1 Hz, H-7), 1.05 (3H, d, J = 6.7 Hz, H-21), 5.28 (2H, m, H-22/23), 0.89 (6H, s, H-18/19), 0.86 (3H, d, J = 6.5 Hz, H-26), 0.87 (3H, d, J = 6.8 Hz, H-27), 0.96 (3H, d, J = 6.7 Hz, H-28), and 3.45 (3H, s, 7-OCH_3); ^{13}C-NMR (150 MHz, $CDCl_3$) δ: 153.6 (q, C-14), 135.6 (d, C-22), 132.5 (d, C-23), 122.8 (q, C-8), 72.9 (d, C-7), 69.0 (d, C-3), 65.5 (q, C-9), 40.2 (t, C-4), 39.6 (d, C-20), 36.8 (t, C-12), 36.3 (q, C-10), 33.3 (d, C-25), 32.5 (t, C-1), 31.5 (t, C-2), 27.5 (t, C-16), 25.2 (t, C-15), 21.5 (q, C-21), 20.2 (q, C-27), 19.9 (q, C-26), 19.5 (t, C-11), 18.5 (q, C-18), 17.9 (q, C-28), and 16.8 (q, C-19).

3β,5α,9α-trihydroxy-ergosta-7,22-dien-6-one (**9**), white powder; ESI-MS *m/z*: 467 $[M+Na]^+$; ^{1}H-NMR (600 MHz, $CDCl_3$) δ: 4.09 (1H, m, H-3), 5.69 (1H, s, H-7), 1.06 (3H, s, H-18), 0.65 (3H, s, H-19), 1.05 (3H, d, J = 6.8 Hz, H-21), 5.20 (1H, dd, J = 15.4, 8.0 Hz, H-22), 5.23 (1H, dd, J = 15.4, 7.8 Hz, H-23), 0.85 (3H, d, J = 6.8 Hz, H-26), 0.87 (3H, d, J = 6.7 Hz, H-27), and 0.95 (3H, d, J = 6.8 Hz, H-28); ^{13}C-NMR (150 MHz, $CDCl_3$) δ: 25.5 (t, C-1), 26.4 (t, C-2), 67.4 (d, C-3), 33.8 (t, C-4),79.9 (s, C-5), 197.8 (d, C-6), 120.1 (d, C-7), 164.5 (s, C-8), 74.9 (d, C-9), 42.0 (s, C-10), 28.9 (t, C-11), 35.1 (t, C-12), 45.5 (s, C-13), 51.9 (d, C-14), 22.6 (t, C-15), 28.0 (t, C-16), 56.3 (d, C-17), 21.3 (q, C-18), 12.5 (q, C-19), 40.5 (d, C-20), 19.9 (q, C-21), 135.4 (d, C-22), 132.6 (d, C-23), 42.9 (d, C-24), 33.4 (d, C-25), 20.3 (q, C-26), 20.5 (q, C-27), and 17.8 (q, C-28).

3β,5α,6β-triol-7,22*E*-diene-ergosta (**10**), white powder; ESI-MS *m/z*: 453 $[M+Na]^+$; ^{1}H-NMR (600 MHz, C_5D_5N) δ: 4.85 (1H, m, H-3), 4.23 (1H, d, J = 10.2 Hz, H-6), 5.74 (1H, m, H-7), 0.65 (3H, s, H-18), 1.53 (3H, s, H-19), 1.05 (3H, d, J = 6.7 Hz, H-21), 5.14 (1H, dd, J = 15.3, 8.2 Hz, H-22), 5.21 (1H, dd, J = 15.3, 7.5 Hz, H-23), 0.84 (3H, d, J = 3.2 Hz, H-26), 0.85 (3H, d, J = 3.1 Hz, H-27), and 0.94 (3H, d, J = 6.8 Hz, H-28); ^{13}C-NMR (150 MHz, C_5D_5N) δ: 32.7 (t, C-1), 33.8 (t, C-2), 67.6 (d, C-3), 42.0 (t, C-4), 76.1 (s, C-5), 74.3 (d, C-6), 120.5 (d, C-7), 141.6 (s, C-8), 43.7 (d, C-9), 38.1 (s, C-10), 22.4 (t, C-11), 39.9 (t, C-12), 43.8 (s, C-13), 55.3 (d, C-14), 23.5 (t, C-15), 28.5 (t, C-16), 56.1 (d, C-17), 12.5 (q, C-18), 18.8 (q, C-19), 40.9 (d, C-20), 21.2 (q, C-21), 136.2 (d, C-22), 132.1 (d, C-23), 43.1 (d, C-24), 33.3 (d, C-25), 19.9 (q, C-26), 20.2 (q, C-27), and 17.8 (q, C-28).

Stigmast-5-ene-3β-yl formate (**11**), colorless solid; ESI-MS *m/z*: 465 $[M+Na]^+$; ^{1}H-NMR (600 MHz, $CDCl_3$) δ: 8.04 (1H, s, H-30), 4.73 (1H, m, H-3), 1.84 (1H, m, H-16), 1.57 (1H, m, H-1), 1.56 (1H, m, H-15), 1.46 (1H, m, H-11), 1.35 (1H, m, H-20), 1.32 (1H, m, H-22), 1.17 (1H, m, H-12), 1.10 (1H, m, H-17), 0.95 (1H, m, H-9), 0.93 (3H, d, J = 4.9 Hz, H-21), 0.84 (3H, d, J = 3.9 Hz, H-26), 0.83 (3H, d, J = 6.2 Hz, H-27), and 0.82 (3H, d, J = 5.0 Hz, H-29); ^{13}C-NMR (150 MHz, $CDCl_3$) δ: 36.9 (C-1), 27.8 (C-2), 74.0 (C-3), 38.1 (C-4), 139.3 (C-5), 123.0 (C-6), 31.9 (C-7), 31.8 (C-8), 50.0 (C-9), 36.6 (C-10), 21.0 (C-11), 39.7 (C-12), 42.3 (C-13), 56.7 (C-14), 24.3 (C-15), 28.2 (C-16), 56.0 (C-17), 19.3 (C-18), 11.9 (C-19), 36.1 (C-20), 18.8 (C-21), 33.9 (C-22), 26.0 (C-23), 45.8 (C-24), 29.1 (C-25), 19.8 (C-26), 12.0 (C-27), 23.0 (C-28), 19.0 (C-29), and 160.7 (C-30).

10.3389/fmicb.2024.1347601

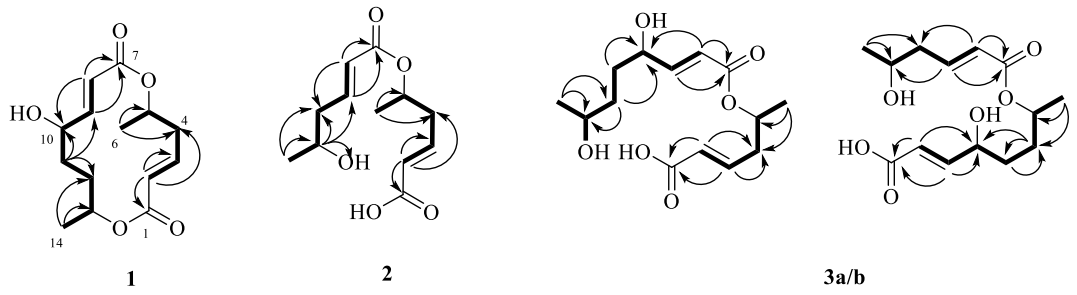

FIGURE 2
Selected HMBC (arrows) and ^{1}H-^{1}H COSY (bold bond) correlations of compounds **1–3**.

2.5 Cytotoxic activity

The cytotoxic activity of several compounds was assessed by conducting an assay using MTS, which is a new type of MTT analog. The method is often regarded as a "one-step" MTT assay as it allows the addition of reagents directly to cell cultures without the intermittent steps required in MTT assays. MTS holds an advantage over XTT owing to its increased solubility and non-toxic nature, enabling the reintroduction of cells to culture for further evaluation. The test concentration of each compound was 40 μM; for compounds with enhanced activity, a comprehensive screening of their activities at varying concentrations was conducted. Following the methods outlined in the literature (Su et al., 2013), five distinct cell lines (leukemia cell line HL-60, liver cancer cell line SMMC-7721, lung adenocarcinoma cell line A549, breast cancer cell line MDA-MB-231, and colon cancer cell line SW480) were selected for analysis. Cisplatin (40 μM) and paclitaxel (5 μM) were used as positive controls. All experiments were conducted in triplicate, and data were expressed as the mean ± standard deviation of three independent experiments.

2.6 Inhibitory activity against protein kinase Cα

According to the existing literature, certain types of polyketides showed antimicrobial bioactivity (Krohn et al., 2007). This finding suggests a limited number of studies exploring the activity of such compounds. To explore other activities of this type of polyketide, SwissTargetPrediction (STP)[1] (accessed on 31 May 2022) was employed to identify potential targets associated with these metabolites (Gfeller et al., 2014). The results indicated that some metabolites may inhibit the activity of protein kinase Cα. Subsequently, compounds **1**, **2**, **3a/b**, **5, 6,** and **7** were evaluated to ascertain their protein kinase Cα inhibitory activity, using an enzyme-linked immunosorbent assay (ELISA) kit (Human Protein Kinase C, PKC ELISA Kit; Product number: kt80184, Wuhan Mosak Biotechnology Co., Ltd.). The experiment was conducted as follows: For sample addition, 50 μL of the standard sample was added to the wells in the microplate-coated plate, including five concentration points and 10 wells; the test samples included 10 μL of sample and 40 μL of diluent, with distilled water as the control. For incubation, the sample was incubated at 37°C for 30 min. For washing, each well was filled with washing solution, kept for 30 s, and subsequently discarded; the procedure was repeated five times. The enzyme was added (50 μL of enzyme-labeled reagent added to each well including the control), incubated, and washed (same as above). For color development, chromogenic agent A from the kit was initially added to each well, followed by the addition of 50 μL of chromogenic agent B from the same kit. The chromogenic agent was then incubated at 37°C in the dark for 15 min. For the termination stage, a termination solution (50 μL) was added to each well. For the determination stage, the absorbance (OD) of each well was measured at 450 nm within 15 min after adding the termination solution.

3 Results and discussion

3.1 Structural identification

Compound **1** is a colorless solid with a molecular weight of 291.1190 $[M+Na]^+$ based on the results of high-resolution mass spectrometry. The molecular formula is determined as $C_{14}H_{20}O_5$. The planar structure of compound **1** was determined based on the key correlations of the two-dimensional nuclear magnetic resonance spectroscopy (2D NMR) data (Table 1): $^{1}H-^{1}H$ COSY spectra revealed the correlations between H-2/H-3/H-4/H-5/H-6, H-8/H-9/H-10/H-11/H-12/H-13/H-14, and –C-2–C-3–C-4–C-5–C-6– and –C-8–C-9–C-10–C-11–C-12–C-13–C-14– fragments (Figure 2). Additionally, long-range heteronuclear multiple bond correlations (HMBCs) revealed specific associations: H-2 (δ_H 5.79) was correlated with C-1 (δ_C 165.5), C-3 (δ_C 143.4), and C-4 (δ_C 40.4); H-3 (δ_H 6.71) was correlated with C-1 (δ_C 165.5) and C-4 (δ_C 40.4); H-6 (δ_H 1.36) was correlated with C-4 (δ_C 40.4) and C-5 (δ_C 68.5); H-9 (δ_H 6.82) was correlated with C-7 (δ_C 165.7), C-8 (δ_C 121.2), and C-10 (δ_C 70.3); H-13 (δ_H 5.18) was correlated with C-11 (δ_C 29.2) and C-14 (δ_C 17.7); and H-14 (δ_H 1.19) was correlated with C-12 (δ_C 26.3) and C-13 (δ_C 69.2; Figure 2). The flat structure of compound **1** mirrored that of colletallol (Kauloorkar and Kumar, 2016). After carefully analyzing the spectral data of compound **1** and colletallol, notable discrepancies were observed in the chemical shift of certain carbons, particularly C-14. In compound **1**, the

1 http://www.swisstargetprediction.ch/

chemical shift differences were δ_C 17.7 for C-14 (Table 1) and δ_C 19.5 for colletallol. In addition, the specific rotation value of compound **1** was $[\alpha]_D^{23} = 75.5$ ($c = 0.10$, MeOH), while the specific rotation of colletallol was $[\alpha]_D^{23} = -107.5$ ($c = 0.40$, CH_2Cl_2).

Among them, H-14 exhibited an NOE effect with H-12β and H-10. The configuration of 6-CH_3 cannot be determined by NMR data, so the calculated ECD spectra and qcc NMR of four stereoisomers, 5*S*,10*S*,13*S* (**1a**), 5*S*,10*R*,13*R* (**1b**), *5R,10S,13S* (**1c**), and 5*R*,10*R*,13*R* (**1d**), were performed. As given in Figure 3A, two cotton effects (CEs) with alternative signals were observed on the experimental spectrum. The 5*S*,10*S*,13*S* (**1a**) and *5R,10S,13S* (**1c**) theoretical spectra exhibited two CEs with alternative signs, which was in good agreement with the experimental ECD spectra. Moreover, the two epimers, 5*S*,10*S*,13*S* (**1a**) and *5R,10S,13S* (**1c**) were subjected to a strict conformational screening procedure, and the NMR chemical shifts were calculated at the mPW1PW91/6–31 + G(d,p)//M06-2X/def2-SVP level of theory with the PCM solvent model in methanol. The ^{13}C NMR data with the correlation coefficient (R^2) of 0.9973 of *5R,10S,13S* (**1c**) were consistent with its experimental values (Figure 3B). So the absolute configuration of compound **1** was assigned as *5R,10S,13S* (Figure 2) and was named gunniiol A.

Compound **2** is colorless oil, and its molecular formula $C_{12}H_{18}O_5$ was determined by HR-ESI-MS with *m/z* 265.1040 ($[M+Na]^+$, calcd for: 265.1046), with four unsaturations. In the ^{13}C-NMR and DEPT analysis (Table 1), the carbon signals of compound **2** appeared in pairs and were characterized by fatty acid chains (δ_C 170.6, 165.7, 146.2, 145.5, 123.8, 123.6, 38.5, 41.8, 69.0, 66.8, 19.9, and 23.2), which was preliminarily judged to be a polyketone compound composed of one or two fatty acids.

The structural units of the two long chains, H-2/H-3/H-4/H-5/H-6 and H-8/H-9/H-10/H-11/H-12, were determined through the ^{1}H-^{1}H COSY experiment of compound **2,** revealing the structural motifs −C-2–C-3–C-4–C-5–C-6– and −C-8–C-9–C-10–C-11–C-12– (Figure 2). The HMBC data were used to determine the planar structure of compound **2**: H-2 (δ_H 5.89) was correlated with C-1 (δ_C 170.6) and C-4 (δ_C 38.5); H-3 (δ_H 6.97) was correlated with C-1 (δ_C 170.6), C-2 (δ_C 123.8), C-4 (δ_C 38.5), and C-5 (δ_C 69.0); H-6 (δ_H 1.29) was correlated with C-4 (δ_C 38.5) and C-5 (δ_C 69.0); H-9 (δ_H 6.94) was correlated with C-7 (δ_C 165.7), C-10 (δ_C 41.8), and C-11 (δ_C 66.8); H-10 (δ_H 2.36) was correlated with C-8 (δ_C 123.6), C-9 (δ_C 145.5), C-11 (δ_C 66.8), and C-12 (δ_C 23.2); and H-12 (δ_H 1.23) was correlated with C-10 (δ_C 41.8) and C-11 (δ_C 66.8). The chemical shift of H-5 exhibited a notable 5.11 ppm shift to the low field, suggesting the connection of the two polyketide chains through 5-OH and C-7 ester bonds. The structure of compound **2** was determined as shown in Figure 2 and named gunniiol B.

Compound **3a/b** is colorless oil. Its molecular formula was determined to be $C_{14}H_{24}O_6$ (*m/z* 309.1300 $[M+Na]^+$, calcd. 309.1309), with four unsaturations, by positive ion mode HR-ESI-MS. According to ^{13}C-NMR and DEPT data (Table 2), the carbon signals of compound **3a/b** indicated paired appearances, akin to compound **2**, suggesting a polyketide. When the ^{1}H- and ^{13}C NMR spectra were analyzed, one fatty acid exhibited a similarity with compound **2**, identified as 5-hydroxyhex-2*E*-enoic acid (δ_C 167.8/167.6, 124.5, 144.2/147.3, 39.3/42.6, 70.9/67.5, and 20.3/23.5). Another fatty acid chain, 4,7-dihydroxyoct-2*E*-enoic acid (δ_C 167.8, 120.8, 152.7, 71.5, 33.9/33.5, 35.9/32.9, 68.3/72.2, and 23.5/20.0), was also identified in the analysis (Table 2).

In the ^{1}H-^{1}H COSY experiment, clear correlations were observed between the two structural units H-2/H-3/H-4/H-5/H-6 and H-8/H-9/H-10/H-11/H-12/H-13/H-14, the structural units of the two long chains −C-2–C-3–C-4–C-5–C-6– and −C-8–C-9–C-10–C-11–C-12–C-13–C-14– (Figure 2) or H-2/H-3/H-4/H-5/H-6/H-7/H-8 and H-10/H-11/H-12/H-13/H-14, and the structural units of the two long chains −C-2–C-3–C-4–C-5–C-6–C-7–C-8– and −C-10–C-11–C-12–C-13–C-14–. HMBC analysis confirmed the planar structure of compound **3a/b** (Figure 2). The two polyketide chains were linked in two ways: The chemical shift of H-5 to the low field reached δ_H 5.08 ppm, indicating that the two polyketide chains were connected by 5-OH and C-7 ester bonds. Alternatively, the chemical shift of H-7 to the low field reached δ_H 4.96 ppm, suggesting that the two polyketide chains were connected by 7-OH and C-9 ester bonds. The structures of compound **3a/b** were determined (Figure 2) and designated as gunniiol C.

Compound **4** is a colorless solid. Its molecular formula was determined to be $C_8H_{14}O_4$ (*m/z* 173.0808 $[M-H]^-$, calcd. 173.0808) with two degrees of unsaturation, by negative ion mode HR-ESI-MS. According to the ^{13}C-NMR and DEPT (Table 3) results, the

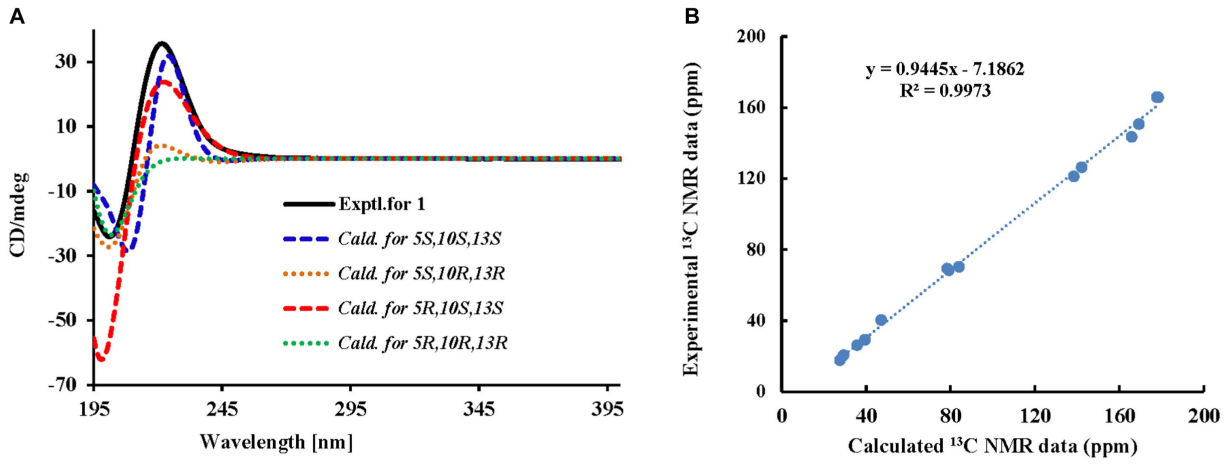

FIGURE 3
Experimental and calculated ECD curves and correlation plots of experimental and ^{13}C NMR data of compound **1**. **(A)** Experimental and calculated ECD curves; **(B)** Correlation plots of experimental and calculated ^{13}C NMR data.

carbon signals of compound **4** were similar to those of compound **1** (Table 1). Careful analysis of the NMR data revealed that compound **4** was one of the two polyketone chains of compound **1** and was 4,7-dihydroxyoct-2*E*-enoic acid. The structure of compound **4** was elucidated through the analysis of HMBC: H-2 (δ_H 5.98) was associated with C-1 (δ_C 170.2) and C-4 (δ_C 71.7); H-3 (δ_H 6.89) was associated with C-4 (δ_C 71.7) and C-1 (δ_C 170.2); H-6 (δ_H 1.54 and 1.47) was associated with C-5 (δ_C 34.0) and C-7 (δ_C 68.6); and H-8 (δ_H 1.16) was associated with C-6 (δ_C 35.9) and C-7 (δ_C 68.6). The structure of compound **4** was determined as 4,7-dihydroxyoct-2*E*-enoic acid (Figure 1).

The other compounds were identified as clonostachydiol (**5**) (Ojima et al., 2018), 7*R*-[[4*R*,5*S*-dihydroxy-1-oxo-2*E*-hexen-1-yl]oxy]-4*S*-hydroxy-2*E*-octenoic acid (**6**) (Ojima et al., 2018), (3*R*,5*R*)-3-hydroxy-5-decanolide (**7**) (Wu et al., 2009), 3β-hydroxy-7α-methoxy-5α,6α-epoxy-8(14),22*E*-dien-ergosta (**8**) (Wu et al., 2015), 3β,5α,9α-trihydroxy-ergosta-7,22-dien-6-one (**9**) (Cai et al., 2013), 3β,5α,6β-triol-7,22*E*-diene-ergosta (**10**) (Zhao et al., 2010), and stigmast-5-ene-3β-yl formate (**11**) (Chumkaew et al., 2010). These identifications were made by comparing the obtained data with the information reported in the respective references.

3.2 Cytotoxic activity

Compounds **1**, **8**, **9,** and **11** were assessed to determine their cytotoxic activity using the MTS method. During an initial active screening, compound concentration was used at 40 μM; the results showed that compounds **1**, **8**, **9,** and **11** had initial inhibitory rates of 21.5%, 100.0%, 15.4%, and 15.6%, respectively, against HL-60; 37.4%, 100.0%, 13.6%, and 0.33%, respectively, against A549 cells; 12.1, 100.0, 30.1, and 6.9%, respectively, against SMMC-7721; 37.9%, 95.5%, 24.4%, and 10.7%, respectively, against MDA-MB-231; and 41.2%, 100.0%, 21.6%, and 4.3%, respectively, against SW480 (Figure 4). Among them, the IC_{50} values of compound **8** were 12.89 ± 0.81 μM (HL-60), 15.69 ± 0.61 μM (A549), 3.00 ± 0.27 μM (SMMC-7721), 4.644 ± 0.270 μM (MDA-MB-231), and 14.02 ± 0.52 μM (SW480).

3.3 Inhibitory activity against protein kinase Cα

In this study, the compounds were analyzed using the data obtained from the SwissTargetPrediction website, revealing that some of them had protein kinase Cα target sites. Subsequently, the effect of these compounds on protein kinase Cα inhibitory activity was assessed, which is determined based on the basic principles of ELISA. Compounds **1**, **2**, **3a/b**, **5, 6,** and **7** were evaluated at a concentration of 20 μg/mL. After substituting the OD values of the six compounds and the blank control, the actual activity concentrations of protein kinase Cα were determined. Compared with the control group, the protein kinase activity of the treated group was obtained. Then according to the inhibition rate formula, the inhibition rates of the six compounds on protein kinase Cα were 43.63%, 15.68%, 30.77%, 8.68%, 40.93%, and 57.66%, respectively. The activity results are shown in Figure 5. Results indicated that compounds **1**, **6,** and **7** had some inhibitory effect on protein kinase Cα activity.

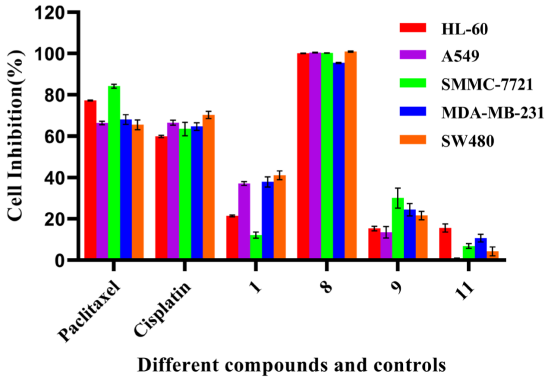

FIGURE 4
Cytotoxic activity of some compounds. The test concentration of each compound (**1**, **8**, **9,** and **11**) was 40 μM; Cisplatin (40 μM) and paclitaxel (5 μM) were used as positive controls. All experiments were conducted in triplicate, and data were expressed as the mean ± standard deviation of three independent experiments.

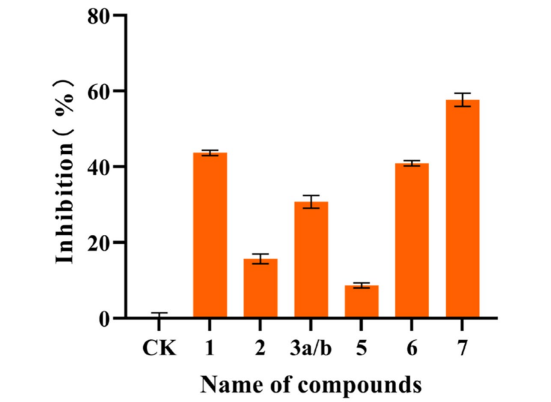

FIGURE 5
Inhibitory activity of some compounds on protein kinase Cα. The inhibitory activity of compounds against protein kinase Cα is determined based on the basic principles of ELISA. Compared with the control, the inhibition rates of the compounds **1**, **2**, **3a/b**, **5**, **6**, and **7** at a concentration of 20 μg/mL on protein kinase Cα were 43.63%, 15.68%, 30.77%, 8.68%, 40.93%, and 57.66%, respectively. All experiments were conducted in triplicate, and data were expressed as the mean ± standard deviation of three independent experiments.

4 Discussion

The investigation of stroma and host complexes of *Cordyceps* has consistently been a focal point in research. However, acquiring these complexes in substantial quantities remains challenging. Consequently, researchers have focused on exploring the activities and components of their anamorphs. In a previous study, we screened *P. gunnii* YMF1.00003 under different culture conditions through the conduct of metabolome analysis and activity comparison and found that the fermentation extract of the mycelium in WGA was similar to the extract of stroma and host complexes and had obvious cytotoxic activity (Qu et al., 2022). Therefore, we further examined the metabolites and activities of *P. gunnii* YMF1.00003 fermented in two different media. Eleven compounds (**1–11**) were

identified, including **1**, **4**, **8,** and **11** from the modified WGA medium and other metabolites from the modified Sabouraud solid medium.

The extract of *P. gunnii* YMF1.00003 showed notable cytotoxic activity. Hence, several isolated compounds were evaluated to ascertain their cytotoxic activity. Compound **8** exhibited moderate cytotoxic activity against five tumor cell lines, with IC_{50} values of 3.00 ± 0.27 μM (SMMC-7721), 4.644 ± 0.270 μM (MDA-MB-231), 12.89 ± 0.81 μM (HL-60), 15.69 ± 0.61 μM (A549), and 14.02 ± 0.52 μM (SW480), respectively. Compound **1** showed weak cytotoxic activity against five tumor cell lines at a concentration of 40 μM. Ergosterols, particularly ergosterol peroxide, have been recognized for their potent cytotoxic activity (Zhabinskii et al., 2022; Hoang et al., 2023). According to the existing literature, the position of hydroxyl substitution, the position of double bonds, and the degree of oxidation are pivotal factors influencing cytotoxicity (Zhabinskii et al., 2022). The mechanism underlying the cytotoxic activity of this compound has been documented: ergosterol peroxide stimulates Foxo3 activity by inhibiting pAKT and c-Myc and activating the pro-apoptotic proteins Puma and Bax to induce cancer cell death (Li et al., 2016). Compound **1** is classified as a non-symmetric macrocyclic bislactone, and this type of bislactone has demonstrated certain antimicrobial bioactivity in previous studies (Krohn et al., 2007). SwissTargetPrediction was launched in 2014 and used as a web-based tool for predicting the potential protein targets of small molecules. It predicts the potential targets of all examined compounds based on their similarity with known bioactive compounds (Gfeller et al., 2014). However, virtual screening is frequently associated with high false-positive rates. Several compounds that receive high rankings for a specific target protein may not exhibit actual activity. During a typical virtual screening, only approximately 12% of the highest-scoring compounds demonstrated activity when subjected to biochemical analysis (Adeshina et al., 2020). Therefore, virtual screening serves as a crucial and beneficial tool, yet necessitating further experimental validation. In the present study, the STP was employed to identify targets associated with the metabolites (Gfeller et al., 2014). The results indicated a potential interaction between this type of bislactone and protein kinase Cα. Our active screening result showed that compounds **1**, **6,** and **7** inhibited the activity of protein kinase Cα by 43.63%, 40.93%, and 57.66% at a concentration of 20 μg/mL, respectively. Protein kinase Cα is implicated in various diseases, such as cardiovascular diseases (Turner et al., 2013), schizophrenia (Carroll et al., 2010), and the neural basis of episodic memory (MacLeod and Donaldson, 2014). However, due to the low inhibition rate of protein kinase Cα activity and the limited amount of compounds, further investigations were not pursued. Protein kinase C, a phospholipid- and calcium-dependent protein kinase, has been marketed as a drug target for multiple drugs, providing significant clinical benefits to patients with cardiovascular and cerebrovascular diseases, leukemia, and diabetes (Carter, 2000). The wild stroma and host complexes of *Cordyceps* fungus have been a focal point of research, but their scarcity has led researchers to concentrate on clonal mycelium. In the initial stages, we evaluated the *Paecilomyces gunnii* extracts under different culture conditions and from the wild stroma and host complexes through the performance of a metabolome analysis and identified the culture conditions for producing metabolites with enhanced cytotoxic activity (Qu et al., 2022). In the present study, fermentation was conducted under screened culture conditions to yield active natural products. The results showed that compound 3β-hydroxy-7α-methoxy-5α,6α-epoxy-8(14),22*E*-dien-ergosta (**8**) exhibited notable antitumor activity, while compounds **1**, **6,** and **7** displayed a certain inhibitory effect on protein kinase Cα.

With the rapid advancements in sequencing technology and bioinformatics, numerous fungal gene clusters have been found to remain "silent" under conventional culture conditions. This suggests the presence of a large number of potentially active compounds with novel structures that are concealed within these "silent" gene clusters and yet to be identified (Nielsen et al., 2017; Kjærbolling et al., 2019). The current study is based on a previous one stain-many compounds (OSMAC) strategy and the isolation and identification of promising compounds under optimized culture conditions (Qu et al., 2022). In recent years, the OSMAC strategy has proven successful in isolating compounds with novel structures and diverse activities from fungi (Bode et al., 2002). Following the screening of culture conditions, hydroxy-substituted fatty acids with nematicidal activity were obtained from *Purpureocillium lavendulum* (Liu et al., 2022). Diketopiperazine alkaloids were purified from a marine endophytic fungus *Penicillium* brocae with strong anti-*Staphylococcus aureus* activity and cytotoxic activity using the "OSMAC" strategy (Meng et al., 2016). The fungal genome harbors numerous transcription regulators, and the transcription and expression of functional genes are often controlled by these regulators. The discovery of new secondary metabolites can be facilitated by manipulating specific transcription factors (Keller, 2019). However, the efficacy of mining fungal metabolites through fermentation conditions remains contingent on factors such as whether the genomic data of the target fungus has been measured, the quality of the genomic data, and the establishment of genetic transformation.

Data availability statement

The original contributions presented in the study are included in the article/supplementary material, further inquiries can be directed to the corresponding author.

Ethics statement

Ethical approval was not required for the studies on humans in accordance with the local legislation and institutional requirements because only commercially available established cell lines were used.

Author contributions

S-SL: Data curation, Investigation, Writing – original draft. S-LQ: Data curation, Investigation, Writing – original draft. JX: Investigation, Writing – original draft. DL: Investigation, Data curation, Writing – original draft. P-JZ: Data curation, Funding acquisition, Investigation, Resources, Writing – review & editing.

Funding

The author(s) declare financial support was received for the research, authorship, and/or publication of this article. This work was

supported in part by the National Key Research and Development Program (2023YFD1400400), the National Natural Science Foundation of China (31970060 and 32270132), the special fund of the Yunnan University "double first-class" construction, and the Applied Basic Research Foundation of Yunnan Province (202201BC070004 and 202102AA100013).

Acknowledgments

The authors are grateful to the Microbial Library of the Germplasm Bank of Wild Species from Southwest China for providing the *Paecilomyces gunnii* YMF1.00003 strain. We are grateful to Shi Bao-Bao for calculating the ECD and qcc NMR of compound **1**.

Conflict of interest

The authors declare that the research was conducted in the absence of any commercial or financial relationships that could be construed as a potential conflict of interest.

Publisher's note

All claims expressed in this article are solely those of the authors and do not necessarily represent those of their affiliated organizations, or those of the publisher, the editors and the reviewers. Any product that may be evaluated in this article, or claim that may be made by its manufacturer, is not guaranteed or endorsed by the publisher.

References

Adeshina, Y. O., Deeds, E. J., and Karanicolas, J. (2020). Machine learning classification can reduce false positives in structure-based virtual screening. *Proc. Natl. Acad. Sci. U. S. A.* 117, 18477–18488. doi: 10.1073/pnas.2000585117

Bode, H. B., Bethe, B., Höfs, R., and Zeeck, A. (2002). Big effects from small changes: possible ways to explore nature's chemical diversity. *ChemBioChem* 3, 619–627. doi: 10.1002/1439-7633(20020703)3:7<619::AID-CBIC619>3.0.CO;2-9

Cai, H. H., Liu, X. M., Chen, Z. Y., Liao, S. T., and Zou, Y. X. (2013). Isolation, purification and identification of nine chemical compounds from *Flammulina velutipes* fruiting bodies. *Food Chem.* 141, 2873–2879. doi: 10.1016/j.foodchem.2013.05.124

Carroll, L. S., Williams, N. M., Moskvina, V., Russell, E., Norton, N., Williams, H. J., et al. (2010). Evidence for rare and common genetic risk variants for schizophrenia at protein kinase Cα. *Mol. Psychiatry* 15, 1101–1111. doi: 10.1038/mp.2009.96

Carter, C. A. (2000). Protein kinase C as a drug target: implications for drug or diet prevention and treatment of cancer. *Curr. Drug Targets* 1, 163–183. doi: 10.2174/1389450003349317

Chumkaew, P., Kato, S., and Chantrapromma, K. (2010). New cytotoxic steroids from the fruits of *Syzygium siamense*. *J. Asian Nat. Prod. Res.* 12, 424–428. doi: 10.1080/10286021003762028

Gfeller, D., Grosdidier, A., Wirth, M., Daina, A., Michielin, O., and Zoete, V. (2014). SwissTargetPrediction: a web server for target prediction of bioactive small molecules. *Nucleic Acids Res.* 42, W32–W38. doi: 10.1093/nar/gku293

Hoang, C. K., Le, C. H., Nguyen, D. T., Tran, H. T. N., Luu, C. V., Le, H. M., et al. (2023). Steroid components of marine-derived fungal strain *Penicillium levitum* N33.2 and their biological activities. *Mycobiology* 51, 246–255. doi: 10.1080/12298093.2023.2248717

Kauloorkar, S. V., and Kumar, P. (2016). Total synthesis of (−)-(6,11,14)-colletallol proline catalyzed α-aminoxylation and Yamaguchi macrolactonization. *RSC Adv.* 6, 63607–63612. doi: 10.1039/C6RA08484B

Keller, N. P. (2019). Fungal secondary metabolism: regulation, function and drug discovery. *Nat. Rev. Microbiol.* 17, 167–180. doi: 10.1038/s41579-018-0121-1

Kjærbolling, I., Mortensen, U. H., Vesth, T., and Andersen, M. R. (2019). Strategies to establish the link between biosynthetic gene clusters and secondary metabolites. *Fungal Genet. Biol.* 130, 107–121. doi: 10.1016/j.fgb.2019.06.001

Krohn, K., Farooq, U., Flörke, U., Schulz, B., Draeger, S., Pescitelli, G., et al. (2007). Secondary metabolites isolated from an endophytic *Phoma* sp. – absolute configuration of tetrahydropyrenophorol using the solid-state TDDFT CD methodology. *Eur. J. Org. Chem.* 2007, 3206–3211. doi: 10.1002/ejoc.200601128

Kuo, Y. C., Tsai, W. J., Shiao, M. S., Chen, C. F., and Lin, C. Y. (1996). *Cordyceps sinensis* as an immunomodulatory agent. *Am. J. Chin. Med.* 24, 111–125. doi: 10.1142/S0192415X96000165

Li, X. M., Wu, Q. P., Bu, M., Hu, L. M., Du, W. W., Jiao, C. W., et al. (2016). Ergosterol peroxide activates Foxo3-mediated cell death signaling by inhibiting AKT and c-Myc in human hepatocellular carcinoma cells. *Oncotarget* 7, 33948–33959. doi: 10.18632/oncotarget.8608

Liu, R., Bao, Z. X., Li, G. H., Li, C. Q., Wang, S. L., Pan, X. R., et al. (2022). Identification of nematicidal metabolites from *Purpureocillium lavendulum*. *Microorganisms* 10:1343. doi: 10.3390/microorganisms10071343

Lu, R., Liu, X., Gao, S., Zhang, W., Peng, F., Hu, F., et al. (2014). New tyrosinase inhibitors from *Paecilomyces gunnii*. *J. Agric. Food Chem.* 62, 11917–11923. doi: 10.1021/jf504128c

Macleod, C. A., and Donaldson, D. I. (2014). PRKCA polymorphism changes the neural basis of episodic remembering in healthy individuals. *PLoS One* 9:e98018. doi: 10.1371/journal.pone.0098018

Meng, L. H., Wang, C. Y., Mándi, A., Li, X. M., Hu, X. Y., Kassack, M. U., et al. (2016). Three diketopiperazine alkaloids with spirocyclic skeletons and one bisthiodiketopiperazine derivative from the mangrove-derived endophytic fungus *Penicillium* brocae MA-231. *Org. Lett.* 18, 5304–5307. doi: 10.1021/acs.orglett.6b02620

Nielsen, J. C., Grijseels, S., Prigent, S., Ji, B. Y., Dainat, J., Nielsen, K. F., et al. (2017). Global analysis of biosynthetic gene clusters reveals vast potential of secondary metabolite production in *Penicillium* species. *Nat. Microbiol.* 2:17044. doi: 10.1038/nmicrobiol.2017.44

Ojima, K. I., Yangchum, A., Laksanacharoen, P., Tasanathai, K., Thanakitpipattana, D., Tokuyama, H., et al. (2018). Cordybislactone, a stereoisomer of the 14-membered bislactone clonostachydiol, from the hopper pathogenic fungus *Cordyceps* sp. BCC 49294: revision of the absolute configuration of clonostachydiol. *J. Antibiot.* 71, 351–358. doi: 10.1038/s41429-017-0008-9

Pu, X. J., Hu, Q. Y., Li, S. S., Li, G. H., and Zhao, P. J. (2021). Sesquiterpenoids and their quaternary ammonium hybrids from the mycelium of mushroom *Stereum hirsutum* by medium optimization. *Phytochemistry* 189:112852. doi: 10.1016/j.phytochem.2021.112852

Qu, S. L., Xie, J., Wang, J. T., Li, G. H., Pan, X. R., and Zhao, P. J. (2022). Activities and metabolomics of *Cordyceps gunnii* under different culture conditions. *Front. Microbiol.* 13:1076577. doi: 10.3389/fmicb.2022.1076577

Su, J., Zhao, P., Kong, L., Li, X., Yan, J., Zeng, Y., et al. (2013). Trichothecin induces cell death in NF-κB constitutively activated human cancer cells via inhibition of IKKβ phosphorylation. *PLoS One* 8:e71333. doi: 10.1371/journal.pone.0071333

Sun, H., Zhu, Z., Tang, Y., Ren, Y., Song, Q., Tang, Y., et al. (2018). Structural characterization and antitumor activity of a novel se-polysaccharide from selenium-enriched *Cordyceps gunnii*. *Food Funct.* 9, 2744–2754. doi: 10.1039/C8FO00027A

Turner, S. T., Boerwinkle, E., O'connell, J. R., Bailey, K. R., Gong, Y., Chapman, A. B., et al. (2013). Genomic association analysis of common variants influencing antihypertensive response to hydrochlorothiazide. *Hypertension* 62, 391–397. doi: 10.1161/HYPERTENSIONAHA.111.00436

Wu, J. Z., Gao, J., Ren, G. B., Zhen, Z. B., Zhang, Y. H., and Wu, Y. K. (2009). Facile access to some chiral building blocks. Synthesis of verbalactone and exophilin a. *Tetrahedron* 65, 289–299. doi: 10.1016/j.tet.2008.10.050

Wu, C. J., Yi, L., Cui, C. B., Li, C. W., Wang, N., and Han, X. (2015). Activation of the silent secondary metabolite production by introducing neomycin-resistance in a marine-derived *Penicillium purpurogenum* G59. *Mar. Drugs* 13, 2465–2487. doi: 10.3390/md13042465

Zhabinskii, V. N., Drasar, P., and Khripach, V. A. (2022). Structure and biological activity of ergostane-type steroids from fungi. *Molecules* 27:2103. doi: 10.3390/molecules27072103

Zhao, J. L., Mou, Y., Shan, T. J., Li, Y., Zhou, L. G., Wang, M. G., et al. (2010). Antimicrobial metabolites from the endophytic fungus *Pichia guilliermondii* isolated from *Paris polyphylla* var. yunnanensis. *Molecules* 15, 7961–7970. doi: 10.3390/molecules15117961

Zheng, Y., Zhang, J., Wei, L., Shi, M., Wang, J., and Huang, J. (2017). Gunnilactams A-C, macrocyclic tetralactams from the mycelial culture of the entomogenous fungus *Paecilomyces gunnii*. *J. Nat. Prod.* 80, 1935–1938. doi: 10.1021/acs.jnatprod.7b00060

frontiers | Frontiers in Microbiology

TYPE Original Research
PUBLISHED 05 March 2024
DOI 10.3389/fmicb.2024.1322316

OPEN ACCESS

EDITED BY
Vijay K. Sharma,
Agricultural Research Organization (ARO), Israel

REVIEWED BY
Sunil Banskar,
University of Arizona, United States
Chandni Talwar,
University of Delhi, India

*CORRESPONDENCE
Hang Jie
✉ jiehangisgood@126.com

RECEIVED 16 October 2023
ACCEPTED 16 February 2024
PUBLISHED 05 March 2024

CITATION
Xu Z, Li F, Liu Q, Ma T, Feng X, Zhao G, Zeng D, Li D and Jie H (2024) Chemical composition and microbiota changes across musk secretion stages of forest musk deer. *Front. Microbiol.* 15:1322316. doi: 10.3389/fmicb.2024.1322316

Chemical composition and microbiota changes across musk secretion stages of forest musk deer

Zhongxian Xu[1,2], Feng Li[1,2], Qian Liu[1], Tianyuan Ma[2], Xiaolan Feng[3], Guijun Zhao[3], Dejun Zeng[3], Diyan Li[2] and Hang Jie[3]*

[1]Sichuan Wildlife Rehabilitation and Breeding Research Center, Key Laboratory of Southwest China Wildlife Resources Conservation (Ministry of Education), China West Normal University, Nanchong, China, [2]Farm Animal Genetic Resources Exploration and Innovation Key Laboratory of Sichuan Province, Sichuan Agricultural University, Chengdu, China, [3]Bio-resource Research and Utilization Joint Key Laboratory of Sichuan and Chongqing, Chongqing Institute of Medicinal Plant Cultivation, Chongqing College of Traditional Chinese Medicine, Chongqing, China

Forest musk deer is the most important animal for natural musk production, and the musk composition changes periodically during musk secretion, accompanied by variation in the com-position of deer-symbiotic bacteria. GC-MS and 16S rRNA sequencing were conducted in this study, the dynamic changes to correlated chemical composition and the microbiota across musk secretion periods (prime musk secretion period, vigorous musk secretion period and late musk secretion period) were investigated by integrating its serum testosterone level in different mating states. Results showed that the testosterone level, musk composition and microbiota changed with annual cycle of musk secretion and affected by its mating state. Muscone and the testosterone level peaked at vigorous musk secretion period, and the microbiota of this stage was distinct from the other 2 periods. Actinobacteria, Firmicutes and Proteobacteria were dominant bacteria across musk secretion period. PICRUSt analysis demonstrated that bacteria were ubiquitous in musk pod and involved in the metabolism of antibiotics and terpenoids in musk. "Carbohydrates and amino acids," "fatty acids and CoA" and "secretion of metabolites" were enriched at 3 periods, respectively. *Pseudomonas*, *Corynebacterium*, *Clostridium*, *Sulfuricurvum* were potential biomarkers across musk secretion. This study provides a more comprehensive understanding of genetic mechanism during musk secretion, emphasizing the importance of *Actinobacteria* and *Corynebacterium* in the synthesis of muscone and etiocholanone during musk secretion, which required further validation.

KEYWORDS

forest musk deer, chemical composition, microbiota, musk secretion stage, mating state

1 Introduction

Musk, a precious raw ingredient in traditional Chinese medicine and perfume manufacturing, is secreted from the glandular sac located between the navel and genitals of male forest musk deer (*Moschus berezovskii*) (FMD) (Meng et al., 2012). The sticky, white and malodorous liquid musk initially secreted by the musk gland is transported by catheters to a musk pod and matured to form

blackish-brown solids with a specific musk odor by eventual fermentation (Bi et al., 1988). The initial liquid musk is synthesized during the prime musk secretion period (PMSP), a large amount of liquid musk is produced and forms semisolid musk during the vigorous musk secretion period (VMSP), and liquid musk stored in the musk pod undergoes full maturation and becomes the final solid musk during the late musk secretion period (LMSP) (Bai et al., 2013).

Testosterone (T) is the most essential factor targeting the testis to induce musk formation (Wilslocki et al., 1947; Wang et al., 2012; Bai et al., 2013; Fan et al., 2018). Studies showed that sex hormones (testosterone and estradiol) levels are consistent with annual cycle of musk formation and secretion (Zheng et al., 2019). Testosterone level increases at first and then decreases across the three stages of musk secretion (Bai et al., 2013; Suo et al., 2020), it reaches the peak at vigorous musk secretion period, and is significantly higher than other periods (Bai et al., 2013; Fan et al., 2018). Meanwhile, testosterone plays a major role in seasonal development of musk glands for musk-secreting animals like musk deer, muskrat, and Indian civet (Zhang et al., 2017). There is a positive correlation between musk yield and serum T levels, and negative correlation with serum estradiol and progesterone levels (Bai, 2012; Bai et al., 2013; Zhang et al., 2015). However, it remains unknown whether the T level is associated with mating status of musk deer in breeding season.

Jie has reported that the number of chemical compositions of musk ascended from June to August and declined from August to October, it varied with the physiological process of musk secretion. They also found ketones were dominant chemicals at vigorous musk secretion period in forest musk deer (Jie et al., 2021). Furthermore, our previous research showed that a greater amount of musk is produced in unmated males (UMs: 22.79 ± 3.6 g, $n = 5$) than mated males (MMs: 1.12 ± 0.34 g, $n = 5$), hinting that the production of musk is associated with its mating states (Li et al., 2016). Muscone, as a preponderant ingredient of natural musk, is claimed to function as pheromone for chemical communication for sexual attractant for females in rutting season (Sokolov et al., 1987), which was verified by more muscone are detected in UMs at LMSP (Li et al., 2016).

Studies have shown that core bacterial communities (Firmicutes, Bacteroidetes, and Proteobacteria) are shared by gut, fecal and musk microbiota in musk deer species, whereas the key genera for different species, mating states, ages, genders, and food-sources are distinct (Hu et al., 2017; Li et al., 2017; Hu et al., 2018; Li et al., 2018; Sun et al., 2019; Zhao et al., 2019). The fermentation hypothesis for mammalian chemical communication states that odorous metabolites secreted by fermentative bacteria in the scent glands can be used by the hosts for communication (Theis et al., 2013). Our study has proven that the maturation of musk is affected by interactions between the complex microbial community and chemical compounds produced by the host, and symbiotic bacteria underlie mating state-specific odors among animals is illustrated by the fact that many bacterial genera were overrepresented in UMs (Li et al., 2016).

2 Materials and methods

2.1 Animals and sample collection

A total of 30 healthy captive FMDs (15 UMs and 15 MMs) aged 2.5 to 6 years were raised in the Chongqing Institute of Medicinal Plant Cultivation (Chongqing, China). We collected the musk at the end of May to June, September, and October corresponding to PMSP, VMSP, LMSP. Six biological replicates for unmated and 7 biological replicates for mated individuals for each stage were sampled. All experiments were conducted in compliance with the guidelines approved by the Institutional Animal Care and Use Committee of Sichuan Agricultural University (approval ID: B20160403), and all efforts were made to minimize animal suffering. The blood samples were collected for serum T quantitative determination during musk secretion and non-secretion season ($n = 10$ for each group); body weight, musk yields were recorded at LMSP ($n = 10$). Serum testosterone was assayed by use of a testosterone ELISA kit (BNIBT, Beijing, China). The operation was conducted according to the specification.

2.2 Musk chemical component extraction and GC–MS determination

Sample preparation was performed as previously described with minor modifications (Li et al., 2016). Twenty milligrams of musk sample from each group were pooled, divided into 2 parts and dissolved in 2.5 mL of diethyl ether and ether alcohol, followed by a 2-h extraction by ultrasonication and centrifugation at 13,000 × g for 5 min. Two milliliters of supernatant was placed into a GC–MS instrument (GCMS-QP2010 Plus, Shanghai, China) for chemical composition detection with the chromatographic conditions as follows: column temperature: 40°C, inlet temperature: 290°C, interface temperature: 220°C, split injection with the pressure of 49.5 kPa. The column temperature program was as follows: 40°C (2 min), 200°C (5 min, 10°C/min), 240°C (5 min, 5°C/min), maintained at 290°C for 15 min. The total and column flow rates were 9.0 and 1.0 mL/min, respectively; the linear velocity was 36.1 cm/s; the purge flow rate was 3.0 mL/min; and the mass scanning range was 33–600 m/z. The acquired data in total ionic chromatograms (TICs) were compared with those in the mass spectral library of the National Institute of Standards and Technology (NIST). A confidence coefficient of above 80% was adopted for the data, and peak area % values were used to determine component variations. Finally, to discriminate the chemical compositions among 6 groups, we performed Partial Least Squares Discriminant Analysis (PLS-DA) after Pareto scaling.

2.3 Bacterial DNA isolation and 16S rRNA sequencing

Total bacterial DNA of each sample was isolated using an UltraClean Microbial DNA Isolation Kit (MOBIO, CA, USA) according to the manufacturer's instructions. DNA quality was tested by 1.0% agarose gel electrophoresis and a NanoDrop spectrophotometer (NanoDrop Technologies, Wilmington, DE). The primers 515-F (5′- GTGCCAGCMGCCGCGG-3′) and 907-R (5'-CCGTCAATTCMTTTRAGTTT-3′) targeting the V3-V4 variable regions of the 16S-rRNA gene were used (Merrifield et al., 2013). The 16S-rRNA gene was amplified by PCR (95°C for 3 min, followed by 35 cycles of 95°C for 30 s, 55°C for 30 s, and 72°C for 45 s, and a final extension of 8 min at 72°C). The PCR products were purified and recovered by the Ezgene TM Gel/PCR Extraction Kit (Biomiga, USA) and submitted for library construction using the TruSeq Nano DNA

LT Library Prep Kit (Illumina). Finally, a total of 39 libraries were constructed, and 250-bp paired-end (PE250) sequencing was performed on an Illumina Hiseq 2,500 platform (Illumina Inc., San Diego, CA, US) at Novogene (Beijing, China).

2.4 Bioinformatic analysis

The obtained low-quality raw reads and chimeras were removed using Cutadapt software (V1.9.1), the preprocessed paired-end reads were merged with FLASH (V1.2.7[1]) followed the criteria that the overlapped base of Read 1 and Read 2 was > = 10 bp and no mismatches allowed. High-quality reads were generated after quality control by FastQC (V0.11.7[2]). High-quality reads were assigned to operational taxonomic units (OTUs) with an unidentity threshold of 3% using UPARSE (V7.0.1001[3]) in QIIME (Quantitative Insights IntoMicrobial Ecology, Boulder, CO, USA, V1.8.0), and microbial taxa were identified from species annotation based on the GreenGenes reference database by Usearch software. We analyzed the relative abundances (RAs) of the top 10 phyla and top 20 genera, estimated four α diversity indices (Shannon, PD whole tree, observed OTU and Chao1), and compared the significant differences among 6 groups using ANOVA with Tukey's HSD test. Prior to the evaluation of β diversity, unweighted pair-group method with arithmetic means (UPGMA) clustering trees were constructed to calculate Bray-Curtis and UniFrac distances, and canonical correspondence analysis (CCA) and principal coordinates analysis (PCoA) were implemented to evaluate the segregation of the microbial community using the R package (V2.15.3). Linear discriminant analysis (LDA) effect size (LEfSe) was performed to determine the differentially abundant microbes among the 6 groups (Segata et al., 2011), and selected bacteria with LDA score > 4 were used to calculate the Spearman correlation with the top 20 chemical components. Finally, the functional prediction of the musk microbiota was performed online using Phylogenetic Investigation of Communities by Reconstruction of Unobserved States (PICRUSt2) (Langille et al., 2013).

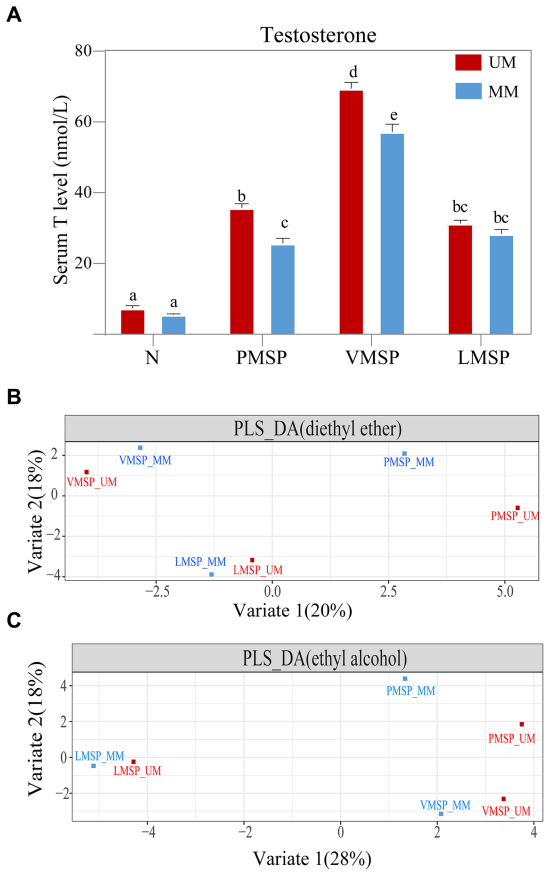

FIGURE 1
The serum testosterone and chemical composition features across musk secretion. **(A)** Histograms of serum testosterone levels and **(B,C)** partial least squares discriminant analysis (PLS-DA) across musk secretion based on diethyl ether and ethyl alcohol, respectively. **(A)** Different letters on the columns in panel A indicated significant differences, the same letters were nonsignificant, $p < 0.05$. N indicates non-musk secretion season. PMSP, VMSP, LMSP indicates prime, vigorous and late musk secretion period, respectively. UM and MM represents unmated and mated males, respectively.

3 Results

3.1 The serum testosterone (T) level varies with musk secretion

The T concentration was significantly higher in the UM group (PMSP and VMSP) than that of MM group. The serum T concentration was at a basal level and as low as 7.37 ± 1.78 nmol/L and 5.54 ± 1.62 nmol/L in UMs and MMs, respectively, in non-secretion season (N). TheT level significantly increased from N to PMSP (35.72 ± 1.28 nmol/L in UMs and 25.68 ± 2.64 nmol/L in MMs), and reached a peak in VMSP (69.44 ± 3.24 nmol/L in UM and 57.24 ± 6.65 nmol/L in MM). It decreased gradually from VMSP to LMSP (31.32 ± 2.03 nmol/L in UMs and 28.34 ± 3.59 nmol/L in MMs) (Figure 1A). We collected 21.161 ± 5.434 g of fully mature secretions from UMs in the late musk secretion period, which was significantly greater than the amount derived from MMs (7.122 ± 1.648 g, $p = 0.018$). And the musk yields were significantly positive correlated ($R = 0.719$, $p = 0.019$) with serum T levels for MM, while no correlation was found for UM (Supplementary Figure S1).

3.2 The chemical composition changes across musk secretion

Generally, the TICs indicated that the number of chemicals extracted by diethyl ether (75.17 ± 8.32) was greater than that extracted by ethyl alcohol (66.00 ± 11.09); as the key medical active and aromatic component of natural musk, 3-methylcyclopentadecanone (muscone) was the most abundant component (26.99% in UM and 25.54% in MM), followed by 3a-hydroxy-5b-androstan-17-one (etiocholanone) (12.95% in UM and 12.30% in MM) and cholesterol (10.99 in UM and

1 http://ccb.jhu.edu/software/FLASH/
2 https://www.bioinformatics.babraham.ac.uk/projects/fastqc/
3 http://drive5.com/uparse/

7.82 in MM) (Supplementary Figures S2, S3; Supplementary Table S1). The PLS-DA results showed metabolites extracted by two solvents of LMSP were more distinct with PMSP and VMSP, and the differences between UM and MM were least within LMSP (Figures 1B,C).

3.3 Statistics of 16S rRNA sequencing data

In addition, we performed 16S rRNA sequencing to evaluate the bacterial dynamics, and a total of 1,869,786 high-quality reads of 39 samples were generated; an average of 52,868, 40,226 and 50,735 reads were obtained in PMSP, VMSP and LMSP; 45,202 and 51,141 high-quality reads were assigned to UMs and MMs, respectively (Supplementary Table S2). There were 1,431 OTUs that were assigned at the 97% similarity level; the average number of OTUs was 977 ± 64 in each group, ranging from 865 (PMSP-MM) to 1,014 (LMSP-UM), and there were 1,075 OTUs in PMSP, 1,157 OTUs in VMSP, and 1,248 OTUs in LMSP. The number of OTUs detected in UMs was significantly higher than that in MMs (~1,024 in UMs and ~930 in MMs, $p = 0.0002$). Taxonomic classification of the OTUs resulted in 39 phyla, 84 classes, 162 orders, 291 families, 569 genera and 654 species, among which, 391 out of 1,431 OTUs, 19 out of 39 phyla and 257 out of 569 genera were shared by all individuals within each group, and most unique OTUs were found in LMSP (37 in UMs and 14 in MMs) and VMSP (23 in MMs and 4 in UMs) (Supplementary Figure S4).

3.4 Different dominant microbiota composition at genus level

We selected the top 10 phyla and top 20 genera in terms of relative proportions to illustrate the dominant microbiota composition. Actinobacteria, Firmicutes, Proteobacteria, and Bacteroidetes were common dominant microbial communities in the 6 groups, and their relative proportions accounted for more than 87% of all phyla (Figure 2 upper). Intriguingly, the relative proportion of Actinobacteria was as high as 77.57% ± 11.24% in the VMSP-MM group, which was much higher than that in UMs (20.39% ± 9.24%) and significantly different from that in the other 2 periods ($p = 0.0017$), indicating the absolute abundant role of Actinobacteria in this group. At the genus level, we found that *Corynebacterium* and an unassigned genus of Aerococcaceae were common dominant microbial communities during PMSP and VMSP. In particular, the genus *Corynebacterium* was an abundant dominant microbe (63.63%) in the VMSP-MM group, with a significantly higher ($p = 0.0261$) relative proportion than the average relative proportions in other groups (6.82%), as well as the relative proportion in UMs (14.21%). During LMSP, the main dominant genera were *Oligella*, *Enterococcus*, and *Cetobacterium* in MMs and *Pseudomonas*, *Cetobacterium*, and *Acinetobacter* in UMs (Figure 2 lower).

3.5 Microbiota diversity variations across musk secretion

We calculated the α and β-diversity to further evaluate the differences in microbiota composition within and among the 6 groups. Overall, the α diversity showed negligible differences because of the inconsistent trends in variation across multiple metrices: the observed significant differences between PMSP and LMSP in MMs ($p = 0.0477$) for the observed OTU and Chao1 index ($p = 0.0451$) did not showed in PD whole tree and Shannon index (Figures 3A-D, Supplementary Table S3). The microbiota composition differences between groups based on Bray-Curtis distance are listed in Supplementary Table S3. A significant discrepancy between PMSP and VMSP was observed ($p = 0.0040$ in MM and 0.0100 in UM), variance between PMSP and LMSP was detected merely within MM ($p = 0.0090$). The CCA result explained 17.7% ($p = 0.001$) of the total variance between samples. All samples in VMSP were clustered and distinctly separated from the communities clustered by the majority of samples in PMSP and LMSP, which could be well explained by PCoA 1 (47.76%). However, this plot revealed negligible differences between the UM and MM groups. As expected, identical results for the musk microbiota in VMSP were revealed by the PCoA plot (Figures 3E,F).

3.6 Distinct bacteria interact with chemical components to mediate musk secretion

We performed LEfSe analysis of the 6 groups to further determine differentially abundant bacterial taxa that might be considered biomarkers. Twenty-one taxa were identified as significantly abundant communities (LDA > 4 and $p < 0.05$) across 3 musk secretion stages, belonging to the top 3 dominant microbial communities (Firmicutes, Proteobacteria, and Actinobacteria). Among them, Firmicutes was dominant in MMs in the 3 periods (LDA > 5). During VMSP, 5 taxa of Proteobacteria including Proteobacteria, Betaproteobacteria, Pseudomonadales, Pseudomonadaceae, and *Pseudomonas*, and 5 taxa of Actinobacteria, including *Corynebacterium*, were distinct bacteria in UM and MM respectively; 6 taxa of Firmicutes (*Clostridium* and an unknown genus of Aerococcaceae) and 2 taxa of Proteobacteria were discrepant microbes in MMs and UMs during LMSP (Figure 4A). Furthermore, we identified 17 taxa as significant biomarkers (LDA > 4 and $p < 0.05$) between UMs and MMs, and more taxa were found in MMs, namely, 5 Firmicutes, 5 Actinobacteria and 1 Proteobacteria, particularly *Corynebacterium* and *Sulfuricurvum*. We identified 2 Firmicutes (including *Clostridium*), 1 Actinobacteria, 2 Proteobacteria (an unidentified genus of Rhodobacteraceae) and 1 Bacteroidetes (an unassigned genus of Bacteroidaceae) as biomarkers in UMs (Figure 4B).

The relative abundances of identified biomarkers were used to conduct spearman correlation analysis with the level of top 20 chemical components, we found that the abundance of p_ Actinobacteria was positively correlated with muscone ($R = 0.886$, $p = 0.019$), normuscone ($R = 0.829$, $p = 0.042$), 17-Oxoandrost-5-en-3-yl hydrogen sulfate ($R = 0.870$, $p = 0.024$), cis-9-Hexadecenal ($R = 0.928$, $p = 0.008$) and cyclotridecanone ($R = 0.928$, $p = 0.008$). The abundance of c_Gammaproteobacteria had a positive relationship with 3a-Hydroxy-5b-androstan-17-one (etiocholanone) ($R = -0.943$, $p = 0.005$) and negative with cholesterol ($R = -0.890$, $p = 0.019$). The abundance of g_*Corynebacterium* was positively correlated with etiocholanone ($R = 0.829$, $p = 0.042$) and cholesterol ($R = 0.886$, $p = 0.019$), but negatively with dihydroandrosterone ($R = -0.943$, $p = 0.005$). And the abundance of f_Aerococcaceae was negatively

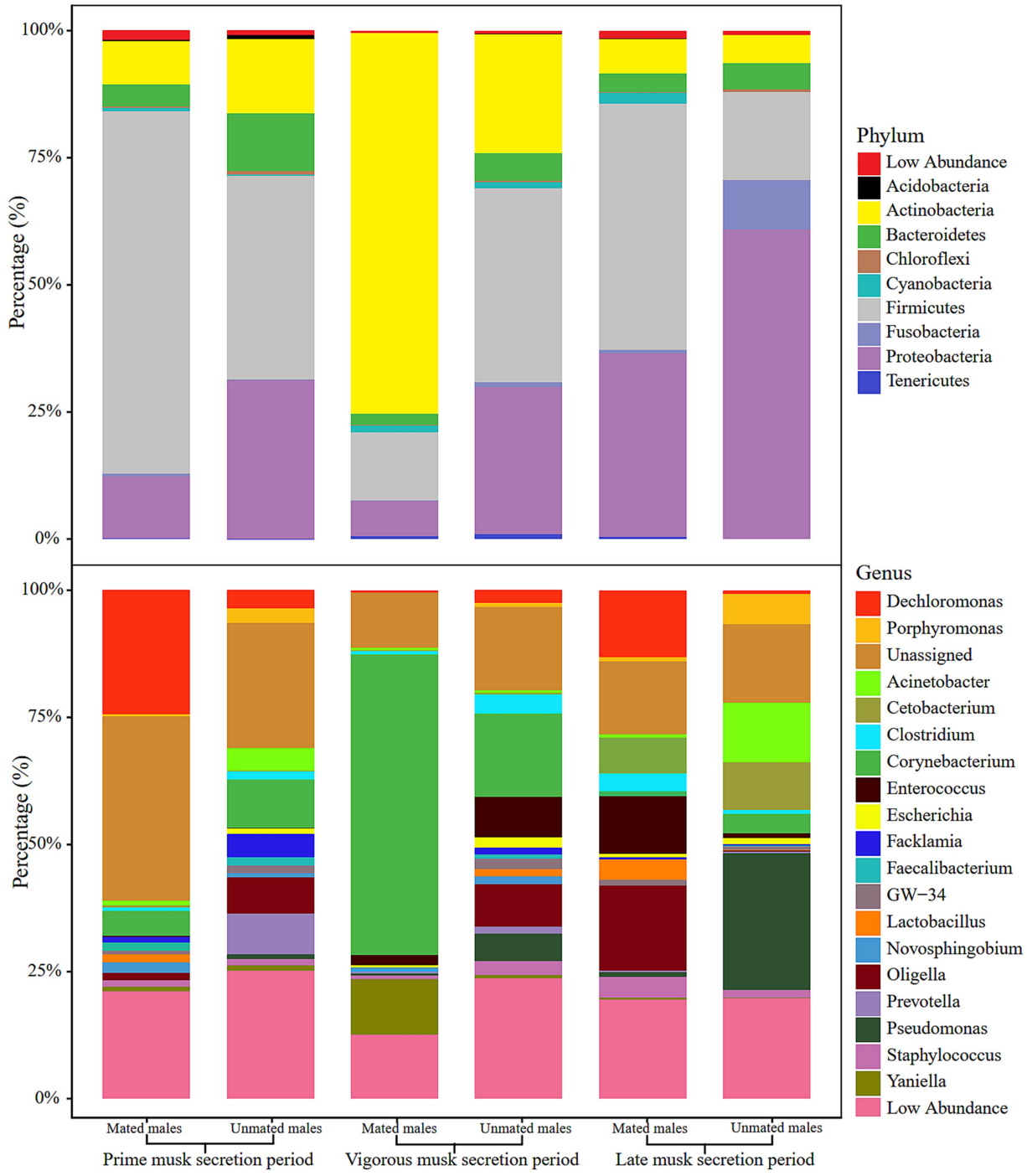

FIGURE 2
Histogram of relative abundance of microbiota composition at phylum (upper) and genus (lower) levels in the 6 groups.

correlated with androstan-17-ol, 2,3-epoxy ($R = -0.845$, $p = 0.034$) (Figure 5).

3.7 Function predictions of musk microbiota

To explore the differences in microbial functions in each group, we used the assigned OTUs to determine the relative abundances of functional categories through PICRUSt2. We found 39 pathways shared predicted functions in the 6 groups. Intriguingly, "Biosynthesis of ansamycins (ko01051)," "Biosynthesis of vancomycin group antibiotics (ko01055)" and "Terpenoid backbone biosynthesis (ko00900)" belonging to metabolism of terpenoids and polyketides, as was "Synthesis and degradation of ketone bodies (ko00072)" were detected in all samples. For stage-specific functions, we found 6 pathways were specifically enriched in PMSP-MM. "Glyoxylate and dicarboxylate metabolism (ko00630)" was uniquely enriched in

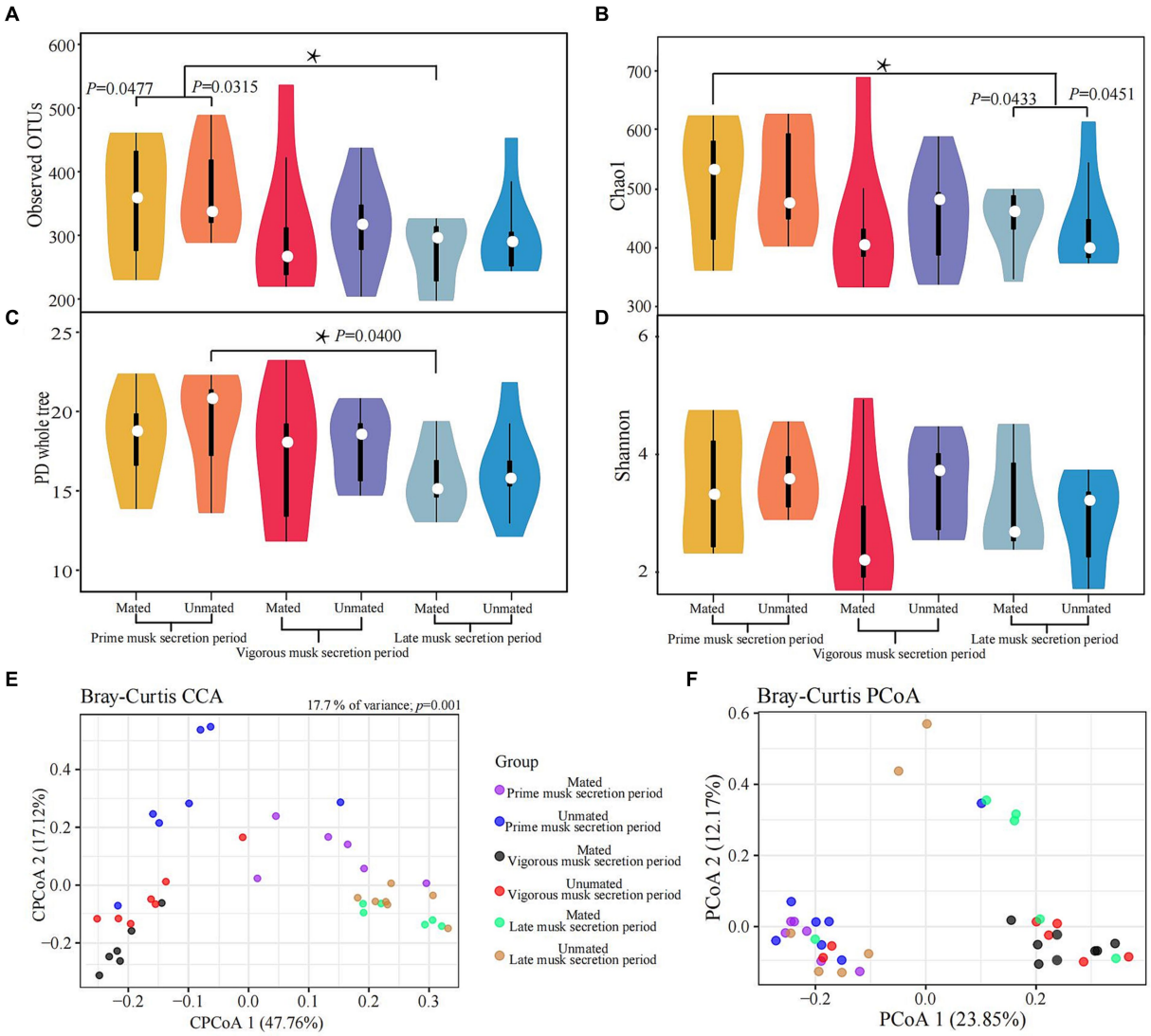

FIGURE 3
Variations in alpha **(A–D)** and beta **(E,F)** diversity of the musk microbiota. Asterisk means $p < 0.05$.

VMSP-MM. Three pathways were uniquely enriched in LMSP-UM. Moreover, "Geraniol degradation (ko00281)" was enriched in UMs during LMSP, and "Bacterial chemotaxis (ko02030)" was assigned only in the UM group across the 3 periods (Figure 6 and Supplementary Table S4).

4 Discussion

The hardship of sample collection and non-invasive principles of sampling limited the sample size in our study. The timid feature and furious reaction of forest musk deer increases the difficulty of sampling. Actually, the collection of musk at the initial stage would decrease the subsequent musk secretion, which would 39 sampling in the following stages. Therefore, it is not possible to collected enough musk of all individuals at one stage. Although we have studied the chemical composition and microbiota in UMs and MMs in our previous study, we merely elucidated the microbiota changes and the important roles of the dominant bacteria during LMSP (Li et al., 2018). Whether the T levels and dynamic composition of musk change with the bacterial communities colonizing the musk glands is unclear, and the relationship between mating states and microbiota across musk secretion stages need additional studies. We selected 30 healthy musk deer, sampled 6 unmated and 7 mated individuals during musk secretion. A total of 39 (18 UM and 21 MM) libraries were constructed for 16S rRNA sequencing. Moreover, due to the musk is one of the most valuable scented animal products and more expensive than gold. Sufficient musk (at least 0.8 g) for DNA extraction was priority, we pooled 20 mg musk of each group for GC–MS determination.

We further investigated the dynamic changes of chemical composition and the microbiota across musk secretion by integrating its serum T level in different mating states. As one of the most important androgens mediated by HPG axis, testosterone can affect the development and physiological responses of the musk gland (Bi et al., 1980; Knol, 1991). Bai found an obvious tendency of the fecal T levels in the musk-secreting period (2–7 years old's male forest musk

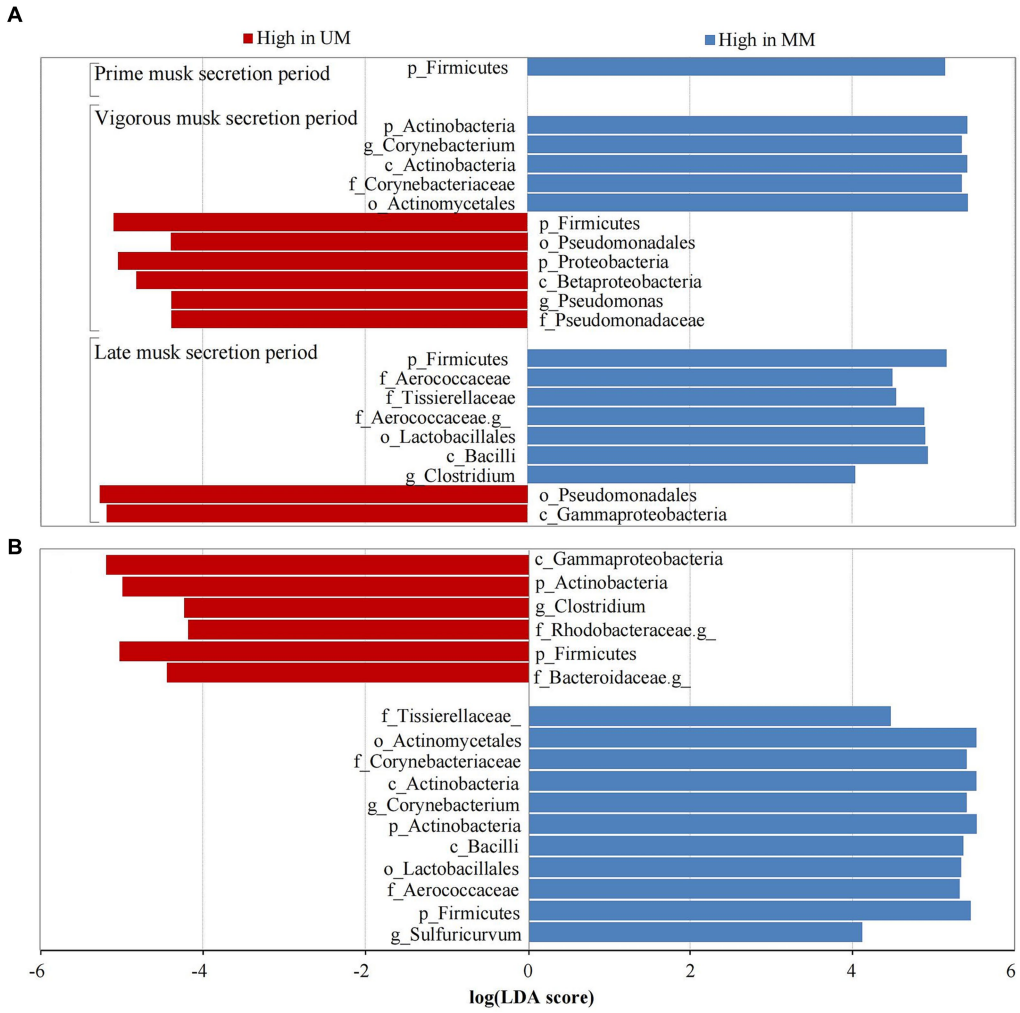

FIGURE 4
Taxa with significant difference (LDA > 4) across musk secretion stages **(A)** between unmated and mated males **(B)**. UM and MM represents unmated and mated males, respectively. A means LEfSe analysis of 21 significantly abundant taxa between Ums and MMs across 3 musk secretion stages. B means LEfSe analysis of 17 taxa were used as significant biomarkers between UMs and MMs.

deer, $n = 30$), a similar pattern was found in estradiol but no obvious trend was detected in progesterone. Compared with the non-secretion season (114.15 ± 15.46 ng/g), T levels of PMSP (1731.50 ± 95.66 ng/g) and VMSP (3766.82 ± 98.48 ng/g) were higher significantly, which raised gradually before musk-secreting period (412.05 ± 54.14 ng/g), increased rapidly in PMSP, and peaked in VMSP, subsequently declined steeply in LMSP (616.79 ± 68.79 ng/g) (Bai, 2012; Bai et al., 2013). Results in this study showed that the serum T levels changed dynamically during musk secretion and peaked at VMSP as well, it increased significantly in musk secretion season and was much higher in UMs than MMs. Zhang et al. (2015) and Suo et al. (2020) reported the serum and fecal T levels increased first and then decreased in the three stages of secretion, respectively. In addition, we found a stronger positive correlation ($R^2 = 0.719$, $p = 0.019$) in MM, but an uncorrelated relationship ($R^2 = 0.084$, $p = 0.816$) in UM. Bai (2012) and Bai et al. (2013) indicated that musk yield was positively correlated with T level ($R^2 = 0.650$, $p < 0.05$). Sun et al. (2020) discovered the musk secretion with higher T level was significantly more than that of with lower T level. Previous studies prompted the musk secretion through intramuscular injection of testosterone (Jie et al., 2014). Fan hinted that sex hormones might determine musk composition in early musk secretion, even facilitate the musk secretion (Fan et al., 2018). The muscone content showed the highest relative abundance among all components. Consistent with previous report (Su et al., 2009), steroids (cholesterol, cholestanol. and etiocholanone) presented at relatively high levels in musk.

Although there were some individual differences in alpha diversity there were no consistent trends in variation across multiple alpha metrics. The principal coordinate analysis of β diversity values illustrated samples in VMSP were distinctly separated from the other 2 periods, which were consistent with the highest T level observed at VMSP. It was speculated that the diversity of microbiota is affected by homeostasis in musk sacs maintained by hosts at different periods, and a slightly richer microbiota is essential for the synthesis of specific odor substances to make fully mature musk in the unmated males for more attractive to females (Li et al., 2016; Jie et al., 2021).

It is generally believed that substantial changes of the bacterial communities colonizing the musk gland are resulted from

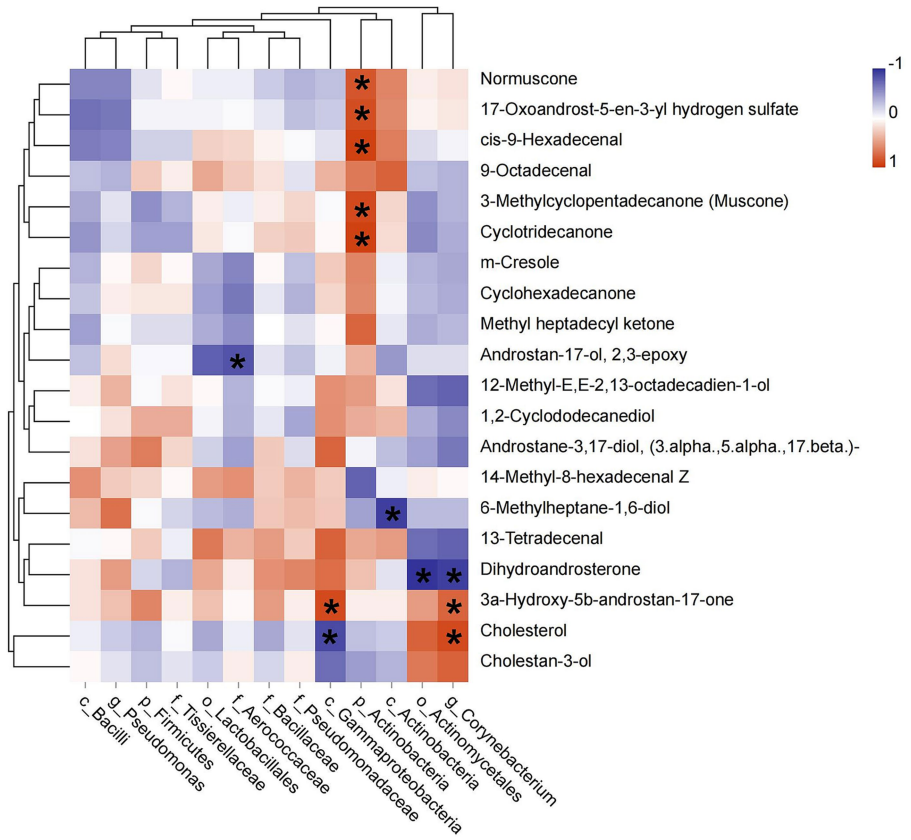

FIGURE 5
Pearson correlation between dominant bacterial taxa and the top 20 chemical components of musk. Asterisk means $p < 0.05$, red square indicates positive correlation and blue square indicates negative correlation.

physiological activities during musk secretion (Li et al., 2018; Jie et al., 2019). Though Actinobacteria, Firmicutes, and Proteobacteria are dominant bacteria in musk deer (Sundset et al., 2007; Gruninger et al., 2014; Ishaq and Wright, 2014), their composition is dynamic across musk secretion, namely, Actinobacteria (especially there were 15 mated and 15 non mated deer in two groups) dominated in VMSP absolutely; Firmicutes and Proteobacteria accounted for majority of bacterial communities during PMSP and LMSP, respectively. Hu et al. have revealed the decline of Firmicutes-Bacteroidetes ratio with the seasonal variation but the dominant genera showed no significant changes of gut microbiota in forest musk deer (Hu et al., 2018). We have reported differences of relative microbiota abundance during forest musk deer development, Clostridiales and Bacteroidales were higher in juvenile, *Pseudomonas* and Lachnospiraceae were more abundant in the adult (Zhao et al., 2019). Li et al. (2021) have found the fecal microbiota composition in young forest musk deer at genus level changed from that found in 7–10 day's old became stabilized after 30 day's old, the relative abundance of *Actinobacteria*, *Spirochaetes*, *Ruminococcaceae_UCG-005*, *Treponema* and *Prevotella* was higher in the post-weaning than in the pre-weaning group (Li et al., 2020).

The LEfSe analysis showed that Firmicutes, which contain cellulolytic bacteria was the dominant bacteria across 3 stages (Hugenholtz, 2002). Proteobacteria which are resistant to antimicrobial compounds (Lee et al., 2012) and Actinobacteria which are the main sources of anti-inflammatory components (Scharf and Brakhage, 2013; O'Connor, 2015; Motoyama and Osada, 2016) in musk were dominant in VMSP. *Pseudomonas aeruginosa* can inhibit the growth of *Trueperella pyogenes* in FMD with abscess diseases (Yuan et al., 2020). Actinobacteria include members with significant economic and medical importance. Filamentous actinomycetes, such as *Corynebacterium* and *Streptomyces* species, can produce a plethora of bioactive secondary metabolites, many of these metabolic compounds are antimicrobial, anticancer, antiviral or immunosuppressive in activity (Prudence et al., 2020; Undabarrena et al., 2021; Seshadri et al., 2022). *Corynebacterium* is used as a commercial bacterial strain to synthesize heterologous terpenoids and as a model system for aromatic hydrocarbon metabolism research (Shen et al., 2012; Lee et al., 2016). The metabolites of *Corynebacterium* play analgesic, anticancer and antioxidant functions in therapy (Heider et al., 2012; Hari et al., 2019). These bacteria were confirmed to have positive correlations with muscone and etiocholanone (Gammaproteobacteria/*Corynebacterium* vs. etiocholanone and Actinobacteria vs. muscone). During LMSP, metabolites of Aerococcaceae might be the source of fatty acids and might protect against foreign bacterial invasion (Hugenholtz, 2002).

Pathways enriched in all groups illustrated that these bacteria are involved in the metabolism antibiotics and terpenoids, which are essential for the synthesis of antibacterial and anti-inflammatory components and specific odor substances in musk. For example, ansamycin and vancomycin are antibiotics used for the treatment of

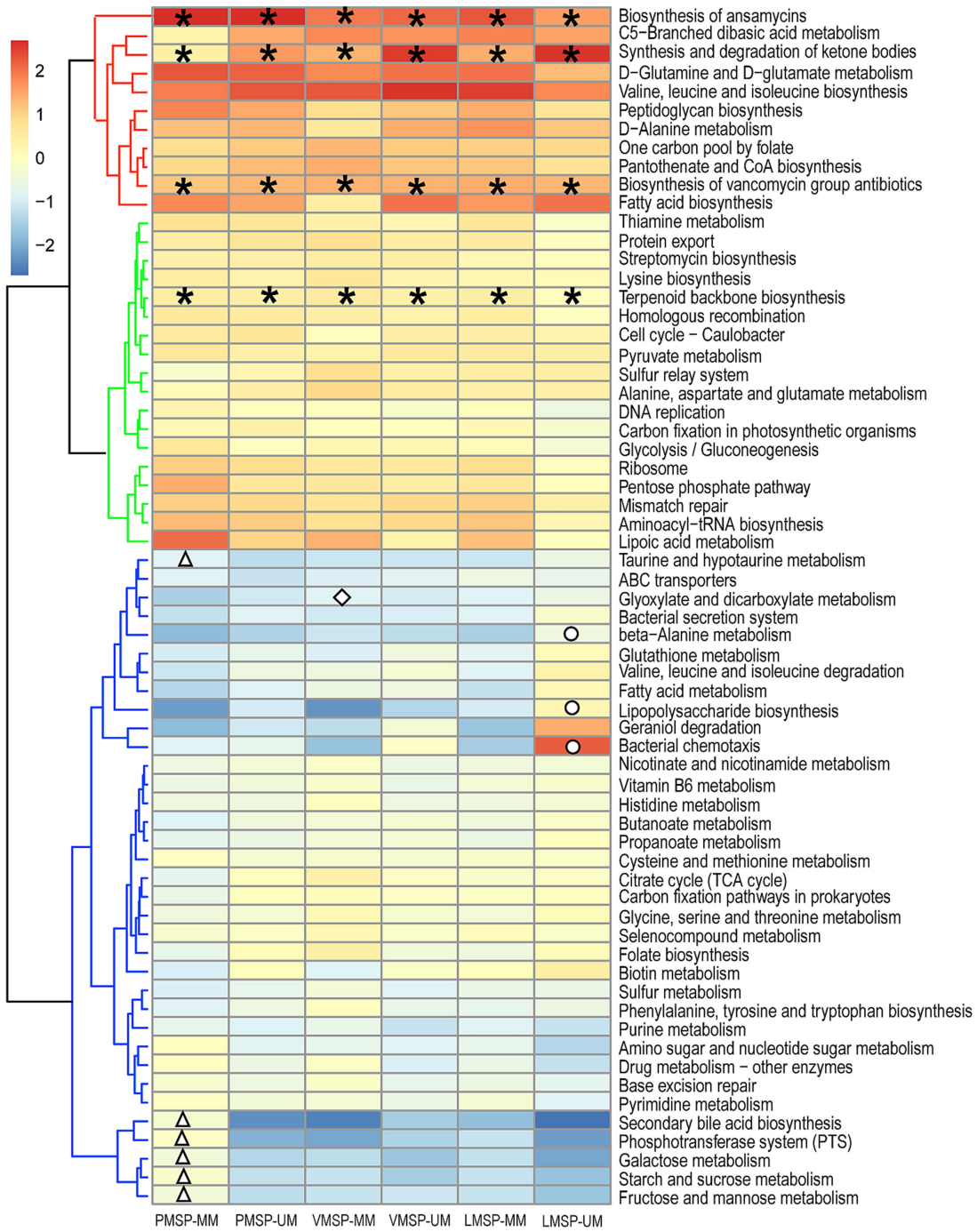

FIGURE 6
Heat map of the functional predictions of musk microbiota (normalized by Z-score). PMSP, VMSP, LMSP indicates prime, vigorous and late musk secretion period, respectively. UM and MM represents unmated and mated males, respectively. *represents pathways enriched in 6 groups, △ means PMSP-MM specific pathways, ◇ and ○ indicates VMSP-MM and LMSP-MM uniquely enriched pathways, respectively.

bacterial infections (Yu et al., 2002; Watanabe et al., 2003; Okano et al., 2017); terpenoids are the precursor of sterols and ketones (Mookherjee and Wilson, 1982; Wriessnegger and Pichler, 2013), and they are microbial metabolites of Streptomycetaceae (Hwang et al., 2014), Actinobacteria (*Actinomycetes* and *Corynebacterium*) (van Bergeijk et al., 2020), Myxobacteria (Schaberle et al., 2014) and Proteobacteria (*Escherichia coli*) in industry (Yamada et al., 2015; Lee et al., 2016; Wang et al., 2018). Among PMSP-specific pathways, the PTS is a major mechanism used by bacteria for the uptake of carbohydrates (Deutscher et al., 2008), which is related to the accumulation of carbohydrates and other amino acids at PMSP. Glyoxylate and dicarboxylate metabolism is associated with the biosynthesis of carbohydrates from fatty acids or CoA (Yoo et al., 2019). Bacterial secretion system has been shown to mediate protein export through the membranes of Gram-negative bacteria (King et al., 2009). Bacterial chemotaxis is an adaptive response to the environment, suggesting

that UMs might be more attractive for females than MMs, and this attraction is driven by aromatic substances produced by bacteria in UMs (Miller et al., 2009).

5 Conclusion

To sum up, the serum T level, chemical composition and microbiota of musk exhibited dynamic changes with musk secretion. The microbiota of VMSP was distinct from the other 2 periods. Actinobacteria, Firmicutes and Proteobacteria are dominant bacteria across musk secretion, *Pseudomonas* and *Corynebacterium* were candidate biomarkers of the VMSP, *Clostridium* was a biomarker of the LMSP; *Corynebacterium* and *Sulfuricurvum* in MMs and *Clostridium* in UMs could be used to distinguish the mating state of FMD. We are also assuming that Actinobacteria and *Corynebacterium* have vital roles in the synthesis of muscone and etiocholanone during musk secretion, and further study is needed to confirm these hypotheses. However, these results predicted the metagenomic function, further validations were required to confirm our hypotheses.

Data availability statement

The 16S rRNA sequencing data presented in the study are deposited at https://ngdc.cncb.ac.cn/bioproject, accession number PRJCA002782.

Ethics statement

The animal study was approved by the Institutional Animal Care and Use Committee of Sichuan Agricultural University (approval ID: B20160403). The study was conducted in accordance with the local legislation and institutional requirements.

Author contributions

ZX: Conceptualization, Methodology, Project administration, Writing – original draft, Writing – review & editing, Funding acquisition. FL: Supervision, Writing – review & editing, Software. QL: Writing – review & editing, Data curation, Formal analysis. TM: Data curation, Writing – review & editing, Visualization. XF: Writing – review & editing, Data curation, Investigation. GZ: Data curation, Writing – review & editing, Resources. DZ: Resources, Writing – review & editing, Software. DL: Software, Writing – review & editing, Data curation, Formal analysis. HJ: Writing – review & editing, Conceptualization, Funding acquisition, Project administration, Supervision.

Funding

The author(s) declare financial support was received for the research, authorship, and/or publication of this article. This research was funded by National Natural Science Foundation of China (81973428 and 82274046), the Fundamental Research Funds of China West Normal University (21E037, 21E038, and KCXTD2022-7) and Chongqing Talent Program (cstc2021jscx-bgzxm0201).

Conflict of interest

The authors declare that the research was conducted in the absence of any commercial or financial relationships that could be construed as a potential conflict of interest.

Publisher's note

All claims expressed in this article are solely those of the authors and do not necessarily represent those of their affiliated organizations, or those of the publisher, the editors and the reviewers. Any product that may be evaluated in this article, or claim that may be made by its manufacturer, is not guaranteed or endorsed by the publisher.

Supplementary material

The Supplementary material for this article can be found online at: https://www.frontiersin.org/articles/10.3389/fmicb.2024.1322316/full#supplementary-material

References

Bai, K. (2012) *Research on the association among polymorphisms of androgen receptor gene, the levels of gonadal hormone and musk yield in the Moschus Berezovskii (forest musk deer)*, Northwest A&F University, Yangling.

Bai, K., Ren, Z. J., Li, F. R., Li, Y., Zhu, C. S., Tang, J., et al. (2013). An association with gonadal hormone level and musk yield in *Moschus berezovskii* during musk-secreting period. *Chinese J. Vet. Sci.* 33, 956–962. doi: 10.16303/j.cnki.1005-4545.2013.06.032

Bi, S. Z., Guan, Q., Jia, L. Z., An, G. L., Zhang, Z. G., and Cheng, J. J. (1988). Studies on microscopic structure and ultrastructure of musk glandular sac of *Moschus* and on musk secretion. *Acta Theriol. Sin.* 8, 4–12.

Bi, S. Z., Yan, Y. H., Jin, S. Z., Wu, Y. M., Chen, C. F., Xu, H. J., et al. (1980). The prelimilary study of musk secretion and musk yield increase regulated by hypothalamic-pituitary-testis system. *Chin. J. Met. Sci. Technol.* 4, 18–20.

Deutscher, J., Francke, C., and Postma, P. W. (2008). How phosphotransferase system-related protein phosphorylation regulates carbohydrate metabolism in bacteria. *Microbiol. Mol. Biol. Rev.* 70, 939–1031. doi: 10.1128/MMBR.00024-06

Fan, M., Zhang, M., Shi, M., Zhang, T., Qi, L., Yu, J., et al. (2018). Sex hormones play roles in determining musk composition during the early stages of musk secretion by musk deer (*Moschus berezovskii*). *Endocr. J.* 65, 1111–1120. doi: 10.1507/endocrj.EJ18-0211

Gruninger, R. J., Sensen, C. W., McAllister, T. A., and Forster, R. J. (2014). Diversity of rumen bacteria in Canadian Cervids. *PLoS One* 9:e89682. doi: 10.1371/journal.pone.0089682

Hari, B., Meriga, B., Muni Swamy, G., and Karunakaran, R., *Recent developments in applied microbiology and biochemistry*. (2019), South Korea: Elsevier.

Heider, S. A., Peters-Wendisch, P., and Wendisch, V. F. (2012). Carotenoid biosynthesis and overproduction in *Corynebacterium glutamicum*. *BMC Microbiol.* 12:198. doi: 10.1186/1471-2180-12-198

Hu, X., Liu, G., Li, Y., Wei, Y., Lin, S., Liu, S., et al. (2018). High-throughput analysis reveals seasonal variation of the gut microbiota composition within Forest musk deer (*Moschus berezovskii*). *Front. Microbiol.* 9:1674. doi: 10.3389/fmicb.2018.01674

Hu, X., Liu, G., Shafer, A. B. A., Wei, Y., Zhou, J., Lin, S., et al. (2017). Comparative analysis of the gut microbial communities in Forest and alpine musk deer using high-throughput sequencing. *Front. Microbiol.* 8:572. doi: 10.3389/fmicb.2017.00572

Hugenholtz, P. (2002). Exploring prokaryotic diversity in the genomic era. *Genome Biol.* 3:REVIEWS0003. doi: 10.1186/gb-2002-3-2-reviews0003

Hwang, K. S., Kim, H. U., Charusanti, P., Palsson, B. O., and Lee, S. Y. (2014). Systems biology and biotechnology of Streptomyces species for the production of secondary metabolites. *Biotechnol. Adv.* 32, 255–268. doi: 10.1016/j.biotechadv.2013.10.008

Ishaq, S. L., and Wright, A. D. (2014). High-throughput DNA sequencing of the ruminal bacteria from moose (*Alces alces*) in Vermont, Alaska, and Norway. *Microb. Ecol.* 68, 185–195. doi: 10.1007/s00248-014-0399-0

Jie, H., Feng, X. L., Zhao, G. J., Zeng, D. J., Zhang, C. L., and Chen, Q. (2014). Research progress on musk secretion mechanism of forest musk deer. *Zhongguo Zhong Yao Za Zhi* 39, 4522–4525. doi: 10.4268/cjcmm20142309

Jie, H., Zhang, C., Zeng, D., Zhao, G., Feng, X., and Lei, M. (2021). Variation of chemical constituents in musk harvested at different maturity stages. *Chin. Trad. Pat. Med.* 43, 144–148. doi: 10.3969/j.issn.1001-1528.2021.01.028

Jie, H., Zhao, G., Zeng, D., Feng, X., Zhang, C., Liang, Z., et al. (2019). Microbial diversity of musk across its maturation process in forest musk deer. *Zhongguo Zhong Yao Za Zhi* 44, 4448–4453. doi: 10.19540/j.cnki.cjcmm.20190729.106

King, J. D., Kocincova, D., Westman, E. L., and Lam, J. S. (2009). Lipopolysaccharide biosynthesis in *Pseudomonas aeruginosa*. *Innate Immun.* 15, 261–312. doi: 10.1177/1753425909106436

Knol, B. W. (1991). Stress and the endocrine hypothalamus-pituitary-testis system: a review. *Vet. Q.* 13, 104–114. doi: 10.1080/01652176.1991.9694292

Langille, M. G. I., Zaneveld, J., Caporaso, J. G., McDonald, D., Knights, D., Reyes, J. A., et al. (2013). Predictive functional profiling of microbial communities using 16S rRNA marker gene sequences. *Nat. Biotechnol.* 31, 814–821. doi: 10.1038/nbt.2676

Lee, L. H., Cheah, Y. K., Nurul Syakima, A. M., Shiran, M. S., Tang, Y. L., Lin, H. P., et al. (2012). Analysis of Antarctic proteobacteria by PCR fingerprinting and screening for antimicrobial secondary metabolites. *Genet. Mol. Res.* 11, 1627–1641. doi: 10.4238/2012.June.15.12

Lee, J. Y., Na, Y. A., Kim, E., Lee, H. S., and Kim, P. (2016). The Actinobacterium *Corynebacterium glutamicum*, an industrial workhorse. *J. Microbiol. Biotechnol.* 26, 807–822. doi: 10.4014/jmb.1601.01053

Li, D. Y., Chen, B. L., Zhang, L., Gaur, U., Ma, T. Y., Jie, H., et al. (2016). The musk chemical composition and microbiota of Chinese forest musk deer males. *Sci. Rep.* 6:18975. doi: 10.1038/srep18975

Li, Y., Hu, X., Yang, S., Zhou, J., Zhang, T., Qi, L., et al. (2017). Comparative analysis of the gut microbiota composition between captive and wild Forest musk deer. *Front. Microbiol.* 8:1705. doi: 10.3389/fmicb.2017.01705

Li, Y., Shi, M., Zhang, T., Hu, X., Zhang, B., Xu, S., et al. (2020). Dynamic changes in intestinal microbiota in young forest musk deer during weaning. *PeerJ* 8:e8923. doi: 10.7717/peerj.8923

Li, Y., Zhang, T., Qi, L., Yang, S., Xu, S., Cha, M., et al. (2018). Microbiota changes in the musk gland of male forest musk deer during musk maturation. *Front. Microbiol.* 9:3048. doi: 10.3389/fmicb.2018.03048

Li, Y., Zhang, T., Shi, M., Zhang, B., Hu, X., Xu, S., et al. (2021). Characterization of intestinal microbiota and fecal cortisol, T3, and IgA in forest musk deer (*Moschus berezovskii*) from birth to weaning. *Integr. Zool.* 16, 300–312. doi: 10.1111/1749-4877.12522

Meng, X., Liu, D., Feng, J., and Meng, Z. (2012). Asian medicine: exploitation of wildlife. *Science* 335:1168. doi: 10.1126/science.335.6073.1168-a

Merrifield, C. A., Lewis, M. C., Claus, S. P., Pearce, J. T. M., Cloarec, O., Duncker, S., et al. (2013). Weaning diet induces sustained metabolic phenotype shift in the pig and influences host response to *Bifidobacterium Lactis* NCC2818. *Gut* 62, 842–851. doi: 10.1136/gutjnl-2011-301656

Miller, L. D., Russell, M. H., and Alexandre, G. (2009). Diversity in bacterial chemotactic responses and niche adaptation. *Adv. Appl. Microbiol.* 66, 53–75. doi: 10.1016/S0065-2164(08)00803-4

Mookherjee, B. D., and Wilson, R. A. (1982). *The chemistry and fragrance of natural musk compounds*. New York: Academic Press

Motoyama, T., and Osada, H. (2016). Biosynthetic approaches to creating bioactive fungal metabolites: pathway engineering and activation of secondary metabolism. *Bioorg. Med. Chem. Lett.* 26, 5843–5850. doi: 10.1016/j.bmcl.2016.11.013

O'Connor, S. E. (2015). Engineering of secondary metabolism. *Annu. Rev. Genet.* 49, 71–94. doi: 10.1146/annurev-genet-120213-092053

Okano, A., Isley, N. A., and Boger, D. L. (2017). Total syntheses of vancomycin-related glycopeptide antibiotics and key analogues. *Chem. Rev.* 117, 11952–11993. doi: 10.1021/acs.chemrev.6b00820

Prudence, S. M. M., Addington, E., Castano-Espriu, L., Mark, D. R., Pintor-Escobar, L., Russell, A. H., et al. (2020). Advances in actinomycete research: an ActinoBase review of 2019. *Microbiology* 166, 683–694. doi: 10.1099/mic.0.000944

Schaberle, T. F., Lohr, F., Schmitz, A., and Konig, G. M. (2014). Antibiotics from myxobacteria. *Nat. Prod. Rep.* 31, 953–972. doi: 10.1039/c4np00011k

Scharf, D. H., and Brakhage, A. A. (2013). Engineering fungal secondary metabolism: a roadmap to novel compounds. *J. Biotechnol.* 163, 179–183. doi: 10.1016/j.jbiotec.2012.06.027

Segata, N., Izard, J., Waldron, L., Gevers, D., Miropolsky, L., Garrett, W. S., et al. (2011). Metagenomic biomarker discovery and explanation. *Genome Biol.* 12:R60. doi: 10.1186/Gb-2011-12-6-R60

Seshadri, R., Roux, S., Huber, K. J., Wu, D., Yu, S., Udwary, D., et al. (2022). Expanding the genomic encyclopedia of Actinobacteria with 824 isolate reference genomes. *Cell Genom.* 2:100213. doi: 10.1016/j.xgen.2022.100213

Shen, X. H., Zhou, N. Y., and Liu, S. J. (2012). Degradation and assimilation of aromatic compounds by *Corynebacterium glutamicum*: another potential for applications for this bacterium. *Appl. Microbiol. Biotechnol.* 95, 77–89. doi: 10.1007/s00253-012-4139-4

Sokolov, V. E., Kagan, M. Z., Vasilieva, V. S., Prihodko, V. I., and Zinkevich, E. P. (1987). Musk deer (*Moschus moschiferus*): reinvestigation of main lipid components from preputial gland secretion. *J. Chem. Ecol.* 13, 71–83. doi: 10.1007/BF01020352

Su, G., Wu, A., Gan, X. N., Yue, B. S., and Li, J. (2009). Quantitative analysis of musk components by gas chromatography/mass spectrometry. *Mol. Boil. Rep.* 54, 2472–2482. doi: 10.1360/972009-1142

Sun, Y., Sun, Y., Shi, Z., Liu, Z., Zhao, C., Lu, T., et al. (2019). Gut microbiota of wild and captive alpine musk deer (*Moschus chrysogaster*). *Front. Microbiol.* 10:3156. doi: 10.3389/fmicb.2019.03156

Sun, T., Wang, J., Cai, Y., Cheng, J., Li, Y., Zhou, M., et al. (2020). Relationship between fecal steroid hormones and musk secretion in captive forest musk deer. *Acta Ecol. Sin.* 40, 9245–9251. doi: 10.5846/stxb202001210162

Sundset, M. A., Praesteng, K. E., Cann, I. K., Mathiesen, S. D., and Mackie, R. I. (2007). Novel rumen bacterial diversity in two geographically separated sub-species of reindeer. *Microb. Ecol.* 54, 424–438. doi: 10.1007/s00248-007-9254-x

Suo, L., Tang, J., Bian, K., Yang, C., Li, F., and Wang, Y. (2020). Preliminary study on the relationship between the levels of cortisol and testosterone and musk yield in secrete sweet period of forest musk deer. *Heilongjiang Anim. Husb. Vet.* 15, 140–142. doi: 10.13881/j.cnki.hljxmsy.2020.01.0173

Theis, K. R., Venkataraman, A., Dycus, J. A., Koonter, K. D., Schmitt-Matzen, E. N., Wagner, A. P., et al. (2013). Symbiotic bacteria appear to mediate hyena social odors. *Proc. Natl. Acad. Sci. USA* 110, 19832–19837. doi: 10.1073/pnas.1306477110

Undabarrena, A., Pereira, C. F., Kruasuwan, W., Parra, J., Selem-Mojica, N., Vind, K., et al. (2021). Integrating perspectives in actinomycete research: an ActinoBase review of 2020-21. *Microbiology* 167:1084. doi: 10.1099/mic.0.001084

van Bergeijk, D. A., Terlouw, B. R., Medema, M. H., and van Wezel, G. P. (2020). Ecology and genomics of Actinobacteria: new concepts for natural product discovery. *Nat. Rev. Microbiol.* 18, 546–558. doi: 10.1038/s41579-020-0379-y

Wang, C. L., Liwei, M., Park, J. B., Jeong, S. H., Wei, G. Y., Wang, Y. J., et al. (2018). Microbial platform for terpenoid production: *Escherichia coli* and yeast. *Front. Microbiol.* 9:2460. doi: 10.3389/fmicb.2018.02460

Wang, Q., Zhang, X. Y., Wang, Z. K., Qi, W. H., Yang, C. Z., and Yue, B. S. (2012). The cloning and analysis of FSHβ, LHβ genes in *Moschus berezovskii*. *Sichuan. J. Zool.* 31, 77–83. doi: 10.3969/j.issn.1000-7083.2012.01.017

Watanabe, K., Rude, M. A., Walsh, C. T., and Khosla, C. (2003). Engineered biosynthesis of an ansamycin polyketide precursor in *Escherichia coli*. *Proc. Natl. Acad. Sci. USA* 100, 9774–9778. doi: 10.1073/pnas.1632167100

Wilslocki, G. B., Aub, J. C., and Waldo, C. M. (1947). The effects of gonadectomy and the administration of testosterone propionate on the growth of antlers in male and female deer. *Endocrinology* 40, 202–224. doi: 10.1210/endo-40-3-202

Wriessnegger, T., and Pichler, H. (2013). Yeast metabolic engineering – targeting sterol metabolism and terpenoid formation. *Prog. Lipid Res.* 52, 277–293. doi: 10.1016/j.plipres.2013.03.001

Yamada, Y., Kuzuyama, T., Komatsu, M., Shin-ya, K., Omura, S., Cane, D. E., et al. (2015). Terpene synthases are widely distributed in bacteria. *Proc. Natl. Acad. Sci. USA* 112, 857–862. doi: 10.1073/pnas.1422108112

Yoo, H. J., Jung, K. J., Kim, M., Kim, M., Kang, M., Jee, S. H., et al. (2019). Liver cirrhosis patients who had normal liver function before liver cirrhosis development have the altered metabolic profiles before the disease occurrence compared to healthy controls. *Front. Physiol.* 10:1421. doi: 10.3389/fphys.2019.01421

Yu, T. W., Bai, L. Q., Clade, D., Hoffmann, D., Toelzer, S., Trinh, K. Q., et al. (2002). The biosynthetic gene cluster of the maytansinoid antitumor agent ansamitocin from *Actinosynnema pretiosum*. *Proc. Natl. Acad. Sci. U. S. A.* 99, 7968–7973. doi: 10.1073/pnas.092697199

Yuan, Y., Li, J., Zhang, A., Lin, J., Chu, Y., Wang, X., et al. (2020). Interspecific interaction between *Pseudomonas aeruginosa* and *Trueperella pyogenes* from the abscesses disease of *Moschus berezovskii*. *Sichuan. J. Zool.* 5, 1–7. doi: 10.11984/j.issn.1000-7083.2020001

Zhang, T., Peng, D., Qi, L., Li, W., Fan, M., Shen, J., et al. (2017). Musk gland seasonal development and musk secretion are regulated by the testis in muskrat (*Ondatra zibethicus*). *Biol. Res.* 50:10. doi: 10.1186/s40659-017-0116-9

Zhang, Z., Yang, J., Wang, J., Fu, W., Wang, Z., Ye, S., et al. (2015). Changes of serum gonadal hormones levels during musk-secreting period and estrus of *Moschus berezovskii*. *Zhong Yao Cai* 38, 240–244. doi: 10.13863/j.issn1001-4454.2015.02.008

Zhao, G., Ma, T., Tang, W., Li, D., Mishra, S. K., Xu, Z., et al. (2019). Gut microbiome of Chinese forest musk deer examined across gender and age. *Biomed. Res. Int.* 2019:9291216. doi: 10.1155/2019/9291216

Zheng, C., Wang, J., Wang, J., Zhou, L., Yang, Y., Feng, D., et al. (2019). Research progress on the relationship between musk components and androgen in captive musk deer. *J. Sichuan Trad. Chin. Med.* 37, 220–222.

frontiers | Frontiers in Microbiology

TYPE Original Research
PUBLISHED 02 April 2024
DOI 10.3389/fmicb.2024.1377965

OPEN ACCESS

EDITED BY
Vijay K. Sharma,
Agricultural Research Organization (ARO), Israel

REVIEWED BY
Rajesh Patel,
Veer Narmad South Gujarat University, India
Khan Mohd. Sarim,
Rudjer Boskovic Institute, Croatia

*CORRESPONDENCE
Aparna Banerjee
aparna.banerjee@uautonoma.cl

RECEIVED 28 January 2024
ACCEPTED 13 March 2024
PUBLISHED 02 April 2024

CITATION
Narsing Rao MP, Singh RN, Sani RK and Banerjee A (2024) Genome-based approach to evaluate the metabolic potentials and exopolysaccharides production of *Bacillus paralicheniformis* CamBx3 isolated from a Chilean hot spring.
Front. Microbiol. 15:1377965.
doi: 10.3389/fmicb.2024.1377965

Genome-based approach to evaluate the metabolic potentials and exopolysaccharides production of *Bacillus paralicheniformis* CamBx3 isolated from a Chilean hot spring

Manik Prabhu Narsing Rao[1], Ram Nageena Singh[2,3], Rajesh K. Sani[2,3,4,5] and Aparna Banerjee[1]*

[1]Instituto de Ciencias Aplicadas, Facultad de Ingeniería, Universidad Autónoma de Chile, Sede Talca, Talca, Chile, [2]Department of Chemical and Biological Engineering, South Dakota Mines, Rapid City, SD, United States, [3]2-Dimensional Materials for Biofilm Engineering, Science and Technology, South Dakota Mines, Rapid City, SD, United States, [4]Data Driven Material Discovery Center for Bioengineering Innovation, South Dakota Mines, Rapid City, SD, United States, [5]BioWRAP (Bioplastics With Regenerative Agricultural Properties), Rapid City, SD, United States

In the present study, a thermophilic strain designated CamBx3 was isolated from the Campanario hot spring, Chile. Based on 16S rRNA gene sequence, phylogenomic, and average nucleotide identity analysis the strain CamBx3 was identified as *Bacillus paralicheniformis*. Genome analysis of *B. paralicheniformis* CamBx3 revealed the presence of genes related to heat tolerance, exopolysaccharides (EPS), dissimilatory nitrate reduction, and assimilatory sulfate reduction. The pangenome analysis of strain CamBx3 with eight *Bacillus* spp. resulted in 26,562 gene clusters, 7,002 shell genes, and 19,484 cloud genes. The EPS produced by *B. paralicheniformis* CamBx3 was extracted, partially purified, and evaluated for its functional activities. *B. paralicheniformis* CamBx3 EPS with concentration 5 mg mL^{-1} showed an optimum 92 mM ferrous equivalent FRAP activity, while the same concentration showed a maximum 91% of Fe^{2+} chelating activity. *B. paralicheniformis* CamBx3 EPS (0.2 mg mL^{-1}) demonstrated β-glucosidase inhibition. The EPS formed a viscoelastic gel at 45°C with a maximum instantaneous viscosity of 315 Pa.s at acidic pH 5. The present study suggests that *B. paralicheniformis* CamBx3 could be a valuable resource for biopolymers and bioactive molecules for industrial applications.

KEYWORDS

***Baciilus paralicheniformis* CamBx3, bioactive compound, exopolysaccharides, genome analysis, pangenome**

Introduction

Thermal environments are considered pinpoint anomalies against a background of ambient life, they contain the most profound insights into the earliest life on Earth (Walter, 1996) and it is assumed that life on Earth evolved in such an environment (Woese, 1987). Culture-dependent and independent microbial diversity analysis of the thermal environment showed that they have diverse microbial diversity and harbor novel candidates (Luo et al., 2020; Narsing Rao et al., 2020, 2021). Ever since the exploration of Taq DNA polymerase from *Thermus aquaticus* and its application in the development of the polymerase chain reaction

(Chien et al., 1976; Brock, 1997), enzymes of thermophiles have been of considerable interest. Apart from thermostable enzymes, thermophiles are a valuable resource for biopolymers (Wang et al., 2019, 2020, 2021; Banerjee et al., 2022). Thermophilic bacteria produce a variety of macromolecules, including exopolysaccharides, as adaptations to help microbial communities withstand extreme temperatures (Wang et al., 2021). Exopolysaccharides from thermophiles have significant potential due to their thermostability and biological activities, which include biocompatibility, antioxidant properties, non-cytotoxicity, antiviral and immunostimulant effects (Arena et al., 2009; Wang et al., 2021). Exopolysaccharides (EPSs) from thermophiles maintain the viscosity of oil drilling fluids at high temperatures and thus can be considered flocculating agents (Dhagat and Jujjavarapu, 2021; Gongi et al., 2021).

Genome sequencing coupled with advancements in bioinformatic tools provides valuable insights into bacterial evolution, ecology, taxonomy, pathogenesis, metabolism, and the design of related therapeutic interventions (Goris et al., 2007; Donkor, 2013; Wang et al., 2022). Our earlier microbial analysis of Chilean hot springs showed that they harbor bacteria with thermostable EPSs and bioactive molecules (Banerjee et al., 2022; Marín-Sanhueza et al., 2022). In continuation of our earlier work in the screening of bioactive molecules and biopolymers from Chilean hot springs, a strain designated CamBx3 was isolated. Initial screening findings indicated that the strain CamBx3 generated EPS. This work aimed to identify genes linked to exopolysaccharide (EPS) production, metabolic capabilities, and heat stress response mechanisms in strain CamBx3 by analyzing its genome. We isolated and purified the EPS from strain CamBx3 to assess its structural characteristics and functional capabilities.

Materials and methods

Isolation of strain CamBx3 and preliminary screening of EPS

Strain CamBx3 was isolated by serial dilution method from the water sample (at a depth of 0.5 m) collected from the Campanario hot spring (35°56′23″ S 70°36′22″ W) located in the central Andean Mountain of Chilean Maule region using nutrient agar. The surface water temperature was 56.4°C, with a pH value of 5.8, hence the same incubation conditions were employed for isolation. Strain CamBx3 was subjected to Gram staining (Gram, 1884). The shape and size of the strain CamBx3 were observed using nucleic acid stain DAPI (excitation/emission = 359 nm/461 nm) using a Leica Stellaris 5 confocal microscope (Leica Microsystems, Wetzlar, Germany). The preliminary production of EPS was analysed using scanning electron microscopy (FESEM, JEOl-JSM 7610FPlus) by following the protocol described by Banerjee et al. (2024).

EPS production and purification

EPS production, recovery, and partial purification were carried out as described by Rimada and Abraham (2003) with a little modification. Strain CamBx3 was grown in nutrient broth at 55°C, pH 5.8 for 3 days. Then, the stationary phase bacterial cells harvested in nutrient broth (NB) (Difco) were treated with 4% trichloroacetic acid (w/v) for 30 min at 37°C to remove the proteins. The cells were centrifuged at 4°C, 5000 × *g* for 20 min to precipitate the proteins out. An equal volume of chilled ethanol was added to the chilled cell-free supernatant and left overnight at 4°C. The solvent-coagulated EPS was then separated by centrifuging the solution at 4°C and 12,000 × *g* for 20 min. The protein-purified EPS was then dialyzed, followed by lyophilization to obtain the EPS powder to see the functional activity. Optimally, 1.75 g L^{-1} of EPS production was achieved.

Functional activity of the EPS

Antioxidant activity of the EPS

To understand the antioxidant activity, the Ferric Reducing Antioxidant Power (FRAP) activity was determined according to the method of Benzie and Strain (1996) with some modifications using a FRAP assay kit (BioVision, Milpitas, United States). The reaction mixture consisted of 10 µL of sample EPS solution (0.2, 0.5, 1.0, 2.0, and 5.0 mg mL^{-1}) with 152 µL of FRAP assay buffer, 19 µL of ferric chloride ($FeCl_3$), and 19 µL of FRAP probe. The reaction mixture was further incubated at 30°C for 60 min in dark condition. The absorbance of the mixture was measured at 594 nm in Mobi-Microplate Spectrophotometer (µ2 MicroDigital, Seoul, South Korea). The FRAP activity was calculated using Eq. 1:

$$\left(B \times \frac{D}{V}\right) \quad (1)$$

Where B is the amount of ferrous ammonium sulfate from the standard curve (nmol), D is the dilution factor, and V is the volume of sample added to the reaction well (in µL). For the calibration curve, different concentrations of the ferrous standard were provided in the kit.

The Fe^{2+} ion chelating activity was analyzed according to Shi et al. (2013). The reaction mixture was composed 50 µL of the sample. EPS (0.2, 0.5, 1.0, 2.0, and 5.0 mg mL^{-1}), 2 µL of 2 mM ferrous chloride ($FeCl_2$) solution, 10 µL of 5 mM ferrozine (Sigma) solution, and 138 µL of distilled water. The reaction mixture was incubated at 30°C for 10 min in dark condition. The absorbance of the mixture was measured at 562 nm in Mobi-Microplate Spectrophotometer (µ2 MicroDigital, Seoul, South Korea). The Fe^{2+} chelating activity was calculated using Eq. 2:

$$\left(1 - \frac{A_1 - A_2}{A_0}\right) \times 100 \quad (2)$$

Where A_0 is the absorbance of the control (water instead of the sample EPS solution), A_1 is the absorbance of the EPS samples, and A_2 is the absorbance with the EPS sample but without the ferrozine solution. EDTA was used as the positive control along with commercial bacterial EPS xanthan gum (Sigma).

Glucosidase inhibition activity

β-glucosidase (*β*-GA) inhibition activity of the EPS was performed using *β*-GA assay kit (Sigma-Aldrich). For this, 200 µL assay buffer and 8 µL of *β*-NPG substrate was mixed to reach a final

concentration of 1 mM β-NPG. From this, 20 µL of the mix was added to 200 µL of EPS samples (0.2, 0.5, 1.0, 2.0, 5.0 mg mL^{-1}) diluted in 50 mM phosphate buffer. About 200 µL of the reaction mixture was added to each well. The initial absorbance was measured at 405 nm with subsequent incubation at 30°C for 20 min. The final absorbance was taken again at 405 nm in Mobi-Microplate Spectrophotometer (µ2 MicroDigital, Seoul, South Korea) using the end-point technique. Eq. 3 was followed to determine the β-GA inhibition activity:

$$\beta - GA = \frac{(Abs_{405})\ \text{final} - (Abs_{405})\ \text{initial}}{(Abs_{405})\ \text{calibrator} - (Abs_{405})\ \text{water}} \times 250 \left(\frac{\text{units}}{1}\right) \quad (3)$$

Rheological property analysis

To analyze the rheological properties of the EPS, 2% hydrocolloidal, aqueous EPS suspension was prepared at 30°C under continuous stirring. Hysteresis plots were recorded by varying the pH level (pH 3, 5, 7, and 9), and temperature (35°C and 45°C) using a dynamic rheometer (MCR 52, Anton Paar, Austria) by execution of small amplitude oscillatory shears (Banerjee et al., 2020). Temperature sweep experiment was performed for 2% EPS suspension at varying pH. For this experiment, evaporative losses were minimized by covering the exposed sample edges with a thin layer of low-viscosity mineral oil. Heating (40–90°C) and successive cooling (90–40°C) was done at 1.5°C min^{-1} and 1 Hz frequency, followed by establishing 0.6 Pa constant stress.

Genome sequencing and analysis

Genomic DNA from strain CamBx3 was extracted using the ZymoBiomics DNA/RNA miniprep kit (Zymo Research) according to the manufacturer's instructions. DNA concentration and quality ($OD_{260/280}$ = 1.8) was assessed by using Nanodrop 1,000 (Thermo Fisher Scientific) and Qubit 4.0 (Thermo Fisher Scientific). The genomic DNA was also checked on 0.7% agarose gel for high molecular size along with Lambda DNA HindIII cut DNA marker (NEB, Inc.). The genomic DNA was sequenced using Oxford-Nanopore single molecule real-time sequencing technology (ONT-SMRT) at Meta-Omics Lab facility of South Dakota Mines (SDM), Rapid City, SD, USA. High-quality genomic DNA was processed for library preparation using a ligation sequencing kit (SQK-LSK109), as recommended (DNA damage repair and end-repair/dA tailing, adapter ligation) by Oxford-Nanopore. The sequencing library was purified three times with AMPureXP beads (Beckman Coulter Genomics, MA, United States) as per the oxford-nanopore library preparation recommendation for purification and capturing of desired library fragment size (~10 kb) for sequencing. The final library was quantified on Qubit 4.0 and 100 fmol of DNA library was loaded with sequencing loading beads in a flow cell (R9.4.1) by following standard procedures. The flow cell was placed on MinION sequencer and sequencing was achieved by 12 h sequencing run with MinKNOW (v22.03.6) with super accuracy base call option (Guppy v6.0.7) (Wick et al., 2019). The quality passed raw sequence data generated from Nanopore sequencing was further processed for the assembly of reads to generate a chromosome-level genome assembly. The super high quality 558,043 reads (241,090,1974 bp) with N_{50} 10.92 kb were assembled using flye (v2.8.3) (Kolmogorov et al., 2020) with 3 iterations of Minimap2 v2.24 (Li, 2018).

The assembled genome has coverage of 529×. After the genome assembly, a separate polishing step was performed using Medaka (v1.6.0) with default parameters.[1] The final polished and finished genome assembly was processed for characterization and annotation. The genome sequence of strain CamBx3 was submitted to GenBank under the accession number GCA_026210435.

The genome quality was estimated by CheckM (Parks et al., 2015). The genome was visualized by using Proksee (Seemann, 2014; Grant et al., 2023). The rRNAs and tRNAs were predicted using RNAmmer (Lagesen et al., 2007) and tRNAscan-SE, respectively (Lowe and Eddy, 1997). The 16S rRNA gene obtained from the CamBx3 genome was compared with the sequences in the NCBI GenBank database and EzBioCloud server (Yoon et al., 2017). The phylogenomic tree was reconstructed using the Anvi'o platform (Eren et al., 2015). The genes in HMM source "Bacteria_71" (Lee, 2019) were taken and aligned using MUSCLE (Edgar, 2004). The resulting tree was visualized using MEGA version 7.0 (Kumar et al., 2016). The average nucleotide identity (ANI) value was calculated using pyani software package with the ANIb parameter (Pritchard et al., 2016).

Functional annotation was performed using Anvi'o version 7.1 platform (Eren et al., 2015). The fasta file was first reformatted with anvi-script-reformat-fasta. The scripts anvi-gen-contigs-database and anvi-run-hmms were executed; this command uses Prodigal to identify open reading frames (Hyatt et al., 2010). Functional annotation was performed by KofamKOALA (Aramaki et al., 2020) using the anvi-run-kegg-kofams program. Pan-genome analysis was carried out using Roary (Page et al., 2015) using genome annotation data (GFF3 format) generated by Prokka (Seemann, 2014). The coding regions were extracted from the input and converted to protein sequences, filtered to remove partial sequences, and iteratively pre-clustered with CD-HIT (Fu et al., 2012), then an all-against-all comparison was performed with a built-in BLASTP on the reduced sequences with the default sequence identity cutoff. The Roary's gene presence/absence dataset was used to build a Venn diagram.

Statistical analysis

All the experiments were performed in triplicate; the statistical analysis was carried out using ANOVA.

Results and discussion

Identification of strain CamBx3 and preliminary screening of EPS

Strain CamBx3 was Gram-stain-positive and creamish white in color. The confocal micrograph revealed that the strain CamBx3 exhibited a rod-shaped morphology (Figure 1A). The 16S rRNA gene sequence extracted from CamBx3 genome showed the highest similarity with *Bacillus paralicheniformis* (100%). In the phylogenomic

1 https://github.com/nanoporetech/medaka

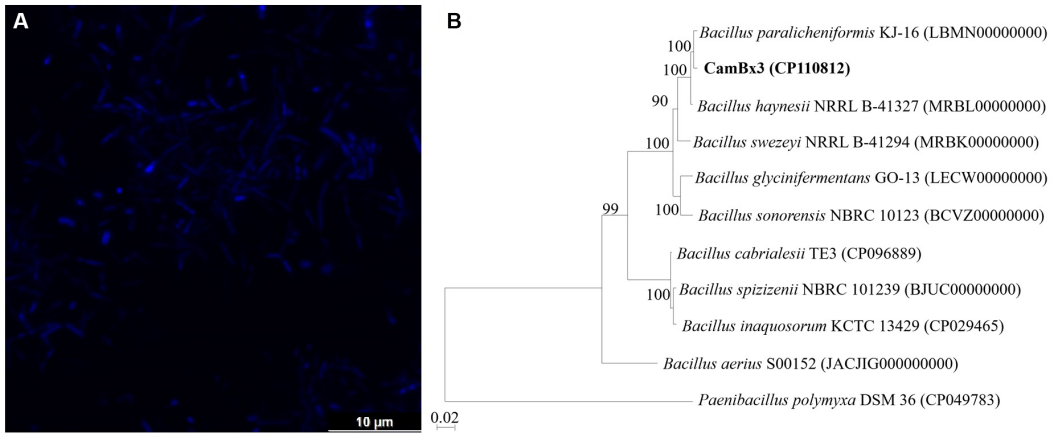

FIGURE 1
(A) Confocal micrograph of *B. paralicheniformis* CamBx3 showing the presence of rod-shaped cells; **(B)** Phylogenomic tree based on 16S rRNA gene sequence showing the relationships of *B. paralicheniformis* CamBx3. Bootstrap values (expressed as percentages of 1,000 replications) greater than 50% are shown at branch points. Bar, 0.02 substitutions per nucleotide position.

tree, CamBx3 clade with *B. paralicheniformis* (Figure 1B). The above results suggest that strain CamBx3 was a member of the genus *Bacillus*. Additionally, it showed a mucoid colony appearance indicating EPS production. The SEM analysis (Supplementary Figure S1) revealed the presence of EPS and optimally, 1.75 g L^{-1} of EPS production was achieved.

Genome attributes of strain CamBx3

The whole genome sequence of strain CamBx3 was assembled in a single circular chromosome (Figure 2) and contains 4,452,754 bp (4.45 Mb). The genomic DNA G + C content was 45.8% and the genome completeness and contamination were 99.5 and 0.1%, respectively, indicating a high-quality genome (Parks et al., 2015). A total of 4,648 genes including 4,541 protein-coding genes, 83 tRNAs and 24 rRNAs were predicted. The ANI value (Supplementary Table S1) of CamBx3 was highest with *B. paralicheniformis* KJ-16 (96.9%). The ANI value between CamBx3 and *B. paralicheniformis* KJ-16 (96.9%) was above the cut-off level (95–96%) for species delineation (Richter and Rosselló-Móra, 2009). The above results suggest that CamBx3 and *B. paralicheniformis* were similar species.

Genes related to EPS

Generally, the biosynthetic process of EPSs comprises regulation, chain-length determination, repeat-unit assembly, polymerization, and export (Ates, 2015). EPS biosynthetic pathway involves the sugar uptake system, and the most efficient sugar transport is the phosphoenolpyruvate-phosphotransferase system (PEP-PTS) (Xiong et al., 2019). The genes responsible for glucose, glucosamine, β-glucoside, *N*-acetylglucosamine, fructose, mannose, oligo-β-mannoside, cellobiose, maltose, trehalose, mannitol, ascorbate, glucitol/sorbitol, and oligo-β-mannoside-specific PEP-PTS systems were noticed in *B. paralicheniformis* CamBx3 genome. Sugars that do not have a particular PEP-PTS were delivered into the cytoplasm via non-PEP-PTS systems (Cui et al., 2016). The genes related to the L-arabinose transport system permease protein, lactose transport system permease protein, D-xylose transporter, and sucrose permease were also identified in the strain CamBx3 genome. These results suggest that strain CamBx3 may uptake glucose, fructose, sucrose, maltose, mannose, galactose, xylose, lactose, arabinose, and cellobiose.

Once sugars enter the cytoplasm, they will be converted to nucleotide sugars via different pathways (Figure 3), which act as active precursors in synthesising the EPS structure. The glycolysis pathway is the first stage in EPS production, and the key enzymes for EPS production include UTP-glucose-1-phosphate uridylyltransferase and uridine diphosphate (UDP)-glucose-4-epimerase for UDP-glucose biosynthesis, and mannose-1-phosphate guanylyltransferase for GDP-mannose biosynthesis (Wang et al., 2019). Glucose is phosphorylated by glucokinase to glucose-6-phosphate, then mutated to glucose-1-phosphate by phosphoglucomutase. UTP-glucose-1-phosphate uridylyltransferase might convert glucose-1-phosphate to UDP-glucose (Li et al., 2018). The enzymes for the conversion of glucose to UDP-glucose were noticed in *B. paralicheniformis* CamBx3 (Figure 3). CamBx3 also contained enzymes for the breakdown of lactose into glucose and galactose (through β-galactosidase) and the conversion of galactose to glucose-1-phosphate to UDP-galactose and UDP-glucose. Sucrose, mannose, xylose, and arabinose were catalyzed to fructose-6-phosphate and then converted to UDP-*N*-acetyl-α-D-glucosamine and UDP-N-acetyl-2-amino-2-deoxy-D-glucuronate. The enzyme mannose-1-phosphate guanylyltransferase for GDP-mannose biosynthesis was not present in *B. paralicheniformis* CamBx3. These results indicate that *B. paralicheniformis* CamBx3 may use UDP-glucose, UDP-galactose, UDP-*N*-acetyl-α-D-glucosamine, and UDP-*N*-acetyl-2-amino-2-deoxy-D-glucuronate as primary precursors for the production of EPS. Recently, *Bacillus* sp. ISTL8 was reported for EPS production and uses UDP-galactose, dTDP-rhamnose, and UDP-glucose as primary precursors for the production of EPS (Gupta et al., 2021).

The genome analysis of *B. paralicheniformis* CamBx3 revealed the presence of EPS biosynthetic gene cluster (*epsB*, *epsD*, *epsE*, *epsF*, *epsG*, *epsH*, *epsI*, *epsJ*, *epsK*, *epsL*, *epsM*, *epsN*, and *epsO*). The EPS gene

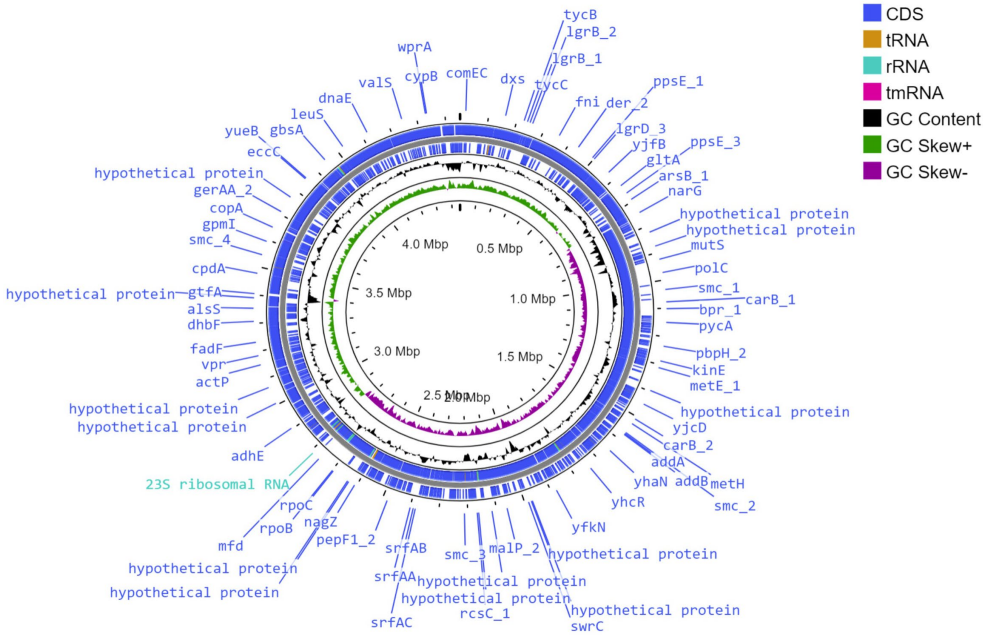

FIGURE 2
Circular genome view of *B. paralicheniformis* CamBx3 created using Proksee.

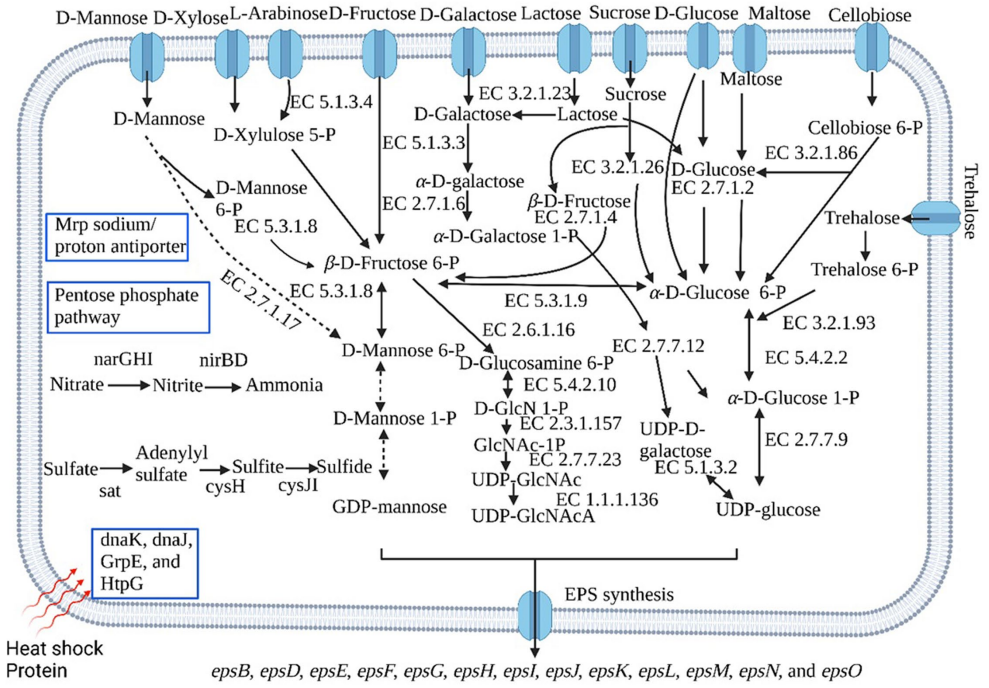

FIGURE 3
Some important metabolic pathways of *B. paralicheniformis* CamBx3 based on *KEGG* (Kyoto Encyclopedia of Genes and Genomes) *databases*. The dashed line arrow indicates the absence of the gene. The figure was created by BioRender.com.

cluster might assemble the nucleotide sugars listed above into repeating units to create EPS. Genes *epsA* and *espB* regulate EPS biosynthesis (Xiong et al., 2019). EPS chain length is determined by the genes *epsC* and *epsD*, while biosynthesis of repeating sugar units is encoded by *epsE*, *epsF*, *epsG*, *epsH*, and *epsI*, and EPS polymerization and export are encoded by *epsJ*, *epsK*, *epsL*, and *epsM* (Wu et al., 2020).

Functional activity of the EPS

Antioxidant activity

In FRAP activity test, CamBx3 EPS demonstrated almost similar ferric-reducing activity to commercial bacterial EPS (xanthan) with more than 90 mM ferrous equivalents (Figure 4A). The ferrous

equivalent was calculated by preparing the ferrous standard curve. The EPS produced by CamBx3 showed 92 mM ferrous equivalents (5 mg mL^{-1} of EPS), which was more than that of commercial bacterial biopolymer xanthan gum at the same concentration (Figure 4B). An exponential increase in the ferrous ion chelation was observed with increasing EPS concentration compared to the positive control.

Reactive oxygen species (ROS) are natural by-products of normal aerobic metabolism or host defence mechanisms involved in various biological processes (Juan et al., 2021). FRAP assay is a simple method to determine the antioxidant activity of a compound that reduces Fe^{3+} to Fe^{2+}. The reducing potentials of antioxidants are associated with their electron-donating abilities to break the free radical chain reactions (Benzie and Strain, 1996). A very high FRAP value was recorded in our study similar to xanthan. The results indicated that the EPS might act as electron donors to react with free radicals and convert them into stable products terminating the free radical chain reactions. *In vitro* antioxidant activity supports the application of CamBx3 EPS for food and pharmaceutical applications as a natural antioxidant and product shelf-life enhancer.

With the increase in consumer-oriented functional food, natural antioxidants have received great attention from researchers because of their ability to inhibit ROS and radicals (Zhao and Liang, 2022). The Fe^{2+} chelating activity is considered an important antioxidant property. The transition of Fe^{2+} is reported to stimulate lipid peroxidation by generating hydroxyl radicals through the Fenton reaction via decomposing lipid hydroperoxides into peroxyl and alkoxyl radicals (Benedet and Shibamoto, 2008). Chelating agents inhibit lipid oxidation by stabilizing transition metals. In our study, the EPS produced by CamBx3 showed a maximum 91% Fe^{2+} ion chelation at a low concentration of EPS (5 mg mL^{-1}) usage same as commercial bacterial polysaccharide xanthan. In a study, *Lactobacillus helveticus* MB2-1 reported to exhibit a chelating capacity on Fe^{2+} at 4.0 mg mL^{-1} of up to 59.1% (Li et al., 2014). More than 90% of *in vitro* Fe^{2+} chelation has been reported earlier for the EPS produced by endophytic *Paenibacillus polymyxa* EJS-3 (Liu et al., 2010), confirming the capacity of bacterial EPS to chelate Fe ions thereby possibly inhibiting the lipid peroxidation. The presence of –OH and –O– groups in structures of bacterial polysaccharides might be responsible for this property (Liu et al., 2010).

Glucosidase inhibition activity

β-glucosidase inhibitors are being extensively studied these days for their use as anti-diabetics, anti-obesity, and anti-tumor compounds (Chaipoot et al., 2023). So far, these compounds have been reported in large numbers from plants, algae, fungi, and marine bacteria (Pandey et al., 2013). The EPS produced by *B. paralicheniformis* CamBx3 showed *β*-GA inhibition activity even at a low concentration (0.5 mg mL^{-1}). An increase in the inhibition was observed with increasing concentrations of EPS and commercial xanthan as a control in the studied concentrations (Figure 4C). For all bioactive compounds; there is a dose-response activity which results in the evolution of the percentage of inhibition according to the increase of concentrations (Chokki et al., 2020). Recent studies reported bioactive compounds from *Momordica charantia* Linn. leaves inhibited the activity of *β*-GA enzyme useful as antiviral, antiadhesive, antibacterial, antimetastatic, or immunostimulatory agents (Chokki et al., 2020).

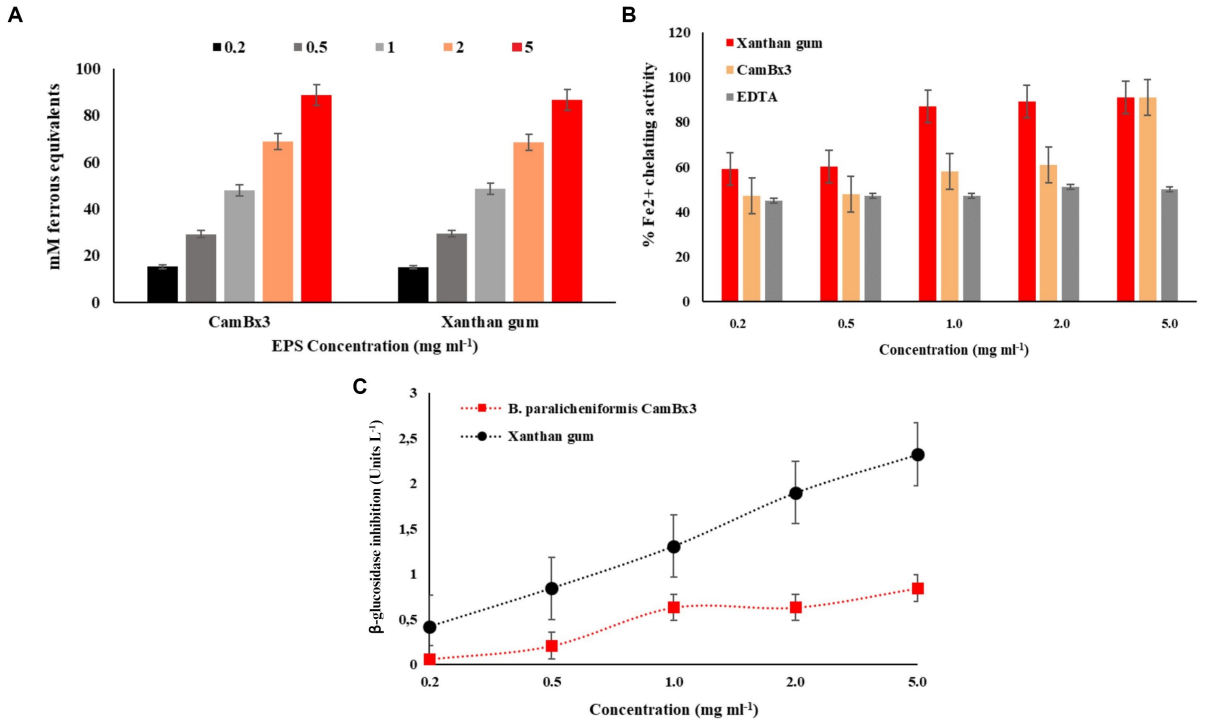

FIGURE 4
Antioxidant activity of the exopolysaccharide (EPS) produced by *B. paralicheniformis* CamBx3; **(A)** FRAP activity, and **(B)** Fe^{2+} chelating activity. **(C)** β-glucosidase enzyme inhibition activity.

Human immunodeficiency virus (HIV), the causative agent of AIDS, contains two heavily glycosylated envelope proteins, gp120 and gp41, and it has been reported that an interaction between glycoprotein gp120 and the cellular protein CD4 is required to initiate the infection cycle (Hart et al., 1991). Metabolites capable of inhibiting β-glucosidase activity have shown anti-HIV activity by inhibiting glycoprotein processing, which in turn affects the formation of the syncytium and results in an alternative site of action for HIV (Gruters et al., 1987). Thus, our study demonstrates important bioactive potential of the CamBx3 EPS as β-GA inhibitor, which might have future applications in biomedicine or biopharmaceutical industry.

Rheological property of the EPS

Exopolysaccharides have unique rheological and physicochemical characteristics and offer advanced functionality (Bamigbade et al., 2023). *B. paralicheniformis* CamBx3 EPS hydrocolloid at 35°C, compared to basic pH of 9.0, both at acidic and neutral pH has demonstrated formation of a gel resistant to flow (Figure 5). At low shear rate, the maximum instantaneous viscosity of 304 Pa.s was observed for a neutral EPS gel followed by a highly acidic EPS gel with 280 Pa.s at a pH of 3.0 (Table 1). An increase in temperature to 45°C resulted in the production of a viscoelastic acid gel with a maximal instantaneous viscosity of 315 Pa.s at pH 5.0 and 203 Pa.s at pH 3.0. Interestingly, the EPS gel at basic pH at both temperatures did show a low viscosity with poor shear thinning behavior. In fact, at 45°C, structural degradation of EPS was observed at pH 9.0 (Table 1). Improved viscoelasticity is typically associated with the structural reversibility of gels, which is a result of the formation of 3D networks facilitated by hydrogen bonding between polysaccharide macromolecules (Li et al., 2011). Acid gels have been noted for their use in drug delivery systems, particularly in seaweed polysaccharides (Zhong et al., 2020). In our study, a similar viscoelastic acid gel formation was observed at both 35°C and 45°C, with steady shear thinning behavior and structural reversibility, suggesting possible applications in the biopharmaceutical industry in the future. The temperature sweep curve of acid gel at pH 3.0 showed a characteristic stability from 50–90°C region followed by the neutral pH EPS gel at pH 7.0. The temperature sweep investigation, like the Carreau model hysteresis experiment, found that EPS has good viscosifying and rheological properties at pH 3.0 and 7.0, as well as structural degradation or instability at pH 9.0. The rheological properties of a polysaccharide are crucial for its application in the food business. Commercial bacterial EPS xanthan maintains structural integrity when it cools, indicating renaturation. In contrast, curdlan polysaccharide, typically insoluble in water, only gels when heated. This process is irreversible (Maalej et al., 2016). In our study, the gel-like behavior of CamBx3 was observed to be maintained even at high temperatures and cooling was favorable for the enhancement of a gel-like network probably due to the aggregation of the polymer chains at both acidic pH and neutral pH as reported earlier by Maalej et al. (2016).

Genes related to nitrogen and sulphur metabolism

Nitrate is the most oxidized form of fixed nitrogen compounds and one of the most important nutrients for microbial and plant life (Kamp et al., 2015). In prokaryotes, dissimilatory nitrate reduction mechanisms have been extensively explored (Kamp et al., 2015; Sun et al., 2018; Keren et al., 2020). Dissimilatory nitrate reduction can occur in several ways, beginning with nitrate reduction to nitrite by respiratory membrane-bound *NarG* or periplasmic nitrate reductase *NapA*, followed by nitrite reduction to ammonia via cytoplasmic nitrite reductase *NirB* or periplasmic nitrite reductase *NrfA* (Sun et al., 2018). *Bacillus subtilis* anaerobically reduces nitrate to ammonium by nitrate reductase *NarGHI* and nitrite reductase *NirBD*, whereas *Bacillus selenitireducens* generates ammonium via the periplasmic nitrite reductase *NrfA* (Nakano et al., 1998; Nakano and Zuber, 1998). *B. paralicheniformis* CamBx3 reduces nitrate to ammonium via nitrate reductase (*NarGHI*) and nitrite reductase (*NirBD*) (Figure 3). Microorganisms use assimilatory sulfate reduction (ASR) pathway to convert inorganic sulfate to sulfide (Koprivova et al., 2001). The genes (*sat*, *cysH* and *cysJI*) involved in the ASR were identified in *B. paralicheniformis* CamBx3 (Figure 3). ASR pathway leads to the biosynthesis of sulfur-containing amino acids, such as cysteine, and does not lead to the direct excretion of sulfide (Kopriva et al., 2007; Longo et al., 2016).

Stress-related genes

Microbes at high temperatures must maintain their protein machinery stable and efficient (Narsing Rao et al., 2022). *DnaK*, *DnaJ*, and *GrpE* from cellular chaperone machinery capable of repairing heat-induced protein damage (Schröder et al., 1993). *B. paralicheniformis* CamBx3 encodes genes for *Dnak*, *DnaJ*, *GrpE*, and *HtpG* (Figure 3). Multiple resistance and pH adaptation (Mrp) antiporters are multi-subunit complexes that link Na^+ (or K^+) ion transport across the membrane to the proton motive force. They play various physiological roles, including pH and Na^+ homeostasis, as well as Na^+ tolerance (Haja and Adams, 2021). *B. paralicheniformis* CamBx3 also encodes genes for Mrp sodium/proton antiporter. Ancient Mrp antiporter has been reported earlier in diverse thermophilic or hyperthermophilic, Gram-positive and Gram-negative bacteria along with archaea for adaptation in polyextremophilic environments (Ito et al., 2017).

Carbohydrates, amino acids, and other metabolic pathways

Genes related to the pentose phosphate and Entner-Doudoroff pathways were present in *B. paralicheniformis* CamBx3. The shikimate pathway is the central metabolic route leading to the formation of tryptophan, tyrosine, and phenylalanine (Averesch and Krömer, 2018). The genes related to the shikimate pathway were noticed in *B. paralicheniformis* CamBx3 (Supplementary Table S2). Further, genes related to tryptophan biosynthesis were also noticed in strain CamBx3 (Supplementary Table S2). A detailed list of the metabolic potentials of *B. paralicheniformis* CamBx3 is mentioned in Supplementary Table S2.

Pangenome analysis

The pangenome analysis of *B. paralicheniformis* CamBx3 was performed with eight *Bacillus* spp. Figure 6A, shows the Roary matrix,

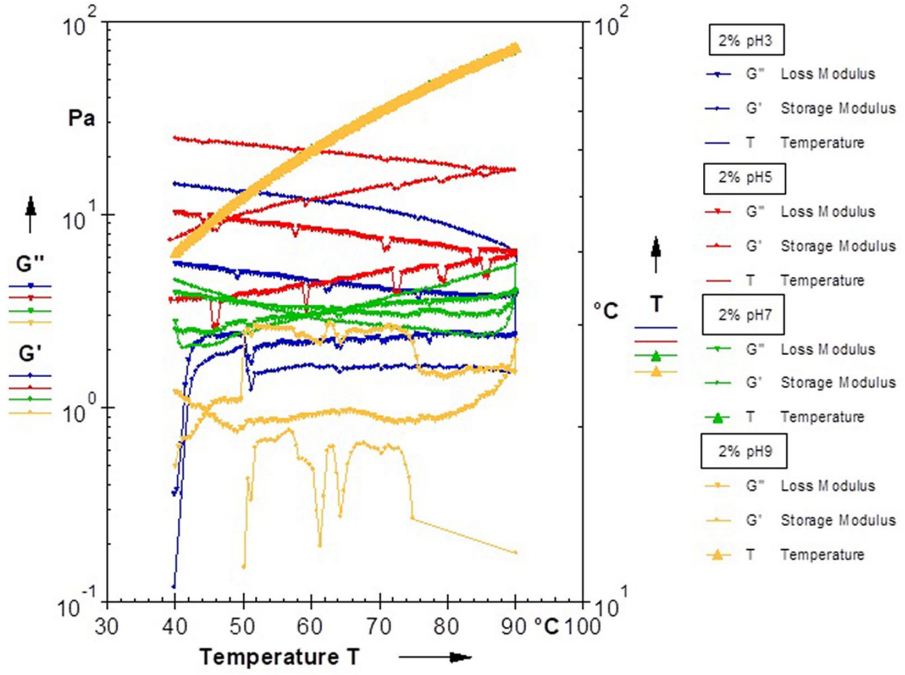

FIGURE 5
Rheological analysis showing temperature sweep of 2% aqueous EPS solution at different pH.

TABLE 1 Dynamic rheological properties of the EPS at different temperatures under pH variation in terms of the Carreau model.

Temperature (°C)	pH	η_o	η_∞ (×10^{-9})	*A*	*p*-value	R^2	SD
35	3.0	280.26	3.8883e^{-9}	96.60	0.49	0.999	0.19
	5.0	148.41	4.2631e^{-9}	38.64	0.49	0.998	0.39
	7.0	303.80	3.8114e^{-9}	82.47	0.50	0.999	0.39
	9.0	91.72	3.4499e^{-9}	22.94	0.51	0.997	0.33
45	3.0	203.36	4.221e^{-9}	58.97	0.49	0.998	0.65
	5.0	315.04	3.5481e^{-9}	80.71	0.51	0.999	0.62
	7.0	177.02	3.6376e^{-9}	42.77	0.51	0.994	0.96
	9.0	−15.62	–	–	–	–	–

Where η_o, instantaneous viscosity; $\eta\infty$, final viscosity after prolonged shearing; *A*, coefficient; *p*, measure of the shape of the curve between shear rate and shear stress; *R*, coefficient of correlation; SD, standard deviation.

which includes 26,562 gene clusters generated from all 9 genomes. These gene clusters were categorized as 7,002 shell genes, and 19,484 cloud genes. Although strains *B. paralicheniformis* CamBx3 and *B. paralicheniformis* KJ-16 were similar species based on 16S rRNA, a clear difference was observed in their gene clusters shown in Figure 6A. A Venn diagram (using the presence and absence gene matrix) was constructed between *B. paralicheniformis* CamBx3, *B. paralicheniformis* KJ-16 and *B. haynesii* NRRL B-41327 (Figure 6B). A total of 854 different genes were found in *B. paralicheniformis* CamBx3 when compared to *B. paralicheniformis* KJ-16 and *B. haynesii* NRRL B-41327 (Supplementary Table S3). The above results show the differences in the genome content of *B. paralicheniformis* CamBx3. Comparing the gene clusters of CamBx3, NRRL B-41327, and KJ-16, EPS formation-related genes (*epsH*, *epsM*, and *epsF*), associated with glycosyl transferase experession, putative acyltransferase, and biofilm formation were noticed in three strains. Additionally, heat stress-related chaperones *dnaJ*, and *dnaK* were also encountered.

Conclusion

In the present study, a thermophilic strain of *B. paralicheniformis*, designated CamBx3 was isolated from the water sample of Campanario hot spring located in Andean Mountain of central Chile. Genome analysis identified genes related to EPS clusters, assimilatory sulfate reduction, heat stress-related machinery along with the major metabolic potentials. Additionally, the pangenome analyses showed that *B. paralicheniformis* CamBx3 has very different genome content compared to the nearby species *B. paralicheniformis* KJ-16 and *B. haynesii* NRRL B-41327. The EPS produced by this thermophilic strain has demonstrated FRAP-mediated antioxidant capacity and Fe^{2+} ion chelating properties. The EPS is additionally a β-glucosidase enzyme inhibitor and rheologically formed a thermo-resistant, viscoelastic gel at acidic pH. Acid gels are known for their application in drug delivery systems. The EPS extracted from *B. paralicheniformis* CamBx3 showed strong antioxidant, and glucosidase inhibition

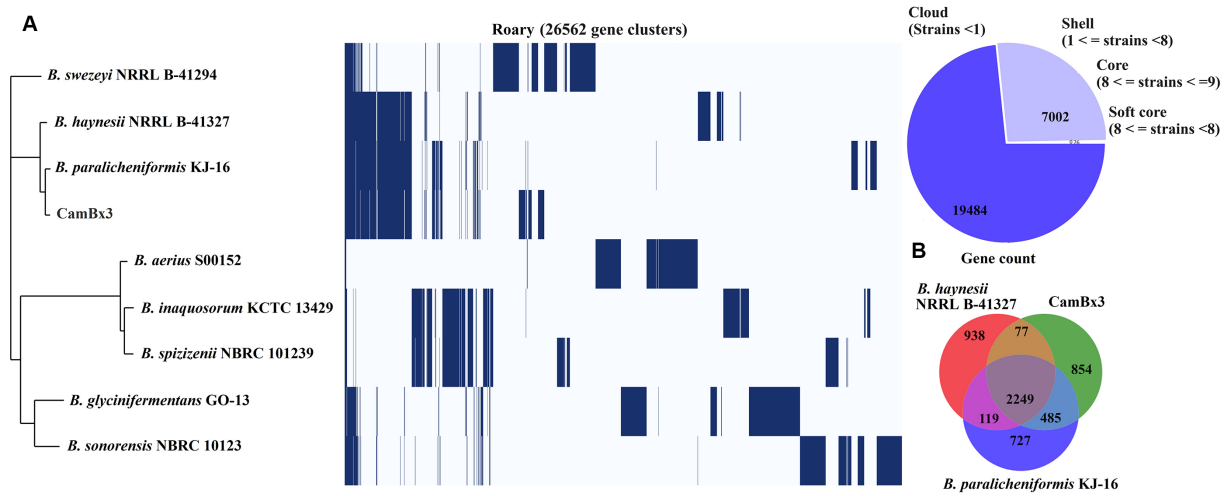

FIGURE 6
Pangenome analysis: **(A)** Roary gene cluster, showing the presence and absence of genes, **(B)** Venn diagram (based on presence and absence of genes) between *B. paralicheniformis* CamBx3 and two closely related *Bacillus* species.

activities, as well as suitable viscoelastic acid gel formation, which could be a valuable resource for biotechnological applications.

Data availability statement

The datasets presented in this study can be found in online repositories. The names of the repository/repositories and accession number(s) can be found at: https://www.ncbi.nlm.nih.gov/, GCA_026210435.

Author contributions

MN: Writing – review & editing, Writing – original draft, Software, Methodology, Investigation, Formal analysis. RSi: Writing – review & editing, Software, Methodology, Investigation, Formal analysis, Data curation. RSa: Writing – review & editing, Resources, Investigation. AB: Writing – review & editing, Writing – original draft, Supervision, Resources, Project administration, Methodology, Investigation, Funding acquisition, Formal analysis, Conceptualization.

Funding

The author(s) declare that financial support was received for the research, authorship, and/or publication of this article. This research was funded by FONDECYT Regular, grant number 1231917 by ANID, Govt. of Chile.

Acknowledgments

AB and RSa are thankful to FOVI220149 grant by ANID, Govt. of Chile.

Conflict of interest

The authors declare that the research was conducted in the absence of any commercial or financial relationships that could be construed as a potential conflict of interest.

The author(s) declared that they were an editorial board member of Frontiers, at the time of submission. This had no impact on the peer review process and the final decision.

Publisher's note

All claims expressed in this article are solely those of the authors and do not necessarily represent those of their affiliated organizations, or those of the publisher, the editors and the reviewers. Any product that may be evaluated in this article, or claim that may be made by its manufacturer, is not guaranteed or endorsed by the publisher.

Supplementary material

The Supplementary material for this article can be found online at: https://www.frontiersin.org/articles/10.3389/fmicb.2024.1377965/full#supplementary-material

References

Aramaki, T., Blanc-Mathieu, R., Endo, H., Ohkubo, K., Kanehisa, M., Goto, S., et al. (2020). KofamKOALA: KEGG Ortholog assignment based on profile HMM and adaptive score threshold. *Bioinformatics* 36, 2251–2252. doi: 10.1093/bioinformatics/btz859

Arena, A., Gugliandolo, C., Stassi, G., Pavone, B., Iannello, D., Bisignano, G., et al. (2009). An exopolysaccharide produced by Geobacillus thermodenitrificans strain B3-72: antiviral activity on immunocompetent cells. *Immunol. Lett.* 123, 132–137. doi: 10.1016/j.imlet.2009.03.001

Ates, O. (2015). Systems biology of microbial exopolysaccharides production. *Front. Bioeng. Biotechnol.* 3:200. doi: 10.3389/fbioe.2015.00200

Averesch, N. J. H., and Krömer, J. O. (2018). Metabolic engineering of the shikimate pathway for production of aromatics and derived compounds-present and future strain construction strategies. *Front. Bioeng. Biotechnol.* 6:32. doi: 10.3389/fbioe.2018.00032

Bamigbade, G., Ali, A. H., Subhash, A., Tamiello-Rosa, C., Al Qudsi, F. R., Esposito, G., et al. (2023). Structural characterization, biofunctionality, and environmental factors impacting rheological properties of exopolysaccharide produced by probiotic Lactococcus lactis C15. *Sci. Rep.* 13:17888. doi: 10.1038/s41598-023-44728-w

Banerjee, A., Das, D., Rudra, S. G., Mazumder, K., Andler, R., and Bandopadhyay, R. (2020). Characterization of exopolysaccharide produced by pseudomonas sp. PFAB4 for synthesis of EPS-coated AgNPs with antimicrobial properties. *J. Polym. Environ.* 28, 242–256. doi: 10.1007/s10924-019-01602-z

Banerjee, A., Mohammed Breig, S. J., Gómez, A., Sánchez-Arévalo, I., González-Faune, P., Sarkar, S., et al. (2022). Optimization and characterization of a novel exopolysaccharide from Bacillus haynesii CamB6 for food applications. *Biomol. Ther.* 12:834. doi: 10.3390/biom12060834

Banerjee, A., Roy, R. K., Sarkar, S., López, J. L., Vuree, S., and Bandopadhyay, R. (2024). Synthesis of hot spring origin bacterial cell wall polysaccharide-based copper nanoparticles with antibacterial property. *Electron. J. Biotechnol.* 68, 11–19. doi: 10.1016/j.ejbt.2023.11.005

Benedet, J. A., and Shibamoto, T. (2008). Role of transition metals, Fe(II), Cr(II), Pb(II), and cd(II) in lipid peroxidation. *Food Chem.* 107, 165–168. doi: 10.1016/j.foodchem.2007.07.076

Benzie, I. F., and Strain, J. J. (1996). The ferric reducing ability of plasma (FRAP) as a measure of "antioxidant power": the FRAP assay. *Anal. Biochem.* 239, 70–76. doi: 10.1006/abio.1996.0292

Brock, T. D. (1997). The value of basic research: discovery of Thermus aquaticus and other extreme thermophiles. *Genetics* 146, 1207–1210. doi: 10.1093/genetics/146.4.1207

Chaipoot, S., Punfa, W., Ounjaijean, S., Phongphisutthinant, R., Kulprachakarn, K., Parklak, W., et al. (2023). Antioxidant, anti-diabetic, anti-obesity, and antihypertensive properties of protein hydrolysate and peptide fractions from black sesame cake. *Molecules* 28:211. doi: 10.3390/molecules28010211

Chien, A., Edgar, D. B., and Trela, J. M. (1976). Deoxyribonucleic acid polymerase from the extreme thermophile Thermus aquaticus. *J. Bacteriol.* 127, 1550–1557. doi: 10.1128/jb.127.3.1550-1557.1976

Chokki, M., Cudălbeanu, M., Zongo, C., Dah-Nouvlessounon, D., Ghinea, I. O., Furdui, B., et al. (2020). Exploring antioxidant and enzymes (A-amylase and B-glucosidase) inhibitory activity of Morinda lucida and Momordica charantia leaves from Benin. *Food Secur.* 9:404034. doi: 10.3390/foods9040434

Cui, Y., Xu, T., Qu, X., Hu, T., Jiang, X., and Zhao, C. (2016). New insights into various production characteristics of Streptococcus thermophilus strains. *Int. J. Mol. Sci.* 17:1701. doi: 10.3390/ijms17101701

Dhagat, S., and Jujjavarapu, S. E. (2021). Biorefinery system for production of thermostable exopolysaccharide by a novel thermophile Brevibacillus borstelensis MK878423 and its study on impact of glucose utilization. *Biomass Convers Biorefin.* 13, 7521–7531. doi: 10.1007/s13399-021-01288-1

Donkor, E. S. (2013). Sequencing of bacterial genomes: principles and insights into pathogenesis and development of antibiotics. *Genes (Basel)* 4, 556–572. doi: 10.3390/genes4040556

Edgar, R. C. (2004). MUSCLE: multiple sequence alignment with high accuracy and high throughput. *Nucleic Acids Res.* 32, 1792–1797. doi: 10.1093/nar/gkh340

Eren, A. M., Esen, Ö. C., Quince, C., Vineis, J. H., Morrison, H. G., Sogin, M. L., et al. (2015). Anvi'o: an advanced analysis and visualization platform for omics data. *PeerJ* 3:e1319. doi: 10.7717/peerj.1319

Fu, L., Niu, B., Zhu, Z., Wu, S., and Li, W. (2012). CD-HIT: accelerated for clustering the next-generation sequencing data. *Bioinformatics* 28, 3150–3152. doi: 10.1093/bioinformatics/bts565

Gongi, W., Cordeiro, N., Pinchetti, J. L. G., and Ben Ouada, H. (2021). Production of exopolymer substances from the thermophilic chlorophyte Graesiella: industrial and ecological applications. *J. Appl. Phycol.* 33, 343–356. doi: 10.1007/s10811-020-02299-7

Goris, J., Konstantinidis, K. T., Klappenbach, J. A., Coenye, T., Vandamme, P., and Tiedje, J. M. (2007). DNA-DNA hybridization values and their relationship to whole-genome sequence similarities. *Int. J. Syst. Evol. Microbiol.* 57, 81–91. doi: 10.1099/ijs.0.64483-0

Gram, H. C. (1884). Über die isolierte Färbung der Schizomyceten in Schnitt- und Trockenpräparaten. *Fortschr. Med.* 2, 185–189.

Grant, J. R., Enns, E., Marinier, E., Mandal, A., Herman, E. K., Chen, C. Y., et al. (2023). Proksee: in-depth characterization and visualization of bacterial genomes. *Nucleic Acids Res.* 51, W484–W492. doi: 10.1093/nar/gkad326

Gruters, R. A., Neefjes, J. J., Tersmette, M., de Goede, R. E., Tulp, A., Huisman, H. G., et al. (1987). Interference with HIV-induced syncytium formation and viral infectivity by inhibitors of trimming glucosidase. *Nature* 330, 74–77. doi: 10.1038/330074a0

Gupta, J., Rathour, R., Dupont, C. L., Kaul, D., and Thakur, I. S. (2021). Genomic insights into waste valorized extracellular polymeric substances (EPS) produced by bacillus sp. ISTL8. *Environ. Res.* 192:110277. doi: 10.1016/j.envres.2020.110277

Haja, D. K., and Adams, M. W. W. (2021). pH homeostasis and sodium ion pumping by multiple resistance and pH antiporters in Pyrococcus furiosus. *Front. Microbiol.* 12:712104. doi: 10.3389/fmicb.2021.712104

Hart, T. K., Kirsh, R., Ellens, H., Sweet, R. W., Lambert, D. M., Petteway, S. R., et al. (1991). Binding of soluble CD4 proteins to human immunodeficiency virus type 1 and infected cells induces release of envelope glycoprotein gp120. *Proc. Natl. Acad. Sci. USA* 88, 2189–2193. doi: 10.1073/pnas.88.6.2189

Hyatt, D., Chen, G. L., Locascio, P. F., Land, M. L., Larimer, F. W., and Hauser, L. J. (2010). Prodigal: prokaryotic gene recognition and translation initiation site identification. *BMC Bioinf.* 11:119. doi: 10.1186/1471-2105-11-119

Ito, M., Morino, M., and Krulwich, T. A. (2017). Mrp antiporters have important roles in diverse bacteria and archaea. *Front. Microbiol.* 8:2325. doi: 10.3389/fmicb.2017.02325

Juan, C. A., Pérez de la Lastra, J. M., Plou, F. J., and Pérez-Lebeña, E. (2021). The chemistry of reactive oxygen species (ROS) revisited: outlining their role in biological macromolecules (DNA, lipids and proteins) and induced pathologies. *Int. J. Mol. Sci.* 22:94642. doi: 10.3390/ijms22094642

Kamp, A., Høgslund, S., Risgaard-Petersen, N., and Stief, P. (2015). Nitrate storage and dissimilatory nitrate reduction by eukaryotic microbes. *Front. Microbiol.* 6:1492. doi: 10.3389/fmicb.2015.01492

Keren, R., Lawrence, J. E., Zhuang, W., Jenkins, D., Banfield, J. F., Alvarez-Cohen, L., et al. (2020). Increased replication of dissimilatory nitrate-reducing bacteria leads to decreased anammox bioreactor performance. *Microbiome* 8:7. doi: 10.1186/s40168-020-0786-3

Kolmogorov, M., Bickhart, D. M., Behsaz, B., Gurevich, A., Rayko, M., Shin, S. B., et al. (2020). metaFlye: scalable long-read metagenome assembly using repeat graphs. *Nat. Methods* 17, 1103–1110. doi: 10.1038/s41592-020-00971-x

Kopriva, S., Fritzemeier, K., Wiedemann, G., and Reski, R. (2007). The putative moss 3′-phosphoadenosine-5′-phosphosulfate reductase is a novel form of adenosine-5′-phosphosulfate reductase without an iron-sulfur cluster. *J. Biol. Chem.* 282, 22930–22938. doi: 10.1074/jbc.M702522200

Koprivova, A., Melzer, M., von Ballmoos, P., Mandel, T., Brunold, C., and Kopriva, S. (2001). Assimilatory Sulfate reduction in C3, C3-C4, and C4 species ofFlaveria. *Plant Physiol.* 127, 543–550. doi: 10.1104/pp.010144

Kumar, S., Stecher, G., and Tamura, K. (2016). MEGA7: molecular evolutionary genetics analysis version 7.0 for bigger datasets. *Mol. Biol. Evol.* 33, 1870–1874. doi: 10.1093/molbev/msw054

Lagesen, K., Hallin, P., Rødland, E. A., Staerfeldt, H. H., Rognes, T., and Ussery, D. W. (2007). RNAmmer: consistent and rapid annotation of ribosomal RNA genes. *Nucleic Acids Res.* 35, 3100–3108. doi: 10.1093/nar/gkm160

Lee, M. D. (2019). GToTree: a user-friendly workflow for phylogenomics. *Bioinformatics* 35, 4162–4164. doi: 10.1093/bioinformatics/btz188

Li, H. (2018). Minimap2: pairwise alignment for nucleotide sequences. *Bioinformatics* 34, 3094–3100. doi: 10.1093/bioinformatics/bty191

Li, B., Ding, X., Evivie, S. E., Jin, D., Meng, Y., Huo, G., et al. (2018). Short communication: genomic and phenotypic analyses of exopolysaccharides produced by Streptococcus thermophilus KLDS SM. *J. Dairy Sci.* 101, 106–112. doi: 10.3168/jds.2017-13534

Li, H. P., Hou, W. G., and Zhang, Y. Z. (2011). Rheological properties of aqueous solution of new exopolysaccharide secreted by a deep-sea mesophilic bacterium. *Carbohydr. Polym.* 84, 1117–1125. doi: 10.1016/j.carbpol.2010.12.072

Li, W., Ji, J., Rui, X., Yu, J., Tang, W., Chen, X., et al. (2014). Production of exopolysaccharides by Lactobacillus helveticus MB2-1 and its functional characteristics in vitro. *LWT – Food Sci. Technol.* 59, 732–739. doi: 10.1016/j.lwt.2014.06.063

Liu, J., Luo, J., Ye, H., Sun, Y., Lu, Z., and Zeng, X. (2010). In vitro and in vivo antioxidant activity of exopolysaccharides from endophytic bacterium Paenibacillus polymyxa EJS-3. *Carbohydr. Polym.* 82, 1278–1283. doi: 10.1016/j.carbpol.2010.07.008

Longo, F., Motta, S., Mauri, P., Landini, P., and Rossi, E. (2016). Interplay of the modified nucleotide phosphoadenosine 5′-phosphosulfate (PAPS) with global regulatory proteins in Escherichia coli: modulation of cyclic AMP (cAMP)-dependent gene expression and interaction with the HupA regulatory protein. *Chem. Biol. Interact.* 259, 39–47. doi: 10.1016/j.cbi.2016.04.016

Lowe, T. M., and Eddy, S. R. (1997). tRNAscan-SE: a program for improved detection of transfer RNA genes in genomic sequence. *Nucleic Acids Res.* 25, 955–964. doi: 10.1093/nar/25.5.955

Luo, Z. H., Narsing Rao, M. P., Chen, H., Hua, Z. S., Li, Q., Hedlund, B. P., et al. (2020). Genomic insights of "Candidatus Nitrosocaldaceae" based on nine new metagenome-assembled genomes, including "Candidatus Nitrosothermus" gen Nov. and two new species of "Candidatus Nitrosocaldus". *Front. Virol.* 11:608832. doi: 10.3389/fmicb.2020.608832

Maalej, H., Hmidet, N., Boisset, C., Bayma, E., Heyraud, A., and Nasri, M. (2016). Rheological and emulsifying properties of a gel-like exopolysaccharide produced by Pseudomonas stutzeri AS22. *Food Hydrocoll.* 52, 634–647. doi: 10.1016/j.foodhyd.2015.07.010

Marín-Sanhueza, C., Echeverría-Vega, A., Gómez, A., Cabrera-Barjas, G., Romero, R., and Banerjee, A. (2022). Stress dependent biofilm formation and bioactive melanin pigment production by a thermophilic bacillus species from Chilean hot spring. *Polymers* 14:40680. doi: 10.3390/polym14040680

Nakano, M. M., Hoffmann, T., Zhu, Y., and Jahn, D. (1998). Nitrogen and oxygen regulation of Bacillus subtilis nasDEF encoding NADH-dependent nitrite reductase by TnrA and ResDE. *J. Bacteriol.* 180, 5344–5350. doi: 10.1128/jb.180.20.5344-5350.1998

Nakano, M. M., and Zuber, P. (1998). Anaerobic growth of a "strict aerobe" (Bacillus subtilis). *Ann. Rev. Microbiol.* 52, 165–190. doi: 10.1146/annurev.micro.52.1.165

Narsing Rao, M. P., Dong, Z. Y., Kan, Y., Xiao, M., Kang, Y. Q., and Li, W. J. (2020). Bacillus tepidiphilus sp. nov., isolated from tepid spring. *Arch. Microbiol.* 202, 2367–2371. doi: 10.1007/s00203-020-01958-0

Narsing Rao, M. P., Dong, Z. Y., Luo, Z. H., Li, M. M., Liu, B. B., Guo, S. X., et al. (2021). Physicochemical and microbial diversity analyses of Indian Hot Springs. *Front. Microbiol.* 12:627200. doi: 10.3389/fmicb.2021.627200

Narsing Rao, M. P., Luo, Z. H., Dong, Z. Y., Li, Q., Liu, B. B., Guo, S. X., et al. (2022). Metagenomic analysis further extends the role of chloroflexi in fundamental biogeochemical cycles. *Environ. Res.* 209:112888. doi: 10.1016/j.envres.2022.112888

Page, A. J., Cummins, C. A., Hunt, M., Wong, V. K., Reuter, S., Holden, M. T., et al. (2015). Roary: rapid large-scale prokaryote pan genome analysis. *Bioinformatics* 31, 3691–3693. doi: 10.1093/bioinformatics/btv421

Pandey, S., Sree, A., Dash, S. S., Sethi, D. P., and Chowdhury, L. (2013). Diversity of marine bacteria producing beta-glucosidase inhibitors. *Microb. Cell Factories* 12:35. doi: 10.1186/1475-2859-12-35

Parks, D. H., Imelfort, M., Skennerton, C. T., Hugenholtz, P., and Tyson, G. W. (2015). CheckM: assessing the quality of microbial genomes recovered from isolates, single cells, and metagenomes. *Genome Res.* 25, 1043–1055. doi: 10.1101/gr.186072.114

Pritchard, L., Glover, R. H., Humphris, S., Elphinstone, J. G., and Toth, I. K. (2016). Genomics and taxonomy in diagnostics for food security: soft-rotting enterobacterial plant pathogens. *Anal. Methods* 8, 12–24. doi: 10.1039/C5AY02550H

Richter, M., and Rosselló-Móra, R. (2009). Shifting the genomic gold standard for the prokaryotic species definition. *Proc. Natl. Acad. Sci. USA* 106, 19126–19131. doi: 10.1073/pnas.0906412106

Rimada, P. S., and Abraham, A. G. (2003). Comparative study of different methodologies to determine the exopolysaccharide produced by kefir grains in milk and whey. *Lait* 83, 79–87. doi: 10.1051/lait:2002051

Schröder, H., Langer, T., Hartl, F. U., and Bukau, B. (1993). DnaK, DnaJ and GrpE form a cellular chaperone machinery capable of repairing heat-induced protein damage. *EMBO J.* 12, 4137–4144. doi: 10.1002/j.1460-2075.1993.tb06097.x

Seemann, T. (2014). Prokka: rapid prokaryotic genome annotation. *Bioinformatics* 30, 2068–2069. doi: 10.1093/bioinformatics/btu153

Shi, M., Zhang, Z., and Yang, Y. (2013). Antioxidant and immunoregulatory activity of Ganoderma lucidum polysaccharide (GLP). *Carbohydr. Polym.* 95, 200–206. doi: 10.1016/j.carbpol.2013.02.081

Sun, Y., De Vos, P., and Willems, A. (2018). Influence of nitrate and nitrite concentration on N_2O production via dissimilatory nitrate/nitrite reduction to ammonium in *Bacillus paralicheniformis* LMG 6934. *MicrobiologyOpen* 7:e00592. doi: 10.1002/mbo3.592

Walter, M. R. (1996), Ancient hydrothermal ecosystems on earth: a new palaeobiological frontier, *Evolution of hydrothermal ecosystems on earth (and Mars?)*, Wiley, Chichester, (Ciba Found Symp 202), 112–130.

Wang, J., Goh, K. M., Salem, D. R., and Sani, R. K. (2019). Genome analysis of a thermophilic exopolysaccharide-producing bacterium – Geobacillus sp. *Sci. Reports* 9:1608. doi: 10.1038/s41598-018-36983-z

Wang, J., Salem, D. R., and Sani, R. K. (2020). Synthesis of biopolymers from a Geobacillus sp. WSUCF1 using unprocessed corn Stover. *ACS Sustain. Chem. Eng.* 8, 9483–9496. doi: 10.1021/acssuschemeng.0c02435

Wang, J., Salem, D. R., and Sani, R. K. (2021). Two new exopolysaccharides from a thermophilic bacterium Geobacillus sp. WSUCF1: characterization and bioactivities. *New Biotechnol.* 61, 29–39. doi: 10.1016/j.nbt.2020.11.004

Wang, S., Sun, L., Narsing Rao, M. P., Fang, B. Z., and Li, W. J. (2022). Comparative genome analysis of a novel Alkaliphilic Actinobacterial species Nesterenkonia haasae. *Pol. J. Microbiol.* 71, 453–461. doi: 10.33073/pjm-2022-040

Wick, R. R., Judd, L. M., and Holt, K. E. (2019). Performance of neural network basecalling tools for Oxford Nanopore sequencing. *Genome Biol.* 20:129. doi: 10.1186/s13059-019-1727-y

Woese, C. R. (1987). Bacterial evolution. *Microbiol. Rev.* 51, 221–271. doi: 10.1128/mr.51.2.221-271.1987

Wu, R., Qin, Y., Shen, Q., and Li, P. (2020). The complete genome sequence of Bacillus velezensis LPL061, an exopolysaccharide-producing bacterium. *Three Biotech* 10:243. doi: 10.1007/s13205-020-02228-y

Xiong, Z.-Q., Kong, L. H., Lai, P. F. H., Xia, Y. J., Liu, J. C., Li, Q. Y., et al. (2019). Genomic and phenotypic analyses of exopolysaccharide biosynthesis in Streptococcus thermophilus S-3. *J. Dairy Sci.* 102, 4925–4934. doi: 10.3168/jds.2018-15572

Yoon, S. H., Ha, S. M., Kwon, S., Lim, J., Kim, Y., Seo, H., et al. (2017). Introducing EzBioCloud: a taxonomically united database of 16S rRNA gene sequences and whole-genome assemblies. *Int. J. Syst. Evol. Microbiol.* 67, 1613–1617. doi: 10.1099/ijsem.0.001755

Zhao, X., and Liang, Q. (2022). EPS-producing Lactobacillus plantarum MC5 as a compound starter improves rheology, texture, and antioxidant activity of yogurt during storage. *Food Secur.* 11:111660. doi: 10.3390/foods11111660

Zhong, H., Gao, X., Cheng, C., Liu, C., Wang, Q., and Han, X. (2020). The structural characteristics of seaweed polysaccharides and their application in gel drug delivery systems. *Mar. Drugs* 18:658. doi: 10.3390/md18120658

frontiers | Frontiers in Microbiology

TYPE Original Research
PUBLISHED 22 April 2024
DOI 10.3389/fmicb.2024.1355369

OPEN ACCESS

EDITED BY
Ragini Bodade,
Savitribai Phule Pune University, India

REVIEWED BY
Thiruchelvi R,
Vels Institute of Science Technology and Advanced Studies (VISTAS), India
Somnath Nandi,
Savitribai Phule Pune University, India

*CORRESPONDENCE
YingWu Shi
✉ syw1973@126.com

†These authors have contributed equally to this work

RECEIVED 13 December 2023
ACCEPTED 15 March 2024
PUBLISHED 22 April 2024

CITATION
Shi Y, Niu X, Yang H, Chu M, Wang N, Bao H, Zhan F, Yang R and Lou K (2024) Optimization of the fermentation media and growth conditions of *Bacillus velezensis* BHZ-29 using a Plackett–Burman design experiment combined with response surface methodology.
Front. Microbiol. 15:1355369.
doi: 10.3389/fmicb.2024.1355369

Optimization of the fermentation media and growth conditions of *Bacillus velezensis* BHZ-29 using a Plackett–Burman design experiment combined with response surface methodology

YingWu Shi[1,2,3*†], XinXiang Niu[3,4†], HongMei Yang[1,2,3], Ming Chu[1,2,3], Ning Wang[1,2,3], HuiFang Bao[1,2], FaQiang Zhan[1,2], Rong Yang[1,2] and Kai Lou[1,2]

[1]Institute of Microbiology, Xinjiang Academy of Agricultural Sciences, Ürümqi, China, [2]Xinjiang Laboratory of Special Environmental Microbiology, Ürümqi, China, [3]Key Laboratory of Agricultural Environment in Northwest Oasis of Ministry of Agriculture and Countryside, Ürümqi, China, [4]Institute of Soil Fertilizer and Agricultural Water Conservation, Xinjiang Academy of Agricultural Sciences, Ürümqi, China

Introduction: *Bacillus velezensis* occurs extensively in the soil environment. It produces a range of antimicrobial compounds that play an important role in the field of biological control. However, during the actual application process it is often affected by factors such as the medium formulation and fermentation conditions, and therefore biocontrol measures often do not achieve their expected outcomes.

Methods: In this study, the *B. velezensis* BHZ-29 strain was used as the research object. The carbon and nitrogen sources, and inorganic salts that affect the number of viable bacteria and antibacterial potency of *B. velezensis* BHZ-29, were screened by a single factor test. A Plackett–Burman design experiment was conducted to determine the significant factors affecting the number of viable bacteria and antibacterial potency, and a Box–Behnken design experiment was used to obtain the optimal growth of *B. velezensis* BHZ-29. The medium formula that produced the highest number of viable bacteria and most antibacterial substances was determined. The initial pH, temperature, amount of inoculant, liquid volume, shaking speed, and culture time were determined by a single factor test. The factors that had a significant influence on the number of viable bacteria of *B. velezensis* BHZ-29 were selected by an orthogonal test. A Box–Behnken design experiment was conducted to obtain the optimal fermentation conditions, and highest number of viable bacteria and antibacterial titer.

Results: Molasses, peptone, and magnesium sulfate had significant effects on the viable count and antibacterial titer of *B. velezensis* BHZ-29. The viable count of *B. velezensis* BHZ-29 increased from 7.83×10^9 to 2.17×10^{10} CFU/mL, and the antibacterial titer increased from 111.67 to 153.13 mm/mL when the optimal media were used. The optimal fermentation conditions for *B. velezensis* BHZ-29 were as follows: temperature 25.57°C, pH 7.23, culture time 95.90 h, rotation speed 160 rpm, amount of inoculant 2%, and liquid volume 100 ml. After the optimization of fermentation conditions, the number of viable bacteria increased to 3.39×10^{10} CFU/mL, and the bacteriostatic titer increased to 158.85 mm/ml.

The plant height and leaf number of cotton plants treated with BHZ-29 fermentation broth were higher than those of cotton inoculated with *Verticillium dahliae*. The number of bacteria was 1.15×10^7 CFU/g, and the number of fungi was 1.60×10^5 spores/g. The disease index of the cotton seedlings treated with the optimized fermentation broth was 2.2, and a control effect of 93.8% was achieved. *B. velezensis* BHZ-29 could reduce the disease index of cotton *Verticillium* wilt and had a controlling effect on the disease. The best effect was achieved in the treatment group with an inoculation concentration of 2×10^8 CFU/ml, the disease index was 14.50, and a control effect of 84.18% was achieved.

Discussion: The fermentation process parameters of the number of viable bacteria and antibacterial titer by strain *B. velezensis* BHZ-29 were optimized to lay a foundation for the practical production and application of strain *B. velezensis* BHZ-29 in agriculture.

KEYWORDS

optimization, fermentation media, fermentation conditions, *Bacillus velezensis* BHZ-29, Plackett–Burman design, response surface methodology

1 Introduction

Xinjiang is the largest cotton production base in China; however, cotton *Verticillium* wilt is an important disease that has seriously hindered the development of the Xinjiang cotton industry (Xue et al., 2013). The occurrence of cotton *Verticillium* wilt in Xinjiang is becoming increasingly serious due to unfavorable factors, such as continuous cropping, returning cotton stalk to the field, and the poor disease resistance of varieties, resulting in huge economic losses (Ma, 2007; Liu et al., 2015a,b). Biological control has become a hot spot in cotton *Verticillium* wilt research because of its advantages of producing no pollution or residues, not harming humans and livestock, and not causing pathogenic fungus resistance (Ma et al., 1997). The use of bacteria for the biocontrol of cotton *Verticillium* wilt is a major focus in biological control research. Antagonistic bacteria are known for their variety, wide distribution, rapid growth, strong stress resistance, and production of many secondary metabolites, and are therefore the main flora used for the biological control of cotton *Verticillium* wilt (Liu J. et al., 2023; Liu L. et al., 2023). It is therefore of great significance to develop environmentally friendly and efficient biocontrol agents for the biological control of important soil-borne diseases of cotton and to promote the green production of cotton.

Bacillus velezensis has great potential in the prevention and control of plant diseases, but some strains have only a single function, and at the same time, there is also a lack of development and utilization of diversified functions of strains. Additionally, the antibacterial activity of strains is usually related to their biomass, the yield of active substances, and colonization ability (Zhang H. et al., 2023; Zhang L. et al., 2023). The optimization of fermentation conditions would create a suitable environment for the growth of various strains, thus promoting growth and increasing the content of active antibacterial substances in the fermentation broth of strains, both of which will improve the biocontrol potential of these strains (Li R. Q. et al., 2018; Li X. Y. et al., 2018).

The growth and reproduction of microorganisms are inseparable from the medium, and the composition of the medium is essential for the growth, development, metabolism, and product accumulation of microorganisms (Ahsan et al., 2017). Due to the use of unsuitable culture media, the number of viable bacteria in the fermentation process is often low, and few antibacterial substances are secreted, which diminishes the biocontrol potential for these microorganisms against diseases. The selection and proportional composition of microbial media components are therefore particularly important. Based on a single-factor test and the central composite design of response surface methodology, the optimum fermentation medium for *Bacillus amyloliquefaciens* antagonistic substance was determined, containing 15 gm/L of semolina flour, 12.5 gm/L of beef extract, and 0.5 gm/L of magnesium sulfate, which inhibited the fungal growth by 91% (Ahsan et al., 2022), and a new optimal formulation was determined as follows: 10% silica, 40% soybean oil, 8% ST, 1.51% AEC-9NA, 2.36% glycol, 0.08% sodium alginate, and 2% SY-6535 (Zhang H. et al., 2023; Zhang L. et al., 2023). Under optimized conditions, the viable count of *B. amyloliquefaciens* Lx−11 SE was up to 9.3×10^8 colony forming units (cfu) per ml. The results showed that the regression equation model had satisfactory accuracy in predicting the viable count of *B. amyloliquefaciens* Lx-11 SE. Under these optimal culture conditions, the titer of antifungal substances produced by the *Paenibacillus polymyxa* DS-R5 was 77.6% higher than that under the initial culture conditions. Response surface methodology can be well applied the optimization of culture conditions for antifungal substance, which lays the foundation for further research on the DS-R5 strain (Sa et al., 2022). Different strains require different nutrients, and the optimal medium for *B. velezensis* BHZ-29 has not been reported.

Different strains have different physiological characteristics and habitat preferences. The optimal fermentation temperature, fermentation time, rotation speed, carbon source, nitrogen source, and inorganic salts are different. Under the optimal parameters level (frequency of 40 kHz, power density of 40 W/L, time of 17.5 min) of *Bacillus amyloliquefaciens*, peptide content of SSF soybean meal in ultrasonic treatment group reached 150.68 mg/g, which increased by 13.10% compared to the control (Wang et al., 2021). The optimal carbon source, nitrogen source, and precursor for *Bacillus siamensis* CAU83 producing gamma-PGA were 30 g/L lactose, 5 g/L yeast

extract, and 60 g/L L-sodium glutamate, respectively. The optimal fermentation conditions were 37°C and pH 7.0. The yield of gamma-polyglycolic acid (PGA) increased by 260% from 8.4 g/L before optimization to 30.1 g/L after optimization (Lin et al., 2022). The average amount of dried extract produced by *Bacillus velezensis* RP137 in the optimum conditions was 131.1 mg/L and the best response was 71.45%, which is more than 28-fold better than the pre-optimized conditions (Pournejati et al., 2020). Therefore, determining the appropriate fermentation conditions for different strains is a key step in the production of functional strains and will enable their biocontrol functions to be realized.

Different microorganisms have different nutritional needs. Before the industrial production of microorganisms, it is necessary to optimize the fermentation medium and culture conditions. The methods used to optimize the fermentation medium include a single factor experiment (Tian et al., 2014), orthogonal test (Tu et al., 2015), uniform design (Ruan et al., 2012), Plackett–Burman design (Quan et al., 2015), Box–Behnken design (Shang et al., 2013; Quan et al., 2015), and central composite design (Lima et al., 2011). The optimization of different microbial fermentation media has been achieved previously using Plackett–Burman design, Box–Behnken design, or central composite design experiments. Using response surface methodology (RSM), the optimal medium or culture conditions can be quickly and effectively determined.

Bacillus velezensis BHZ-29 was isolated from cotton plants in our laboratory (Zhang et al., 2018). The results of an indoor bioassay showed that the strain had a strong control effect on cotton *Verticillium* wilt, jujube black spot, melon postharvest rot, and grape rot, and had some value in the development of microbial pesticide products. In this study, *B. velezensis* BHZ-29 was used as the research object, and a Plackett–Burman design experiment was conducted to optimize the components of a shaken flask formula for the nutrient broth fermentation medium to screen out the significant influencing factors. Then, the steepest ascent test and Box–Behnken design experiment were conducted, enabling a nonlinear equation to be fitted between the significant factors and spore yield, and the fermentation sporulation medium formula of the strain was optimized. Taking the number of viable bacteria as the index, the range of fermentation conditions was determined by a single factor test. An orthogonal test was used to select the significant factors affecting the viable count of *B. velezensis* BHZ-29. A Box–Behnken design experiment was then conducted according to the orthogonal test results, and the simulation fitting equation was established based on the test results. The optimal fermentation conditions were obtained, which resulted in improved viable bacteria numbers. Validation of fermentation processes was carried out in a 1,000 L fermentor to provide support for the expansion of production and industrialization of the BHZ-29 strain.

2 Materials and methods

2.1 Microorganisms and media

Bacillus velezensis BHZ-29 was isolated, purified, and preserved by the laboratory of Institute of Microbial Application, Xinjiang Academy of Agricultural Sciences (Zhang et al., 2018). *Verticillium dahlia* 2015–007 was isolated from diseased plants in the Shihezi cotton area and preserved with moderate to strong pathogenicity. Potato dextrose water medium (PDB) was prepared as follows: potato extract 6.0 g, glucose 20.0 g, distilled water 1,000 mL, pH 5.6 ± 0.2. Nutrient broth medium (NB) was prepared as follows: peptone 10.0 g, beef extract 3.0 g, sodium chloride 5.0 g, distilled water 1,000 mL, pH 7.2 ± 0.2.

2.2 Preparation of inoculum and flask cultures

The preserved *B. velezensis* BHZ-29 was streaked and inoculated on nutrient agar (NA) medium and cultured at 32°C for 48 h. The volume of liquid medium was 100 mL per 500 mL Erlenmeyer flask. A single colony of *B. velezensis* BHZ-29 was selected and inoculated into 100 mL NB liquid medium, and the seed liquid was obtained by shaking a culture at 32°C and 180 rpm for 12 h (Hassan et al., 2011). *Fusarium oxysporum* cakes were placed on a potato dextrose agar (PDA) medium, and cultured at 28°C for 5 days. The liquid volume of PDB liquid medium was 200 mL per 500 mL Erlenmeyer flask. Small fungal cakes (6 mm) were prepared by a punching method. Each bottle was inoculated with 15 fungal cakes, and cultured at 28°C and 160 rpm for 5 days. The filtrate was filtered through a sterile gauze, and the filtrate was collected and used as the spore suspension of *F. oxysporum* (Shim et al., 2013).Erlenmeyer flask.

2.3 Fermentation medium screening

2.3.1 Screening of significant variables by a Plackett–Burman design experiment

Fermentation medium composition was based on NB medium. Glucose, sucrose, lactose, fructose, maltose, soluble starch, starch, molasses, and Indian meal, each with a concentration of 10 g/L, were selected to replace the carbon source in the basic fermentation medium, while the other components remained unchanged. Beef extract, peptone, yeast extract, urea, ammonium nitrate, ammonium sulfate, sodium nitrate, soybean powder, and cottonseed meal, each with a concentration of 10 g/L, were selected to replace peptone and beef powder in the basic fermentation medium, while the other components remained unchanged. Potassium chloride, calcium chloride, magnesium sulfate, zinc sulfate, ferrous sulfate, calcium carbonate, manganese sulfate, and dipotassium hydrogen phosphate, each with a concentration of 5 g/L, were selected to replace sodium chloride in the basic fermentation medium, while the other components remained unchanged. Experiments were carried in triplicates. A 0.5 ml portion of fermentation broth was added to 4.5 ml of 0.03% Tween 80, the solution was successively diluted 10 times, and 100 µl was evenly coated on NA medium. It was cultured at 32°C for 2 days, and the number of viable bacteria was counted. Then, 100 µl of *F. oxysporum* spore suspension was evenly coated on PDA medium where it was left to stand for 30 min. Four 6 mm diameter holes were punched equidistantly on the medium using a sterile puncher, and 100 µl of fermentation broth was injected, respectively. The fermentation broth was cultured at 28°C for 4 days, the diameter of the inhibition zone was measured, and the bacteriostatic titer was calculated. The bacteriostatic titer was defined as the diameter of the 1 mm inhibition zone produced by each 1 ml fermentation broth. Bacteriostatic titer $(mm/mL) = (X - Y)/V \times 1{,}000$, where X is the

diameter of the inhibition zone (mm), Y is the diameter of the puncher (6 mm), and V is the volume of bacterial suspension (μL).

The Plackett–Burman design experimental was conducted using DesignExpert 10.0 software to further screen the condition factors determined by the single factor experiment. Each factor was divided into low and high levels, and a total of 12 experiments were conducted.

2.3.2 The steepest climbing test and Box–Behnken design experiment

According to the proportion of important factor effects determined by the results of the Plackett–Burman design experiment, the gradient direction and range of test value changes were set, and the optimal optimization conditions were selected as the central point of the RSM results. A three-level RSM analysis was conducted on three significant influencing factors using a Box–Behnken design experiment. The data were fitted by a quadratic regression to obtain a quadratic equation with interaction and square terms. The variance analysis of the regression equation was carried out to evaluate the influence of each factor and its interaction on the response value. At the same time, the level of each factor when the response value was largest was obtained, and the optimal conditions determined by the regression model were verified. The experimental scheme and regression analysis were designed using the Design Expert 10.0 software.

2.4 Optimization of the fermentation conditions

2.4.1 Optimization of the fermentation conditions of *Bacillus velezensis* BHZ-29 by a single factor test

The culture conditions were optimized using the optimized medium. The volume of liquid in a 500 ml conical flask was 100 ml. The single factor test had the basic culture conditions of: initial pH 7.2, amount of inoculant 1%, temperature 32°C, and rotation speed 180 rpm for 72 h. The number of viable bacteria and antibacterial titer of the *B. velezensis* BHZ-29 fermentation broth were determined, and the antibacterial titer was measured by the diameter of the inhibition zone.

2.4.2 Optimization of the fermentation conditions of *Bacillus velezensis* BHZ-29 by an orthogonal test and RSM

The orthogonal test was conducted under the range of conditions obtained by the single factor test. Assuming that there was an interaction between the factors, an orthogonal test of six factors and three levels L18 (36) was designed (Table 1). Based on the results of the orthogonal test, the temperature (A), pH (C), and culture time (F) that had a significant effect on the number of viable *B. velezensis* BHZ-29 bacteria were selected for optimization, and a Box–Behnken design experiment was conducted with the number of viable bacteria as the response value.

TABLE 1 Fermentation factor and level of BHZ-29.

Variables	Code	Level		
		–1	0	1
Temperature	A	24	26	28
Rotational speed	B	160	180	200
Initial pH	C	7.0	7.2	7.4
Inoculation amount	D	1	2	3
Broth content	E	50	100	150
Time	F	48	72	96

2.5 Shaken flask fermentation verification test

The optimized medium was adjusted as follows: molasses 20.38 g/L, peptone 19.40 g/L, and magnesium sulfate 3.56 g/L. The number of viable bacteria in the fermentation broth of *B. velezensis* BHZ-29 was determined, and the fitting degree between the actual and predicted values of the number of viable bacteria was verified. The optimized medium was adjusted to 19.44 g/L molasses, 20.42 g/L peptone, and 3.51 g/L magnesium sulfate. The antibacterial titer of the fermentation broth of *B. velezensis* BHZ-29 was determined to verify the fitting degree between the actual and predicted values of the antibacterial titer. The experiment was repeated five times.

2.6 The control effect of the *Bacillus velezensis* BHZ-29 optimized fermentation culture on cotton *Verticillium* wilt

The soil was sterilized at 180°C for 3 h, and Xinluzao 36 cotton seeds were planted with six plants per pot. When the cotton seedlings grew to two leaves and one heart, the fermentation broth of *V. dahliae* with a concentration of 2×10^7 spores/mL was inoculated by the root injury perfusion method at 20 mL/plant. After 7 days, the fermentation broths with different concentrations of antagonistic bacteria were inoculated by a root irrigation method at 20 mL/plant. Three treatments were established: (1) *V. dahliae* fermentation broth + strain *B. velezensis* BHZ-29 fermentation broth; (2) *V. dahliae* fermentation broth; and (3) clear water control. The inoculation concentration of the antagonistic bacteria fermentation broth was set to three levels of 2×10^8, 2×10^6, or 2×10^5 CFU/mL. A pot disease prevention test for each of the three pot treatments was conducted with three replicates. After 60 days of cotton seedling growth, the plants were graded according to the classification method of Zhu et al. (2013): grade 0: healthy plant; grade 1: 1–2 cotyledons were diseased; grade 2: 1 true leaf diseased; grade 3: more than 2 true leaves diseased or fallen off; and grade 4: all leaves fallen off or the apex withered. The disease index and control effect of cotton *Verticillium* wilt were calculated according to the grading of the cotton *Verticillium* wilt disease index. Disease index = ∑(grade value × plant number)/(highest grade value × total plant number) × 100; control effect (%) = (control disease index-treatment disease index)/control disease index × 100.

2.7 Statistical analysis

The Plackett–Burman design experiment, Box–Behnken design experiment, and RSM were conducted using DesignExpert12 software. The results of the experiments were statistically analyzed using SPSS 22.0 software, and the least significant difference method was used to test for significant differences.

10.3389/fmicb.2024.1355369

3 Results

3.1 Selection of carbon, nitrogen, and mineral sources

As shown in Figure 1A, the different carbon sources had different promotional effects on the number of viable bacteria and antibacterial potency of *B. velezensis* BHZ-29. The number of viable bacteria in the fermentation broth was highest (3.55×10^9 CFU/mL) when molasses were used as the carbon source. When glucose, lactose, maltose, soluble starch, fructose, and molasses were used as carbon sources, the numbers of viable *B. velezensis* BHZ-29 bacteria were significantly different from that of the control. When sucrose, starch, and corn flour were used as carbon sources, the numbers of viable *B. velezensis* BHZ-29 bacteria were not significantly different from that of the control. The antibacterial titer was highest (128.89 mm/mL) when starch was used as the carbon source, but the number of viable bacteria was lower and there was no significant difference with the control. For molasses, maltose, and corn flour the antibacterial titers were 112.44, 108.89, and 106.11 mm/mL, respectively. Therefore, molasses and maltose were selected as the carbon source of the medium.

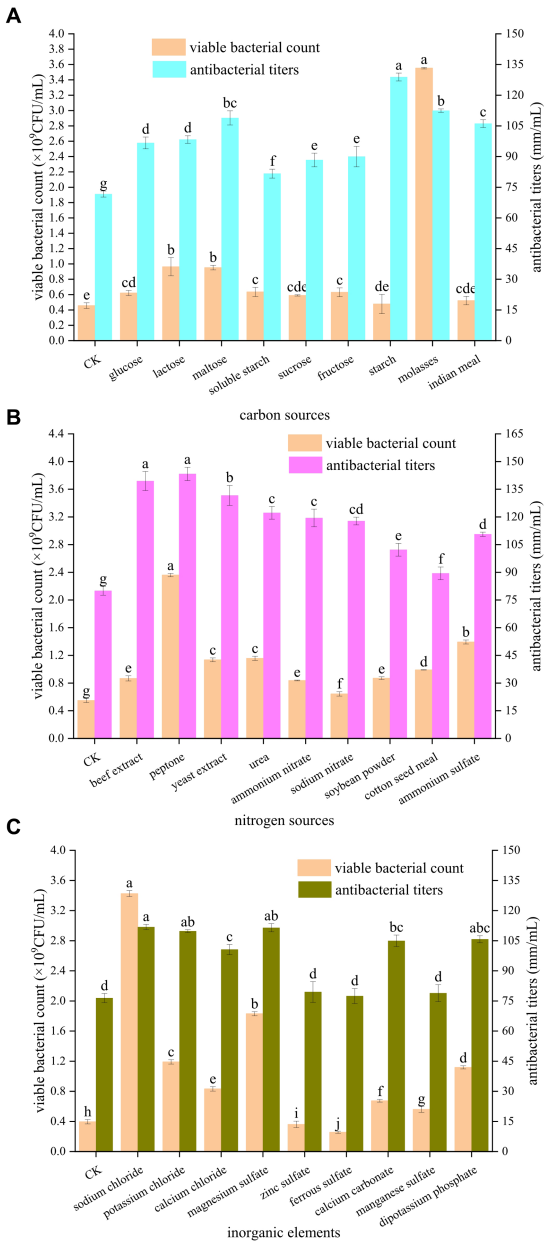

FIGURE 1
Effects of different carbon sources **(A)**, nitrogen sources **(B)**, and inorganic elements **(C)** on the fermentation of strain BHZ-29. Different lowercase letters mean significant difference. ($P < 0.05$).

As shown in Figure 1B, the different nitrogen sources also had different effects on the number of viable bacteria and antibacterial titer of *B. velezensis* BHZ-29. Among the organic nitrogen sources, peptone and yeast extract were the most suitable for the growth and reproduction of *B. velezensis* BHZ-29, producing numbers of viable bacteria of 2.36×10^9 and 1.14×10^9 CFU/mL, respectively. Among the inorganic nitrogen sources, ammonium sulfate and urea were the most suitable for the growth and reproduction of *B. velezensis* BHZ-29, producing numbers of viable bacteria of 1.39×10^9 and 1.16×10^9 CFU/mL, respectively. For organic nitrogen sources, the fermentation broth had the best inhibitory effect on the target pathogen when peptone and beef extract were used, and the difference between the two nitrogen sources was not significant. The bacteriostatic titers were 143.33 and 139.44 mm/mL, respectively. For inorganic nitrogen sources, the fermentation broth had the best inhibitory effect on the target pathogen when urea and ammonium nitrate were used, and the difference between the two nitrogen sources was not significant. The antibacterial titers were 122.22 and 119.44 mm/ml, respectively. Based on the effects of different nitrogen sources on the number of viable bacteria and bacteriostatic titer of *B. velezensis* BHZ-29, peptone and ammonium sulfate were selected as the nitrogen sources of the medium.

As shown in Figure 1C, the different inorganic salts also had different effects on the number of viable bacteria and the antibacterial activity of *B. velezensis* BHZ-29. Ferrous sulfate and zinc sulfate had a significant inhibitory effect on the number of viable *B. velezensis* BHZ-29 bacteria. Sodium chloride, calcium chloride, magnesium sulfate, calcium carbonate, manganese sulfate, dipotassium hydrogen phosphate, and potassium chloride had significant promotional effects on the number of viable *B. velezensis* BHZ-29 bacteria. The number of viable cells produced in the presence of sodium chloride, magnesium sulfate, and potassium chloride were 3.43×10^9, 1.83×10^9, and 1.19×10^9 CFU/mL, respectively. All inorganic salts promoted antibacterial activity. The fermentation broth with sodium chloride, magnesium sulfate, and potassium chloride as inorganic salts had a stronger antibacterial effect on the target pathogen, with antibacterial titers of 111.82, 111.46, and 109.76 mm/ml, respectively. Therefore, sodium chloride and magnesium sulfate were selected as inorganic salts for incorporation in the medium.

3.2 Screening of significant variables by the Plackett–Burman design experiment

A Plackett–Burman design experiment ($N = 12$) was conducted. According to the results of the single factor test, molasses (X1), maltose (X2), peptone (X3), ammonium sulfate (X4), sodium chloride (X5), and magnesium sulfate (X6) were selected as six factors to investigate. The high and low levels of these variables were selected, and the number of viable bacteria (Y1) and the bacteriostatic titer (Y2)

were used as experimental indexes. The experimental design and results are shown in Table 2. A multiple linear regression equation was obtained by a regression analysis of the data in Table 2: $Y1 = 1.039 + 0.165 \times 1 + 0.080 \times 2 + 0.390 \times 3 + 0.192 \times 4\text{-}0.012 \times 5 + 0.295 \times 6$; $Y2 = 139.569 + 0.779 \times 1\text{-}0.234 \times 2 + 1.371 \times 3 + 0.562 \times 4 + 0.617 \times 5 + 0.941 \times 6$.

The effects of various factors on the number of *B. velezensis* BHZ-29 colonies were analyzed. The results are shown in Table 2. The effects of these factors on the antibacterial titer of *B. velezensis* BHZ-29 are also shown in Table 2. The importance of the six factors on the colony number of *B. velezensis* BHZ-29 was peptone > magnesium sulfate > ammonium sulfate > molasses > maltose > sodium chloride. Peptone and magnesium sulfate had a significant effect on the colony number at the 0.05 level. The importance of the six factors on the antibacterial titer of *B. velezensis* BHZ-29 was peptone > magnesium sulfate > molasses > ammonium sulfate > sodium chloride > maltose. After a comprehensive consideration, molasses was selected as the carbon source, peptone as the nitrogen source, and magnesium sulfate as the inorganic salt for further optimization.

3.3 Determination of the central point levels by the steepest ascent experiments and determination of the optimal medium

According to Table 3, with increased amounts of molasses, peptone, and magnesium sulfate, the number of viable bacteria and bacteriostatic titer displayed a trend of first increasing and then decreasing. When the molasses concentration was 20 g/L, peptone concentration was 20 g/L, and magnesium sulfate concentration was 3.5 g/L, the number of viable bacteria and bacteriostatic titer reached their maximum values. Therefore, the proportional composition of the treatment 3 fermentation medium was used as the central point of the RSM for further optimization.

Based on the results of the steepest ascent test, three concentrations of molasses (15, 20, and 25 g/L), peptone (15, 20, and 25 g/L) and magnesium sulfate (3, 3.5, and 4 g/L) were established with the proportional composition of the treatment 3 fermentation medium as the central point. A regression analysis was performed on the data in Supplementary Table S1, and the following quadratic polynomial equation was obtained: $Y1 = 1.900 - 0.240 \times 1 + 0.150 \times 3\text{-}0.063 \times 6\text{-}0.160X1X3 - 0.0170X1X6 + 0.092X3X6 - 0.430 \times 12\text{-}0.440 \times 32\text{-}0.490 \times 62$ ($R^2 = 0.9952$, R^2 adjustment = 0.8976); $Y2 = 151.09 - 3.57 \times 1 + 2.41 \times 3\text{-}0.77 \times 6 + 0.10X1X3 - 1.53X1X6 + 2.48X3X6 - 5.31 \times 12\text{-}4.45 \times 32\text{-}5.31 \times 62$ ($R^2 = 0.9405$, R^2 adjustment = 0.8640).

The results of the variance analysis of the regression model with the number of colonies as the response value are shown in Table 4, and the results of the variance analysis of the regression model with the antibacterial potency as the response value are shown in Supplementary Table S2. The results showed that at the 0.05 level, the regression of the two models was significant, and the first (X1 and X3) and second ($X1^2$, $X3^2$, and $X6^2$) terms had significant effects on the experiment.

The RSM and contour maps for when the number of colonies was used as the response value, are shown in Figures 2A–F. According to Figures 2A,B, when the molasses concentration was constant, with an increase in the peptone concentration, the number of viable bacteria first increased, and then began to decrease at a certain point. When the peptone concentration was constant, with the increase in the molasses concentration, the number of colonies also showed a trend of first increasing and then decreasing. Figures 2C,D shows that when the molasses concentration was constant, the number of *B. velezensis* BHZ-29 colonies first increased and then decreased as the magnesium sulfate concentration increased, and the vertex of the surface was the point with the maximum number of colonies. Similarly, the surface shown in Figures 2E,F reflects the interaction between peptone and magnesium sulfate.

The results when the antibacterial titer was used as the response value are shown in Supplementary Figures S1A–F. It can be seen from Supplementary Figures S1A,B that when the molasses concentration was constant, the antibacterial titer of *B. velezensis* BHZ-29 first increased with the increase of peptone, and then began to decrease when it reached a certain value. When the peptone concentration was constant, with an increase in the molasses concentration, the antibacterial titer of *B. velezensis* BHZ-29 also displayed a trend of first increasing and then decreasing. Supplementary Figures S1C,D shows that when the molasses concentration was constant, the antibacterial

TABLE 2 The design and results of Plackett–Burman experiment.

Run numbers	X1	X2	X3	X4	X5	X6	Y1 (10^{10} CFU/mL)	Y2 (mm/mL)
1	1	1	1	−1	1	1	2.24	140.24
2	1	−1	−1	−1	1	1	0.63	135.78
3	−1	1	1	−1	1	−1	0.57	141.89
4	1	1	−1	1	−1	−1	0.84	138.13
5	1	1	−1	1	1	−1	0.74	138.60
6	−1	−1	−1	−1	−1	−1	0.36	139.80
7	−1	−1	1	1	1	−1	1.23	137.74
8	−1	1	−1	−1	-1	-1	0.56	137.05
9	-1	1	1	1	-1	1	1.77	141.06
10	1	-1	1	1	-1	1	2.06	143.43
11	-1	-1	-1	1	1	1	0.76	139.39
12	1	-1	1	-1	-1	-1	0.72	141.72

TABLE 3 Regression analysis of experimental results based on Plackett–Burman design.

Factors		Levels		T	P	Order
Symbols	Variables	low(−1)	high(1)			
X_1	Molasses (g/L)	5	10	2.643	0.046	3
X_2	Maltose (g/L)	5	10	−0.792	0.464	6
X_3	Peptone (g/L)	5	10	4.635	0.006	1
X_4	Ammonium sulfate (g/L)	5	10	1.902	0.116	5
X_5	Sodium chloride (g/L)	0.5	2.5	2.088	0.091	4
X_6	Magnesium sulfate (g/L)	0.5	2.5	3.181	0.025	2

TABLE 4 The design scheme and test results of the Box–Behnken design.

Run numbers	X_1	X_3	X_6	Y_1 (10^{10} CFU/mL)	Y_2 (mm/mL)
1	−1	−1	0	0.91	142.08
2	−1	1	0	1.54	146.10
3	1	1	0	0.84	140.77
4	0	0	0	1.99	153.97
5	1	−1	0	0.84	136.35
6	0	−1	1	0.76	135.31
7	0	−1	−1	0.93	142.28
8	1	0	1	0.54	134.21
9	0	0	0	1.85	151.18
10	0	1	1	1.21	145.68
11	−1	0	1	1.16	146.00
12	0	0	0	1.66	147.51
13	−1	0	1	1.16	144.03
14	1	0	−1	0.84	138.35
15	0	0	0	1.89	149.60
16	0	0	0	2.11	153.17
17	0	1	−1	1.01	142.74

titer of *B. velezensis* BHZ-29 first increased and then decreased as the magnesium sulfate concentration increased. The vertex of the surface was the maximum point of the antibacterial titer of *B. velezensis* BHZ-29. Similarly, the surface shown in Supplementary Figures S1E,F reflects the interaction between peptone and magnesium sulfate.

The results when the optimized medium was adjusted to 20.38 g/L molasses, 19.40 g/L peptone, and 3.56 g/L magnesium sulfate are shown in Supplementary Table S3. The average number of colonies was 2.17×10^{10} CFU/mL, which was 1.14 times the predicted value, and showed a good degree of fitting with the predicted value. Under these conditions, the bacteriostatic titer was 149.60 mm/mL. When the optimized medium was adjusted to molasses 19.44 g/L, peptone 20.42 g/L, and magnesium sulfate 3.51 g/L, the measured bacteriostatic titer was 153.13 mm/mL, which was 1.01 times the predicted value, and the predicted value had a good fit. The average number of colonies under these conditions was 1.63×10^{10} CFU/mL. In summary, the medium selected as the test medium had a molasses concentration of 20.38 g/L, peptone concentration of 19.40 g/L, and magnesium sulfate concentration of 3.56 g/L.

3.4 Optimization of the single factor fermentation conditions for *Bacillus velezensis* BHZ-29

The effects of the initial pH of the medium on the number of viable bacteria and the antibacterial titer of *B. velezensis* BHZ-29 are shown in Supplementary Figure S2. When the initial pH value was in the range of 5–9, *B. velezensis* BHZ-29 was able to grow. The number of viable bacteria and antibacterial titer of *B. velezensis* BHZ-29 were highest when the initial pH value was 7 and 8. Therefore, the initial pH values of 7 and 8 were selected for the next optimization. The results are shown in Figure 3A. With the increase in the pH value, the number of viable bacteria and the bacteriostatic titer displayed a trend of first increasing and then decreasing. When the pH value increased to 7.2, the number of viable bacteria increased to 2.25×10^{10} CFU/ml, which was significantly higher than for the other pH values, and the bacteriostatic titer reached 97.70 mm/ml.

As shown in Figure 3B, with an increase in the culture temperature, the number of viable bacteria and bacteriostatic titer displayed a trend of first increasing and then decreasing. When the temperature was 24°C, the viable count of *B. velezensis* BHZ-29 was 1.27×10^{10} CFU/ml. When the culture temperature was 26°C, the viable count of *B. velezensis* BHZ-29 was 1.27×10^{10} CFU/ml. BHZ-29 had the highest viable count of 1.49×10^{10} CFU/mL and highest antibacterial titer of 129.93 mm/ml.

As shown in Figure 3C, with an increase in shaking speed, the number of viable bacteria and antibacterial titer displayed a trend of first increasing and then decreasing. When the shaking speed was 180 rpm, the number of viable bacteria reached a maximum of 1.69×10^{10} CFU/ml, and the antibacterial titer reached a maximum of 98.33 mm/ml.

As shown in Figure 3D, with an increase in the amount of inoculant, the number of viable bacteria in the fermentation broth and the antibacterial titer displayed a trend of first increasing and then decreasing, but the trend did not change significantly. When the amount of inoculant was 2%, the number of viable bacteria and the bacteriostatic titer reached the maximum value. At this time, the number of viable bacteria was 1.72×10^{10} CFU/ml, and the bacteriostatic titer reached 114.44 mm/ml.

As shown in Figure 3E, with an increase in the liquid volume, the number of viable bacteria displayed a trend of first increasing, then decreasing, and then increasing again, while the antibacterial titer

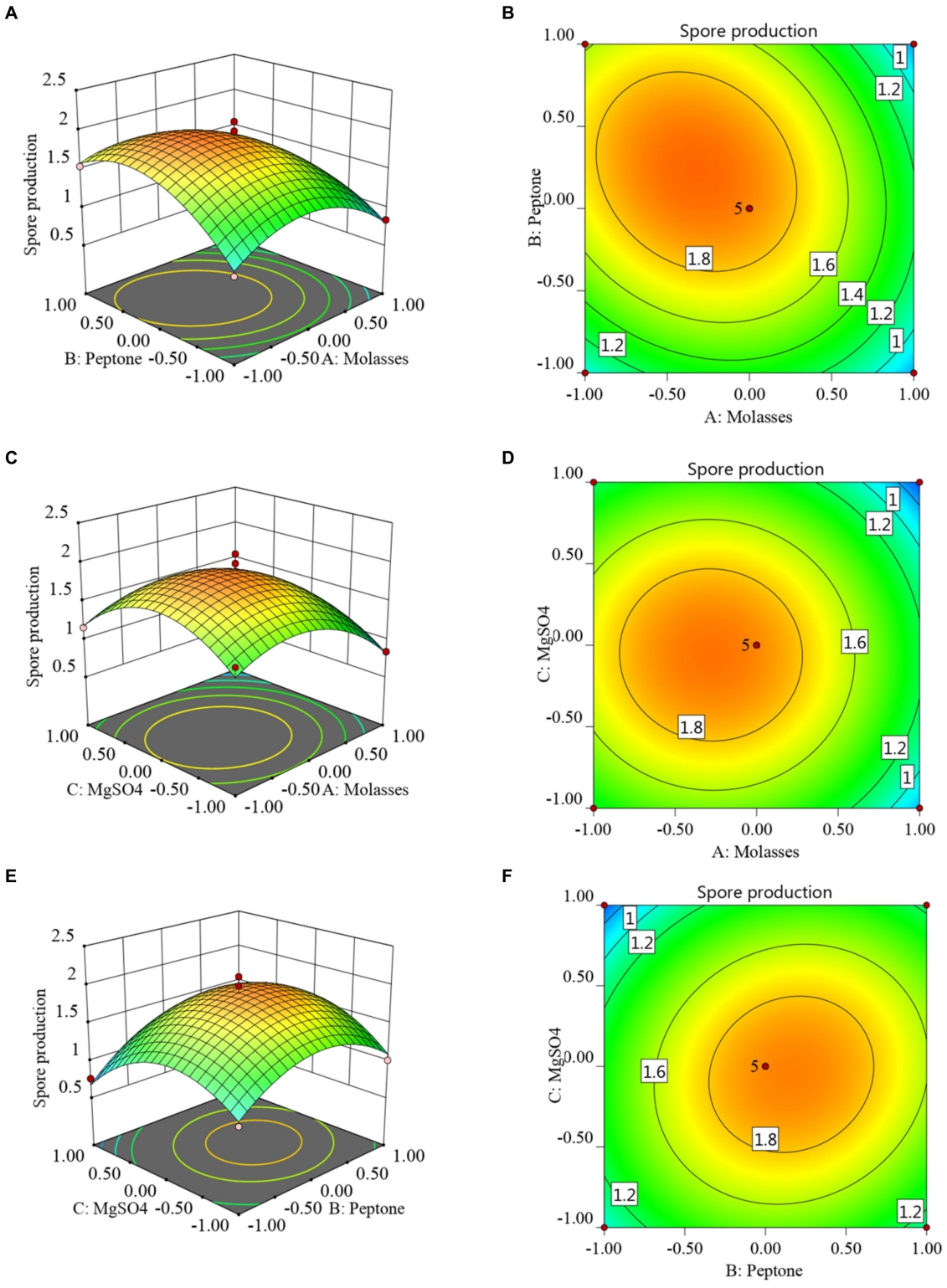

FIGURE 2
Response surface **(A, C, E)** and contour lines **(B, D, F)** of the interaction among three factors of medium components, molasses (X1), peptone (X3), and MgSO4 (X6) on the yield of viable cells.

displayed a trend of first increasing and then decreasing. When the liquid volume was 100 mL, the number of viable bacteria and the antibacterial titer reached their maximum values of 1.45×10^{10} CFU/ml and 126.56 mm/ml, respectively.

As shown in Figure 3F, with the prolongation of culture time, the number of viable bacteria and the antibacterial titer displayed a trend of first increasing and then decreasing. When the culture time reached 72 h, the number of viable bacteria reached a

10.3389/fmicb.2024.1355369

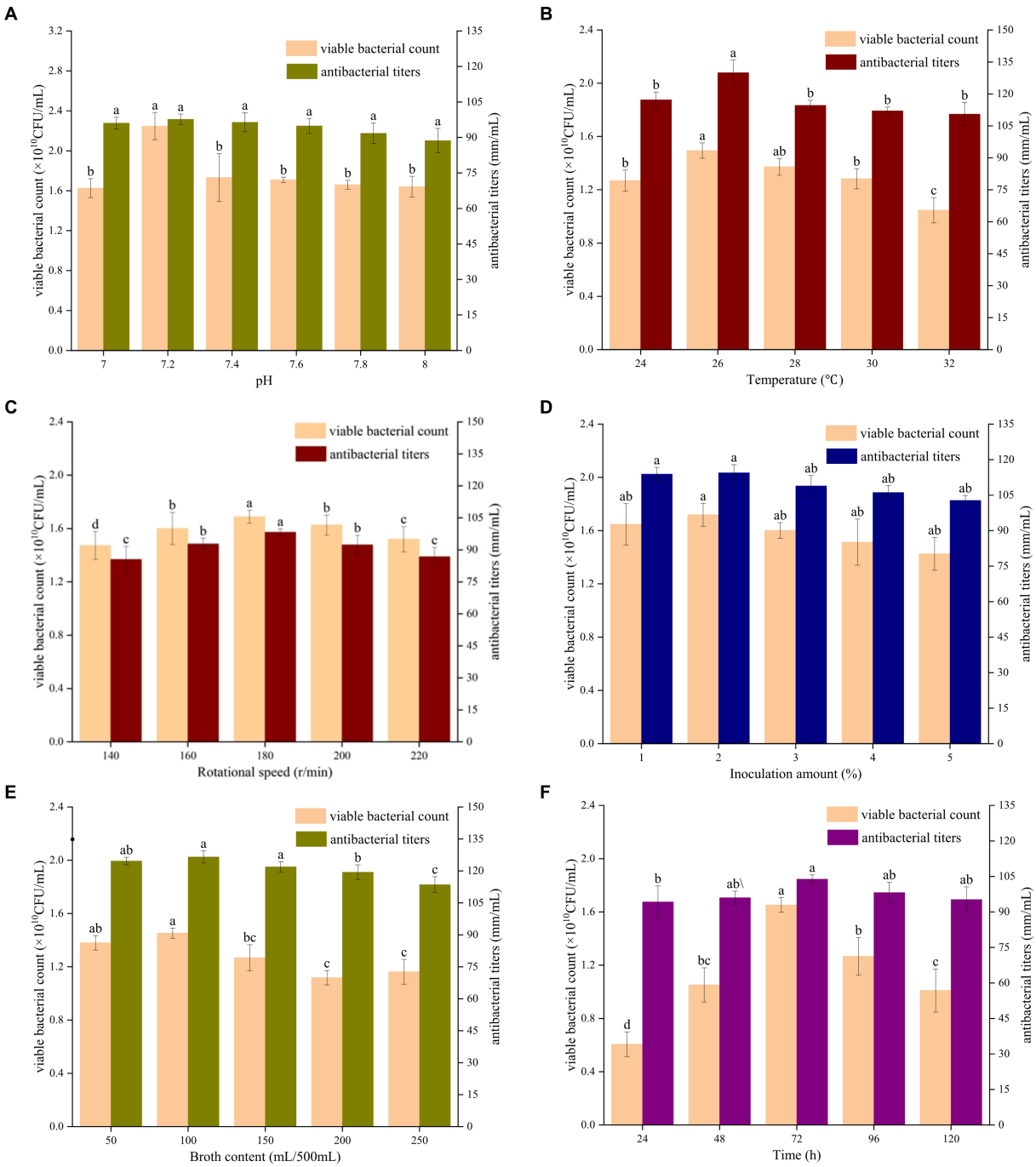

FIGURE 3
Effects of different initial pH value **(A)**, culture temperature **(B)**, shaking speed **(C)**, amount of inoculant **(D)**, liquid volume **(E)**, and culture time **(F)** on the fermentation of strain BHZ29. Different lowercase letters mean significant difference ($p < 0.05$).

maximum of 1.65×10^{10} CFU/ml, and the bacteriostatic titer was 103.84 mm/ml.

3.5 The significant influencing factors of fermentation conditions as determined by an orthogonal test

Based on the results of the single factor test, six factors of temperature (A), rotation speed (B), pH (C), amount of inoculant (D), liquid volume (E), and culture time (F) were selected for an orthogonal test. The test factors and levels are shown in Table 1. The orthogonal test design and results are shown in Table 5. Y1 and Y2 are the number of viable bacteria and bacteriostatic titer, respectively.

The results of the orthogonal test are as shown in Table 5. The changes of F, A, and C (i.e., culture time, temperature, and pH, respectively) had a large influence on the number of viable bacteria, while changes in E, D, and B (i.e., liquid volume, amount of inoculant, and rotation speed, respectively) had little influence. The order of

influence on the number of viable bacteria was culture time > temperature > pH > liquid volume > amount of inoculant > rotation speed. The results of the orthogonal test showed that the optimal fermentation conditions were as follows: temperature 26°C, rotation speed 160 rpm, pH 7.2, amount of inoculant 2%, liquid volume 100 ml, and culture time 96 h.

The results of the variance analysis are shown in Supplementary Table S4. Culture time, temperature, and pH had significant effects on the number of viable bacteria. The effects of rotation speed, amount of inoculant, and liquid volume on the number of viable bacteria were not significant. Therefore, the culture time, temperature, and pH, all of which had significant effects on the number of viable bacteria, were selected for the Box–Behnken design experiment.

3.6 The Box–Behnken design experiment and analysis of significant influencing factors of fermentation conditions

A regression analysis was performed on the data in Table 6, and the following quadratic polynomial equation was obtained: $Y1 = 3.040 - 0.520A + 0.270C - 0.073F + 0.043AC - 0.130AF + 0.200CF - 1.170A^2 - 0.750C^2 - 1.040F^2$ ($R^2 = 0.8853$, R^2 adjustment = 0.7379).

According to the variance analysis results in Supplementary Table S5, the regression model showed that unknown factors resulted in little interference and the model was stable. According to the F value, the effect on the number of viable *B. velezensis* BHZ-29 bacteria was: temperature > pH > culture time. According to the p value, A2 and F2 were extremely significant ($p < 0.01$), A and C2 were significant ($p < 0.05$), and the other parameters were not significant.

3.7 The RSM analysis and determination of the optimal fermentation conditions

The RSM diagram and contour diagram between the factors when the number of viable bacteria was taken as the response value are shown in Figures 4A–F. It can be seen from Figures 4A,B that when the temperature was constant, the number of viable bacteria first increased and then decreased with the extension of culture time. When the culture time was constant, with an increase in temperature, the number of viable bacteria also displayed a trend of first increasing and then decreasing. Figures 4C,D shows that when the pH was constant, the number of viable bacteria in *B. velezensis* BHZ-29 first increased and then decreased with the increase of temperature, and the vertex of the surface was the maximum point of the number of viable bacteria. Similarly, the surface of Figures 4E,F reflected the

TABLE 5 L_{18} (3^6) Orthogonal experimental design results.

Run numbers	A	B	C	D	E	F	Y_1 (10^{10} CFU/ml)	Y_2 (mm/ml)
1	1	1	1	1	1	1	0.59	150.10
2	1	2	2	2	2	2	1.96	150.32
3	1	3	3	3	3	3	1.85	161.04
4	2	1	1	2	2	3	3.02	145.70
5	2	2	2	3	3	1	1.95	150.40
6	2	3	3	1	1	2	2.34	152.58
7	3	1	2	1	3	2	1.87	150.51
8	3	2	3	2	1	3	2.49	149.62
9	3	3	1	3	2	1	0.43	149.65
10	1	1	3	3	2	2	1.78	149.73
11	1	2	1	1	3	3	0.84	175.12
12	1	3	2	2	1	1	1.08	150.00
13	2	1	2	3	1	3	3.00	147.87
14	2	2	3	1	2	1	1.76	146.78
15	2	3	1	2	3	2	2.10	151.95
16	3	1	3	2	3	1	0.56	147.70
17	3	2	1	3	1	2	0.87	149.93
18	3	3	2	1	2	3	2.66	146.23
K_1	8.10	10.82	7.85	10.06	10.37	6.37		
K_2	14.17	9.87	12.52	11.21	11.61	10.92		
K_3	8.88	10.46	10.78	9.88	9.17	13.86		
R	6.07	0.95	4.67	1.33	2.44	7.49		

TABLE 6 The design scheme and test results of the Box–Behnken design.

Run numbers	A	C	F	Y_1 (10^{10} CFU/ml)	Y_2 (mm/ml)
1	−1	−1	0	1.77	133.63
2	−1	1	0	1.52	132.63
3	1	1	0	0.54	133.60
4	0	0	0	3.23	162.00
5	1	−1	0	0.61	126.73
6	0	−1	1	0.32	160.07
7	0	−1	−1	0.92	124.70
8	1	0	1	0.14	133.60
9	0	0	0	2.22	154.67
10	0	1	1	1.96	166.53
11	−1	0	1	1.40	127.37
12	0	0	0	3.29	143.73
13	−1	0	−1	1.24	132.90
14	1	0	−1	0.49	114.77
15	0	0	0	2.76	153.93
16	0	0	0	3.68	154.53
17	0	1	−1	1.75	132.53

interaction between pH and incubation time. In summary, there was a strong interaction between the factors.

The 3D response surfaces plots were employed to determine the interaction of the fermentation conditions and the optimum levels that have the most significant effect on antibacterial titer. The response surfaces plots based on the model are depicted in Supplementary Figures S3A–F. It is clear from Supplementary Figures S3A that the maximum response of antibacterial titer (156.037 mm) occurred when temperature was at its −0.228075 level. Antibacterial titer increased considerably as temperature increased, indicating that temperature for antibacterial titer has a significant effect on the responses. As the temperature increased, the responses were maximal at 0.725735 level of initial pH and at 0.328792 level of time. The response was also varied at different levels of initial pH and time along the axis, suggesting that there is a considerable interaction between temperature and initial pH, temperature and time, initial pH and initial time (Supplementary Figures S3A–F).

The optimized fermentation conditions were verified, and the results are shown in Supplementary Table S6. The average number of viable *B. velezensis* BHZ-29 bacteria was 3.39×10^{10} CFU/mL, which showed a good fit with the predicted value. Under these conditions, the antibacterial titer of *B. velezensis* BHZ-29 was 158.85 mm/ml.

3.8 Determination of the inhibitory effect and the control effect of the fermentation broth of *Bacillus velezensis* BHZ-29 before and after optimization on *V. dahlia* in cotton

Based on the above optimization results, an indoor pot experiment was conducted, and the disease index, incidence rate, and agronomic traits of cotton seedlings under each treatment were measured after 30 days. The results are shown in Table 7 and Supplementary Table S7, and revealed that the strain could effectively inhibit the occurrence of cotton *Verticillium* wilt both before and after optimization. The control treatment inoculated only with pathogen (CK1) was most seriously affected. The cotton growth was relatively short, and the leaves were yellow, withered, and the edges were rolled up. These are typical symptoms of *Verticillium* wilt, and the disease index was also high (92.22). *B. velezensis* BHZ-29 had a growth-promoting effect on the cotton seedlings. Compared with the control, agronomic traits (e.g., plant height, stem circumference, root length, root weight, fresh weight and dry weight of aboveground parts of cotton seedlings) were significantly improved after treatment with strain fermentation broth (Supplementary Table S7).

The disease index of the *B. velezensis* BHZ-29 treatment group was significantly different from that of the *V. dahlia* treatment group at the 95% level, indicating that *B. velezensis* BHZ-29 could reduce the disease index of cotton *Verticillium* wilt and had control effect on cotton *Verticillium* wilt (Figure 5). The best effect was obtained at the inoculation concentration of 2×10^8 CFU/mL, with a disease index of 14.50 and control effect of 84.28%. The worst effect was obtained at an inoculation concentration of 2×10^5 CFU/ml, with a disease index of 56.67 and control effect of 38.55%. With the decrease in the inoculation concentration, the disease index of cotton treated with bacteria gradually increased and the control effect gradually decreased, indicating that the higher the inoculation concentration of antagonistic bacteria, the lower the disease index and the better the control effect (Supplementary Table S7).

4 Discussion

4.1 Harm and control status of cotton *Verticillium* wilt

Xinjiang is the largest cotton production base in China, and cotton *Verticillium* wilt is one of the most important diseases affecting the Xinjiang cotton industry (Xue et al., 2013). Due to perennial continuous cropping, the return of cotton stalks to the field, poor disease resistance, and other unfavorable factors, the occurrence of cotton *Verticillium* wilt in Xinjiang is becoming increasingly serious (Liu et al., 2015a,b), resulting in huge economic losses (Zhu et al., 2023). Biological control has become a hot spot in cotton *Verticillium* wilt research because of its advantages of producing no pollution or residues, not harming humans and livestock, and the lack of resistance to pathogenic bacteria (Liu J. et al., 2023; Liu L. et al., 2023). *Bacillus velezensis* BHZ-29, a highly effective antagonistic bacterium against cotton *Verticillium* wilt, was studied in our laboratory in the early stage of the disease and control effect of 84.18% on cotton *Verticillium* wilt was achieved.

In recent years, the application of *B. velezensis* in agriculture has become increasingly extensive. In previous studies, to take advantage of its antagonistic effects *B. velezensis* has often been isolated from water, soil, air, plant roots, plant surfaces, and animal intestines (Sahal et al., 2023). *Bacillus velezensis* BHZ-29 isolated from healthy cotton plants has a strong adaptability to the natural environment. Previous studies have shown that *B. velezensis* can synthesize lipopeptides, polyketides, bacteriocins, and antibacterial proteins through the polyketide synthase synthesis pathway,

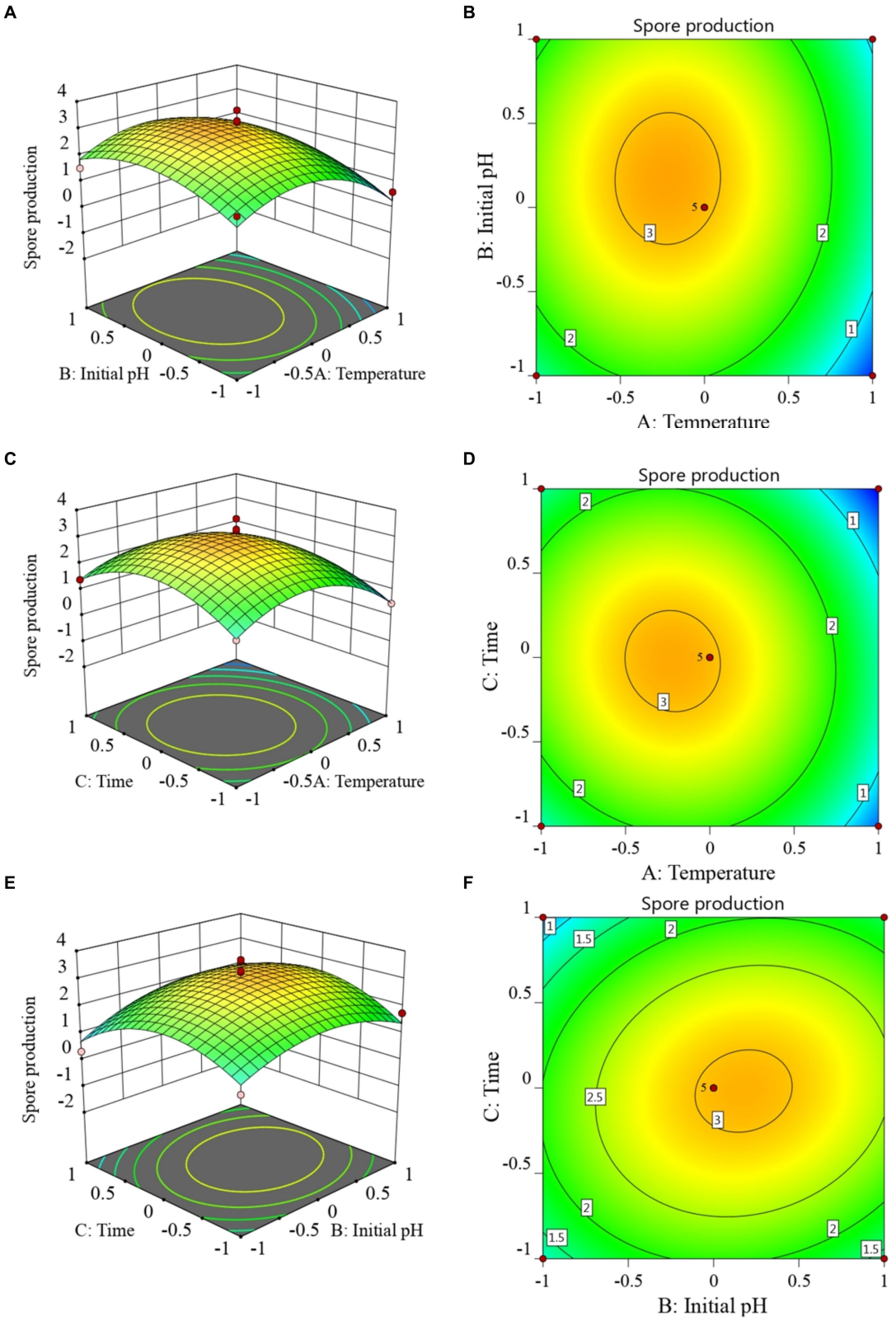

FIGURE 4
Response surface **(A, C, E)** and contour lines **(B, D, F)** of the interaction among three factors of culture condition, Temperature **(A)**, Time **(C)**, and Initial pH **(E)** on the yield of viable cells.

ribosome pathway, and non-ribosomal pathway to inhibit the growth of pathogens (Huang et al., 2023). The genome of the *B. velezensis* TSA32−1 strain contains genes related to the biosynthesis of lipopeptide antimicrobial substances, such as surfactin, and fengycin family compounds, secondary metabolites known as key factors in biological control (Kim et al., 2022). Similarly, the results of this study showed that

B. velezensis BHZ-29 bacteria and a sterile fermentation broth had a strong inhibitory effect on *V. dahliae*, and could significantly improve the agronomic traits such as plant height, root length and root weight of cotton seedlings. Similarly to the *B. velezensis* ND (Tang et al., 2023), *B. velezensis* BHZ-29 has a strong biocontrol potential by inhibiting the growth of *V. dahliae*, activating the disease resistance of the cotton system, enhancing the resistance of cotton to *Verticillium* wilt, and increasing cotton yield.

4.2 Screening of the fermentation medium and optimization of fermentation conditions for *Bacillus velezensis*

The medium composition has a large influence on the number of viable bacteria and antibacterial products resulting from microbial fermentation, and will determine the ability of microorganisms to inhibit pathogens. After optimizing the culture medium by single factor test and response surface method, the diameter of the inhibition zone of *Bacillus velezensis* P9 fermentation broth was 1.7 times larger than that of the initial inhibition zone (Liu J. et al., 2023; Liu L. et al., 2023). By orthogonal test, the optimal fermentation medium constitutes 40 g/L glucose, 20 g/L corn starch, 25 g/L hot-pressed soybean flour, 3 g/L $CaCO_3$. Verification tests suggested the yield of chrysomycin A under optimized conditions reaches up to 3,648 +/− 119 mg/L, which is increased by almost five times (Ni et al., 2021).

TABLE 7 Biocontrol efficacy of different treatments on cotton *Verticillium* wilt.

Treatment	Inoculation concentration (cfu/ml)	Disease index	Biocontrol efficacy (%)
BHZ-29 + VD	3×10^8	14.50 ± 1.80^{d}	84.28 ± 1.65^{a}
	3×10^6	20.56 ± 4.19^{c}	70.71 ± 5.43^{ac}
	3×10^5	56.67 ± 7.64^{b}	38.55 ± 4.12^{b}
CK	–	0.00 ± 0.00^{e}	–
VD	–	92.22 ± 2.55^{a}	–

Values followed by different letters within a column are significantly different ($P<0.05$) according to Duncan's new multiple range test.

In this study, an NB medium was used as the basic medium for the testing of different carbon sources, nitrogen sources, and inorganic salts, and the effects of different medium components on the number of viable bacteria and antibacterial activity of *B. velezensis* BHZ-29 were determined. The optimal medium composition for the colony number fermentation culture *B. velezensis* BHZ-29 was molasses 20.38 g/L, peptone 19.40 g/L, and magnesium sulfate 3.56 g/L, and the populations of the viable organisms were increased to 2.17×10^{10} CFU/mL using the optimal fermentation medium. The optimal medium composition for the fermentation culture of *B. velezensis* BHZ-29 was molasses 19.44 g/L, peptone 20.42 g/L, and magnesium sulfate 43.51 g/L, and the bacteriostatic titer in the optimum medium was 131.1 mg/L and the best response was 71.45%, which is more than 28-fold better than the pre-optimized conditions.

4.3 Comparison of the effects of fermentation conditions of *Bacillus velezensis* on the number of viable bacteria and antibacterial titer

The optimization of the fermentation conditions of the strain determines the biomass of the strain and the strength of the antibacterial activity (Guo et al., 2014). Optimizing the culture

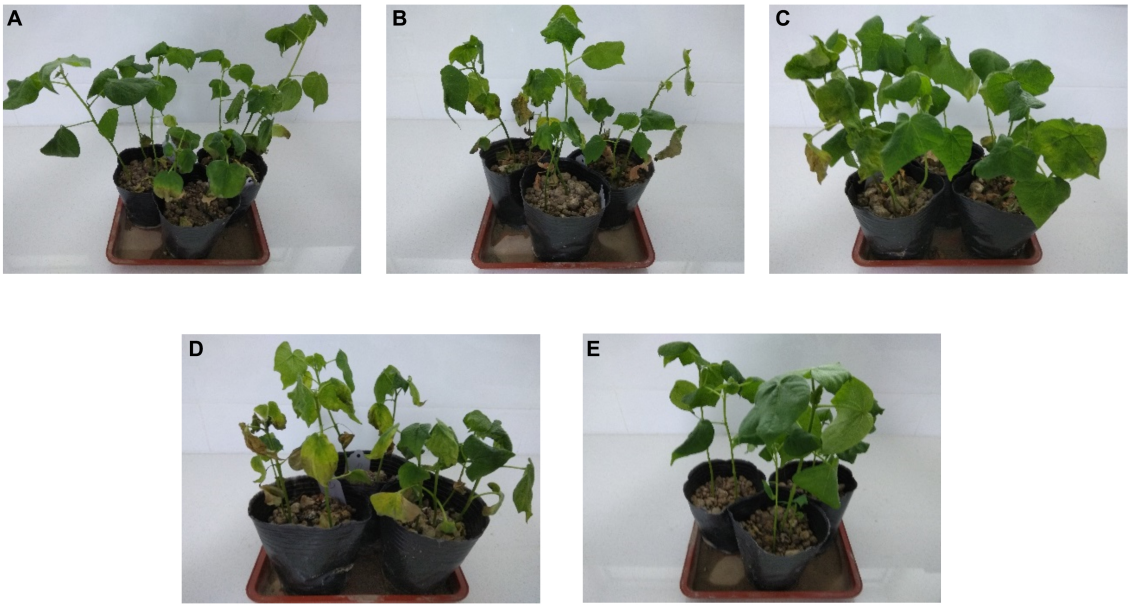

FIGURE 5
Inhibition effect of four different inoculation concentrations of antagonistic bacteria against *V. dahliae*. **(A)** 2×10^8 cfu/mL; **(B)** 2×10^6 cfu/mL; **(C)** 2×10^5 cfu/mL; **(D)** *V. dahliae*; **(E)** control.

conditions of biocontrol bacteria can increase the amount of bacteria and the yield of antimicrobial substances, thereby improving the biocontrol effect (Naeimi et al., 2020; He et al., 2023). It has previously been reported that the optimal inorganic salt for *B. amyloliquefaciens* HF-01 fermentation is magnesium sulfate, the optimal pH value is slightly acidic to neutral, and the culture temperature is 28°C (Hong et al., 2014), with these values being similar to those reported for *B. velezensis* in this study. This was also similar to the results of this study, but its optimal initial pH was 8.0, while the optimal pH in this study was 7.2, which may be due to the different long-term growth environments of the strains (Hong et al., 2014). The optimal culture conditions of *B. velezensis* BHZ-29 and other biocontrol strains are very different, and the possible mechanisms for this difference need to be further explored.

The culture conditions have a large influence on fermentation, as revealed by their different effects on the number of viable bacteria and antibacterial titer. The fermentation conditions that produced the maximum viable count were likely inconsistent with those that produced the strongest antibacterial potency. When the number of viable bacteria reached 10^9 CFU/ml or more, antibacterial substances were produced, and therefore the fermentation supernatant had an antibacterial effect (Wu et al., 2020).

4.4 Prevention and control of cotton *Verticillium* wilt by *Bacillus velezensis*

Bacillus velezensis has long attracted attention as an efficient and safe biocontrol strain that has inhibitory effects on a variety of pathogens (Pandin et al., 2019; Zhang et al., 2022). The biological control of soil-borne cotton *Verticillium* wilt has received increasing attention worldwide (Hasan et al., 2020; Bai et al., 2022; Liu J. et al., 2023; Liu L. et al., 2023; Zhang H. et al., 2023; Zhang L. et al., 2023). The antagonistic bacteria *B. velezensis* BHZ-29 screened in our laboratory can effectively inhibit the growth of *V. dahliae* and increase the peroxidase and superoxide dismutase activities in cotton, indicating that its mechanism of action has antibiosis and induces resistance. Whether there are other mechanisms involved requires further exploration. The highest control effect of cotton treated with *B. velezensis* BHZ-29 on *Verticillium* wilt was 84.18%, and the indoor pot experiment revealed a strong biocontrol potential.

Hasan et al. observed that antagonistic bacteria caused the tip of *V, dahliae* mycelium to expand, hyphae to become abnormal, the number of vacuoles to increase, mitochondria to expand, hyphae to rupture, cytoplasm to overflow, and abnormal microsclerotia (Hasan et al., 2020). Soliman et al. showed that the *Bacillus amyloliquefaciens* could cause the mycelium of the pathogen to break, swell, and deform (Soliman et al., 2022). The results of this study showed that the *B. velezensis* BHZ-29 strain could promote mycelium deformity, overflow, spore perforation, and the depression of *V. dahliae*, resulting in changes to the mycelium and spore morphology.

The induced resistance of biocontrol bacteria could interact with competition, hyperparasitism, antagonism, plant growth promotion, and other mechanisms to exert synergistic effects (Saraf et al., 2014). The reported results of the plate determination of protease, cellulase activity, glucanase activity, and dinitro salicylate method enzyme activity analyses are inconsistent, indicating that the use of the transparent circle diameter as the only indicator of enzyme production capacity is unreliable. Bao et al. (2007) and Jiang and Ding (2015) also reported similar results. With a decrease in the number of bacteria, the enzyme activity also decreased to varying degrees with the prolongation of fermentation time. This may be due to the accumulation of metabolites, apoptosis, and the decreased pH of the fermentation broth with the prolongation of fermentation time, thereby reducing enzyme activity. The *B. velezensis* BHZ-29 strain is rich in cell wall degrading enzymes, especially proteases, which are widely used in feed, leather, and food production (Bao et al., 2012). The antagonistic bacteria *B. velezensis* BHZ-29 can be used as a protease- and other enzyme-producing strain. The *B. velezensis* BHZ-29 strain produces glucanase, protease, and cellulase, with only a low-yield of chitinase. The enzyme activity is greatly affected by the stationary and logarithmic phases of the antagonistic bacteria growth, with a positive correlation between enzyme activity and growth phase (Li R. Q. et al., 2018; Li X. Y. et al., 2018).

Data availability statement

The original contributions presented in the study are included in the article/Supplementary material, further inquiries can be directed to the corresponding author/s.

Author contributions

YS: Data curation, Formal analysis, Funding acquisition, Investigation, Visualization, Writing – original draft, Writing – review & editing. XN: Investigation, Resources, Writing – original draft, Writing – review & editing. HY: Investigation, Resources, Writing – original draft. MC: Investigation, Resources, Writing – review & editing. NW: Data curation, Formal analysis, Investigation, Writing – review & editing. HB: Data curation, Resources, Writing – review & editing. FZ: Formal analysis, Investigation, Writing – review & editing. RY: Formal analysis, Investigation, Supervision, Writing – review & editing. KL: Formal analysis, Software, Supervision, Writing – review & editing.

Funding

The author(s) declare financial support was received for the research, authorship, and/or publication of this article. This work was supported by the Major Scientific and Technological Project of Xinjiang Uygur Autonomous Region of China (2022B02053-2, 2021B02004), Xinjiang Uygur Autonomous Region Science and Technology Plan Major Projects (2022A02005-3), the National Key Research and Development Program of China (2022YFD1400300, 2021YFD1400200), the National Nature Science Foundation of China (31860024).

Conflict of interest

The authors declare that the research was conducted in the absence of any commercial or financial relationships that could be construed as a potential conflict of interest.

Publisher's note

All claims expressed in this article are solely those of the authors and do not necessarily represent those of their affiliated organizations, or those of the publisher, the editors and the reviewers. Any product that may be evaluated in this article, or claim that may be made by its manufacturer, is not guaranteed or endorsed by the publisher.

Supplementary material

The Supplementary material for this article can be found online at: https://www.frontiersin.org/articles/10.3389/fmicb.2024.1355369/full#supplementary-material

References

Ahsan, T., Chen, J., Wu, Y., Irfan, M., and Shafi, J. (2017). Screening, identification, optimization of fermentation conditions, and extraction of secondary metabolites for the biocontrol of *Rhizoctonia solani* AG-3. *Biotechnol. Biotechnol. Equip.* 31, 91–98. doi: 10.1080/13102818.2016.1259016

Ahsan, T., Zang, C., Yu, S., Pei, X., Xie, J., Lin, Y., et al. (2022). Screening, and optimization of fermentation medium to produce secondary metabolites from *Bacillus amyloliquefaciens*, for the biocontrol of early leaf spot disease, and growth promoting effects on Peanut (*Arachis hypogaea* L.). *J. Fungi* 8:1223. doi: 10.3390/jof8111223

Bai, H., Feng, Z., Zhao, L., Feng, H., Wei, F., Zhou, J., et al. (2022). Efficacy evaluation and mechanism of *Bacillus subtilis* EBS03 against cotton *Verticillium* wilt. *J. Cotton Res.* 5, 1–11. doi: 10.1186/s42397-022-00134-7

Bao, H. Z., Wang, S. F., Ma, G. Z., Fu, H. R., and Ge, P. H. (2012). Activity of extracellular enzymes in marine *Bacterium* BN−1 against Vibrio. *Fish. Sci.* 31, 354–357. doi: 10.16378/j.cnki.1003-1111.2012.06.011

Bao, K., Wang, X. H., Zhang, W. Q., Luo, J. L., Nie, M., and Xiao, M. (2007). Screening of celluloytic microbes and determination of cellulase activity. *J. Biol.* 24, 56–58.

Guo, L., Zhu, W., and Zheng, A. (2014). Identification and fermentation optimization of an antibacterial *Aspergillus tubingensis* associated with the crab *Portunus trituberculatus*. *J. Pure Appl. Microbiol.* 8, 1627–1633.

Hasan, N., Farzand, A., Heng, Z., Khan, I. U., Moosa, A., Zubair, M., et al. (2020). Antagonistic potential of novel endophytic *Bacillus* strains and mediation of plant defense against *Verticillium* wilt in upland cotton. *Plan. Theory* 9:1438. doi: 10.3390/plants9111438

Hassan, M., Nadeem, S., Khaliq, K., and Perveen, I. (2011). Efficacy of bacterial isolates from soil for L-phenylalanine (L-Phe) production in different fermentation media. *J. Animal. Plant. Sci.* 21, 197–201.

He, J., Zhang, X., Wang, Q., Li, N., Ding, D., and Wang, B. (2023). Optimization of the fermentation conditions of *Metarhizium robertsii* and its biological control of wolfberry root rot disease. *Microorganisms* 11:2380. doi: 10.3390/microorganisms11102380

Hong, P., Hao, W., Luo, J., Chen, S., Hu, M., and Zhong, G. (2014). Combination of hot water, *Bacillus amyloliquefaciens* HF-01 and sodium bicarbonate treatments to control postharvest decay of mandarin fruit. *Postharvest Biol. Technol.* 88, 96–102. doi: 10.1016/j.postharvbio.2013.10.004

Huang, W., Qu, L., Gao, P., and Du, G. (2023). Bioassay and whole-genome analysis of *Bacillus velezensis* FIO1408, a biocontrol agent against pathogenic bacteria in aquaculture. *Curr. Microbiol.* 80:354. doi: 10.1007/s00284-023-03423-9

Jiang, M. X., and Ding, X. F. (2015). Screening of cellulose-decomposing bacteria and enzymatic activity determination. *Chin. Agric. Sci. Bull.* 31, 161–164.

Kim, J. A., Song, J. S., Kim, P. I., Kim, D. H., and Kim, Y. (2022). *Bacillus velezensis* TSA32−1 as a promising agent for biocontrol of plant pathogenic fungi. *J. Fungi* 8:1053. doi: 10.3390/jof8101053

Li, R. Q., Li, J. F., Zhou, Z. Y., Guo, Y., Zhang, T. T., Tao, F. F., et al. (2018). Antibacterial and antitumor activity of secondary metabolites of endophytic fungi ty5 from Dendrobium officinale. *J. Biobaased Mater. Bioenergy* 12, 184–193. doi: 10.1166/jbmb.2018.1769

Li, X. Y., Zhang, T., Yang, H. M., Chu, M., Gao, Y., Zeng, J., et al. (2018). Detection of extracellular enzymes of antagonizing cotton *Verticillium* wilt bacteria and determination of enzyme activity. *Xinjiang Agric. Sci.* 55, 1663–1673.

Lima, C. A., Viana Marques, D. A., Neto, B. B., Lima Filho, J. L., Carneiro-da-Cunha, M. G., and Porto, A. L. (2011). Fermentation medium for collagenase production by *Penicillium aurantiogriseum* URM4622. *Biotechnol. Prog.* 27, 1470–1477. doi: 10.1002/btpr.664

Lin, G., Liu, H., Liu, H. J., Yan, Q. J., and Jiang, Z. Q. (2022). Optimization of fermentation conditions for poly-gamma-glutamic acid production by *Bacillus siamensis*. *Microbiol. China* 49, 3335–3345. doi: 10.13344/j.microbiol.china.211134

Liu, L., Medison, R. G., Zheng, T. W., Meng, X. J., Sun, Z. X., and Zhou, Y. (2023). Biocontrol potential of *Bacillus amyloliquefaciens* YZU-SG146 from *Fraxinus hupehensis* against Verticillium wilt of cotton. *Biol. Control* 183:105246. doi: 10.1016/j.biocontrol.2023.105246

Liu, H. Y., Wang, W., Zhang, R. F., Wu, G., and Yao, J. (2015a). Occurrence overviews of cotton Verticillium wilt in Xinjiang. *Crop Prot.* 41, 138–142. doi: 10.3969/j.issn.0529-1542.2015.03.027

Liu, H. Y., Wang, W., Zhang, R. F., Wu, G., and Yao, J. (2015b). Occurrence research of cotton Verticillium wilt and the phylogenetic evolution analysis of *Verticillium dahliae* in Xinjiang. *Xinjiang Agricult. Sci.* 52, 65–71. doi: 10.6048/j.issn.1001-4330.2015.01.011

Liu, J., Zhang, C. Z., and Zhao, H. (2023). Optimization of medium and fermentation conditions of *Bacillus velezensis* P9 resistant to *Fusarium oxysporum*. *China Brewing* 42, 157–162. doi: 10.11882/j.issn.0254-5071.2023.02.026

Ma, C. *Study on fusarium wilt and Verticillium wilt of cotton*. Beijing: China Agriculture Press (2007), 185–246.

Ma, C., Jian, G. L., and Sun, W. J. (1997). Current status, problem and countermeasure on resistance breeding to Verticillium wilt of cotton in China. *Sci. Agric. Sin.* 32, 58–64.

Naeimi, S., Khosravi, V., Varga, A., Vagvolgyi, C., and Kredics, L. (2020). Screening of organic substrates for solid-state fermentation, viability and bioefficacy of *Trichoderma harzianum* AS12-2, a biocontrol strain against rice sheath blight disease. *Agronomy* 10:1258. doi: 10.3390/agronomy10091258

Ni, H. J., Lv, S. Y., Sheng, Y. T., Wang, H., Chu, X. H., and Zhang, H. W. (2021). Optimization of fermentation conditions and medium compositions for the production of chrysomycin a by a marine-derived strain *Streptomyces* sp. 891. *Prep. Biochem. Biotechnol.* 51, 998–1003. doi: 10.1080/10826068.2021.1885046

Pandin, C., Darsonval, M., Mayeur, C., Le Coq, D., Aymerich, S., and Briandet, R. (2019). Biofilm formation and synthesis of antimicrobial compounds by the biocontrol agent *Bacillus velezensis* QST713 in an *Agaricus bisporus* compost micromodel. *Appl. Environ. Microbiol.* 85, e00327–e00319. doi: 10.1128/AEM.00327-19

Pournejati, R., and Karbalaei-Heidari, H. R. (2020). Optimization of fermentation conditions to enhance cytotoxic metabolites production by *Bacillus velezensis* strain RP137 from the Persian Gulf. *Avicenna J. Med. Biotechnol.* 12, 116–123.

Quan, Y., Wang, L., Liu, Y., Cong, J., Xie, S., and Wu, X. (2015). Optimization of fermentation medium for glycyrrhizin biotransformation to monoglucuronyl-glycyrrhetinic acid by Plackett-Burman and box-Behnken design. *Korean Chem. Engin. Res.* 53, 321–326. doi: 10.9713/kcer.2015.53.3.321

Ruan, Z., Cui, Z., Liu, S., Xu-gang, S., Dai, Z., Luo, C., et al. (2012). Optimization of fermentation medium for beta-fructofuranosidase production from *Arthrobacter* sp 10138 using artificial neural network and genetic algorithms. *J. Food Agric. Environ.* 10, 176–181. doi: 10.1016/S0032-9592(01)00204-7

Sa, R., He, S., Han, D., Liu, M., Yu, Y., Shang, R., et al. (2022). Isolation and identification of a new biocontrol bacteria against *Salvia miltiorrhiza* root rot and optimization of culture conditions for antifungal substance production using response surface methodology. *BMC Microbiol.* 22:231. doi: 10.1186/s12866-022-02628-5

Sahal, G., Donmez, H. G., and Beksac, M. S. (2023). Cervicovaginal *Bacillus velezensis* isolate: a potential probiotic and an antagonist against *Candida* and *Staphylococcus*. *Curr. Microbiol.* 80:332. doi: 10.1007/s00284-023-03447-1

Saraf, M., Pandya, U., and Thakkar, A. (2014). Role of allelochemicals in plant growth promoting rhizobacteria for biocontrol of phytopathogens. *Microbiol. Res.* 169, 18–29. doi: 10.1016/j.micres.2013.08.009

Shang, Z. F., Fan, D. D., Deng, J. J., Ma, P., Ma, X. X., and Mi, Y. (2013). Optimization of fermentation medium for cell yield of recombinant *Pichia pastoris* during growth stage using response surface methodology. *J. Pure Appl. Microbiol.* 7, 1207–1212.

Shim, S. A., Kim, J. C., Jang, K. S., Choi, Y. H., Kim, H. T., and Choi, G. J. (2013). Role of a phytotoxin produced by *Fusarium oxysporum* f. sp. *raphani* on pathogenesis of and

resistance to the fungus. *Horticult. Sci. Technol.* 31, 626–632. doi: 10.7235/hort.2013.13052

Soliman, S. A., Khaleil, M. M., and Metwally, R. A. (2022). Evaluation of the antifungal activity of *Bacillus amyloliquefaciens* and *B. Velezensis* and characterization of the bioactive secondary metabolites produced against plant pathogenic fungi. *Biology* 11:1390. doi: 10.3390/biology11101390

Tang, Z., Cao, X., and Zhang, H. (2023). Production of iturin a by *Bacillus velezensis* ND and its biological control characteristics. *J. Basic Microbiol.* 63, 179–189. doi: 10.1002/jobm.202200473

Tian, Y., Fan, Y., Zhao, X., Zhang, J., Yang, L., and Liu, J. (2014). Optimization of fermentation medium for acetoin production by *Bacillus subtilis* SF4-3 using statistical methods. *Prep. Biochem. Biotechnol.* 44, 529–543. doi: 10.1080/10826068.2013.835731

Tu, Q., Zhao, H., and Chen, J. (2015). Optimization of medium for biological potency of fermentation supernatant of *Paenibacillus brasilensis* YS−1. *Minerva Biotechnol.* 27, 93–98.

Wang, Y., Xu, K., Lu, F., Wang, Y., Ouyang, N., and Ma, H. (2021). Increasing peptide yield of soybean meal solid-state fermentation of ultrasound-treated *Bacillus amyloliquefaciens*. *Innov. Food Sci. Emerg. Technol.* 72:102704. doi: 10.1016/j.ifset.2021.102704

Wu, H. Z., Xia, F. G., Chen, Z., Huang, K. Y., and Lin, W. F. (2020). The influence of carbon source on the antimicrobial effect of *Lactobacillus reuteri* fermentation supernatant. *Modern Food Sci. Technol.* 36, 119–125. doi: 10.13982/j.mfst.1673-9078.2020.4.016

Xue, L., Xue, Q. H., Chen, Q., Lin, C. F., Shen, G. H., and Zhao, J. (2013). Isolation and evaluation of rhizosphere actinomycetes with potential application for biocontrol of *Verticillium* wilt of cotton. *Crop Prot.* 43, 231–240. doi: 10.1016/j.cropro.2012.10.002

Zhang, T., Li, X. Y., Yang, H. M., Chu, M., and Shi, Y. W. (2018). Isolation, screening and identification of antagonistic bacteria against *Verticillium dahliae* Kleb. in Xinjiang. *Microbiol. China* 45, 2418–2428. doi: 10.13344/j.microbiol.china.180003

Zhang, L., Wang, Y., Lei, S., Zhang, H., Liu, Z., Yang, J., et al. (2023). Effect of volatile compounds produced by the cotton endophytic bacterial strain *Bacillus* sp. T6 against Verticillium wilt. *BMC Microbiol.* 23:8. doi: 10.1186/s12866-022-02749-x

Zhang, R. S., Wang, F. G., Qi, Z. Q., Qiao, J. Q., Du, Y., Yu, J. J., et al. (2022). Iturins produced by *Bacillus velezensis* Jt84 play a key role in the biocontrol of rice blast disease. *Biol. Control* 174:105001. doi: 10.1016/j.biocontrol.2022.105001

Zhang, H., Zhang, R., Qiao, J., Yu, J., Qi, Z., Du, Y., et al. (2023). Optimization of *Bacillus amyloliquefaciens* lx−11 suspoemulsion by response surface methodology to control rice bacterial blight. *Biol. Control* 68, 169–179. doi: 10.1007/s10526-023-10186-6

Zhu, H. Q., Feng, Z. L., Li, Z. F., Shi, Y. Q., Zhao, L. H., and Yang, J. R. (2013). Characterization of two fungal isolates from cotton and evaluation of their potential for biocontrol of Verticillium wilt of cotton. *J. Phytopathol.* 161, 70–77. doi: 10.1111/jph.12027

Zhu, Y., Zhao, M., Li, T., Wang, L., Liao, C., Liu, D., et al. (2023). Interactions between *Verticillium dahliae* and cotton: pathogenic mechanism and cotton resistance mechanism to *Verticillium* wilt. *Front. Plant Sci.* 14:1174281. doi: 10.3389/fpls.2023.1174281

frontiers | Frontiers in Microbiology

TYPE Original Research
PUBLISHED 29 April 2024
DOI 10.3389/fmicb.2024.1387222

OPEN ACCESS

EDITED BY
Ragini Bodade,
Savitribai Phule Pune University, India

REVIEWED BY
Jianhua Fan,
East China University of Science and Technology, China
Han Sun,
Shenzhen University, China

*CORRESPONDENCE
Dongzhe Sun
✉ merdzsun@sina.com
Zhao Zhang
✉ zhangzhao900626@sina.com

†These authors share first authorship

RECEIVED 17 February 2024
ACCEPTED 01 April 2024
PUBLISHED 29 April 2024

CITATION
Yuan Y, Zhao T, Gao W, Ye W, Chen Y, Sun D and Zhang Z (2024) Reactive oxygen species derived from NADPH oxidase as signaling molecules regulate fatty acids and astaxanthin accumulation in *Chromochloris zofingiensis*. *Front. Microbiol.* 15:1387222. doi: 10.3389/fmicb.2024.1387222

Reactive oxygen species derived from NADPH oxidase as signaling molecules regulate fatty acids and astaxanthin accumulation in *Chromochloris zofingiensis*

Yi Yuan[1†], Tiantian Zhao[1†], Weizheng Gao[2], Wenqi Ye[2], Yuling Chen[1], Dongzhe Sun[1*] and Zhao Zhang[1*]

[1]Ministry of Education Key Laboratory of Molecular and Cellular Biology, Hebei Collaborative Innovation Center for Eco-Environment, Hebei Research Center of the Basic Discipline of Cell Biology, College of Life Sciences, Hebei Normal University, Shijiazhuang, China, [2]School of Life Sciences, Hebei University, Baoding, China

Abiotic stresses can increase the total fatty acid (TFA) and astaxanthin accumulation in microalgae. However, it remains unknown whether a unified signal transduction mechanism exists under different stresses. This study explored the link between nicotinamide adenine dinucleotide phosphate (NADPH) oxidase-derived reactive oxygen species (ROS) and the accumulation of fatty acids and astaxanthin in *Chromochloris zofingiensis* under three abiotic stresses. Results showed significant increases in fatty acid, astaxanthin, and ROS levels under nitrogen deficiency, phosphorus deficiency, and high-salinity stress. The introduction of the NADPH oxidase inhibitor diphenyleneiodonium (DPI) decreased the content of these components. This underscores the pivotal role of NADPH oxidase-derived ROS in the accumulation of fatty acid and astaxanthin under abiotic stress. Analysis of transcriptomes across three conditions following DPI addition revealed 1,445 shared differentially expressed genes (DEGs). Enrichment analysis revealed that biotin, betalain, thiamine, and glucosinolate may be important in stress responses. The heatmap demonstrated that DPI notably suppressed gene expression in the fatty acid and carotenoid biosynthesis pathways. Our findings underscore the pivotal role of NADPH oxidase-derived ROS in the accumulation of fatty acid and astaxanthin under abiotic stresses.

KEYWORDS

NADPH oxidase, ROS, fatty acid, astaxanthin, transcriptomic analysis, WGCNA analysis, *Chromochloris zofingiensis*

1 Introduction

Microalgae respond rapidly to environmental changes and can accumulate large amounts of bioactive compounds such as proteins, fatty acids, vitamins, and pigments in a short time, which makes them ideal sources for the production of energy, medicine, food, and feed, including biodiesel, DHA, EPA, beta-carotene, and astaxanthin (Maity et al., 2014; Goh et al., 2019; Sun et al., 2019; Chen et al., 2020). Among them, fatty

acids and carotenoids are the typical stress-induced valuable substances in microalgae. Numerous studies have attempted to elucidate the metabolic mechanisms underlying fatty acid and carotenoid accumulation under abiotic stresses. High light intensity, nutrient deficiency (nitrogen, phosphorus, and sulfur), and high salinity are the most commonly used strategies for promoting fatty acid and carotenoid accumulation in microalgae (Mao et al., 2018; Liu et al., 2019; Chen et al., 2020; Hang et al., 2020). Under stress conditions, the growth of algal cells generally tends to decrease, and the metabolism of algal cells shifts toward lipid synthesis and accumulation (Nanda et al., 2021). Carotenoid metabolism s also enhanced, resulting in a significant increase in the production of secondary carotenoids. For instance, astaxanthin, is a secondary carotenoid with powerful antioxidant properties that helps cells resist unfavorable environments (Kubo et al., 2022). However, whether a universal signal transduction mechanism exists under different stress conditions remains unclear. Reactive oxygen species (ROS) are by-products of oxygen metabolism and are considered important signaling molecules in algal cells. In particular, ROS can regulate defense responses under adverse conditions (Waszczak et al., 2018; Signorelli et al., 2019). However, excess ROS can cause oxidative damage, leading to apoptosis (Baxter et al., 2014). Studies have speculated that ROS have a potential relationship with fatty acid and carotenoid biosynthesis and are positively correlated with lipid content under nutrient-deprived conditions (Seo et al., 2019; Roy et al., 2021; Liu et al., 2023). In *Chlorella sorokiniana*, nitrogen limitation and hydrogen peroxide (H_2O_2) treatment induced ROS elevation, upregulated the expression of lipogenic genes (mitogen-activated protein kinase, heteromeric acetyl-CoA carboxylase beta subunit, β-ketoacyl-ACP synthase III, and diacylglycerol acyltransferase), and promoted lipid synthesis (Wang L. et al., 2023). In *Haematococcus pluvialis*, ROS treatment and abiotic stress treatment can significantly increase astaxanthin production (Cray and Levine, 2022). ROS can be generated by multiple sources, including the mitochondrial electron transport chain, electron transport chain of chloroplast photosystem I, nicotinamide adenine dinucleotide phosphate (NADPH) oxidase, and other organelles associated with ROS production (Shi et al., 2017). However, the source of ROS, which plays a key role in abiotic stress-induced fatty acid and carotenoid accumulation in microalgae, remains unknown.

Plant NADPH oxidase, also known as the respiratory burst oxidase homolog (RBOH), is a homolog of the mammalian macrophage NADPH oxidase gp91phox (Kaur et al., 2014). ROS produced by plant NADPH oxidase can act as secondary messengers in numerous biological processes, such as plant growth and development, plant reproduction, hormone regulation, and biotic and abiotic stress responses. Modulation of NADPH oxidase activity improves seed germination and root growth tolerance to water and oxidative stress (Wang Q. et al., 2023). Application of an NADPH oxidase inhibitor reversed the negative effects of chromium (Cr) stress (Singh et al., 2023). The structure of the plant NADPH oxidase is conserved and comprises two EF-hands structures, six α-transmembrane helical domains, one flavin adenine dinucleotide (FAD) domain, and one NADPH domain. Two EF chiral structures in the N-terminal region of *Arabidopsis thaliana AtRBOH* bind to calcium ion (Ca^{2+}) to activate *AtRBOH*, which catalyzes the transfer of electrons from NADPH (electron donor) to O_2 (electron acceptor) via FAD, membranes, and heme to generate O_2^-, which is involved in ROS production (Kaya et al., 2019). Diphenyleneiodonium (DPI) is an NADPH oxidase inhibitor that inhibits ROS production by NADPH oxidase (Foreman et al., 2003). Inhibition of NADPH oxidase by DPI treatment can lead to abnormal pollen tube growth in spruce plants (Liu et al., 2009). Following the treatment of *A. thaliana* tissues with DPI under high-intensity light or heat stress, it was observed that ROS production was hindered by the inhibition of NADPH oxidase, ultimately preventing systematic tissue adaptation (Suzuki et al., 2013). Although NADPH oxidase-derived ROS have been extensively studied in higher plants, the universal signaling role in microalgae under abiotic stresses remains unknown.

To fill this gap in the relationship between NADPH oxidase-derived ROS and fatty acid and carotenoid accumulation under abiotic stress, we investigated the effects of the NADPH oxidase inhibitor DPI on the cellular ROS level, total fatty acid (TFA) content, and carotenoid content in *Chromochloris zofingiensis* under three abiotic stress conditions, including nitrogen deficiency, phosphorus deficiency, and high salinity stress. In addition, comparative transcriptome analysis was conducted to provide a theoretical basis for future studies related to TFA metabolism in microalgae and potential loci for molecular biological modifications of microalgae. Our study aimed to reveal the correlation between intracellular ROS levels and lipid accumulation and carotenoids, and elucidate the role of NADPH oxidase-derived ROS in the response to abiotic stress in *C. zofingiensis*.

2 Materials and methods

2.1 Strains and culture conditions

Chromochloris zofingiensis from the American Typical Culture Conservation Center (ATCC, Rockville, MD, USA) was used in this study. To activate the *C. zofingiensis* cells, 10 ml of seed solution was inoculated into a 500 ml conical flask (with filter membrane) containing 100 ml of Kuhl growth medium (Gao et al., 2023). Glucose was used as the carbon source at a concentration of 5 g L^{-1} and incubated in the dark at 150 rpm in an incubator at 25°C. After incubation for 4 days, when the cells were in the late exponential stage, the active cells were inoculated into 100 ml of Kuhl medium and kept in darkness for 4 days to improve the viability of the cells. The resulting culture was used as a seed for further growth. In order to investigate the influence of NADPH oxidase-derived ROS on fatty acid accumulation, the seed culture was gathered, resuspended in 0.5 g L^{-1} dry weight (DW), and cultivated in the dark under nitrogen deficiency (KNO_3^- deficient medium, denoted as -N group), phosphorus deficiency (PO_4^- deficient medium, denoted as -P group), and high-salinity stress (additional 20 g L^{-1} NaCl, denoted as HS group). To study the effect of the NADPH oxidase inhibitor, 25 μg ml^{-1} DPI (DPI uses DMSO for dissolution) added to nitrogen-deficient medium was denoted as the -N + DPI group, 5 μg ml^{-1} DPI added to phosphorus deficient medium and high salt medium, and denoted as the -N + DPI, -P + DPI, and HS + DPI groups, respectively. Fresh Kuhl medium without any additional chemicals was used as the control. After 6 h of induction, fresh algal cells were collected to measure the intracellular ROS and Ca^{2+}

levels. After 4 days of induction, fresh algal cells were collected and lyophilized in a vacuum freeze dryer to measure TFA and carotenoid contents. To rule out the cytotoxic effect of DMSO, 100 μl DMSO was added to group C for a validation experiment (**Supplementary Figure 1**).

For comparative transcriptome sequencing, samples were collected 6 h after induction. The samples were centrifuged at 7,000 × *g* for 1 min at 4°C and the cells were rapidly frozen in liquid nitrogen. Stored at −80°C for subsequent experiments. All measurements were performed in triplicates.

To make a clear description, the experimental design was drawn and showed in **Supplementary Figure 2**.

2.2 Evaluate microalgal growth status by cell count

Chromochloris zofingiensis cells were cultured in different stress-treated media, and cell culture suspensions from 0, 24, 48, 72, 96, 120, and 144 h were taken for cell counting using hemocytometer. The cell suspension at each time point was first blown and mixed with a pipette gun. Then 10 μl of cell suspension was aspirated and quickly punched along the lower edge of the coverslip of the hemocytometer. Waiting for the microalgal cells to fall into the grid of the hemocytometer, they were counted using a light microscope and the total number of cells was calculated. All measurements were performed in triplicate.

2.3 Evaluate microalgal growth status by DW

After 4 days of cultivation 5 ml of algal cells were collected from different culture conditions, and the dry cell weight was measured. Each sample was washed three times with distilled water and filtered onto pre-weighted Whatman 0.47 mm filter paper sheets using a diaphragm pump, followed by vacuum drying at 50°C for 4 h to evaporate the water from the cells, and the difference in the filter paper was the DW of the cells. All measurements were performed in triplicate.

2.4 Measurement of cellular ROS level

Intracellular ROS levels were measured with a ROS assay kit (Beyotime Institute of Biotechnology, China). This kit uses intracellular ROS to oxidize diethyl 2′,7′-dichlorofluorescein diacetate (DCFH-DA) to the highly fluorescent compound dichlorofluorescein (DCF), and the fluorescence of DCF was measured to calculate intracellular ROS level (Cash et al., 2007). Dilution of DCFH-DA with fresh culture medium solution was carried out in 1:1,000 to 10 μmol L^{-1} final concentration. The cells were collected and incubated at 25°C for 20 min. The mixture was inverted every 5 min during incubation to ensure sufficient contact between the probe and the cells. At the end of the incubation period, the cells were washed three times with the fresh culture medium to remove any residual DCFH-DA which did not enter the cells. Finally, the fluorescence intensity was measured with a Tecan (Switzerland, Spark Cyto) enzyme marker at 480 and 530 nm respectively. Meanwhile, fluorescence imaging of ROS was observed using an inverted microscope (Axio Vert.A1). All measurements were performed in triplicates.

2.5 Measurement of cellular calcium ions level

Intracellular Ca^{2+} levels were measured using a Fluo-4 Calcium Assay Kit (Beyotime Institute of Biotechnology, China). The Ca^{2+} fluorescent probe Fluo-4 AM is almost non-fluorescent; once it enters the cell, it is hydrolyzed by intracellular esterases and binds to Ca^{2+}, which emits green fluorescence. Cells were inoculated in 96-well black multi-well plates according to the kit instructions, and the number of cells per well was maintained at 100–10,000. The cells were then centrifuged at 1,000 × *g* for 5 min, the supernatant was discarded, the cells were washed with PBS, and incubated for 20 min at 25°C in the dark. Finally, the fluorescence intensity was measured at 490 nm excitation and 525 nm emission wavelengths using a Tecan enzyme marker. All measurements were performed in triplicates.

2.6 Carotenoid extraction and measurement

After lyophilization, 20 mg of algal powder was thoroughly crushed with a mortar. Extraction was performed using chromatographic-grade acetone, and the algal residue was collected by centrifugation at 10,000 rpm at 4°C for 5 min after shaking. The algal residue was extracted twice with chromatographic acetone until it became colorless. The filtered acetone extracts were combined and the pigments were dried with nitrogen before being dissolved in 1 ml of chromatographic acetone. The resulting solution was then filtered with an organic filter membrane of 0.22 μm and stored in a brown sample bottle (Zhang Z. et al., 2017). The carotenoid content was quantified using a Waters 2695 HPLC system. Measurements according to the method proposed by Ip and Chen (2005). The chemical standards of β-carotene, lutein and astaxanthin were purchased from Sigma (St. Louis, MO, USA). All measurements were performed in triplicate.

2.7 Total fatty acid content analysis

Lyophilized cells (20 mg) were incubated with 2 ml of 1% methanol sulfate solution (v/v, containing 0.01% BHT) and 0.5 ml of heptadecanoic acid at 85°C for 2.5 h for fatty acid methyl ester (FAMEs). The reaction mixture was then shaken for 30 min. After cooling, 1 ml of 0.75% NaCl solution was added and the FAMEs were extracted using 2 ml of chromatographic-grade hexane. The supernatant was collected via centrifugation at 5,000 × *g* for 5 min, and the samples were subsequently nitrogen blown using a pressurized nitrogen concentrator. The sample was filtered through a disposable microporous filter (13 mm × 0.22 μm). FAMEs

were performed by 7890A gas chromatography (Agilent, USA). All measurements were performed in triplicates.

2.8 Comparative transcriptome analysis

After 6 h of cultivation under each culture condition, 50 ml of algal cell cultures was collected in sterile enzyme-free centrifuge tubes, centrifuged at 5,000 × *g* for 3 min at 4°C, the supernatant was discarded, and the precipitated cells were rapidly frozen in liquid nitrogen. The TRIzol reagent (Invitrogen) was used to extract total cell RNA, and the genomic DNA was removed with DNase I (Code No. 9108/9109, Beijing, China). To determine the quality of the extracted RNA, a 2100 Bioanalyzer (Agilent, Santa Clara, CA, USA) and NanoDrop-2000 (NanoDrop Technologies, Wilmington, DE, USA) were used. RNA-seq transcriptome libraries were prepared using the TruSeq RNA sample preparation kit (Illumina, San Diego, CA, USA) with 1 μg of total RNA. Under the effect of reverse transcriptase, single-stranded cDNA was synthesized by reversing the mRNA as a template using random primers, followed by two-stranded synthesis to form a stable double-stranded structure. A cDNA library with a cDNA target fragment of 300 bp was chosen and amplified via PCR on 2% low-range super agarose, and 15 cycles of PCR were carried out using Phusion DNA polymerase (NEB) to produce the final library. RNA-seq data are publicly available through the Genome Sequence Archive under the accession number CRA012296.

Following the retrieval of gene read counts, samples were scrutinized for differentially expressed genes (DEGs) between groups. Genes that showed differential expression were identified, and their functions were explored. The difference analysis software was: DESeq2, the screening threshold was: $|\log_2(\text{fold change})(\log_2\text{FC})| \geq 1$ and p-adjust < 0.05, when a gene met both conditions, then the gene was considered as a DEGs (Wang et al., 2010). To control for calculated false positive rates, four multiplex tests (Bonferroni, Holm, BH, and BY) were used to correct P values, and in general, the Gene Ontology (GO) function and Kyoto Encyclopedia of Genes and Genomes (KEGG) pathway were considered significantly enriched when the corrected $P \leq 0.05$. All measurements were performed in triplicate.

2.9 Weighted correlation network analysis

Weighted correlation network analysis (WGCNA) is a systems biology method used to characterize gene association patterns between different samples by clustering highly correlated genes into modules (Langfelder and Horvath, 2008). After background correction and normalization of gene expression data, abnormal and small variation genes were filtered and outlier samples were excluded. The strength of the correlation between processed genes followed a scale-free distribution, as demonstrated by the coefficient matrix constructed using Spearman's linear correlation coefficients. The key parameter β value for the WGCNA analysis was then determined. Clustering of similar gene expression patterns into modules. Association between the gene network and the phenotype of interest, as well as the hub genes in the network.

2.10 Quantitative real-time PCR analysis

Real-time fluorescence quantitative PCR (RT-qPCR) was used to verify the transcriptome data using a real-time fluorescence quantitative PCR system (Bio-Rad, Hercules, CA, USA). Ten genes were selected and Primer Premier 5 was used to design primers (**Supplementary Table 1**). One microgram of RNA in each sample was reverse-transcribed into cDNA using the QuantScript RT Kit (Tiangen, China), and then amplified by RT-qPCR. Three PCR were performed for each sample. Evaluation of relative gene expression by $2^{-\Delta\Delta CT}$ method (Livak and Schmittgen, 2001).

2.11 Statistical analysis

All experiments were performed with three biological replicates. Variability is shown as mean and standard deviation (SD). The experimental plots were plotted using Origin 2023. The data were analyzed quantitatively and statistically by one-way analysis of variance (ANOVA) using SPSS version 19.0. The differences were statistically significant ($P < 0.05$).

3 Results and discussion

3.1 Effect of NADPH oxidase-derived ROS on cells, DW, ROS, and Ca^{2+} of *C. zofingiensis* under abiotic stress conditions

The growth curves of *C. zofingiensis* under different abiotic stresses with or without DPI addition were firstly measured. As the cultivation time increased, the cell number in the control group increased at a faster rate, but cell division was inhibited to varying degrees in all treatment groups (**Figure 1A**). Different with the cell number, the DW of -N, -P, and HS groups were not significantly different from the control group, but the DW of all the DPI-added groups were significantly reduced (**Figures 1B, C**). The average DW of *C. zofingiensis* cell in DPI addition groups were generally lower than that in stress treatment groups (**Figure 1D**). Consequently, the DW per cell was significantly decreased by DPI. These suggested that NADPH oxidase derived ROS might be a key regulator in abiotic stressed induced storage components accumulation. After 4 days of cultivation, DW was slightly reduced in the -N, -P, and HS groups compared with that in the control group (**Figure 1C**). In addition, the addition of DPI significantly decreased DW in the -N, -P, and HS groups by 27.11%, 23.04%, and 40.11%, respectively. This result is in agreement with previous study, which showed that *C. zofingiensis* DW gradually decreased with an increase in DPI concentration compared to the control (Sun and Zhang, 2021).

The intracellular ROS levels were measured at 0, 6, 24, 48, and 96 h of cultivation, which were firstly increased at 6 h of cultivation, and then gradually decreased along the cultivation (**Supplementary Figure 3**). As the incubation time increased, the ROS level gradually decreased, so we focused on analyzing the ROS level after 6 h of cultivation. Compared with the control group, the ROS level increased significantly under -N, -P, and HS conditions at 6 h,

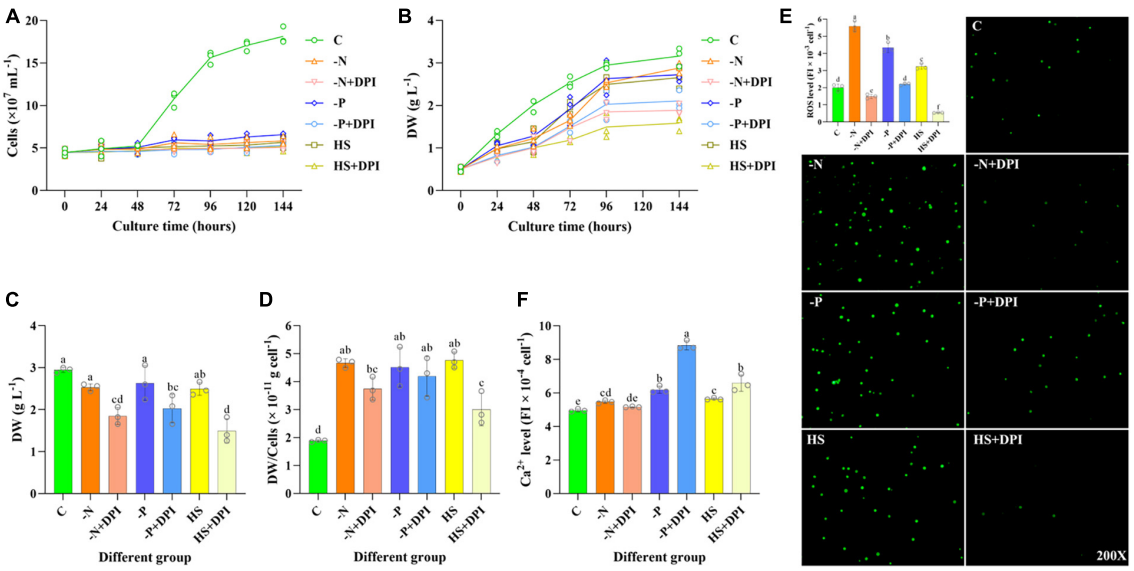

FIGURE 1
Growth status, ROS and Ca^{2+} levels of *Chromochloris zofingiensis*. **(A)** *C. zofingiensis* growth curve. **(B)** Dry weight (DW) change of *C. zofingiensis* from 0 to 6 days. **(C)** DW of *C. zofingiensis* cultured for 4 days. **(D)** Average DW per cell of *C. zofingiensis* cultured for 4 days. **(E)** ROS level of *C. zofingiensis* in control, stress, and DPI group after 6 h of induction. The 200× means that the inverted microscope is 200 times larger. **(F)** Ca^{2+} level of *C. zofingiensis* in control, stress, and DPI group after 6 h of induction. The error bars show the standard deviation. Different letters (a, b, c, d, e) indicate a significant difference between groups ($P < 0.05$).

with respective ratios of 2.78, 2.16, and 1.61 times higher than the control (Figure 1E). This was consistent with the previous studies that microalgal ROS are elevated under stress conditions (Cui et al., 2020; Liu et al., 2023). Specifically, the addition of DPI significantly decreased ROS levels by 73.32%, 49.06%, and 83.13% under -N, -P, and HS conditions, respectively (Figure 1E). Meanwhile, the imaging results of ROS levels were observed by using an inverted microscope to aid in verifying the reliability of the above data (Figure 1E). The -N, -P, and HS groups showed stronger fluorescence level compared to the control group and the treatment group with DPI addition, indicating that -N, -P, and HS increased the intracellular ROS level, but the addition of DPI inhibited ROS production. These results suggest that NADPH oxidase is a universal producer of intracellular ROS in *C. zofingiensis* under stressful conditions.

Apart from ROS, Ca^{2+} is also involved in a variety of signaling pathways in microalgae, affecting a variety of metabolic pathways (Sagi and Fluhr, 2001; Chen et al., 2014). Ca^{2+} may be involved in the regulation of lipid accumulation, as it was previously shown that lipid accumulation increased after the addition of 100 mM $CaCl_2$ in *Chlamydomonas reinhardtii* and a synergistic effect was observed between NaCl and $CaCl_2$ (Hang et al., 2020). In higher plants, ROS production leads to the activation of plasma membrane Ca^{2+} channels, which in turn increases the cytosolic free Ca^{2+} concentration and regulates root growth (Pei et al., 2000). Thus, we measured the cytosolic free Ca^{2+} concentration to determine whether it is another universal signaling molecule in *C. zofingiensis* under abiotic stress. As shown in Figure 1F, intracellular Ca^{2+} levels were slightly higher under -N, -P, and HS stress conditions compared to the control group, whereas TFA content showed the same trend, indicating that intracellular Ca^{2+} levels under stress conditions may be correlated with fatty acid accumulation. However, the addition of DPI significantly increased the intracellular Ca^{2+} levels under phosphorus deficiency and high-salinity conditions. From the above results, it can be inferred that NADPH oxidase mediates ROS generation and triggers cytoplasmic calcium signaling; however, Ca^{2+} is not regulated in the same way as NADPH oxidase-derived ROS under different stresses.

3.2 Effect of NADPH oxidase-derived ROS on fatty acid accumulation under abiotic stresses

Increased fatty acid accumulation is a typical response of microalgae to abiotic stresses (Yu et al., 2018; Shetty et al., 2019; Latsos et al., 2020; Nanda et al., 2021). Our experiments showed that the intracellular TFA content of *C. zofingiensis* was approximately 23.07% of DW in the control group, whereas it accumulated to 45.75%, 29.59%, and 29.36% of DW under -N, -P, and HS conditions, which was 1. 98-, 1. 28-, and 1.27-fold of that in the control group, respectively (Figure 2A). This suggests that fatty acid accumulation in *C. zofingiensis* can be enhanced by multiple stressors, and the addition of the NADPH oxidase inhibitor DPI significantly reduced TFA content from 45.75% to 34.26%, 29.36% to 21.23%, and 29.59% to 22.60% under -N, -P, and HS conditions, respectively. Given the decrease in ROS levels in the DPI-treated groups, it is reasonable to speculate that NADPH oxidase-derived ROS may play an important role in regulating fatty acid metabolism in *C. zofingiensis* under various abiotic stresses.

Compared to the control group, the percentage of saturated fatty acids (SFA) decreased from 24.26% to 16.79%, 17.45%, and 19.28%, under -N, -P, and HS stress conditions, respectively,

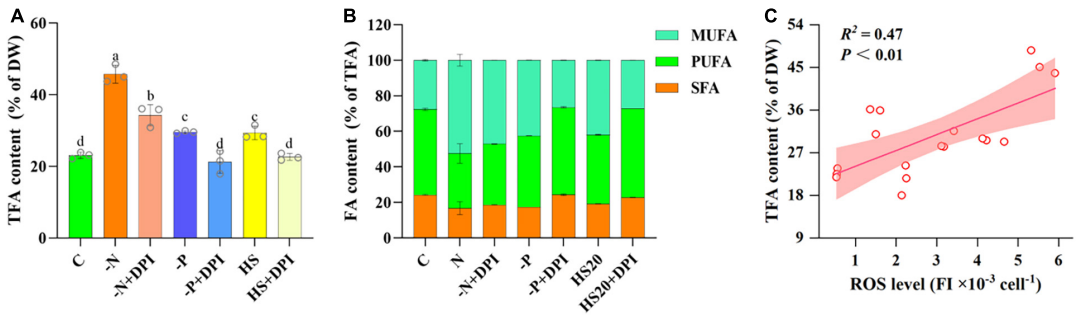

FIGURE 2
Fatty acids content. **(A)** TFA of *Chromochloris zofingiensis* in control, stress, and DPI group after 4 days of cultivation. **(B)** Percentage of fatty acids to TFAs content of *C. zofingiensis* after 4 days of cultivation. **(C)** Relationship between the ROS level and TFA content of *C. zofingiensis* under different culture conditions. Lines are linear fit with Pearson correlation coefficient (R^2). Shaded areas indicate 95% confidence bands. The error bars show the standard deviation. Different letters (a, b, c, d) indicate a significant difference between groups ($P < 0.05$).

and the percentage of unsaturated fatty acids (USFA) increased from 75.74% to 83.21%, 82.55%, and 80.72%, respectively. The percentage of monounsaturated fatty acids (MUFA) increased from 27.59% to 52.50%, 42.59%, and 41.96%, whereas the percentage of polyunsaturated fatty acids (PUFA) decreased from 48.15 to 30.71%, 39.97%, and 38.76%, respectively (**Figure 2B** and **Table 1**). It has been shown that nitrogen starvation could increase the SFA content but decrease the USFA in microalgae (*Dunaliella tertiolecta*, *Dunaliella salina*, *Chlorella minutissima*, and *Desmodesmus* sp. MCC34) (Nagappan and Kumar, 2021). On the contrary, the USFA and MUFA percentages of *C. zofingiensis* were significantly increased under high salt stress (Vitali et al., 2023). These results indicate that the relative abundance of fatty acids in microalgae is highly dependent on the culture conditions (Liu et al., 2016; Mao et al., 2018; Zhang et al., 2021). It is worth noting that in our study, the addition of DPI reversed the variation trends of SFA, MUFA, and PUFA percentages under three stresses.

Palmitic acid (C16:0), oleic acid (C18:1), linoleic acid (C18:2), and α-linolenic acid (C18:3) were the main fatty acids in *C. zofingiensis*, accounting for more than 85% of the TFAs. Under the three stress treatment conditions, the ratio of C18:1 increased significantly compared to the control, where it was 48.84%, 39.13%, and 40.30% of TFA under -N, -P, and HS, respectively, which was significantly higher than the 25.57% TFA of the control group. This is in agreement with Zhang et al. (2021) that the production of C18:1 increased under nitrogen deficiency stress conditions. C18:1 can balance oxidative stability and low temperature performance, and its high abundance is beneficial to improve the quality of biodiesel. DPI does restore the stressed cultures to control for the most part, but it is quite interesting to note that C18:1 in the nitrogen starved DPI culture remains elevated, which contributes to a reduction in the PUFA content. In contrast to C18:1, the content of C16:2 and C18:3 in TFAs was significantly lower under stress conditions than in the control group. Similarly, the addition of DPI reversed this increase and significantly decreased C18:1 content. However, the C16:2 and C18:3 contents showed a slight increase after adding DPI. Compared to the control group, the trends of fatty acid ratio changes under the three stresses tended to be consistent, and the similar trends of all three stresses were reversed after the addition of DPI. Thus, inhibition of NADPH oxidase could reverse the fatty acid changes that arise from abiotic stress in *C. zofingiensis*. This suggests that NADPH oxidase-derived ROS may play a key role in the regulation of TFA content and fatty acid ratio under abiotic stress.

The relationship between ROS and fatty acid biosynthesis was verified by Pearson correlation analysis (**Table 2**). The Pearson correlation coefficients of intracellular TFA content and ROS levels were 0.909, 0.910, and 0.960 under -N, -P, and HS conditions, respectively. Thus, it can be concluded that the accumulation of TFAs was strongly correlated with intracellular ROS levels. The accumulation of TFAs in *C. zofingiensis* increased with an increase in intracellular ROS levels within a certain range (**Figure 2C**). Several studies have indicated that ROS levels may be correlated with lipid accumulation. For instance, the accumulation of stress induced lipid in *Tetradesmus obliquus* KMC24 has been linked to elevated intracellular levels of ROS (Roy et al., 2021). In *C. reinhardtii*, high salt concentration could inhibit the growth of microalgae and induce three main stresses: osmotic, ionic (salt), and oxidative stress (Khona et al., 2016). Excessive cadmium has also been shown to elevate intracellular the concentration of lipid and ROS levels in *Monoraphidium* sp. QLY-1 simultaneously (Zhao et al., 2019). However, our results further confirmed that NADPH oxidase-derived ROS levels under different stress conditions were positively correlated with TFA content. These results indicate that NADPH oxidase-derived ROS may act as universal signaling molecules to regulate fatty acid accumulation under abiotic stress conditions.

3.3 Effect of NADPH oxidase-derived ROS on carotenoids content under abiotic stresses

Apart from TFAs, secondary carotenoids are another typical component that would accumulate under stress conditions. Astaxanthin is a valuable secondary carotenoid produced by *C. zofingiensis* (Zhang K. et al., 2017). ROS is been considered an important regulator of astaxanthin accumulation in microalgae cells (Cray and Levine, 2022). In the present study, the carotenoid content of *C. zofingiensis* was measured 96 h after induction. All primary carotenoids, including lutein and β-carotene, showed a severe decrease in response to -N, -P,

TABLE 1 The percentage of fatty acid profiles (% of TFA) of *Chromochloris zofingiensis* in different stress treatment groups.

Fatty acid component	Control	-N	-N + DPI	-P	-P + DPI	HS	HS + DPI
C16:0	22.48 ± 0.09	16.37 ± 3.36	18.68 ± 0.14	17.45 ± 0.02	23.04 ± 0.35	19.28 ± 0.08	21.42 ± 0.05
C16:1	2.03 ± 0.29	3.66 ± 1.99	2.52 ± 0.12	1.50 ± 0.05	1.94 ± 0.30	1.66 ± 0.24	2.12 ± 0.05
C16:2	6.80 ± 0.19	5.12 ± 0.85	5.22 ± 0.07	4.85 ± 0.04	6.59 ± 0.61	5.68 ± 0.09	7.37 ± 0.07
C16:3	1.73 ± 0.06	0.49 ± 0.26	0.72 ± 0.01	1.83 ± 0.05	2.65 ± 0.26	1.37 ± 0.04	1.79 ± 0.01
C18:1	25.57 ± 1.08	48.84 ± 3.60	44.54 ± 0.10	41.09 ± 0.06	24.47 ± 0.17	40.30 ± 0.26	24.98 ± 0.03
C18:2	26.36 ± 0.71	17.27 ± 6.87	20.60 ± 0.08	21.35 ± 0.06	23.97 ± 0.10	22.04 ± 0.11	26.88 ± 0.10
C18:3	12.03 ± 0.12	7.22 ± 0.66	7.09 ± 0.05	8.31 ± 0.09	14.66 ± 0.21	9.14 ± 0.08	12.50 ± 0.16
SFA	24.26 ± 0.25	16.79 ± 3.64	18.68 ± 0.14	17.45 ± 0.02	24.30 ± 0.44	19.28 ± 0.08	22.89 ± 0.06
USFA	75.74 ± 0.25	83.21 ± 3.64	81.32 ± 0.14	82.55 ± 0.02	75.70 ± 0.44	80.72 ± 0.08	77.11 ± 0.06
MUFA	27.59 ± 0.42	52.50 ± 3.33	47.06 ± 0.08	42.59 ± 0.11	26.41 ± 0.15	41.96 ± 0.19	27.09 ± 0.06
PUFA	48.15 ± 0.67	30.71 ± 5.50	34.26 ± 0.14	39.97 ± 0.08	49.29 ± 0.36	38.76 ± 0.27	50.02 ± 0.01

TABLE 2 Correlation coefficients of ROS and TFA in the stress and DPI groups.

Index	All	-N/-N + DPI	-P/-P + DPI	HS/HS + DPI
ROS	0.687**	0.909*	0.910*	0.960**

The symbol "*" denotes significant at the 0.05 level, while "**" indicates significant at the 0.01 level.

and HS stress conditions (Figure 3A). Previous studies have shown that under nitrogen deficiency and high light stress, intracellular levels of lutein and β-carotene decrease (Zhang et al., 2019). Additionally, secondary carotenoids, such as astaxanthin and adonixanthin, were present in trace amounts under normal conditions, but significantly accumulated under stressed conditions (Figure 3B). The -N, -P, and HS stress also increased astaxanthin accumulation by 223.64%, 73.07%, and 110.39%, respectively, compared with the control group. However, secondary carotenoids content decreased significantly after the addition of DPI under stress conditions (Figure 3B). Since DPI may block the production of NADPH oxidase-derived ROS under stress conditions, fewer signaling molecules were produced; thus, the astaxanthin content was significantly reduced by the addition of DPI under stress conditions. The correlation between NADPH oxidase-derived ROS levels and astaxanthin biosynthesis in *C. zofingiensis* under stress conditions was also verified using Pearson correlation analysis (Table 3). The Pearson correlation coefficients between intracellular astaxanthin accumulation and ROS levels in *C. zofingiensis* under -N, -P, and HS conditions were 0.866, 0.911, and 0.961, respectively. The Pearson's correlation coefficients for the different groups were greater than 0.7. These results indicated that the accumulation of intracellular astaxanthin in *C. zofingiensis* was closely related to its intracellular NADPH oxidase-derived ROS levels under stress conditions. Astaxanthin content increased with an increase in intracellular ROS levels within a certain range (Figure 3C). These results further confirmed that ROS levels, especially NADPH oxidase-derived ROS, may have a regulatory effect on astaxanthin accumulation under abiotic stress conditions.

3.4 Differential expression genes and enrichment analysis under abiotic stresses

In order to elucidate the molecular mechanism of NADPH oxidase-derived ROS in microalgal cell substance synthesis under stress conditions, comparative transcriptome analysis was performed. On the basis of principal component analysis (PCA), the transcriptional profiles of the eight groups in this study were highly reproducible in three replicates (Supplementary Figure 4). Based on the results of expression quantification, differential gene analysis between groups was performed to identify the genes that were differentially expressed of both groups. Log_2FC was used to express the expression changes in the differential ratio analysis groups, and the number of genes that were down- and up-regulated in each differential ratio analysis group was determined (Supplementary Table 2).

The DEGs were analyzed across the three abiotic stresses after the addition of DPI, and Venn diagrams were generated. As depicted in Figures 4A, B, there are 5,622, 2,803, and 7,615 DEGs of the "-N + DPI/-N," "-P + DPI/-P," and "HS + DPI/HS" groups, respectively. A total of 1,445 DEGs were shared among the three groups. KEGG enrichment analysis was performed on the DEGs of each group and their common DEGs (Figure 4C–F). The "-N + DPI/-N," "-P + DPI/-P," and "HS + DPI/HS" gene sets were all enriched for pathways associated with fatty acid biosynthesis and terpenoid quinone biosynthesis (precursors of carotenoid synthesis) (Figures 4C–E). These results indicated that ROS derived from NADPH oxidase would be a regulator of fatty acids and astaxanthin biosynthesis under abiotic stresses. Besides, 11 pathways were enriched in the common DEGs, the first two enriched pathways were the fatty acid biosynthesis and fatty acid elongation pathways, further supported the role of NADPH oxidase-derived ROS in regulating fatty acid biosynthesis under stress conditions (Figure 4F). In addition, the ubiquinone and other terpenoid-quinone biosynthesis pathways were also enriched. Ubiquinone is an important isoprenoid quinone that acts as an antioxidant in plant responses to stress that regulate gene expression and cell signaling (Abby et al., 2020). Terpenoids are

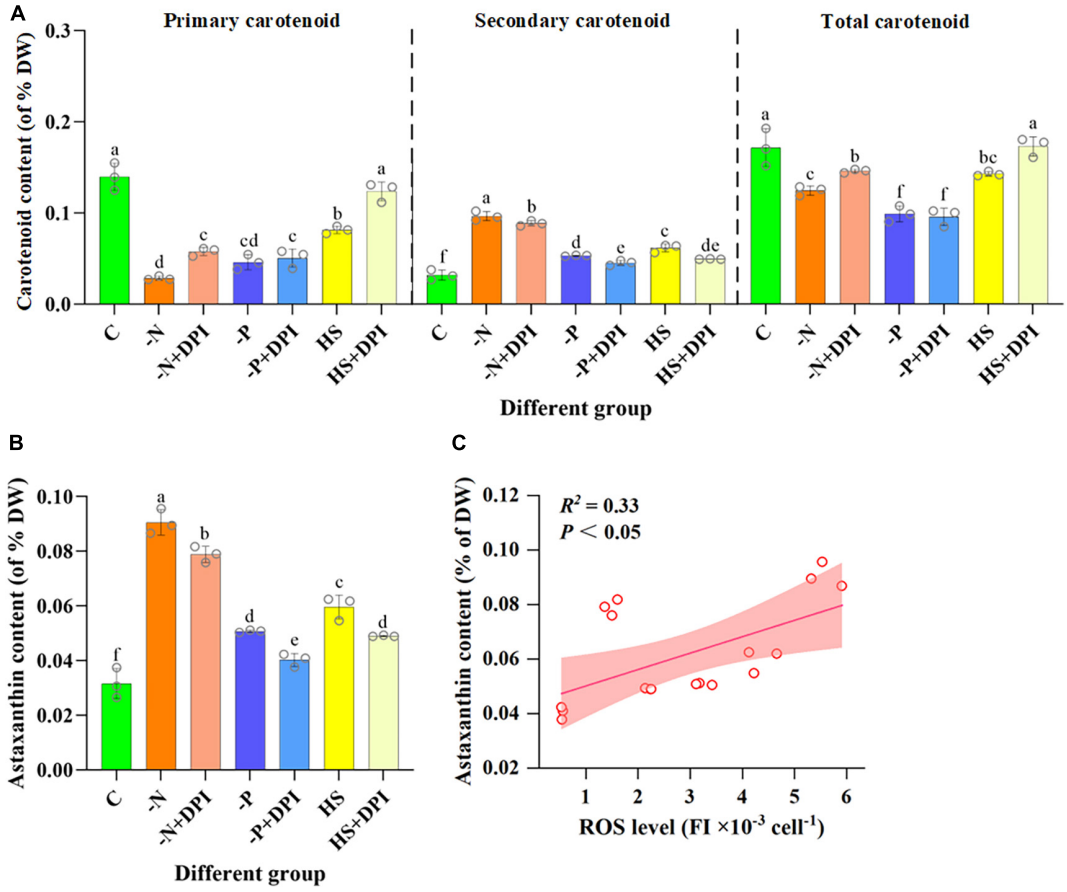

FIGURE 3
Carotenoid content after 4 days of cultivation. Carotenoid **(A)**, astaxanthin **(B)** content of *Chromochloris zofingiensis* after 4 days of induction under different conditions. **(C)** Relationship between the ROS level and astaxanthin content of *C. zofingiensis* under different culture conditions. Lines are linear fit with Pearson correlation coefficient (R^2). Shaded areas indicate 95% confidence bands. The error bars show the standard deviation. Different letters (a, b, c, d, e, f) indicate a significant difference between groups ($P < 0.05$).

a large group of organic molecules found widely in nature, and are a major type of pigment (Lin et al., 2023). Biotin, betalain, thiamine, and glucosinolate biosynthesis pathways, which play crucial roles in plant growth, development, and stress coping, were found to be enriched (Barba-Espin et al., 2018; Wang et al., 2020; Deng et al., 2022; Zhang et al., 2023). Biotin is essential for fatty acid carbon chain extension as it catalyzes the formation of CoA malonate from acetyl-CoA, which is a two-carbon unit supplier. Biotin deficiency alters the intracellular fatty acid composition and decreases SFA synthesis, explaining the reversal of saturated fatty acid reduction after DPI addition under stress conditions. Betalain reduces damage to cell membranes, enzymes, and protein structure and function caused by osmotic water loss under adverse conditions, thus increasing plant resistance to various stress factors. Thiamine plays an integral role as a cofactor in key metabolic reactions in all organisms, including glycolysis, pentose phosphate pathway, and tricarboxylic acid cycle (Goyer, 2010). Previous studies have shown that thiamine and its intermediates, acting as signaling molecules, are involved in systemic acquired resistance in various plant species (Tunc-Ozdemir et al., 2009). Thiamine accumulation was induced by the three stress treatments, thereby reducing oxidative stress damage to microalgal cells. Li et al. (2023) showed that $CaCl_2$-HCl electrolyzed water induces calcium signaling to activate NADPH oxidase-derived ROS to regulate the growth and metabolism of glucosinolate. Our analysis of DEGs under stress treatments revealed that inhibition of NADPH oxidase significantly affected glucosinolate biosynthesis. Except for the component biosynthesis, peroxisome related pathway was found to be enriched. The peroxisome is an organelle present in all eukaryotic cells, and its main function is to catalyze fatty acid β-oxidation to break down very long-chain fatty acids (VLCFAs) into short-chain fatty acids. Thus, inhibition of NADPH oxidase-derived ROS under different stress conditions can significantly regulate a range of cellular component synthesis and environmental stress-related pathways, suggesting that NADPH oxidase-derived ROS play an important regulatory role in a variety of stress processes.

TABLE 3 Correlation coefficients of ROS and astaxanthin in the stress and DPI groups.

Index	All	-N/-N + DPI	-P/-P + DPI	HS/HS + DPI
ROS	0.578*	0.866*	0.911*	0.961**

The symbol "*" denotes significant at the 0.05 level, while "**" indicates significant at the 0.01 level.

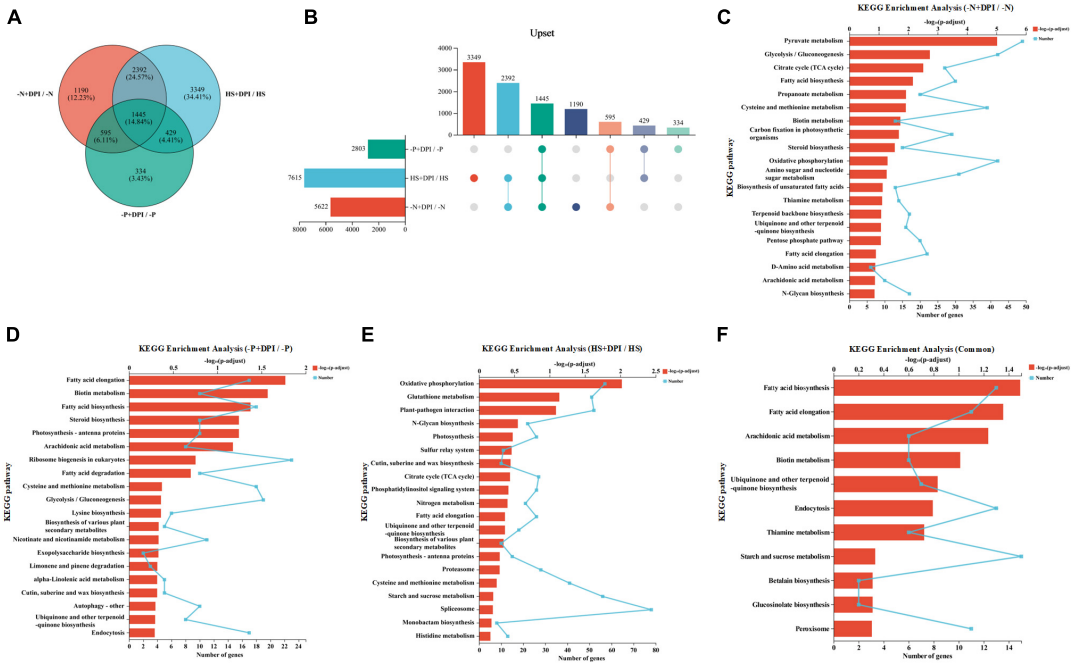

FIGURE 4
Venn analysis and functional enrichment analysis. **(A)** The number of shared and unique differentially expressed genes at 6 h. Different colored circles represent DEGs sets and the values represent the number of common and unique genes among DEGs sets. **(B)** Upset figure. The horizontal bar chart on the left represents the statistical values of the elements of each set, the individual points in the middle matrix represent the elements specific to a set, the lines between the points represent the intersections specific to different sets, and the vertical bar charts represent the values of the elements of the corresponding intersections, respectively. **(C–F)** KEGG enrichment analysis of the three groups including "-N + DPI/-N," "-P + DPI/-P," "HS + DPI/HS," and "Common." The vertical coordinate indicates the KEGG pathway, and the lower horizontal coordinate indicates the number of genes in this pathway on the ratio, corresponding to the different points on the fold; the upper horizontal coordinate indicates the significance level of enrichment, corresponding to the height of the bar, where the smaller the false discovery rate and the larger the $-\log_{10}(p\text{-adjust})$ value, the more significantly enriched the KEGG pathway is (p-adjust < 0.5).

We selected ten important genes for RT-qPCR confirm the validity of the comparative transcriptome data. These genes were involved in fatty acid biosynthesis, carotenoid biosynthesis, and the peroxisome pathway. As shown in **Supplementary Figure 5**, the expression profiles of all selected genes showed changes similar to those observed in the comparative transcriptome analysis. Therefore, transcriptome data were considered plausible.

3.5 Typical pathways analysis

To elucidate the role of NADPH oxidase-derived ROS in the regulation of fatty acid and carotenoid accumulation, we analyzed the enriched pathways. Biochemical data showed that fatty acid and carotenoid contents were significantly decreased in all stress treatment groups after the addition of DPI. Moreover, the primary function of peroxisomes is to catalyze fatty acid β-oxidation, which can also affect the fatty acid content. Therefore, we focused our analysis on the biosynthesis of fatty acids, carotenoids, and peroxisome pathways. Detailed information on the genes involved in the biological pathways selected above is provided in **Supplementary File 1**.

Acetyl-CoA carboxylase (*ACCase*) is considered the first key rate-limiting enzyme in the fatty acid biosynthetic pathway. Comparative transcriptome analysis showed that *ACCase* was downregulated by DPI-treatment, especially under nitrogen starvation conditions. Other genes involved in the fatty acid biosynthesis pathway included S-malonyltransferase (*FabD*), 3-oxoacyl-(acyl-carrier-protein) synthase II (*FabF*), 3-oxoacyl-(acyl-carrier-protein) synthase III (*FabH*) and, 3-hydroxyacyl-[acyl-carrier-protein] dehydratase (*FabZ*), and enoyl-(acyl carrier protein) reductase (*FabI*) (**Figure 5A**). The biochemical data indicated that large amounts of fatty acids accumulated under various stress conditions, but this accumulation was significantly hindered by the inclusion of DPI. These findings corroborate the molecular viewpoint that NADPH oxidase-derived ROS play a regulatory role in fatty acid synthesis.

In the carotenoid synthesis pathway, β-carotene is the precursor for astaxanthin biosynthesis, followed by hydroxylation and ketolation (Zhou et al., 2019). In bacteria and algae, the synthesis of zeaxanthin from β-carotene is mainly catalyzed by β-carotene hydroxylase (*CrtZ*) and β-carotene ketolase (*BKT*) (Liu et al., 2014). Zeaxanthin is further ketonized to astaxanthin via *BKT*. The addition of DPI under -N, -P, and HS stress conditions down regulated the expression of *CrtZ* and *BKT* (**Figure 5B**). These transcriptomic results are in agreement with biochemical data, implying that hindering NADPH oxidase activity under stress conditions obstructs ROS signaling, which leads to a decrease in astaxanthin biosynthesis by downregulating the expression of genes related to astaxanthin synthesis.

Peroxisomes are single membrane-covered vesicles present in most eukaryotic cells. Its main function is to participate

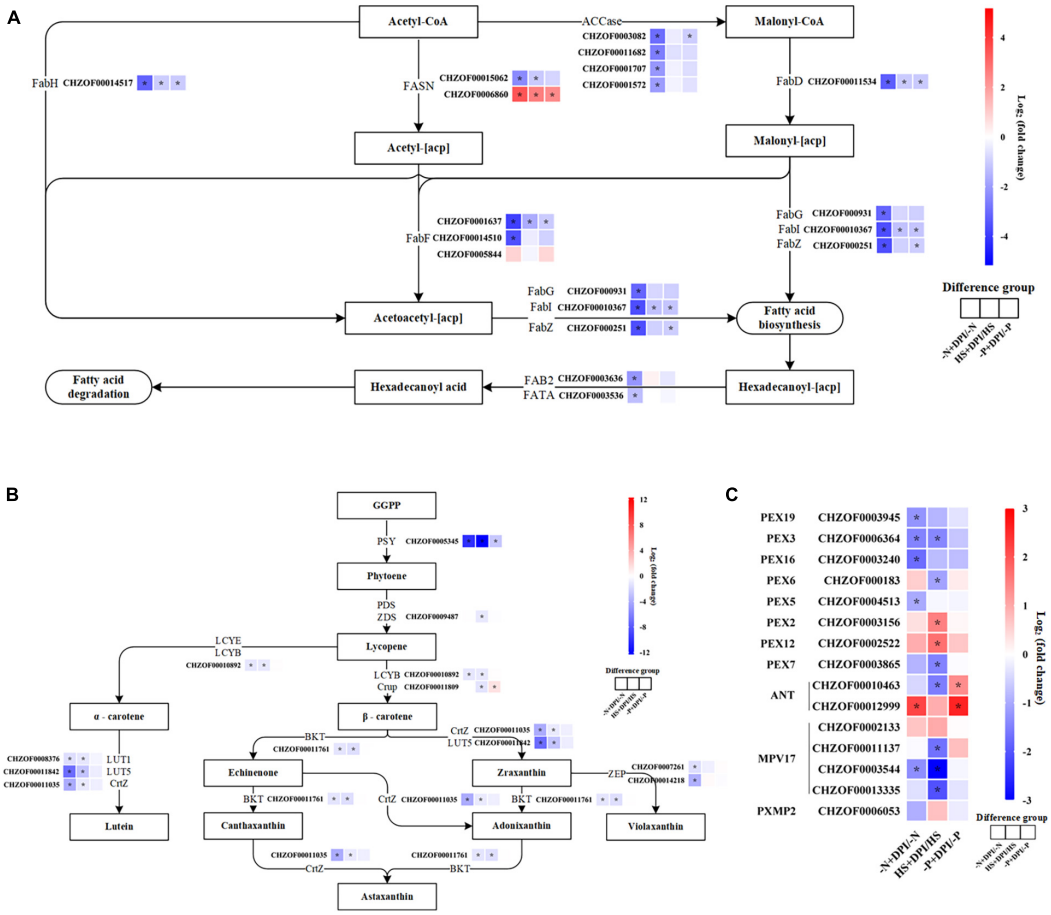

FIGURE 5
Up-down-regulation of typical pathway genes. The expression changes in the fatty acid biosynthesis pathway **(A)**, carotenoid biosynthesis pathway **(B)**, and peroxisome pathway **(C)**. [Heat map indicates the variation of $\log_2$FC in the differential comparison analysis groups. Genes are displayed in red (upregulated) and blue (downregulated). The isozymes are ranked in descending order of expression. Significantly differentially expressed genes $|\log_2 FC| \geq 1$, $P < 0.05$].

in lipid metabolism, such as catabolism of long-chain fatty acids. Glutathione S-transferase kappa 1 (*GSTK1*) and superoxide dismutase (*SOD*) have antioxidant effects and are involved in the regulation of plant secondary metabolism, detoxification, and defense (Ferreira et al., 2023). Peroxidase is one of the key enzymes in the enzymatic defense system of plants under adverse conditions, and acts synergistically with *SOD* and catalase (*CAT*) to scavenge excess free radicals in the body, thereby increasing plant resistance (Dazy et al., 2009). The peroxisome gene encoded by peroxidase plays a crucial role in the cellular metabolism and pathogenicity of microalgae (Kato et al., 2022). Our results showed that most peroxidase genes were down-regulated upon inhibition of NADPH oxidase-derived ROS under various stress conditions, such as peroxin-3 (*PEX3*), peroxin-5 (*PEX5*), peroxin-7 (*PEX7*), peroxin-16 (*PEX16*), and peroxin-19 (*PEX19*) genes (**Figure 5C**). Inhibition of NADPH oxidase-derived ROS led to the suppression of signal transduction and downregulation of peroxidase genes, which in turn weakened the plant defense system. The upregulation of the adenine nucleotide transporter (*ANT*) gene may be due to its role as a reverse transporter that transports adenosine diphosphate (*ADP*) from the cytoplasm to the mitochondrial matrix and adenosine 5′-triphosphate (*ATP*) synthesized by the mitochondrial matrix to the cytoplasm, thus providing energy to the organism. **Supplementary Table 3** shows the peroxisomal proteins, in which long-chain acyl-CoA synthesis (*ACSL*), acyl-CoA oxidase (*ACOX*) and 2,4-dienoyl-CoA reductase (*DECR2*) are involved in fatty acid β-oxidation. All three genes were significantly upregulated. This explains the significant decrease in TFA content after the inhibition of NADPH oxidase-derived ROS.

3.6 WGCNA analysis

A variety of abiotic stresses lead to the accumulation of TFAs and carotenoids in *C. zofingiensis*, and transcriptome analysis can be used to determine variations in gene expression levels for fatty acid and carotenoid biosynthesis. However, it is unclear whether a universal regulatory mechanism exists under various stress conditions. To address this, we performed WGCNA and established gene clusters that were highly correlated with phenotypic characteristics. After filtering abnormal and small variant genes, we ensured that the intensity of the correlation effects among processed genes conformed to a scale-free distribution following background correction and normalization. Intracellular

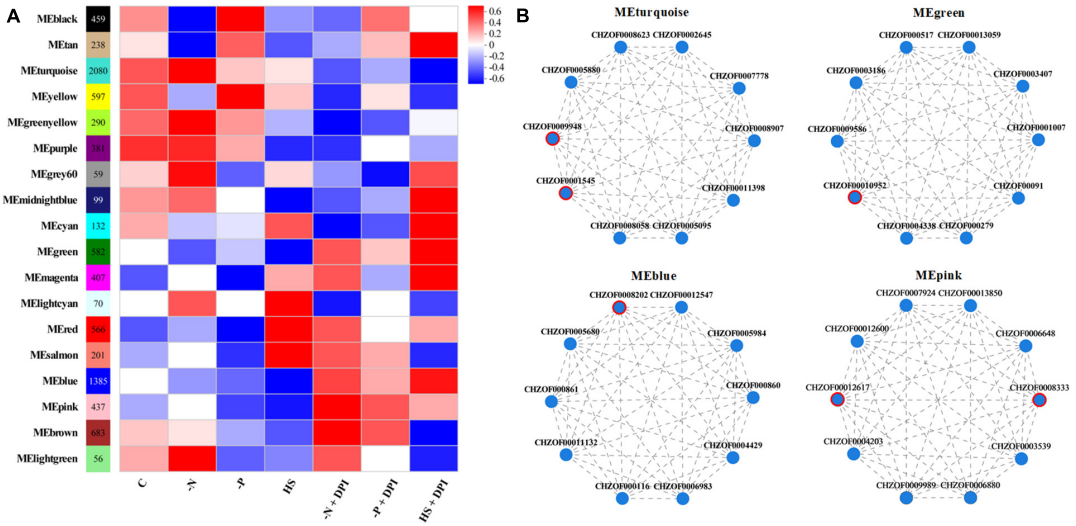

FIGURE 6
Weighted correlation network analysis (WGCNA). **(A)** Correlation between module and trait. **(B)** Visualization and analysis images of the top 10 hub genes. The genes marked in red circle are key genes.

genes and genes with similar expression profiles were clustered into modules. The correlation between phenotypes and modules was analyzed to identify the key modules that were significantly regulated by NADPH oxidase under stress conditions. As shown in Figure 6A, 8,749 genes were clustered into 18 modules. Correlation analysis with the phenotypic data revealed that 582 and 1,385 genes in the MEgreen and MEblue modules, respectively, were negatively correlated with stress conditions but positively correlated with the addition of DPI under stress conditions. The MEturquoise module contains 2,080 genes in the MEturquoise module that were positively associated with phenotype under stress conditions, but negatively associated with the addition of DPI under stress conditions. We also searched for modules containing genes involved in fatty acid biosynthesis, carotenoid biosynthesis, and peroxisome-related processes, and found 58 genes in the three pathways. Of these, 39 genes were included in the WGCNA analysis, and more than half of the genes were found to be distributed in the three most abundant clusters (MEturquoise, MEpink, and MEblue). Therefore, we considered the MEturquoise, MEgreen, MEblue, and MEpink modules as key modules. The top 10 hub genes for connectivity within the target modules were screened using BLAST, and the top ten hub genes in the different modules are shown in Figure 6B, and the hub genes relevant to this study are listed in Table 4.

Among the key modules screened, protein phosphatase PTC7 (*PPTC7*, CHZOF0009948), 5′-AMP-activated protein kinase (*AMPK*, CHZOF00010952), mechanosensitive ion channel protein (*MSL*, CHZOF0008202), and ubiquitin-like 1-activating enzyme E1 A (*UBLE1A*, CHZOF00012617) are all involved in signal transduction and are important for cells to perform normal physiological functions. Previous research showed that up-regulation of the pyruvate dehydrogenase E2 component (*aceF*) would promote the production of acetyl-CoA in *H. pluvialis*, resulting in an increase of fatty acid accumulation (Zhao et al., 2020). Therefore, the down-regulated expression of *aceF* (CHZOF0001545) by the addition of DPI might be the reason for the decrease fatty acid content under stress conditions. Stimulation of ROS production leads to the activation of *AMPK* (Ohishi et al., 2021). *AMPK* regulates fatty acid biosynthesis through phosphorylation and inactivation by acetyl-CoA carboxylase. CHZOF0008333 is a methyltransferase that converts demethylmenaquinone (*DMKH2*) to menaquinone (*MKH2*) and functions in the plant and microbial electron transport chains. Moreover, cellular signaling pathways primarily involved in nitrogen fixation have been identified in *Klebsiella pneumoniae* (Thummer et al., 2007). *UBLE1A* is the ultimate step in the downstream signaling pathway, which interacts with downstream ubiquitination mechanisms to regulate gene expression. In summary, we propose a plausible signal transduction pathway in which microalgal cells perceive stress and generate ROS signals, which continue to signal downward through phosphorylation and ubiquitination, ultimately resulting in fatty acid and carotenoid biosynthesis. However, the above speculations are only based on histological data, and more work is needed to

TABLE 4 The hub genes of different modules.

Module	Gene ID	Annotated	Degree
MEturquoise	CHZOF0009948	Protein phosphatase PTC7	840.800
	CHZOF0001545	Pyruvate dehydrogenase E2 component	837.534
MEgreen	CHZOF00010952	5′-AMP-activated protein kinase	324.218
MEblue	CHZOF0008202	Mechanosensitive ion channel protein	483.858
MEpink	CHZOF0008333	Methyltransferase	189.934
	CHZOF00012617	Ubiquitin-like 1-activating enzyme E1 A	183.900

verify the regulation of NADPH oxidase under stress conditions. In summary, through WGCNA analysis, this study identified six potential core regulatory-related genes in *C. zofingiensis*, providing a framework for future research.

4 Conclusion

This study examined the correlation between the generation of ROS by NADPH oxidase and the accumulation of fatty acids and astaxanthin under -N, -P, and HS stress conditions. The results showed that these stresses induced fatty acid and astaxanthin accumulation, whereas treating the plants with DPI under stress conditions reduced ROS generation and significantly decreased fatty acid and astaxanthin accumulation. The correlation between ROS and TFA and astaxanthin content was strong, with Pearson correlation coefficients of over 0.9 and 0.8, respectively. Comparative transcriptome analysis showed that the expression levels of key enzymes involved in the fatty acid and carotenoid biosynthesis pathways were downregulated in the DPI group. Moreover, biotin, betaine, thiamine, and glucosinolate metabolism pathways were enriched in the DPI group under different stress conditions, indicating that these pathways may be regulated by NADPH oxidase-derived ROS and may play important roles in regulating the biosynthesis of TFAs and carotenoids. However, the exact regulatory mechanisms underlying these pathways require further functional verification. In summary, this study proved that NADPH oxidase-derived ROS might play a universal regulatory role in the production of fatty acids and astaxanthin under stress conditions, which suggests that NADPH oxidase as well as its downstream regulating pathways could be promising manipulation points for the production of lipids and carotenoids in microalgae.

Data availability statement

The datasets presented in this study can be found in online repositories. The names of the repository/repositories and accession number(s) can be found in the article/ **Supplementary material**.

Author contributions

YY: Data curation, Formal analysis, Investigation, Validation, Writing – original draft, Writing – review & editing. TZ: Data curation, Formal analysis, Investigation, Writing – original draft. WG: Data curation, Formal analysis, Writing – review & editing. WY: Methodology, Writing – review & editing. YC: Data curation, Writing-review & editing. DS: Conceptualization, Supervision, Writing – review & editing. ZZ: Conceptualization, Investigation, Supervision, Writing – review & editing.

Funding

The author(s) declare financial support was received for the research, authorship, and/or publication of this article. This study was financially supported by the National Natural Science Foundation of China (Project No. 32101925), Science Foundation of Hebei Normal University (Project Nos. L2023B20 and L2024B22), and Post-graduate's Innovation Fund Project of Hebei University (HBU2023SS016).

Conflict of interest

The authors declare that the research was conducted in the absence of any commercial or financial relationships that could be construed as a potential conflict of interest.

Publisher's note

All claims expressed in this article are solely those of the authors and do not necessarily represent those of their affiliated organizations, or those of the publisher, the editors and the reviewers. Any product that may be evaluated in this article, or claim that may be made by its manufacturer, is not guaranteed or endorsed by the publisher.

Supplementary material

The Supplementary Material for this article can be found online at: https://www.frontiersin.org/articles/10.3389/fmicb.2024.1387222/full#supplementary-material

References

Abby, S. S., Kazemzadeh, K., Vragniau, C., Pelosi, L., and Pierrel, F. (2020). Advances in bacterial pathways for the biosynthesis of ubiquinone. *Biochim. Biophys. Acta Bioenerg.* 1861:148259. doi: 10.1016/j.bbabio.2020.148259

Barba-Espin, G., Glied-Olsen, S., Dzhanfezova, T., Joernsgaard, B., Lütken, H., and Müller, R. (2018). Preharvest application of ethephon and postharvest UV-B radiation improve quality traits of beetroot (*Beta vulgaris* L. ssp. *vulgaris*) as source of colourant. *BMC Plant Biol.* 18:316. doi: 10.1186/s12870-018-1556-2

Baxter, A., Mittler, R., and Suzuki, N. (2014). ROS as key players in plant stress signalling. *J. Exp. Bot.* 65, 1229–1240. doi: 10.1093/jxb/ert375

Cash, T. P., Pan, Y., and Simon, M. C. (2007). Reactive oxygen species and cellular oxygen sensing. *Free Radic. Biol. Med.* 43, 1219–1225. doi: 10.1016/j.freeradbiomed.2007.07.001

Chen, H., Zhang, Y., He, C., and Wang, Q. (2014). Ca^{2+} signal transduction related to neutral lipid synthesis in an oil-producing green alga *Chlorella* sp. C2. *Plant Cell Physiol.* 55, 634–644. doi: 10.1093/pcp/pcu015

Chen, J., Wei, D., and Lim, P. E. (2020). Enhanced coproduction of astaxanthin and lipids by the green microalga *Chromochloris zofingiensis*: Selected phytohormones

as positive stimulators. *Bioresour. Technol.* 295:122242. doi: 10.1016/j.biortech.2019.122242

Cray, R., and Levine, I. (2022). Oxidative stress modulates astaxanthin synthesis in *Haematococcus pluvialis*. *J. Appl. Phycol.* 34, 2327–2338. doi: 10.1007/s10811-022-02792-1

Cui, J., Yu, C., Zhong, D. B., Zhao, Y., and Yu, X. (2020). Melatonin and calcium act synergistically to enhance the coproduction of astaxanthin and lipids in *Haematococcus pluvialis* under nitrogen deficiency and high light conditions. *Bioresour. Technol.* 305:123069. doi: 10.1016/j.biortech.2020.123069

Dazy, M., Masfaraud, J.-F., and Férard, J.-F. (2009). Induction of oxidative stress biomarkers associated with heavy metal stress in *Fontinalis antipyretica Hedw*. *Chemosphere* 75, 297–302. doi: 10.1016/j.chemosphere.2008.12.045

Deng, B., Chen, L., Tian, S., Shi, H., and Zhao, X. (2022). Vitamin B1 delays postharvest senescence and enhances antioxidant accumulation by activating NADPH oxidase in *Ziziphus jujuba* fruit. *Lwt* 165:113743. doi: 10.1016/j.lwt.2022.113743

Ferreira, M. J., Rodrigues, T. A., Pedrosa, A. G., Silva, A. R., Vilarinho, B. G., Francisco, T., et al. (2023). Glutathione and peroxisome redox homeostasis. *Redox Biol.* 67:102917. doi: 10.1016/j.redox.2023.102917

Foreman, J., Demidchik, V., Bothwell, J. H. F., Mylona, P., Miedema, H., Torres, M. A., et al. (2003). Reactive oxygen species produced by NADPH oxidase regulate plant cell growth. *Nature* 422, 442–446. doi: 10.1038/nature01485

Gao, W., Guan, Y., Li, Y., Zhang, X., Fu, Z., and Zhang, Z. (2023). Treatment of nitrogen and phosphorus in wastewater by heterotrophic N- and P-starved microalgal cell. *Appl. Microbiol. Biotechnol.* 107, 1477–1490. doi: 10.1007/s00253-023-12380-z

Goh, B. H. H., Ong, H. C., Cheah, M. Y., Chen, W.-H., Yu, K. L., and Mahlia, T. M. I. (2019). Sustainability of direct biodiesel synthesis from microalgae biomass: A critical review. *Renew. Sustain. Energy Rev.* 107, 59–74. doi: 10.1016/j.rser.2019.02.012

Goyer, A. (2010). Thiamine in plants: Aspects of its metabolism and functions. *Phytochemistry* 71, 1615–1624. doi: 10.1016/j.phytochem.2010.06.022

Hang, L. T., Mori, K., Tanaka, Y., Morikawa, M., and Toyama, T. (2020). Enhanced lipid productivity of *Chlamydomonas reinhardtii* with combination of NaCl and $CaCl_2$ stresses. *Bioprocess Biosyst. Eng.* 43, 971–980. doi: 10.1007/s00449-020-02293-w

Ip, P.-F., and Chen, F. (2005). Production of astaxanthin by the green microalga *Chlorella zofingiensis* in the dark. *Process Biochem.* 40, 733–738. doi: 10.1016/j.procbio.2004.01.039

Kato, N., McCuiston, C., Szuska, K. A., Lauersen, K. J., Nelson, G., and Strain, A. (2022). *Chlamydomonas reinhardtii* alternates peroxisomal contents in response to trophic conditions. *Cells* 11:2724. doi: 10.3390/cells11172724

Kaur, G., Sharma, A., Guruprasad, K., and Pati, P. K. (2014). Versatile roles of plant NADPH oxidases and emerging concepts. *Biotechnol. Adv.* 32, 551–563. doi: 10.1016/j.biotechadv.2014.02.002

Kaya, H., Takeda, S., Kobayashi, M. J., Kimura, S., Iizuka, A., Imai, A., et al. (2019). Comparative analysis of the reactive oxygen species-producing enzymatic activity of *Arabidopsis* NADPH oxidases. *Plant J.* 98, 291–300. doi: 10.1111/tpj.14212

Khona, D. K., Shirolikar, S. M., Gawde, K. K., Hom, E., Deodhar, M. A., and D'Souza, J. S. (2016). Characterization of salt stress-induced palmelloids in the green alga, *Chlamydomonas reinhardtii*. *Algal Res.* 16, 434–448. doi: 10.1016/j.algal.2016.03.035

Kubo, Y., Morimoto, D., Shiroi, M., Yoshimi, T., Ohara, K., Higashine, T., et al. (2022). Transcriptional responses of *Aurantiochytrium limacinum* under light conditions. *J. Appl. Microbiol.* 132, 4330–4337. doi: 10.1111/jam.15527

Langfelder, P., and Horvath, S. (2008). WGCNA: An R package for weighted correlation network analysis. *BMC Bioinformatics* 9:559. doi: 10.1186/1471-2105-9-559

Latsos, C., van Houcke, J., and Timmermans, K. R. (2020). The effect of nitrogen starvation on biomass yield and biochemical constituents of *Rhodomonas* sp. *Front. Mar. Sci.* 7:563333. doi: 10.3389/fmars.2020.563333

Li, C., Song, S., He, Y., Han, S., and Liu, H. (2023). $CaCl_2$–HCl electrolyzed water promotes glucosinolate metabolism in broccoli sprouts via calcium signalling. *Chem. Biol. Technol. Agric.* 10:42. doi: 10.1186/s40538-023-00416-5

Lin, J.-L., Chen, L., Wu, W.-K., Guo, X.-X., Yu, C.-H., Xu, M., et al. (2023). Single-cell RNA sequencing reveals a hierarchical transcriptional regulatory network of terpenoid biosynthesis in cotton secretory glandular cells. *Mol. Plant* 16, 1990–2003. doi: 10.1016/j.molp.2023.10.008

Liu, J., Mao, X., Zhou, W., and Guarnieri, M. T. (2016). Simultaneous production of triacylglycerol and high-value carotenoids by the astaxanthin-producing oleaginous green microalga *Chlorella zofingiensis*. *Bioresour. Technol.* 214, 319–327. doi: 10.1016/j.biortech.2016.04.112

Liu, J., Sun, Z., Gerken, H., Liu, Z., Jiang, Y., and Chen, F. (2014). *Chlorella zofingiensis* as an alternative microalgal producer of astaxanthin: Biology and industrial potential. *Mar. Drugs* 12, 3487–3515. doi: 10.3390/md12063487

Liu, J., Sun, Z., Mao, X., Gerken, H., Wang, X., and Yang, W. (2019). Multiomics analysis reveals a distinct mechanism of oleaginousness in the emerging model alga *Chromochloris zofingiensis*. *Plant J.* 98, 1060–1077. doi: 10.1111/tpj.14302

Liu, M., Liu, Y., Zhang, L., and Qiu, F. (2023). NADPH oxidase contributes to the production of reactive oxygen species in *Chlorella pyrenoidosa*. *Biotechnol. Lett.* 45, 199–207. doi: 10.1007/s10529-022-03330-2

Liu, P., Li, R.-L., Zhang, L., Wang, Q.-L., Niehaus, K., Baluska, F., et al. (2009). Lipid microdomain polarization is required for NADPH oxidase-dependent ROS signaling in *Picea meyeri* pollen tube tip growth. *Plant J.* 60, 303–313. doi: 10.1111/j.1365-313X.2009.03955.x

Livak, K. J., and Schmittgen, T. D. (2001). Analysis of relative gene expression data using real-time quantitative PCR and the $2^{(-\Delta\Delta C_T)}$ Method. *Methods* 25, 402–408. doi: 10.1006/meth.2001.1262

Maity, J. P., Bundschuh, J., Chen, C.-Y., and Bhattacharya, P. (2014). Microalgae for third generation biofuel production, mitigation of greenhouse gas emissions and wastewater treatment: Present and future perspectives – A mini review. *Energy* 78, 104–113. doi: 10.1016/j.energy.2014.04.003

Mao, X., Wu, T., Sun, D., Zhang, Z., and Chen, F. (2018). Differential responses of the green microalga *Chlorella zofingiensis* to the starvation of various nutrients for oil and astaxanthin production. *Bioresour. Technol.* 249, 791–798. doi: 10.1016/j.biortech.2017.10.090

Nagappan, S., and Kumar, G. (2021). Investigation of four microalgae in nitrogen deficient synthetic wastewater for biorefinery based biofuel production. *Environ. Technol. Innovat.* 23:101572. doi: 10.1016/j.eti.2021.101572

Nanda, M., Jaiswal, K. K., Kumar, V., Vlaskin, M. S., Gautam, P., Bahuguna, V., et al. (2021). Micro-pollutant Pb(II) mitigation and lipid induction in oleaginous microalgae *Chlorella sorokiniana* UUIND6. *Environ. Technol. Innovat.* 23:101613. doi: 10.1016/j.eti.2021.101613

Ohishi, T., Fukutomi, R., Shoji, Y., Goto, S., and Isemura, M. (2021). The beneficial effects of principal polyphenols from green tea, coffee, wine, and curry on obesity. *Molecules* 26:453. doi: 10.3390/molecules26020453

Pei, Z.-M., Murata, Y., Benning, G., Thomine, S., Klüsener, B., Allen, G. J., et al. (2000). Calcium channels activated by hydrogen peroxide mediate abscisic acid signalling in guard cells. *Nature* 406, 731–734. doi: 10.1038/35021067

Roy, M., Bera, S., and Mohanty, K. (2021). Nutrient starvation-induced oxidative stress-mediated lipid accumulation in *Tetradesmus obliquus* KMC24. *J. Appl. Phycol.* 33, 3617–3635. doi: 10.1007/s10811-021-02614-w

Sagi, M., and Fluhr, R. (2001). Superoxide production by plant homologues of the gp91(phox) NADPH oxidase. Modulation of activity by calcium and by tobacco mosaic virus infection. *Plant Physiol.* 126, 1281–1290. doi: 10.1104/pp.126.3.1281

Seo, S. H., Srivastava, A., Han, M. S., Lee, H. G., and Oh, H. M. (2019). Maximizing biomass and lipid production in Ettlia sp. by ultraviolet stress in a continuous culture. *Bioresour. Technol.* 288:121472. doi: 10.1016/j.biortech.2019.121472

Shetty, P., Gitau, M. M., and Maroti, G. (2019). Salinity stress responses and adaptation mechanisms in eukaryotic green microalgae. *Cells* 8:1657. doi: 10.3390/cells8121657

Shi, K., Gao, Z., Shi, T. Q., Song, P., Ren, L. J., Huang, H., et al. (2017). Reactive oxygen species-mediated cellular stress response and lipid accumulation in oleaginous microorganisms: The state of the art and future perspectives. *Front. Microbiol.* 8:793. doi: 10.3389/fmicb.2017.00793

Signorelli, S., Tarkowski, L. P., Van den Ende, W., and Bassham, D. C. (2019). Linking autophagy to abiotic and biotic stress responses. *Trends Plant Sci.* 24, 413–430. doi: 10.1016/j.tplants.2019.02.001

Singh, S., Dubey, N. K., Tripathi, D. K., Gupta, R., and Singh, V. P. (2023). Nitric oxide and hydrogen peroxide mediated regulation of chromium (VI) toxicity in wheat seedlings involves alterations in antioxidants and high affinity sulfate transporter. *Plant Sci.* 332:111697. doi: 10.1016/j.plantsci.2023.111697

Sun, D., and Zhang, Z. (2021). Reactive oxygen species derived from NADPH oxidase regulate astaxanthin and total fatty acid accumulation in *Chromochloris zofingiensis*. *J. Appl. Phycol.* 33, 819–827. doi: 10.1007/s10811-020-02327-6

Sun, D., Zhang, Z., Zhang, Y., Cheng, K. W., and Chen, F. (2019). Light induces carotenoids accumulation in a heterotrophic docosahexaenoic acid producing microalga, Crypthecodinium sp. SUN. *Bioresour. Technol.* 276, 177–182. doi: 10.1016/j.biortech.2018.12.093

Suzuki, N., Miller, G., Salazar, C., Mondal, H. A., Shulaev, E., Cortes, D. F., et al. (2013). Temporal-spatial interaction between reactive oxygen species and abscisic acid regulates rapid systemic acclimation in plants. *Plant Cell* 25, 3553–3569. doi: 10.1105/tpc.113.114595

Thummer, R., Klimmek, O., and Schmitz, R. A. (2007). Biochemical studies of *Klebsiella pneumoniae* NifL reduction using reconstituted partial anaerobic respiratory chains of *Wolinella succinogenes*. *J. Biol. Chem.* 282, 12517–12526. doi: 10.1074/jbc.M609826200

Tunc-Ozdemir, M., Miller, G., Song, L., Kim, J., Sodek, A., Koussevitzky, S., et al. (2009). Thiamin confers enhanced tolerance to oxidative stress in *Arabidopsis*. *Plant Physiol.* 151, 421–432. doi: 10.1104/pp.109.140046

Vitali, L., Lolli, V., Sansone, F., Kumar, A., Concas, A., and Lutzu, G. A. (2023). Lipid content and fatty acid methyl ester profile by *Chromochloris zofingiensis* under chemical and metabolic stress. *Biomass Convers. Biorefinery* doi: 10.1007/s13399-023-04153-5

Wang, L., Feng, Z., Wang, X., Wang, X., and Zhang, X. (2010). DEGseq: An R package for identifying differentially expressed genes from RNA-seq data. *Bioinformatics* 26, 136–138. doi: 10.1093/bioinformatics/btp612

Wang, L., Ming, D., Pan, Y., Shi, L., and Wei, W. (2023). Nitrogen limitation and hydrogen peroxide act synergistically to enhance lipids accumulation via ROS/Ca^{2+} dependent mechanism in *Chlorella sorokiniana*. *Algal Res.* 70:102974. doi: 10.1016/j.algal.2023.102974

Wang, Q., Shen, T., Ni, L., Chen, C., Jiang, J., Cui, Z., et al. (2023). Phosphorylation of OsRbohB by the protein kinase OsDMI3 promotes H_2O_2 production to potentiate ABA responses in rice. *Mol. Plant* 16, 882–902. doi: 10.1016/j.molp.2023.04.003

Wang, Y., Wang, M., Ye, X. X., Liu, H., Takano, T., Tsugama, D., et al. (2020). Biotin plays an important role in seedlings under carbonate stress. *Plant Sci.* 300:110639. doi: 10.1016/j.plantsci.2020.110639

Waszczak, C., Carmody, M., and Kangasjarvi, J. (2018). Reactive oxygen species in plant signaling. *Annu. Rev. Plant Biol.* 69, 209–236. doi: 10.1146/annurev-arplant-042817-040322

Yu, Z., Pei, H., Jiang, L., Hou, Q., Nie, C., and Zhang, L. (2018). Phytohormone addition coupled with nitrogen depletion almost tripled the lipid productivities in two algae. *Bioresour. Technol.* 247, 904–914. doi: 10.1016/j.biortech.2017.09.192

Zhang, K., Chen, L., Liu, J., Gao, F., He, R., Chen, W., et al. (2017). Effects of butanol on high value product production in *Schizochytrium limacinum* B4D1. *Enzyme Microb. Technol.* 102, 9–15. doi: 10.1016/j.enzmictec.2017.03.007

Zhang, R., Yang, W., Pan, Q., Zeng, Q., Yan, C., Bai, X., et al. (2023). Effects of long-term blue light irradiation on carotenoid biosynthesis and antioxidant activities in Chinese cabbage (*Brassica rapa* L. ssp. *pekinensis*). *Food Res. Int.* 174:113661. doi: 10.1016/j.foodres.2023.113661

Zhang, Y., Shi, M., Mao, X., Kou, Y., and Liu, J. (2019). Time-resolved carotenoid profiling and transcriptomic analysis reveal mechanism of carotenogenesis for astaxanthin synthesis in the oleaginous green alga *Chromochloris zofingiensis*. *Biotechnol. Biofuels* 12:287. doi: 10.1186/s13068-019-1626-1

Zhang, Y., Ye, Y., Bai, F., and Liu, J. (2021). The oleaginous astaxanthin-producing alga *Chromochloris zofingiensis*: Potential from production to an emerging model for studying lipid metabolism and carotenogenesis. *Biotechnol. Biofuels* 14:119. doi: 10.1186/s13068-021-01969-z

Zhang, Z., Huang, J. J., Sun, D., Lee, Y., and Chen, F. (2017). Two-step cultivation for production of astaxanthin in *Chlorella zofingiensis* using a patented energy-free rotating floating photobioreactor (RFP). *Bioresour. Technol.* 224, 515–522. doi: 10.1016/j.biortech.2016.10.081

Zhao, Y., Hou, Y., Chai, W., Liu, Z., Wang, X., He, C., et al. (2020). Transcriptome analysis of *Haematococcus pluvialis* of multiple defensive systems against nitrogen starvation. *Enzyme Microb. Technol.* 134:109487. doi: 10.1016/j.enzmictec.2019.109487

Zhao, Y., Song, X., Yu, L., Han, B., Li, T., and Yu, X. (2019). Influence of cadmium stress on the lipid production and cadmium bioresorption by *Monoraphidium* sp. QLY-1. *Energy Convers. Manage.* 188, 76–85. doi: 10.1016/j.enconman.2019.03.041

Zhou, P., Li, M., Shen, B., Yao, Z., Bian, Q., Ye, L., et al. (2019). Directed coevolution of β-carotene ketolase and hydroxylase and its application in temperature-regulated biosynthesis of astaxanthin. *J. Agric. Food Chem.* 67, 1072–1080. doi: 10.1021/acs.jafc.8b05003

Frontiers in Microbiology

Explores the habitable world and the potential of microbial life

The largest and most cited microbiology journal which advances our understanding of the role microbes play in addressing global challenges such as healthcare, food security, and climate change.

Discover the latest Research Topics

See more →

Frontiers

Avenue du Tribunal-Fédéral 34
1005 Lausanne, Switzerland
frontiersin.org

Contact us

+41 (0)21 510 17 00
frontiersin.org/about/contact